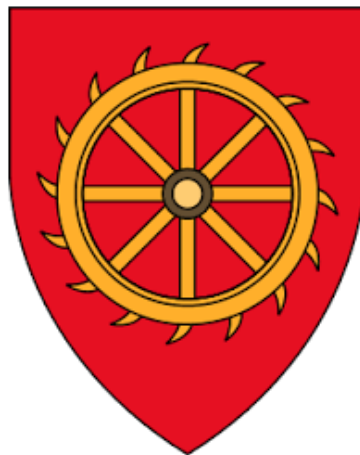


**Investigating the role of histone H3 lysine 9 dimethylation in
regulating disease-associated vascular smooth muscle cell
gene expression**



**Jennifer Louise Harman
St Catherine's College**



This dissertation is submitted for the degree of Doctor of Philosophy

University of Cambridge

30/09/2018

Preface

Declaration

This dissertation is the result of my own work and includes nothing which is the outcome of work done in collaboration except as declared in the Preface and specified in the text.

It is not substantially the same as any that I have submitted, or, is being concurrently submitted for a degree or diploma or other qualification at the University of Cambridge or any other University or similar institution except as declared in the Preface and specified in the text. I further state that no substantial part of my dissertation has already been submitted, or, is being concurrently submitted for any such degree, diploma or other qualification at the University of Cambridge or any other University or similar institution except as declared in the Preface and specified in the text.

It does not exceed the prescribed word limit for the relevant Degree Committee.

- Helle Jorgensen supervised this work and was involved in experimental design and mouse breeding.
- Greg Strachan and Joel Chappell aided in teaching confocal microscopy.
- Alison Finigan aided in performing and teaching insertion of the osmotic mini pumps.
- Joel Chappell and Kirsty Foote performed the carotid ligation injury surgeries.
- Amanda Dalby performed some of the chromatin immunoprecipitation experiments used to analyse H3K9me2 levels at the promoters of mouse contractile VSMC genes.
- The NIHR Cambridge BRC Cell Phenotyping Hub helped with FACS.

Acknowledgments

I would first like to thank my supervisor Dr Helle Jorgensen for her excellent guidance in choosing what questions to ask and how to design experiments to answer them. Helle's incredible knowledge and enthusiasm drove this project forward and gave me an enjoyable and rewarding PhD experience for which I am extremely grateful. I would also like to thank everyone within the Division of Cardiovascular Medicine for their support during my time as a PhD student. In particular, I would like to thank Dr Joel Chappell, Dr Kirsty Foote and Allie Finigan for their help and expertise in setting up the *in vivo* models of vascular disease. I must also thank Annabel Taylor, Lina Dobnikar and Dr Anna Uryga for always having time to help me out the best they could. I also thank my family, Mike and Anna for keeping me calm and collected when ever times felt a little tough. Last but certainly not least, I would like to thank the mice as without them I would not have been able to complete this project.

Abstract

Widespread changes in gene expression accompany vascular smooth muscle cell (VSMC) phenotypic switching, a hallmark of vascular disease. Upon insult, VSMCs downregulate contractile proteins and upregulate genes linked to vascular remodelling, such as matrix metalloproteinases (MMPs) and pro-inflammatory cytokines. However, the epigenetic mechanisms which regulate VSMC phenotypic switching remain unclear. This thesis explores the role of histone 3 lysine 9 dimethylation (H3K9me2), a repressive epigenetic mark, in regulating the expression of disease-associated VSMC genes.

Intriguingly, murine models of VSMC phenotypic switching revealed reduced levels of H3K9me2 upon loss of the contractile state while chromatin immunoprecipitation (ChIP) identified a subset of IL-1 α /injury-responsive VSMC gene promoters enriched for H3K9me2. To test the functional importance of H3K9me2 for VSMC gene regulation the methyltransferase G9A/GLP was pharmacologically inhibited *in vitro* and *in vivo*. The resulting loss of H3K9me2 attenuated the expression of contractile VSMC markers and significantly potentiated IL-1 α /injury-induced expression of MMP and pro-inflammatory genes.

H3K9me2-mediated regulation of contractile and IL-1 α -responsive VSMC gene expression was confirmed in cultured human VSMCs (hVSMCs). This prompted the use of hVSMCs to investigate the mechanism underlying H3K9me2-dependent regulation of IL-1 α -mediated VSMC genes. Interestingly, G9A/GLP inhibition did not influence the level of IL-1 α -induced nuclear localisation of the NF κ B transcription factor p65 but significantly increased IL-1 α -induced p65 binding to the *IL6* promoter, correlating with reduced H3K9me2 levels. In contrast, enrichment of p65 was not observed at reported NF κ B sites within the *MMP3* promoter after IL-1 α stimulation. Rather, IL-1 α -induced *MMP3* expression was dependent on JNK activity and G9A/GLP inhibition potentiated IL-1 α -induced binding of the AP-1 transcription factor cJUN to the *MMP3* promoter.

Collectively, these findings suggest that H3K9me2 plays a role in maintaining the contractile VSMC state and prevents binding of both NF κ B and AP-1 transcription factors at specific IL-1 α -regulated genes to possibly block spurious induction of a pro-inflammatory state.

Contents

Preface	2
Declaration	2
Acknowledgments	3
Abstract.....	4
List of figures	9
List of tables.....	12
Abbreviations.....	13
CHAPTER 1 - INTRODUCTION	15
1.1 Cardiovascular function and disease	16
1.1.1 Vascular structure and function	16
1.1.2 Atherogenesis	17
1.2 VSMC function and phenotype.....	18
1.2.1 VSMC phenotypic switching in vascular disease	19
1.2.2 Cytokines in vascular function and disease	21
1.2.3 Matrix metalloproteinases in vascular function and disease.....	23
1.3 Transcriptional regulation of VSMC gene expression	25
1.3.1 Transcriptional regulation of contractile VSMC genes.....	25
1.3.2 Transcriptional regulation of injury/inflammation-induced VSMC genes	26
1.3.3 The NFκB signalling pathway	27
1.3.4 The AP-1 signalling pathway.....	29
1.4 Epigenetic regulation of gene expression	31
1.4.1 Histone modifications mark regulatory DNA elements	32
1.4.2 Histone methylation	34
1.5 H3K9me2	34
1.5.1 H3K9me2 regulates cell lineage commitment and reprogramming.....	34
1.5.2 H3K9me2 regulates the expression of inflammation-induced genes.....	35
1.6 G9A/GLP are required for H3K9 dimethylation.....	36
1.6.1 G9A/GLP structure and function	36
1.6.2 G9A/GLP have non-histone targets.....	37
1.6.3 Inhibition of G9A/GLP by chemical probes	39
1.7 H3K9me2 demethylases	39

1.8 Epigenetic regulation of VSMC phenotype	39
1.8.1 Histone methylation regulates VSMC gene expression	40
1.8.2 H3K9me2 and G9A/GLP regulate VSMC phenotype	40
1.9 <i>In vivo</i> mouse models of vascular remodelling and disease	40
1.9.1 VSMC-specific conditional lineage tracing	41
1.9.2 Carotid ligation model	43
1.9.3 ApoE ^{-/-} , high fat diet mouse model of atherosclerosis	45
1.10 Hypothesis and aims.....	46
CHAPTER 2 - METHODS	49
2.1 Mouse VSMC isolation.....	50
2.2 Primary mouse VSMC culture.....	50
2.3 Derivation of human VSMCs.....	50
2.4 Animal experiments.....	51
2.4 Western blot.....	52
2.5 Quantitative Real Time-Polymerase Chain Reaction (RT-qPCR)	54
2.5.1 Primer design and validation	54
2.6 ChIP for histone modifications	59
2.7 UNC0638 (UNC)/SP600125/IL-1 α /TNF α treatment	60
2.8 DQ-gelatin ECM degradation assay	61
2.9 FACS of lineage labelled VSMCs	61
2.10 RT-qPCR analysis of mRNA levels from lineage labelled YFP ⁺ VSMCs isolated by FACS	61
2.11 Tissue processing for immunofluorescent staining.....	62
2.12 Immunofluorescent staining of cryosections	62
2.13 Imaging and image processing of immunofluorescent stained cryosections	62
2.14 G9A SiRNA knock down	63
2.15 ChIP for NFkB-p65 and AP-1-cJUN.....	63
2.16 NFkB-p65 immunofluorescent staining of cultured VSMCs	64
2.17 Statistics.....	64

CHAPTER 3 - RESULTS: Assessing the role of H3K9me2 in maintaining the contractile VSMC state.	66
3.1 Introduction	67
3.2 Results.....	68
3.2.1 Global levels of H3K9me2, and the associated histone methyltransferase GLP, are reduced in cultured relative to ex vivo VSMCs, concomitant with loss of the contractile state.	68
3.2.2 Assessing the role of H3K9me2 in VSMC phenotypic switching using in vivo mouse models of CVD.	71
3.2.3 H3K9me2 is enriched at contractile VSMC gene promoters upon culture-induced phenotypic switching.....	76
3.2.4 Loss of H3K9me2 accelerates downregulation of contractile VSMC marker genes upon culture.	78
3.3 Summary and Conclusions.....	79
CHAPTER 4 - RESULTS: H3K9me2 plays a functional role in regulating inflammation/injury-induced gene expression in VSMCs.	81
4.1 Introduction	82
4.2 Results.....	84
4.2.1 H3K9me2 marks IL-1 α -responsive gene promoters in mVSMCs.	84
4.2.2 Loss of H3K9me2, by pharmacological inhibition of G9A/GLP (UNC0638), potentiates MMP gene expression in cultured mVSMCs.....	86
4.2.3 Loss of H3K9me2, by pharmacological inhibition of G9A/GLP (UNC0638), potentiates IL-1 α -induced ECM degradation of gelatin by cultured mVSMCs.	88
4.2.4 Loss of H3K9me2, by pharmacological inhibition of G9A/GLP (A366), significantly potentiates injury-induced Mmp3, Mmp12 and Il6 gene expression in the VSMCs in vivo.....	89
4.3 Summary and conclusions	96
CHAPTER 5 - RESULTS: The functional role of H3K9me2 in regulating VSMC gene expression changes associated with vascular disease is conserved in human	99
5.1 Introduction	100
5.2 Results.....	101
5.2.1 Global levels of H3K9me2 are reduced in cultured relative to ex vivo human VSMCs, concomitant with loss of the contractile state.	101
5.2.2 H3K9me2 marks IL-1 α -responsive gene promoters in human VSMCs.	104
5.2.3 Inhibition of H3K9me2 potentiates IL6 and MMP gene expression in human VSMCs.....	105

5.2.4 SiRNA knockdown of G9A attenuates the expression of contractile VSMC genes.	108
5.3 Summary and Conclusions.....	110
CHAPTER 6 - RESULTS: Investigating the mechanism behind G9A/GLP -mediated regulation of IL-1 α -responsive VSMC genes	113
6.1 Introduction	114
6.2 Results.....	115
6.2.1 Loss of H3K9me2, by pharmacological inhibition of G9A/GLP, does not influence the upstream NF κ B signalling pathway.	115
6.2.2 Pharmacological inhibition of G9A/GLP potentiates IL-1 α -induced p65 binding to the IL6 promoter, correlating with reduced H3K9me2 levels in cultured hVSMCs.	122
6.2.3 Loss of H3K9me2, by pharmacological inhibition of G9A/GLP, does not influence IL-1 α -induced MAPK phosphorylation.	124
6.2.4 Pharmacological inhibition of G9A/GLP potentiates IL-1 α -induced cJUN binding to the MMP3 and IL6 promoter, correlating with reduced H3K9me2 levels in cultured hVSMCs.....	128
6.3 Summary and Conclusions.....	129
CHAPTER 7- DISCUSSION	131
7.1 Global levels of H3K9me2 and the associated methyltransferase GLP are reduced upon VSMC phenotypic switching.	132
7.2 H3K9me2 inhibits inflammation-induced gene upregulation in VSMCs <i>in vitro</i> and <i>in vivo</i>	134
7.3 H3K9me2 hinders inflammation-induced TF binding at target VSMC gene promoters	135
7.4 Limitations of study	137
7.5 Future experiments	138
References	141

List of figures

Figure 1.1: Vascular wall structure.

Figure 1.2: Atherogenesis.

Figure 1.3: Schematic of VSMC phenotypic switching in atherosclerosis.

Figure 1.4: Hypothetical VSMC phenotypic spectrum.

Figure 1.6: Results of *in vivo* studies evaluating the effects of MMPs on atherosclerotic plaque.

Figure 1.7: Stimuli that activate the NFκB and AP-1 signalling pathways and genes under NFκB and AP-1 transcriptional control.

Figure 1.8: The canonical NFκB signalling pathway.

Figure 1.9: The MAPK/AP-1 signalling pathway.

Figure 1.10: Epigenetic regulation of gene expression.

Figure 1.11: Histone modifications mark functional elements in mammalian genomes.

Figure 1.12: Structure of G9A and GLP.

Figure 1.13: A Lys methylation network is presented for known Lys methyltransferase (KMT)–substrate associations based on currently published literature.

Figure 1.14: Schematic of 'Confetti' multi-colour and EYFP single-colour VSMC lineage tracing system.

Figure 1.15: The carotid ligation-injury mouse model.

Figure 1.16: Overview of atherosclerosis model in ApoE-knockout mice fed on a high-fat diet.

Figure 3.1: Schematic of culture-induced VSMC phenotypic switching.

Figure 3.2: Global levels of H3K9me2 are reduced upon culture-induced VSMC phenotypic switching.

Figure 3.3: Schematic of the mouse carotid ligation model of vascular injury.

Figure 3.4: Global levels of H3K9me2 are reduced in VSMCs upon vascular injury.

Figure 3.5: Schematic of the mouse model of atherosclerosis.

Figure 3.6: Global levels of H3K9me2 are reduced in VSMCs within atherosclerotic lesions compared to healthy vessels.

Figure 3.7: Local levels of histone modifications at contractile VSMC gene promoters in *ex vivo* and cultured murine VSMCs.

Figure 3.8: Loss of H3K9me2 accelerates downregulation of contractile VSMC marker genes.

Figure 4.1: IL-1 α -responsive MMP gene promoters are highly enriched for H3K9me2 in both *ex vivo* and cultured mVSMCs.

Figure 4.2: Global reduction of H3K9me2, by pharmacological inhibition of G9A/GLP, significantly potentiates IL-1 α -mediated MMP gene induction in cultured mVSMCs.

Figure 4.3: In cultured mVSMCs, H3K9me2 protects against IL-1 α -induced ECM degradation.

Figure 4.4: Experimental protocol to test the effect of A366, a small molecule inhibitor of G9A/GLP, on H3K9me2 levels in mVSMCs *in vivo*.

Figure 4.5: A366, a small molecule inhibitor of G9A/GLP, reduces H3K9me2 in VSMCs *in vivo*.

Figure 4.6: Schematic of pharmacological model to test whether H3K9me2-mediated regulation of VSMC gene expression is functional *in vivo*.

Figure 4.7: Global reduction of H3K9me2, by pharmacological inhibition of G9A/GLP (A366), significantly potentiates injury-mediated *Mmp3*, *Mmp12* and *Il6* gene induction in VSMCs *in vivo*.

Figure 4.8: Levels of bone marrow-derived endothelial and adventitial cell marker gene expression is independent of sample treatment.

Figure 5.1: The repressive H3K9me2 mark is absent while the active H3K4me3 mark is retained at contractile VSMC gene promoters in cultured human VSMCs, despite their transcriptional silencing.

Figure 5.2: Loss of H3K9me2 correlates with the downregulation of contractile genes in human VSMCs.

Figure 5.3: A subset of IL-1 α -responsive gene promoters, including *MMP3*, *MMP9* and *IL6*, are highly enriched for H3K9me2 in cultured hVSMCs.

Figure 5.4: H3K9me2 regulates IL-1 α -responsive genes in cultured hVSMCs.

Figure 5.5: SiRNA knock down of G9A reduced global H3K9me2 levels, attenuated contractile VSMC gene expression and potentiated IL-1 α -induced *MMP3* and *IL6* expression in cultured hVSMCs.

Figure 6.1: Loss of H3K9me2, by pharmacological inhibition of G9A/GLP (UNC), influences a feature common to both IL-1 α and TNF α signalling pathways in cultured hVSMCs.

Figure 6.2: Pharmacological inhibition of G9A/GLP does not influence levels of I κ B α upon IL-1 α stimulation or alter IL-1 α -induced upregulation of p65.

Figure 6.3: Pharmacological inhibition of G9A/GLP does not influence IL-1 α -mediated nuclear translocation of p65.

Figure 6.4: Pharmacological inhibition of G9A/GLP does not influence TNF α -mediated nuclear translocation of p65.

Figure 6.5: Pharmacological inhibition of G9A/GLP potentiates IL-1 α -induced p65 binding to the *IL6* promoter, correlating with reduced H3K9me2 levels in cultured hVSMCs.

Figure 6.6: Pharmacological inhibition of G9A/GLP does not influence IL-1 α -induced phosphorylation of JNK, ERK1/2 or p38 but potentiates IL-1 α -induced cJUN phosphorylation at Ser63.

Figure 6.7: IL-1 α -induced *MMP3* expression, but not *IL6* or *CCL2* expression, is dependent on JNK-mediated cJUN phosphorylation at Ser63.

Figure 6.8: Pharmacological inhibition of G9A/GLP potentiates IL-1 α -induced cJUN binding to the *IL6* promoter, correlating with reduced H3K9me2 levels in cultured hVSMCs.

Figure 7.1: Proposed mechanism underlying G9A/GLP-mediated attenuation of inflammation-responsive VSMC gene expression.

List of tables

Table 1: Human donor information

Table 2: Primary antibodies used for western blot

Table 3: Secondary antibodies used for western blot

Table 4: Mouse RT-qPCR primer sequences

Table 5: Human RT-qPCR primer sequences

Table 6: Mouse CHIP-qPCR Primers

Table 7: Human CHIP-qPCR primer sequences

Table 8: Antibodies used for CHIP of histone modifications

Table 9: Antibodies used for CHIP for NFkB-p65 and AP1-cJUN

Abbreviations

ApoE	Apolipoprotein E
AP-1	Activator protein-1
BAC	Bacterial artificial chromosome
BSA	Bovine serum albumin
CArG	CC(AT) ₆ GG
CCA	Common carotid artery
CDM	Chemically defined medium
CFP	Cyan fluorescent protein
ChIP	Chromatin immunoprecipitation
CVD	Cardiovascular disease
DAPI	4', 6 diamidino-2-phenylindole
DMEM	Dulbecco's Modified Eagles Medium
DQ	Dye-quenched
EC	Endothelial Cell
ECM	Extracellular matrix
EMT	Epithelial to mesenchymal transition
ERK1/2	Extracellular signal-regulated kinase 1/2
EtOH	Ethanol
EYFP	Enhanced yellow fluorescent protein
FACS	Fluorescence-activated cell sorting
GFP	Green fluorescent protein
HDL	High density lipoprotein
HDM	Histone demethylase
HFD	High fat diet
HMT	Histone methyltransferase
hVSMC	Human vascular smooth muscle cell
H3K4me2	Histone H3 lysine 4 dimethylation
H3K4me3	Histone H3 lysine 4 trimethylation
H3K27me2	Histone H3 lysine 27 trimethylation
H3K9me2	Histone H3 lysine 9 dimethylation
H4ac	Histone H4 acetylation
IL-1α	Interleukin 1 alpha
IL6	Interleukin 6
JNK	c-Jun N-terminal kinase
KLF4	Kruppel-like factor 4
LDL	Low density lipoprotein
LCCA	Left common carotid artery
MAPK	Mitogen-activated protein kinase
MMP	Matrix metalloproteinase
MSC	Mesenchymal stem cell
mVSMC	Mouse vascular smooth muscle cell

NFkB	Nuclear factor kappa beta-light-chain-enhancer of activated B cells
p38	p38 mitogen-activated protein kinase
p65	NFkB transcription factor p65
p-	Phosphorylated-
PBS	Phosphate buffered saline
PDGF	Platelet derived growth factor
Pol II	RNase polymerase II
RCCA	Right common carotid artery
RFP	Red fluorescent protein
RT	Room temperature
RT-qPCR	Real time-quantitative polymerase chain reaction
SD	Safe diet
Ser	Serine
Scr siRNA	Scrambled siRNA
SiRNA	Small interfering RNA
SMC	Smooth muscle cell
SRF	Serum response factor
ssUVR	solar-stimulated ultraviolet radiation
TGFβ	Transforming growth factor beta
Thr	Threonine
TNFα	Tumour necrosis factor alpha
TSS	Transcriptional start site
Tyr	Tyrosine
VSMC	Vascular smooth muscle cell
WHO	World health organisation
YFP	Yellow fluorescent protein

CHAPTER 1 - INTRODUCTION

1.1 Cardiovascular function and disease

Cardiovascular disease (CVD) is a major financial and health concern worldwide. Across Europe, approximately 47% of all deaths are attributed to CVD, costing the EU economy almost €196 billion a year (ESC, 2012). Moreover, the CVD burden is predicted to rise due to an aging population with increasing rates of obesity and diabetes (WHO, 2015). Therefore, it is important to understand the mechanisms underlying CVD to both prevent and improve therapies against such diseases.

CVDs are predominately the clinical manifestation of atherosclerosis, a chronic and progressive disease of large and medium sized blood vessels. Atherosclerosis is characterised by vascular inflammation, fibrosis, necrosis and calcification, which leads to the formation of plaques. Subsequent narrowing of the blood vessels and plaque rupture can trigger a range of complications affecting multiple organ systems. Atherosclerosis is a multi-factorial disease and normally develops many years before clinical symptoms manifest. Proposed risk factors include high cholesterol, hypertension, smoking and diabetes (Libby 2013).

1.1.1 Vascular structure and function

Most blood vessels consist of three layers: an intima, media and adventitia (Figure 1.1). Each layer is distinct in its composition and functionality but all participate in vascular growth, homeostasis, repair and disease (Stenmark et al., 2013). The inner most layer, the intima, is a single endothelial cell layer, mediating the passage of material into and out of the bloodstream. Endothelial cells respond to environmental stimuli and can signal surrounding tissue to react and remodel (Pugsley and Tabrizchi, 2000; Ross and Pawlina, 2011).

The muscular middle layer, the media, predominantly contains vascular smooth muscle cells (VSMCs) and extra cellular matrix (ECM). In the healthy blood vessel, VSMCs align in concentric layers, separated by elastic fibers, to form a highly ordered structure. VSMCs are heterogeneous but primarily function to regulate blood flow and pressure through contraction (Pugsley and Tabrizchi, 2000; Ross and Pawlina, 2011). Unlike their cardiac and skeletal smooth muscle relatives, VSMCs can reversibly alter their quiescent "contractile" phenotype to a more active "synthetic" state in response to changing environmental cues. Such phenotypic switching is essential for vascular growth, homeostasis and repair but can become dysregulated in disease (Alexander and Owens, 2012).

The adventitia forms the protective outermost connective tissue layer of the blood vessel. The adventitia is mainly composed of fibroblasts and ECM but also contains a variety of other cell types, including dendritic cells, macrophages and vascular progenitor cells. Within large arteries, the

adventitia contains smaller vessels, important for the trafficking of material such as leukocytes, into and out of the vessel wall. Recent studies have shown that adventitial cells mediate communication between vascular endothelial cells and VSMCs with their surrounding tissues (Ross and Pawlina, 2011; Stenmark et al., 2013).

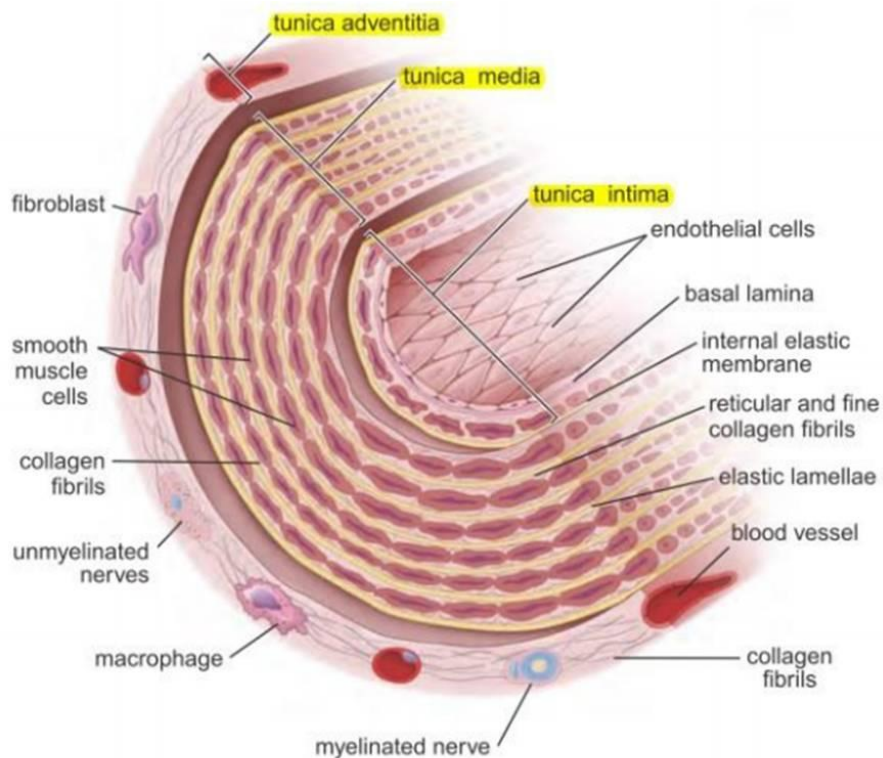


Figure 1.1: Vascular wall structure. The three structural layers of an elastic blood vessel wall (intima, media and adventitia), including cellular and extra cellular components (adapted from Ross and Pawlina, 2011).

1.1.2 Atherogenesis

Atherogenesis is complex but can typically be classified into four main stages (Figure 1.2): 1) Firstly, endothelial cell damage and dysfunction stimulates the accumulation and oxidation of low-density lipoprotein (LDL) within the vessel wall. Oxidised LDL attracts monocytes from the blood into the subendothelial intima where they transform into macrophages which ingest lipoproteins to become foam cells. 2) The subsequent production of inflammatory mediators and cytokines stimulates VSMCs to migrate from the media to the intima where they proliferate and secrete ECM proteins. 3) In progressing plaques, macrophages and VSMCs die, releasing lipids which accumulate within the centre of the plaque to form the necrotic core. VSMCs are thought to migrate and proliferate to create the fibrous cap and encage the necrotic core to stabilise the plaque. 4) In advanced plaques,

the fibrous cap can rupture and trigger thrombus, which can lead to a number of complications including heart attack and stroke (Libby et al., 2011).

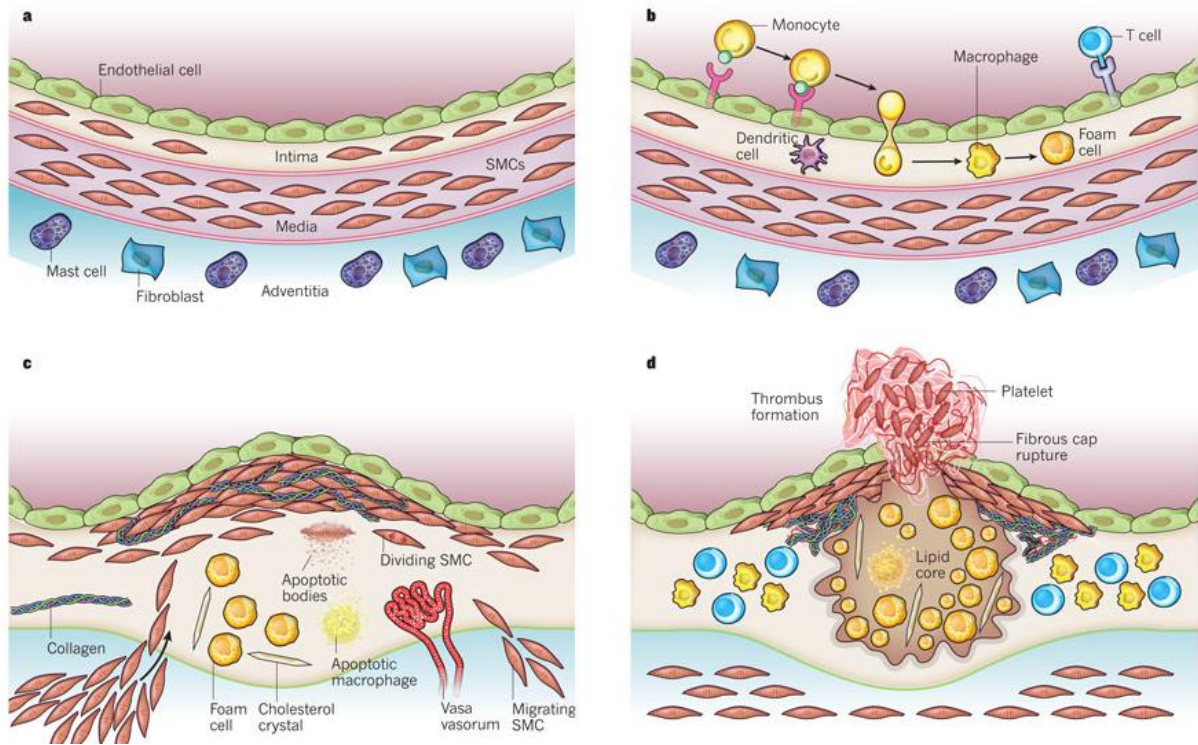


Figure 1.2: Atherogenesis. A) The healthy vasculature. B) Initiation of atherogenesis. Blood leukocytes adhere to endothelial cells and infiltrate the intima. In the intima, monocytes mature to macrophages and uptake lipid to form foam cells. C) VSMCs migrate into the intima and proliferate. A proportion of VSMCs uptake lipid to form foam cells. Extracellular lipid released from dead and dying VSMCs and macrophages accumulate at the centre of the plaque to form the necrotic core. VSMCs on the luminal side of the vessel wall secrete strength giving ECM components, forming the fibrous cap which helps to stabilise the plaque. D) Plaque rupture and subsequent thrombosis can block blood flow and lead to numerous complications including heart attack and stroke (from Libby et al., 2011).

1.2 VSMC function and phenotype

In the healthy blood vessel, VSMCs primarily function to regulate blood flow and pressure. These VSMCs exhibit a low rate of proliferation, low synthetic activity and express a unique set of contractile proteins, essential for the contraction and relaxation of the vascular wall. These proteins either act as structural components of the contractile apparatus or as regulators of contraction and include: transgelin (TAGLN), smooth muscle α actin (ACTA2), calponin (CNN1), smoothelin (SMTN) and smooth muscle myosin heavy chain (MYH11) (Rensen et al., 2007). These contractile VSMCs are also marked by myocardin (MYOCD) expression, a myogenic transcriptional co-activator specifically

expressed in cardiac and contractile smooth muscle (Rensen et al., 2007). However, despite being a highly differentiated and specialised cell type, VSMCs retain remarkable plasticity and can alter their quiescent "contractile" phenotype to a more active "synthetic" state (Alexander and Owens, 2012). Synthetic VSMCs can re-acquire many characteristics of the contractile phenotype, suggesting the phenotypic switch is reversible (Aikawa et al., 1997; Christen et al., 2001; Manderson et al., 1989; Sottirai et al., 1989; Thyberg et al., 1995; Thyberg et al., 1997). Such phenotypic switching is required to maintain vascular homeostasis and regulate vascular response to injury and inflammation. "Synthetic" VSMCs are characterised by the loss of contractile marker expression and the upregulation of selective gene sets, including pro-inflammatory cytokines and matrix metalloproteinases (MMPs), leading to increased cell migration, proliferation and secretion of pro-inflammatory cytokines (Alexander and Owens, 2012; Clarke et al., 2010; Owens et al., 2004).

1.2.1 VSMC phenotypic switching in vascular disease

VSMC phenotypic switching can become dysregulated in vascular disease. Injury, inflammation, endothelial cell dysfunction and the accumulation of lipids within the vessel wall are known to induce VSMCs to phenotypically switch (Alexander and Owens, 2012). Initially, VSMC-derived cells were difficult to identify due to the down regulation of contractile VSMC genes. Furthermore, although the expression of contractile genes marks contractile VSMCs, many of these genes are also expressed by other cell types (Gomez and Owens, 2012). However, recent genetic fate mapping studies using transgenic mice with tamoxifen regulated smooth muscle specific cre recombinase and fluorescent cre-dependent reporter genes, have definitively shown the neointimal cells that arise following vascular injury are largely derived from medial "contractile" VSMCs (Herring et al., 2014; Nemenoff et al., 2011). Moreover, immunofluorescent quantification has revealed that these fluorescent VSMC/VSMC-derived cells comprise approximately 80% of the cellular component of the neointima formed following carotid artery ligation (Herring et al., 2014). Such genetic fate mapping studies have shown that VSMCs can modulate their gene expression profile to resemble various cell types. For example, VSMC-derived cells have been reported to express macrophage (*Lgals3*), mesenchymal stem cell (*Sca1*) and myofibroblast (*Acta2* and *Pdgfrb*) markers (Shankman et al., 2015). A number of studies also suggest VSMCs can acquire an osteo-chondrocytic transcriptional repertoire (*Alp*, *Bglap*, *Opn*, *Runx2* and *Bmp2*) (Briot et al., 2014; Rong et al., 2014; Speer et al., 2009; Steitz et al., 2001). Combined, these findings suggest VSMCs can switch to a number of distinct phenotypes (Figure 1.3).

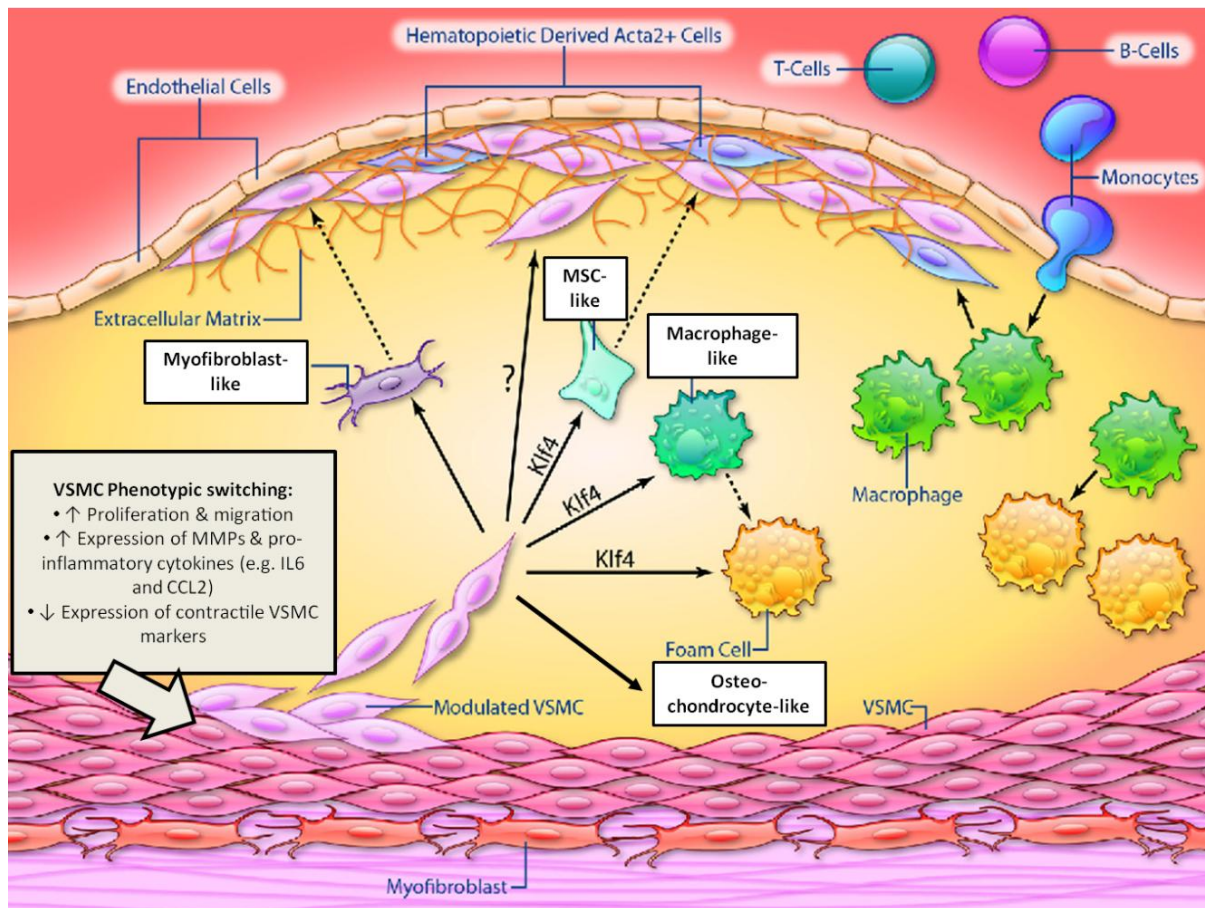


Figure 1.3: Schematic of VSMC phenotypic switching in atherosclerosis. VSMCs undergo phenotypic switching to multiple distinct phenotypes within advanced atherosclerotic lesions. VSMCs within the core of the plaque can acquire myofibroblast, mesenchymal stem cell (MSC), macrophage and osteo-chondrocyte markers, while VSMCs forming the cap resemble the contractile VSMC state (adapted from Bennett et al., 2016).

Another widely held view is that contractile and synthetic VSMCs represent two ends of a diverse phenotypic spectrum, with VSMCs also existing in a range of intermediate phenotypes (Figure 1.4) (Rensen et al., 2007).

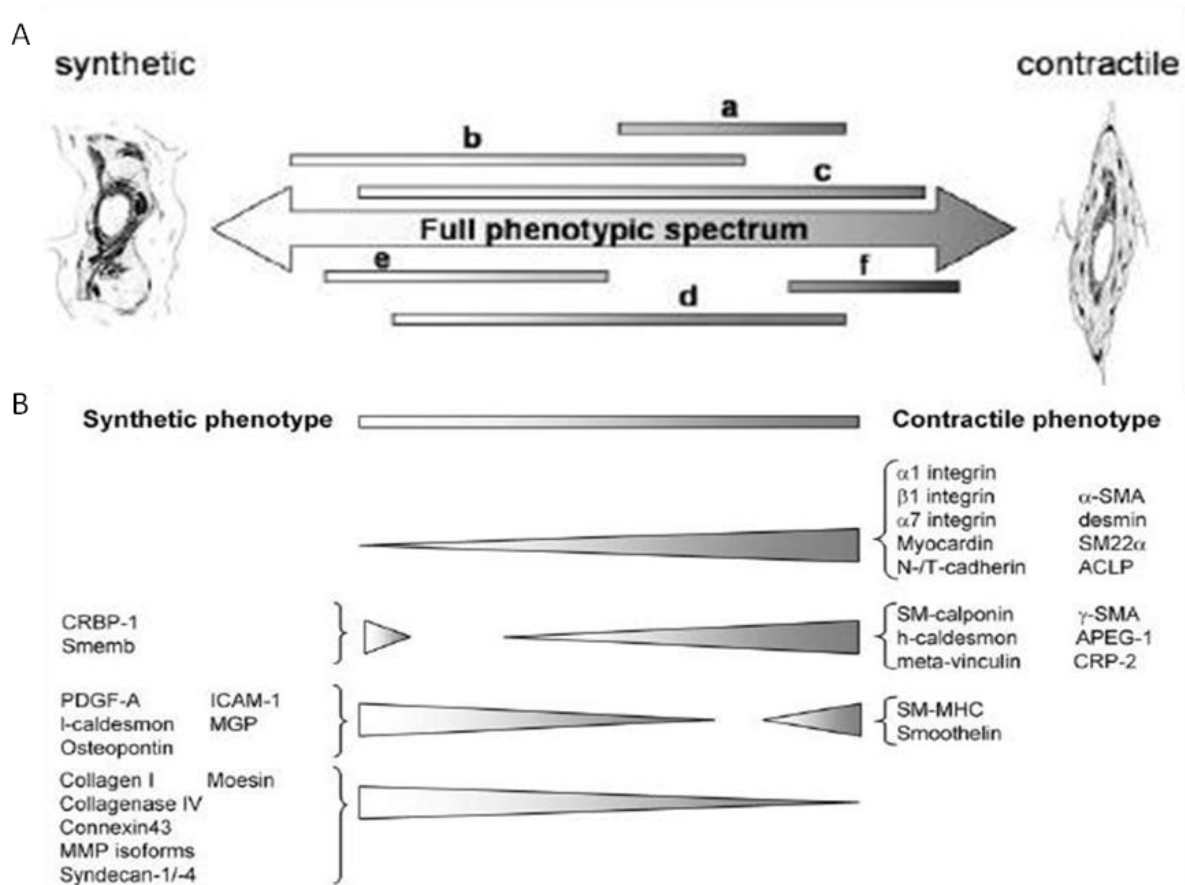


Figure 1.4: Hypothetical VSMC phenotypic spectrum. (A) Distinct VSMC populations (represented a to f) have different potentials to phenotypically switch (from Rensen et al., 2007). (B) Schematic representation of expression levels of genes associated with a particular SMC phenotype (from Rensen et al, 2007).

1.2.2 Cytokines in vascular function and disease

The vascular inflammatory response requires complex interaction between resident vascular cells and inflammatory cells which is governed, in part, by cytokines. Cytokines describe a diverse group of small soluble proteins (~5-30 kDa) involved in cell-to-cell communication and can act to both promote and/or inhibit inflammation and atherogenesis (Figure 1.5). Cytokines are clustered into several categories such as interleukins (e.g. IL-1 α), tumor necrosis factors (e.g. TNF α), growth factors (e.g. PDGF and TGF β), lymphokines (e.g. LPS) and interferons. Bone marrow derived, adventitial, endothelial and VSMCs are all known to produce and respond to cytokines via cell surface receptors which stimulate NF κ B, AP-1, JAK-STAT and Smad signalling pathways. Activation of such signalling pathways influence VSMC adhesion, migration, growth, proliferation, apoptosis and the composition of the ECM (Schober, 2008; Sprague and Khalil, 2009).

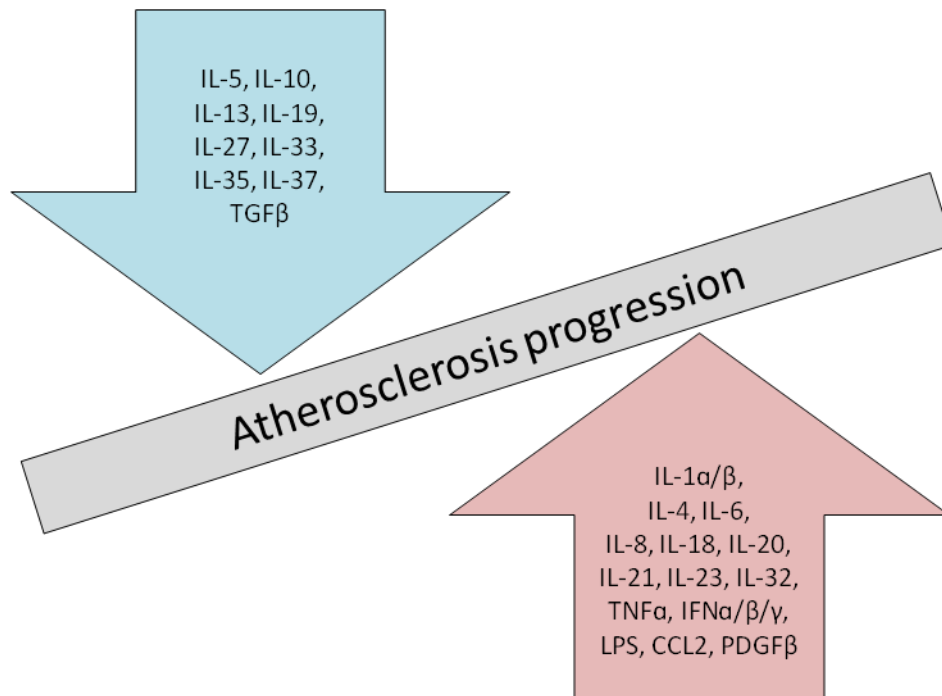


Figure 1.5: Pro- and anti-atherogenic cytokines. Cytokines can be classified broadly into two groups depending on whether they promote or suppress atherogenesis (adapted from Tousoulis et al., 2016).

Several cytokines affect VSMC phenotype and are associated with vascular dysfunction. For example, activation of the platelet-derived growth factor (PDGF) signalling pathway is known to promote the synthetic VSMC phenotype (Chen et al., 2015a; Chen et al., 2015b; Nurminkaya et al., 2014) whereas transforming growth factor beta (TGFβ) signalling promotes the contractile state (Hao et al., 2002; Hautmann et al., 1997; Liu et al., 2003). The pro-inflammatory cytokines interleukin 1 alpha (IL-1α) and tumor necrosis factor alpha (TNFα) also induce VSMCs to switch to a more synthetic phenotype. Both cytokines stimulate the VSMC inflammatory response and activate NFκB and AP-1-dependent transcription of cytokines (e.g. *Il6* and *Ccl2*) and matrix metalloproteinases (MMPs) (Lim and Park, 2014). Interleukin 6 (IL6) has been observed to upregulate VSMC migration, proliferation and vascular calcification whilst attenuating VSMC contraction (Kurozumi et al., 2016; Lee et al., 2016; Watanabe et al., 2004). Also, IL6 treatment of VSMCs activates the JAK-STAT pathway which induces the expression of monocyte chemoattractant protein-1 (*Ccl2*) (Watanabe et al., 2004). CCL2 plays a major role in the recruitment of monocytes and T cells to the vessel wall and has been shown to stimulate VSMC migration and proliferation (Schober, 2008; Selzman et al., 2002). Together, these findings suggest IL6 and CCL2 promote the progression of vascular disease.

However, the role of many cytokines in vascular disease is often not clear cut. For example, IL6 can also act in an anti-inflammatory manner by inhibiting TNFα production while inducing the expression of anti-inflammatory cytokines (e.g. IL1 receptor antagonist and the soluble p55 TNFα receptor) in

leukocytes (Scheller et al., 2011). TNF α also has conflicting roles in the development of vascular disease. Initially, it was widely accepted that, in cultured VSMCs, TNF α activates the NF κ B signalling pathway and decreases the expression of myocardin and myocardin-dependent genes by NF κ B (p65) binding to the *Myocd* promoter (Singh and Zheng, 2014; Tang et al., 2008b; Yoshida et al., 2013). Conversely, Singh and colleagues have shown that TNF α treatment in *Myocd* over expressing cultured VSMCs significantly potentiates myocardin and myocardin-dependent contractile gene expression by stabilising myocardin mRNA via the NF κ B and MAPK pathway (Singh and Zheng, 2014). This finding suggests TNF α differentially regulates myocardin depending on the VSMC phenotypic state.

1.2.3 Matrix metalloproteinases in vascular function and disease

MMPs comprise a family of proteases and play a central role in many CVDs which are associated with structural changes in blood vessels (Galis and Khatri, 2002; Johnson, 2014). Some MMPs are induced by inflammatory signals, such as interleukin 1 (IL-1 α), to regulate vascular remodelling (Nagase et al., 2006). VSMCs only constitutively express MMP2 (Newby, 2005) but exhibit enhanced expression of several MMPs within diseased blood vessels (Choudhary et al., 2006). VSMCs from human atherosclerotic plaque shoulder regions and areas of foam cell accumulation display increased MMP3, MMP9 and MMP12 activity compared to their medial counterparts. However, even though MMP2 activity is enhanced in atherosclerotic plaques, there is no difference in MMP2 activity between these regions. The increase in MMP3, MMP9 and MMP12 activity corresponds to regions containing higher levels of IL-1 α released from necrotic VSMCs and macrophages (Galis et al., 1994b). This IL-1 α -induced expression of MMP genes can be observed *in vitro*. IL-1 α treatment of cultured VSMCs induces the transcription of *MMP3*, *MMP9* and *MMP12* while *MMP2* is unaffected (Galis et al., 1994a).

MMPs can promote angiogenesis, the accumulation of macrophage cells and degrade major components of the ECM. MMPs are known to influence the migration and proliferation of VSMCs, infiltration of inflammatory cells into tissue and the stability of atherosclerotic plaques (Figure 1.6) (Galis and Khatri, 2002; Johnson, 2014; Nagase et al., 2006). Studies using MMP knockout mice have shown that MMP2 and MMP9 contribute to the development of atherosclerosis in apolipoprotein E (ApoE) deficient mice (Cho and Reidy, 2002; Galis and Khatri, 2002; Kuzuya et al., 2003; Kuzuya et al., 2006; Luttun et al., 2004). Furthermore, it has been observed that MMP3 is required to activate MMP9 for neointima formation after carotid ligation in mice and for VSMC migration *in vitro*, whereas MMP12 plays a redundant role (Johnson et al., 2011b). Some MMPs are thought to stabilise atherosclerotic plaques by increasing VSMC migration and proliferation to thicken the fibrous cap.

For instance, ApoE and MMP2/ MMP9 double knockout mice exhibit less stable lesions with fewer VSMCs than macrophages compared to ApoE single knockout controls (Johnson et al., 2005a; Kuzuya et al., 2006). In contrast, other MMPs appear to promote plaque rupture by destruction of the ECM, which induces thinning of the fibrous cap. For example, a selective MMP12 inhibitor has been shown to slow atherosclerotic plaque rupture in ApoE knockout mice (Johnson et al., 2011a). As MMPs can both promote plaque stability and rupture, the development of direct MMP inhibitors to treat vascular disease has been problematic (Galis and Khatri, 2002; Newby, 2012).

MMP/TIMP	Modulation	Site	Effect on plaque size and composition	Reference
Collagenases				
MMP-1	Over-expression	Aorta	Size (↓), VSMCs (↔), Mø (↔)	Lemaître et al, 2001
MMP-8	Knockout	Aorta	Size (↓), VSMCs (↔), Mø (↓)	Laxton et al, 2009
MMP-13	Knockout	Aorta	Size (↔), VSMCs (↔), Mø (↔)	Deguchi et al, 2005
	Inhibitor	Carotid	Size (↔), VSMCs (↔), Mø (↔)	Quillard et al, 2014
Gelatinases				
MMP-2	Knockout	Aorta	Size (↓), VSMCs (↓), Mø (↔)	Kuzuya et al, 2006
MMP-9	Knockout	Aorta/BCA	Size (↓/↑), VSMCs (ND/↓), Mø (↓/↑)	Luttun et al, 2004 Johnson et al, 2005
	Over-expression	Arch/carotid	Size (↔), VSMCs (↔), Mø (↔)	Gough et al, 2006 de Nooijer et al, 2006
Stromelysins				
MMP-3	Knockout	Aorta/BCA	Size (↑/↑), VSMCs (ND/↓), Mø (↔/↑)	Silence et al, 2001 Johnson et al, 2005
MMP-10	Not assessed			
MMP-11	Not assessed			
Others				
MMP-7	Knockout	BCA	Size (↔), VSMCs (↑), Mø (↔)	Johnson et al, 2005
MMP-12	Knockout	Aorta/BCA	Size (↔/↓), VSMCs (↔/↑), Mø (↔/↓)	Luttun et al, 2004 Johnson et al, 2005
	Over-expression	Aorta	Size (↑), VSMCs (↑), Mø (↑)	Yamada et al, 2008 Liang et al, 2006
	Inhibitor	Aorta/BCA	Size (↓), VSMCs (↑), Mø (↓)	Johnson et al, 2011
MT-MMPs				
MMP-14	Knockout	Root	Size (↔), VSMCs (↔), Mø (↔)	Schneider et al, 2008

Figure 1.6: Results of *in vivo* studies evaluating the effects of MMPs on atherosclerotic plaque. Abbreviations: VSMCs, vascular smooth-muscle cells; Mø, macrophages; BCA, brachiocephalic artery; ND, not determined; ↓, decreased; ↑, increased; ↔, no change. In separate studies where different vascular sites have been assessed and discrepancies in effects are observed, red and green text colour are used to define the different sites (from Johnson, 2017).

1.3 Transcriptional regulation of VSMC gene expression

1.3.1 Transcriptional regulation of contractile VSMC genes

Many contractile VSMC genes are regulated by serum response factor (SRF), a transcription factor which binds to CC(A/T-rich)₆GG (CArG) *cis*-elements of all known CArG dependent contractile VSMC genes, including *ACTA2*, *CNN1*, *TAGLN* and *MYH11*. *MYOCD*, a gene only expressed in the vasculature by VSMCs, associates with SRF to activate the expression of CArG dependent contractile VSMC genes (Rensen et al., 2007). It has been suggested that the presence of H4 acetylation and H3K4me2

exclusively at VSMC CArG boxes may permit binding of MYOCD/SRF complexes to specifically activate VSMC-marker genes rather than other SRF-dependent genes, such as cFOS (Liu et al., 2015b; McDonald et al., 2006). Interestingly, Myocd +/- mice on ApoE -/- background exhibit accelerated atherosclerosis with increased numbers of VSMC-derived macrophage like cells compared with Myocd +/- littermate controls (Ackers-Johnson et al., 2015).

The pluripotency factor KLF4 is also widely reported to influence VSMC phenotype. KLF4 both down regulates MYOCD expression and interacts with SRF to repress MYOCD-induced activation of contractile VSMC genes (He et al., 2015; Liu et al., 2005; Liu et al., 2003). In addition, KLF4 has been shown to repress contractile VSMC gene expression in VSMCs by binding to the TGF β control element within their promoters, blocking the recruitment of activating complexes (Guo and Chen, 2012; Liu et al., 2003). Furthermore, VSMC specific conditional knockout of Klf4 results in reduced numbers of VSMC-derived macrophage and mesenchymal stem cell like cells in mice (Shankman et al., 2015). Many studies have also shown that the nuclear factor kappa-light-chain-enhancer of activated B cells (NF κ B) family of transcription factors play a role in regulating the expression of contractile VSMC genes. Activation of the NF κ B signalling pathway in VSMCs eventuates in NF κ B (p65 subunit) binding to the MYOCD promoter, decreasing the expression of MYOCD and MYOCD-dependent contractile genes (e.g. ACTA2, TAGLN and MYH11) (Singh and Zheng, 2014; Tang et al., 2008b; Yoshida et al., 2013).

1.3.2 Transcriptional regulation of injury/inflammation-induced VSMC genes

From *in vitro* and *in vivo* studies, it has long been recognised that both the NF κ B and activator protein-1 (AP-1) family of transcription factors regulate numerous processes in the cardiovascular system, including inflammation, apoptosis, differentiation, proliferation and cell migration (Chistiakov et al., 2018; Muslin, 2008; van der Heiden et al., 2010). Therefore, it is not surprising that dysregulation of NF κ B and AP-1 signalling is strongly associated with the initiation and progression of vascular dysfunction. Figure 1.7 summarises the stimuli that activate NF κ B and AP-1 signalling pathways and the genes under NF κ B and AP-1 transcriptional control.

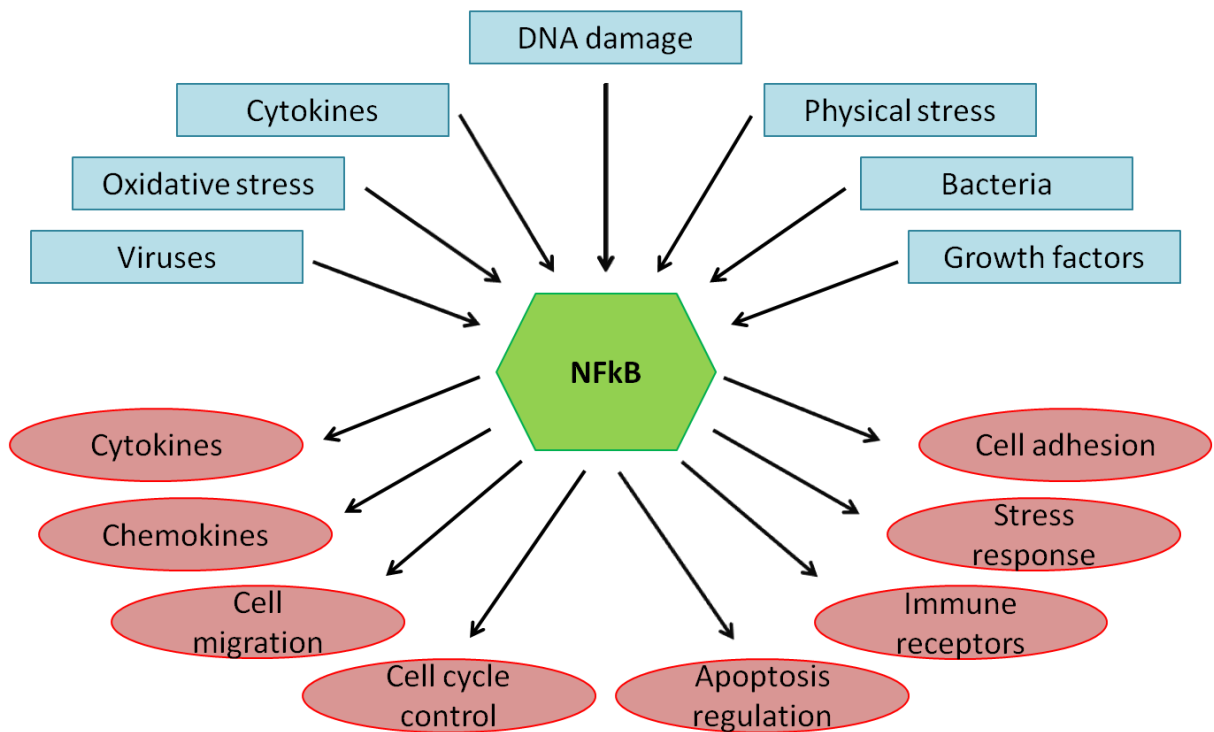


Figure 1.7: Stimuli that activate the NFκB and AP-1 signalling pathways (blue squares) and genes under NFκB and AP-1 transcriptional control (red circles).

1.3.3 The NFκB signalling pathway

The NFκB family of transcription factors is composed of five structurally related proteins: p50, p52, p65 (RelA), RelB and cRel. These proteins share a N-terminal Rel homology domain (RHD), which mediates DNA binding, dimerisation and nuclear translocation. The RHD allows NFκB family members to form homo- and hetero-dimers, which constitute their biologically active form. RelB, cRel and p65 contain C-terminal transcriptional activation domains (TADs), which enable them to participate in a number of protein-protein interactions with various regulatory proteins including other co-activating transcription factors (e.g. AP-1 family members) and chromatin modifying complexes (e.g. HDMs and HATs). In contrast, p50 and p52 do not contain TADs and are therefore involved in transcriptional repression unless they dimerise with a protein containing a TAD, such as p65 (Liu et al., 2017; Zhang et al., 2017).

In unstimulated cells, NFκB is sequestered in the cytoplasm by the IκB kinase (IKK) complex. The IKK complex consists of catalytic kinase subunits (IKKα and IKKβ) and the regulatory non-enzymatic scaffold protein NEMO (NFκB essential modulator otherwise known as IKKγ). In response to a variety of stimuli (Figure 1.7) NFκB dimers are activated by IKK-mediated phosphorylation of IκB. Phosphorylation of IκB triggers the rapid ubiquitination of IκBα and its subsequent degradation

releasing NFκB from its inactive cytoplasmic state. NFκB subunits are then able to migrate to the nucleus and promote the expression of target genes (Figure 1.8). To add further complexity, recent studies have shown that NFκB proteins, especially the p65 subunit, are subject to a wide variety of post translational modifications including phosphorylation, acetylation and ubiquitination. These modifications determine the activation status of NFκB transcription factors and can either enhance or repress their transcriptional activity (Liu et al., 2017; Zhang et al., 2017).

Hundreds of genes contain the NFκB consensus sequence (GGGRNNYYCC) within their regulatory DNA elements. The genes transcriptionally regulated by NFκB include cytokines, chemokines, immunoreceptors, MMPs, growth factors and other transcription factors and are involved in numerous cellular processes (Figure 1.7). As NFκB signalling plays a pathogenic role in various inflammatory diseases, several inhibitors have been developed to block different steps of the NFκB signalling pathway. Pharmacological compounds can inhibit IκBα degradation (e.g. BAY11-7082 (Ghashghaie et al., 2011)), block the nuclear translocation of NFκB subunits and prevent NFκB binding with target DNA (Liu et al., 2017; Zhang et al., 2017).

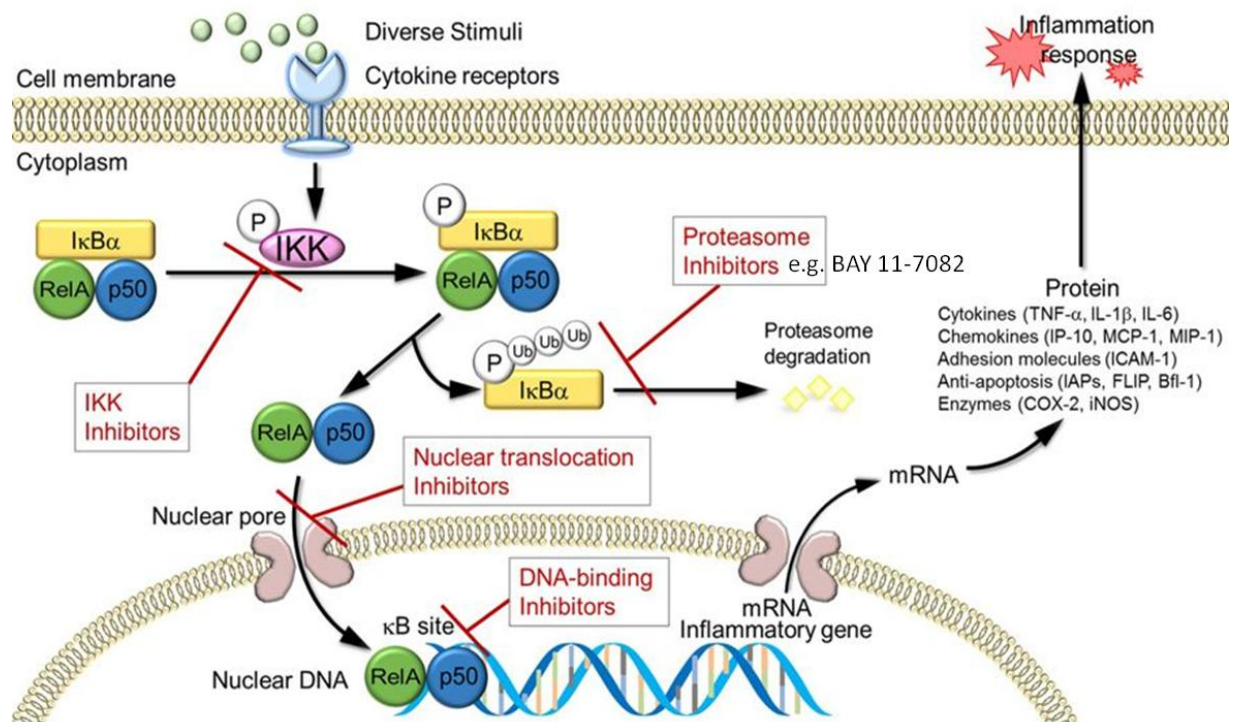


Figure 1.8: The canonical NFκB signalling pathway. Ligand binding to a receptor activates the IKK complex which phosphorylates IκBα and triggers its proteosomal degradation. NFκB is then released and translocates to the nucleus to activate target gene expression. Multiple pharmacological compounds can block different steps of the NFκB signalling pathway (adapted from Liu et al., 2017).

1.3.4 The AP-1 signalling pathway

Like NF κ B, the mitogen-activated protein kinase (MAPK)/AP-1 signalling pathway orchestrates gene expression in response to a variety of stimuli and therefore plays an important role in various cellular processes (Figure 1.7). MAP Kinases make up a family of serine/threonine kinases which function in tiered protein kinase cascades. Extracellular stimuli activate MAPKK kinases (MAPKKKs) via receptor-dependent and -independent mechanisms. MAPKKKs then phosphorylate and activate a downstream MAPK kinase (MAPKK), which in turn phosphorylates threonine and tyrosine residues on MAPKs leading to their activation. There are three main subfamilies of MAPKs: c-Jun N-terminal kinases (JNK1, JNK2 and JNK3), extracellular signal regulated kinases (ERK1 and ERK2) and p38 (p38 α , p38 β , p38 δ and p38 γ) (Figure 1.8) (Kim and Choi, 2015; Sun et al., 2015; Yang et al., 2013).

MAPKs regulate AP-1 transcription factors at the transcriptional and post transcriptional level (Figure 1.9) (Kim and Choi, 2015; Sun et al., 2015; Yang et al., 2013). AP-1 transcription factors describe a group of proteins that belong to the Jun (cJUN, JUNB, and JUND) and Fos (cFOS, FOSB, FRA1, and FRA2) subfamilies. These proteins share an evolutionary conserved basic leucine zipper domain (LZD), essential for AP-1 dimerisation. AP-1 dimerisation is required to bring two DNA binding domains (DBDs) into juxtaposition, thereby facilitating the interaction of protein dimers with the AP-1 DNA consensus sequence (5'--TGAG/CTCA-3'), which is present at many regulatory DNA elements. In contrast to Jun proteins, Fos proteins cannot homodimerize among themselves due to a small difference in the composition of their LZD. However, Fos proteins can partner with Jun proteins to form Jun-Fos heterodimers, which are more stable and have a higher DNA binding activity compared to Jun-Jun homodimers. Apart from FRA1 and FRA2, AP-1 proteins also possess a transactivation domain (TAD), which contains binding sites for other proteins such as transcriptional co-regulators and chromatin modifying enzymes (Cargnello and Roux, 2011; Ye et al., 2014). cJUN, cFOS and FOSB are considered strong activators, while JUNB, JUND, FRA1 and FRA2 are relatively weaker and may sometimes act as repressors by displacing stronger dimers (Hess et al., 2004). More recently, other groups of structurally related transcription factors, including Atf (ATF α , ATF2, and ATF3) and Jdp (JDP1 and JDP2) proteins, have been shown to form heterodimers with AP-1 and bind to the AP-1 consensus motif (Cargnello and Roux, 2011; Ye et al., 2014).

After MAPKs are activated, they regulate downstream transcription factors which induce the transcription of AP-1 family genes. Activation of *FOS* and *JUN* transcription occurs via MAPK-dependent phosphorylation of transcription factors such as TCF, MEF2C, ATF2 and cJUN. At the post translational level, via phosphorylation and dephosphorylation, the MAPK pathway modifies AP-1

subunit stability, transactivation activity and binding to target DNA (Zhang et al., 2017). For example, cJUN phosphorylation at serine 63 and 73 is known to increase its transcriptional output (Smeal et al., 1992).

Historically, MAPKs were not considered to regulate transcriptional outcomes at the chromatin level. However, recent studies have shown that in some cases MAPKs can bind to DNA directly and indirectly via transcriptional regulators and chromatin bound factors (Klein et al., 2013; Pokholok et al., 2006; Sugauma et al., 2010; Tiwari et al., 2012). Furthermore, regulatory proteins that modulate MAPK function can be co-recruited to chromatin (Klein et al., 2013). Interestingly, constitutive tethering of JNK to AP-1 response elements at the *cJUN* promoter has been observed in HeLa cells (Bruna et al., 2003). Such data suggests JNK can be activated in the nucleus while pre-assembled in transcription complexes.

As MAPK signalling is involved in many cellular processes associated with disease, numerous compounds have been developed to inhibit each MAPK family (English and Cobb, 2002; Uehling and Harris, 2015). For example, SP600125, a small molecule drug, has been reported to specifically inhibit JNK activity without influencing ERK, p38 β or NF κ B signalling *in vitro* (Han et al., 2001).

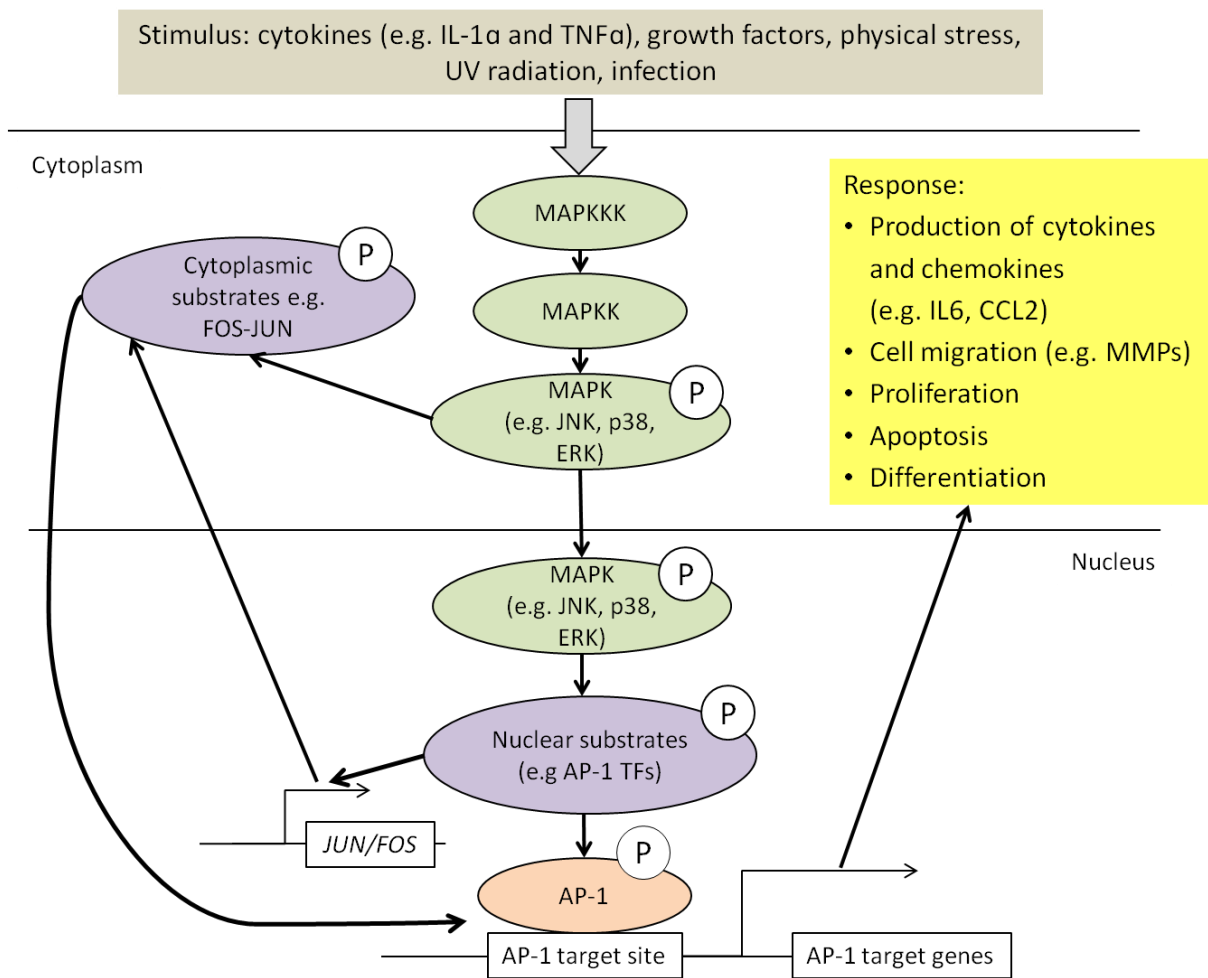


Figure 1.9: The MAPK/AP-1 signalling pathway. A simplified schematic of the MAPK/AP-1 signalling pathway. Ligand binding to a receptor initiates a signalling cascade leading to MAPK phosphorylation. Phosphorylation of MAPK allows it to function as an enzyme to phosphorylate and activate a range of AP-1 family transcription factors, culminating in the expression of AP-1 target genes.

1.4 Epigenetic regulation of gene expression

Eukaryotic cells package DNA into a highly ordered compact structure to actively regulate gene expression and ultimately cell phenotype. In the nucleus, DNA wraps around histone proteins forming nucleosomes. Each nucleosome consists of a 147bp segment of DNA wound around eight core histone proteins (H2A, H2B, H3 and H4). Nucleosomes are connected by linker chromatin, composed of mainly DNA and histone H1 (Figure 1.10). Epigenetic modifications of DNA and histone proteins remodel the chromatin and result in either increased or reduced accessibility to the transcription machinery. Such epigenetic modifications therefore regulate gene expression without changing the underlying DNA sequence (Kouzarides, 2007). The N-terminal tails of histone proteins, which are not bound to the nucleosome core particle and are exposed to the nuclear environment,

are prone to numerous reversible post translational modifications at specific residues (Figure 1.10, 2) (Chi et al., 2010; Kouzarides, 2007; Strahl and Allis, 2000).

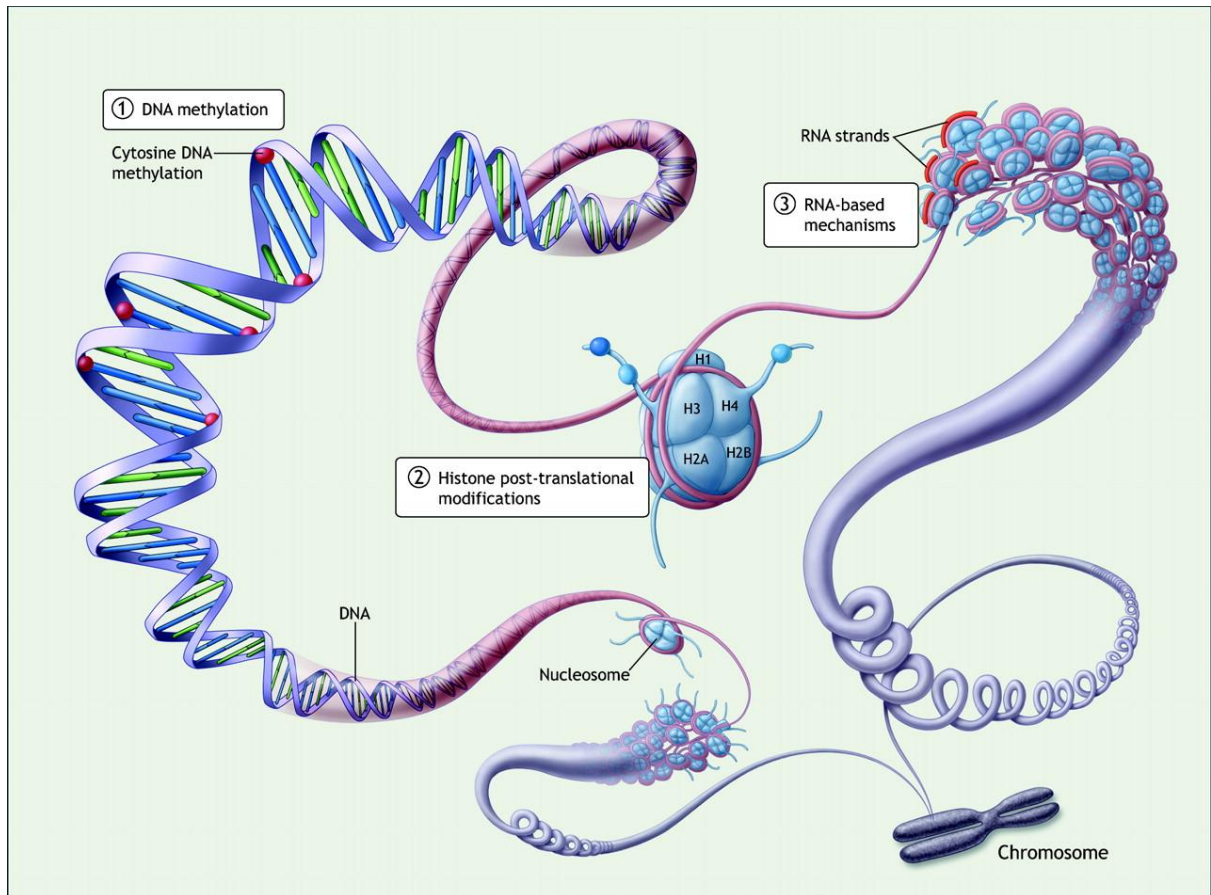


Figure 1.10: Epigenetic regulation of gene expression. DNA methylation, histone modifications and RNA-based mechanisms regulate chromatin structure and gene expression (from Matouk and Marsden, 2008).

1.4.1 Histone modifications mark regulatory DNA elements

Gene transcription is mediated by regulatory DNA regions such as promoters and enhancers. Promoters are located close to the transcriptional start site (TSS) and are required to initiate transcription. Enhancers specify when, in which cell type and at what level each of our genes is expressed by binding to transcriptional activators or repressors. Enhancers can be located almost anywhere in relation to the gene to be influenced and often relay their regulatory information over long distances to a gene's promoter. Historically, promoters and enhancers were thought to be distinct from each other but recent studies have shown significant overlap in their functionality (Kowalczyk et al., 2012; Mikhaylichenko et al., 2018).

Histone post-translational modifications are known to regulate promoter and enhancer activity to control gene expression. Histone modifications are particularly labile and are subject to over 60 different types of modification including methylation, acetylation, phosphorylation, ubiquitylation and sumoylation (Kouzarides, 2007). Certain histone modifications are associated with particular functional DNA elements within mammalian genomes. For instance, active gene promoters often display high levels of histone acetylation, H3K4me2 and H3K4me3 whereas repressed gene promoters are commonly enriched for H3K9me2, H3K9me3 and H3K27me3. Furthermore, increased levels of H3K36me3 and H3K79me2 have been observed at transcribed regions while enhancers are linked to greater H3K4me1, H3K4me2 and H3K27ac (Figure 1.11) (Zhou et al., 2011).

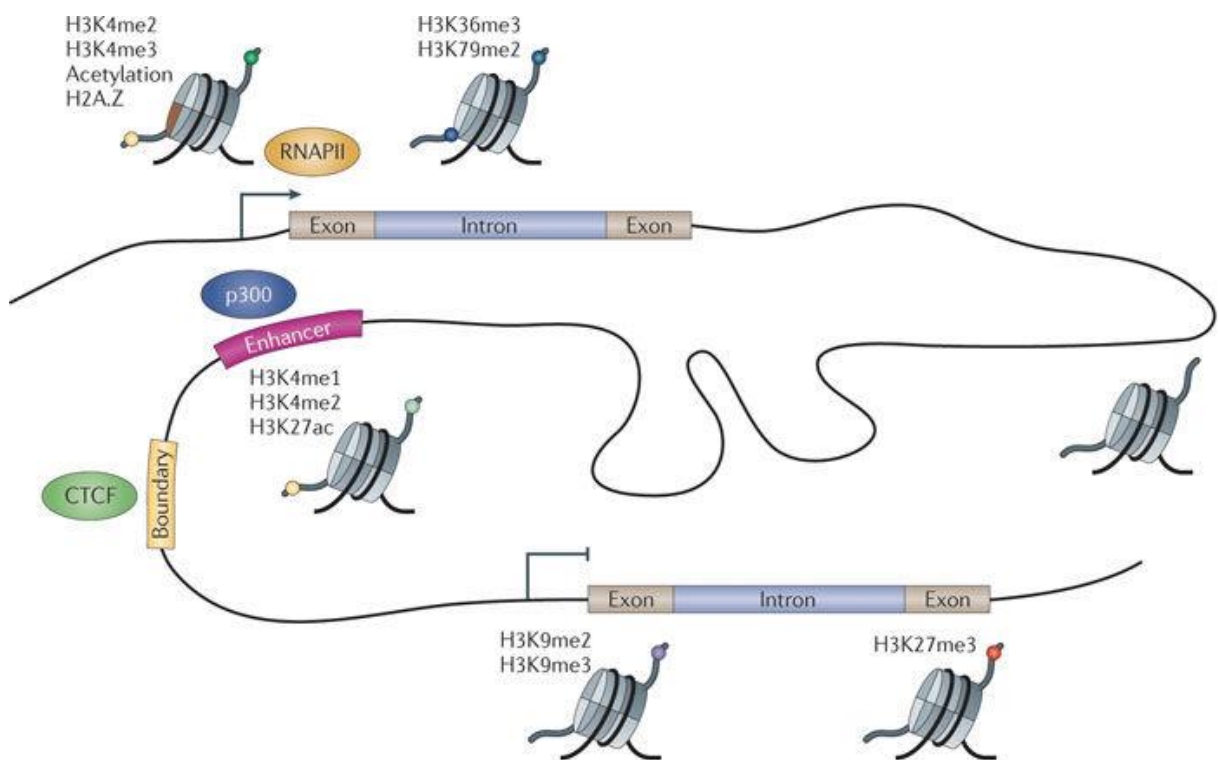


Figure 1.11: Histone modifications mark functional elements in mammalian genomes (from Zhou et al., 2011). Histone modifications can coexist and influence each other and often cannot be generalised with respect to transcriptional outcome. This observation has led to the histone code hypothesis, which proposes that the transcription of genetic information is regulated by different combinations of histone modifications (Chi et al., 2010; Strahl and Allis, 2000). Studies suggest that a combination of active and inactive histone modifications control the expression of lineage-specific genes (Azua et al., 2006). This has been termed gene priming and is associated with rapid changes in gene expression following physiological alterations in the cellular environment (Shah et al., 2014). Such gene priming provides a possible mechanism to explain how VSMCs reversibly switch between a spectrum of phenotypes.

1.4.2 Histone methylation

Histone methylation is associated with both gene repression and activation depending on which residue is modified. Histone residues can be mono-, di- or tri-methylated by a range of specific histone methyltransferases (HMTs) (Chi et al., 2010; Kouzarides, 2007). Histone methylation was thought to be an irreversible mark of both gene activation and silencing for decades. However, the discovery of a number of histone demethylases (HDMs) uncovered the dynamic nature of this mark (Klose and Zhang, 2007).

1.5 H3K9me2

Multiple studies have shown that H3K9me2 is associated with transcriptional repression (Hublitz et al., 2009; Peters et al., 2003; Wen et al., 2009). H3K9me2 levels are higher at silent compared to active genes in a 10kb region surrounding the transcriptional start site (TSS) (Barski et al., 2007). H3K9me2 represses gene expression both passively, by prohibiting acetylation (Wang et al., 2008) and therefore binding of RNA polymerase or its regulatory factors, and actively, by recruiting transcriptional repressors (Nakayama et al., 2001; Shinkai and Tachibana, 2011; Zhang et al., 2016). H3K9me2 has also been found in megabase blocks, termed Large Organised Chromatin K9 domains (LOCKS), which are primarily located within gene-sparse regions but also encompass genic and intergenic intervals (Filion and van Steensel, 2010; McDonald et al., 2011; Wen et al., 2009). In recent years, many studies have reported that H3K9me2 is important for various biological processes including cell lineage commitment, the reprogramming of somatic cells to induced pluripotent stem cells and regulation of the inflammatory response (Chen et al., 2013; Rodriguez-Madoz et al., 2017; Shi et al., 2008).

1.5.1 H3K9me2 regulates cell lineage commitment and reprogramming

H3K9me2 plays a key role in regulating cell lineage commitment and reprogramming. Interestingly, Wen and colleagues found that H3K9me2 LOCKS cover 10-46% of the genome in differentiated cells compared to only 4% in embryonic stem cells (ESCs), can be lineage specific and are substantially lost in cancer cell lines (Wen et al., 2009). These findings prompted speculation over the role of H3K9me2 in establishing and maintaining cell identity. However, Filion and van Steensel reanalyzed the original data sets and disputed these findings, claiming that there are no significant differences in H3K9me2 LOCKS in ESCs compared to differentiated cells and suggest that the algorithm used by Wen et al may have introduced a detection bias (Filion and van Steensel, 2010). Nevertheless, other groups have found evidence to suggest H3K9me2 LOCKS are functionally relevant. For instance, reduction of

H3K9me2 LOCKS was observed in epithelial-to-mesenchymal transition (EMT), a process in which cells acquire a multipotent phenotype (McDonald et al., 2011). Additionally, hematopoietic stem and progenitor cells display lower global levels of H3K9me2 compared to mature bone marrow cells (Li et al., 2018).

Furthermore, studies have shown that inhibition of H3K9me2 improves the reprogramming efficiency of human cells by heterochromatin relaxation and facilitating transcription factor binding (Chen et al., 2013; Rodriguez-Madoz et al., 2017). Interestingly, inhibition of H3K9me2 potentiates the inflammatory activation of fibroblasts in response to IFN (Fang et al., 2012) and inflammation is known to improve the reprogramming efficiency of somatic cells to induced pluripotent stem cells (Lee et al., 2012). Together, these observations point towards a role of H3K9me2 in the maintenance of differentiated cell states.

1.5.2 H3K9me2 regulates the expression of inflammation-induced genes

H3K9me2 often marks genes that are involved in processes that require tight and dynamic regulation, including the inflammatory response. For instance, enriched levels of H3K9me2 at IFN-stimulated genes (ISGs) in fibroblasts, cardiac myocytes and neuroblastoma cells results in a far weaker type 1 IFN response compared to bone marrow-derived macrophages and dendritic cells where H3K9me2 is either absent or present at low levels at ISGs (Fang et al., 2012). Furthermore, elevated levels of G9A-dependent H3K9me2 have been linked to endotoxin and LPS tolerance associated gene repression in various immune cell types (Chen et al., 2009; Liu et al., 2014; Yoshida et al., 2015).

Many studies report that the aberrant expression of a number of MMP and inflammatory genes is associated with H3K9me2-depletion at their promoters. For example, loss of H3K9me2 has been observed at inflammatory and MMP gene promoters, which display increased expression, in monocytes (Miao et al., 2007) and retinal endothelial cells (Zhong and Kowluru, 2013b) derived from diabetic patients compared to controls.

1.6 G9A/GLP are required for H3K9 dimethylation

In mammals, the G9A/GLP enzymatic complex functions to establish and maintain H3K9me₂ (Shankar et al., 2013; Shinkai and Tachibana, 2011). G9A and GLP are expressed ubiquitously and play multiple roles in development, physiology and disease (Shinkai and Tachibana, 2011; Tachibana et al., 2008). Interestingly, G9a and Glp *-/-* mouse embryos display early lethality at E9.5 to E12.5, due to severe growth defects (Tachibana et al., 2002). In addition, dysregulation of G9A and/or GLP has been implicated in many inflammatory (Chang et al., 2011; Chen et al., 2009) and cardiovascular diseases (Thienpont et al., 2017).

1.6.1 G9A/GLP structure and function

G9A and its highly related homologue G9A-like protein (GLP) share an evolutionary SET domain, responsible for their methyltransferase activity (Shinkai and Tachibana, 2011). The SET domains of G9A and GLP share the same substrate specificity and primarily function to establish and maintain H3K9 mono and di-methylation. However, both enzymes have also been reported to catalyze H1, H3K27 and H3K56 methylation (Shankar et al., 2013; Shinkai and Tachibana, 2011; Xiong et al., 2017). When transiently over expressed, G9A and GLP form homo- and heterodimers via their SET domain. However, endogenously both enzymes function exclusively as a heteromeric complex (Tachibana et al., 2005). Although G9A and GLP can exert their methyltransferase activities independently *in vitro*, if either G9a or Glp are knocked out *in vivo*, global levels of H3K9me₂ are severely reduced and are equivalent to H3K9me₂ levels in G9a and Glp double knockout mice (Shinkai and Tachibana, 2011). Therefore, it is thought that G9A cannot compensate for the loss of GLP methyltransferase activity *in vivo*, and vice versa (Shinkai and Tachibana, 2011).

Another important functional domain, which G9A and GLP both share, is a region containing ankyrin repeats, which is involved in protein-protein interactions. The ankyrin repeat domain also contains H3K9me₁ and H3K9me₂ binding sites (Figure 1.12) (Shinkai and Tachibana, 2011). Therefore, the G9A/GLP complex can both methylate histone tails and bind to mono- and di-methylated H3K9 to recruit molecules, such as DNA methyltransferases, to the chromatin (Shinkai and Tachibana, 2011; Zhang et al., 2016). H3K9me₂ is a reversible modification and can be removed by a wide range of histone lysine demethylases (KDMs) including KDM1, KDM3, KDM4 and KDM7 family members (Cloos et al., 2008; Delcuve et al., 2009; Shinkai and Tachibana, 2011).

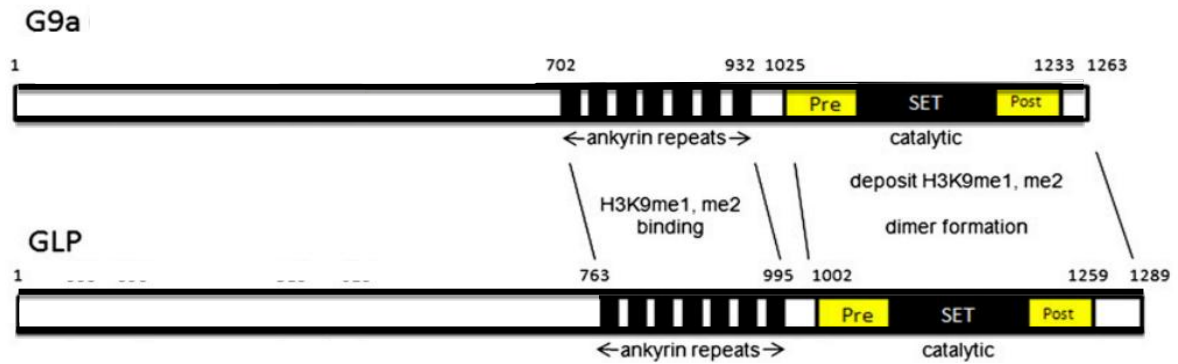


Figure 1.12: Structure of G9A and GLP. (Pre) pre-SET domain; (SET) SET domain; (Post) post-SET domain. The pre-SET, SET and post-SET domains are important for substrate recognition and enzymatic activity. The ankyrin repeats are important for protein-protein interactions and binding to H3K9me1/2 (adapted from Shinkai and Tachibana, 2011).

1.6.2 G9A/GLP have non-histone targets

In addition to their role as histone lysine methyltransferases (HMTs), several studies have shown that G9A/GLP are also able to methylate a wide range of non-histone proteins (Figure 1.13) (Biggar and Li, 2015). However, as most of the reported methylation sites have been derived from mass spectrometry analyses, the function of many of these modifications remain unknown. Nevertheless, increasing evidence suggests methylation of non-histone proteins may influence protein stability (Lee et al., 2015), protein-protein interactions (Lee et al., 2010; Ling et al., 2012) and regulate cellular signalling pathways (Biggar and Li, 2015; Pless et al., 2008). For example, G9A has been shown to methylate the SOX2 protein to regulate its stability in breast cancer cells and mouse embryonic stem cells (Lee et al., 2015). In addition, G9A/GLP can methylate a number of transcription factors to regulate their transcriptional activity, including MyoD (Ling et al., 2012), C/EBP (Pless et al., 2008), Reptin (Lee et al., 2010), p53 (Huang et al., 2010b), MEF2D (Choi et al., 2014), MEF2C (Ow et al., 2016) and MTA1 (Nair et al., 2013). Furthermore, G9A/GLP are able to methylate non-histone proteins to regulate complexes which recruit DNA methyltransferases to gene promoters to repress transcription via the methylation of CpG islands (Chang et al., 2011; Leung et al., 2011; Zhang et al., 2011). Therefore, G9A and/or GLP have wide-ranging roles in development (Choi et al., 2014; Ling et al., 2012; Ow et al., 2016), establishing and maintaining cell identity (Ling et al., 2012; Purcell et al., 2012), cell cycle regulation (Huang et al., 2010a) and cellular responses to environmental stimuli (Lee et al., 2010; Leung et al., 2011), which are dependent on their non-histone protein methyltransferase activity.

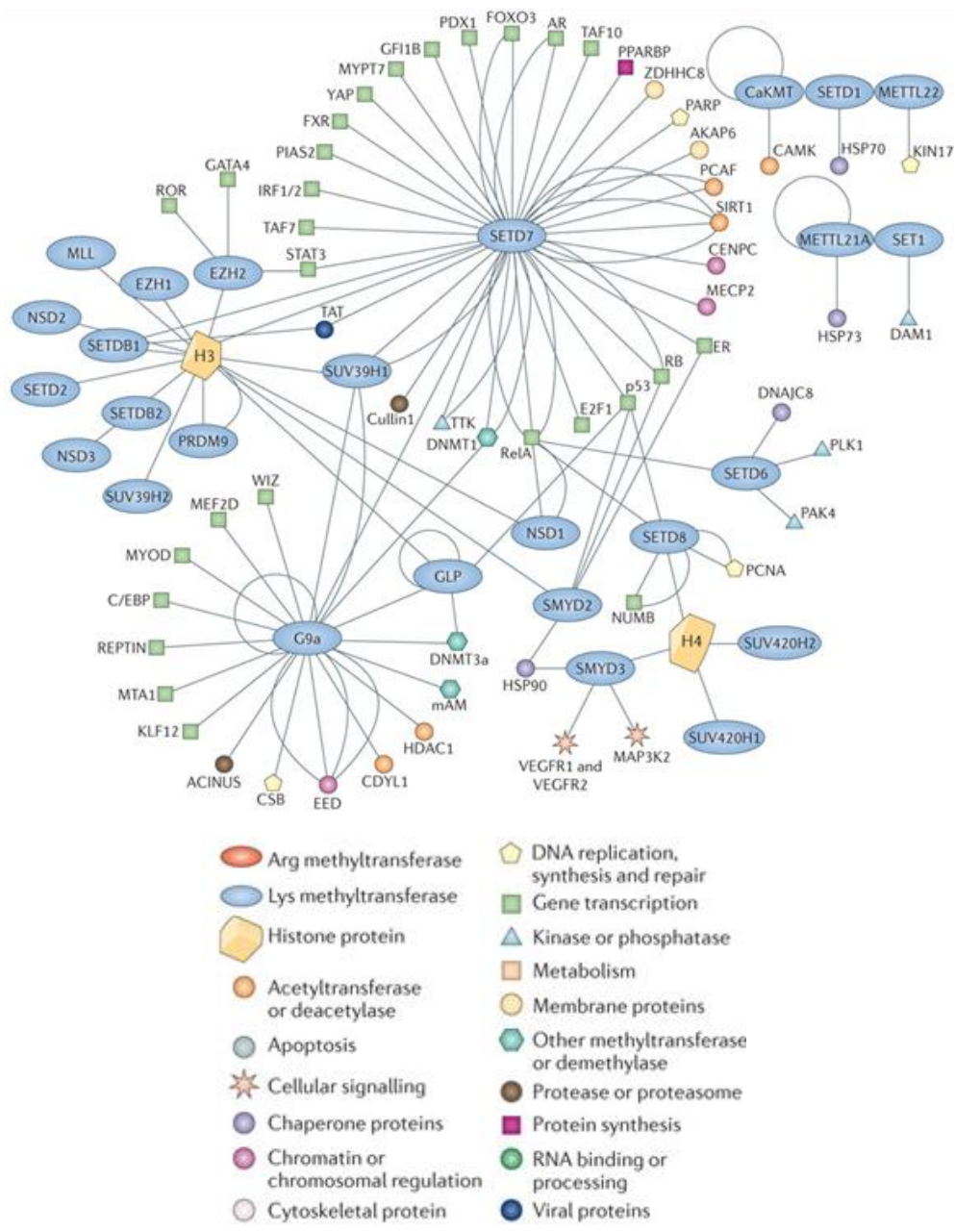


Figure 1.13: A Lys methylation network is presented for known Lys methyltransferase (KMT)–substrate associations based on currently published literature. G9A can methylate at least 17 non-histone proteins, whereas GLP can methylate at least 4 non-histone proteins (from Biggar and Li, 2015).

Apart from their ability to methylate proteins, G9A and GLP also have methyltransferase-independent activities through their N-terminal domain. For example, the Stallcup group demonstrated that G9A binds to co-activators GRIP1, CARM1 and p300 to initiate transcription of a subset of hormone receptors. Here, G9A acts as a positive regulator of transcription independent of its methyltransferase activity, as demonstrated by the insensitivity of G9A co-activator function to UNC0646 (a small molecule G9A-specific methyltransferase inhibitor) (Bittencourt et al., 2012).

1.6.3 Inhibition of G9A/GLP by chemical probes

Several chemical probes have been developed to specifically inhibit the methyltransferase activity of G9A/Glp. A high throughput screen identified BIX-01294 (Kubicek et al., 2007) as the first small molecule inhibitor, which acts by binding to the SET domain of G9A and GLP in the peptide binding site, preventing methylation (Chang et al., 2009). BIX-01294 was further optimised through structure-activity relationships to produce UNC0224, UNC0321, E72, UNC0642 and UNC0638 (Chang et al., 2010; Liu et al., 2013; Liu et al., 2009). For the *in vitro* experiments described in this thesis UNC0638 was used; a potent, specific, stable and cell-permeable inhibitor of G9A/Glp (Liu et al., 2013; Vedadi et al., 2011). However, UNC0638 has poor pharmacokinetics for *in vivo* use (Liu et al., 2013). Therefore, for the *in vivo* experiments described in this thesis A366 was used; a G9A/Glp inhibitor with better pharmacokinetics and no overt toxicity (Sweis et al., 2014). The Roderick group successfully administered mice with A366 via osmotic mini pump (30 mg/kg/ for 10 days) to inhibit G9A/Glp and lower H3K9me2 in cardiomyocytes (Thienpont et al., 2017).

1.7 H3K9me2 demethylases

Historically, like other methylated histone modifications, H3K9me2 was thought to be irreversible due to the high thermodynamic stability of the N-CH₃ bond (Cloos et al., 2008). It was previously thought that histone methylation could only be removed by histone exchange or by cleavage of the methylated histone tail (Cloos et al., 2008). However, the discovery of the histone demethylase (HDM) KDM1A in 2004 changed this perception (Shi et al., 2004). Since then, a number of HDMs have been reported to target H3K9me2, including KDM1A, KDM3A, KDM3B, KDM4A, KDM4B, KDM4C, KDM4D, JHDM1D and PHF8 (Cloos et al., 2008; Hyun et al., 2017). Many of these HDM proteins are also known to target other protein substrates and can be found in bacteria that do not contain histones (Cloos et al., 2008). These observations suggest HDM proteins serve other purposes in addition to demethylating histones.

1.8 Epigenetic regulation of VSMC phenotype

It is becoming increasingly evident that epigenetic mechanisms, including histone modifications, play an important role in controlling VSMC phenotype (Alexander and Owens, 2012; McDonald et al., 2006; Turunen et al., 2009; Villeneuve et al., 2008b).

1.8.1 Histone methylation regulates VSMC gene expression

Interestingly, the activating H3K4me2 mark has been shown to persist at contractile VSMC marker genes in VSMCs after phenotypic switching despite their transcriptional silencing (Alexander and Owens, 2012). Therefore, it has been suggested histone lysine methylation serves as a mechanism for epigenetic cell lineage memory to enable phenotypically modulated VSMCs to switch back to their contractile state (Alexander and Owens, 2012). This information has been used to identify phenotypically switched VSMCs in human atherosclerotic plaque, using in situ hybridisation proximity ligation to detect H3K4me3 at VSMC marker gene promoters. This work combined with fluorescent in situ hybridisation for other cell type and VSMC marker genes demonstrated that VSMCs are able to transition to macrophage and mesenchymal stem cell-like cells within human atheroma (Shankman et al., 2015).

1.8.2 H3K9me2 and G9A/GLP regulate VSMC phenotype

Intriguingly, H3K9me2 has been reported to affect the growth rate, migration and contractility of different smooth muscle cell types (Clifford et al., 2012; Yang et al., 2012). For example, global loss of H3K9me2, by pharmacological inhibition of the associated methyltransferases G9A/Glp, reduced the expression of Calponin and the contractility of ovine foetal pulmonary artery SMCs (Yang et al., 2012). Moreover, compared to VSMCs from healthy aortic tissue, global levels of H3K9me2 are reduced in human VSMCs from atherosclerotic lesions that contain phenotypically modulated VSMCs. In addition, Chen et al observed that VSMCs derived from diabetic rats display lower levels of H3K9me2 compared to non-diabetic controls and found evidence to suggest that dysregulation of H3K9me2 might underlie vascular complications associated with diabetes (Chen et al., 2017; Zhang et al., 2018). Together, these findings implicate H3K9me2 in the regulation of VSMC phenotype.

1.9 *In vivo* mouse models of vascular remodelling and disease

The vasculature is comprised of multiple cell types, which are influenced by a variety of signals in the surrounding milieu including shear stress, circulating blood cells and cytokines. *In vitro* studies fail to mimic this complex environment; therefore *in vivo* models are required to validate and substantiate *in vitro* results. The mouse has proven to be a powerful and flexible model system to explore the development of human CVD and assess therapeutic feasibility. Remarkably, 50% of coronary artery disease-associated pathways derived from mouse genome wide association studies overlapped with those identified from human studies (von Scheidt et al., 2017). We share 95% of our protein encoding genes with mice (von Scheidt et al., 2017) and regulatory elements often share

evolutionary conserved histone modifications which can signify their function (Diehl and Boyle, 2018).

However, despite phylogenetic similarities between mice and humans there are still many differences between the two species and conserved chromatin signatures do not always equate to conserved regulatory functions (Diehl and Boyle, 2018; von Scheidt et al., 2017). For instance, in contrast to mice, a significant number of VSMCs exist within the intima in conserved locations, including branch sites and areas of turbulent blood flow, prior to disease within human vasculature (Doran et al., 2008). Furthermore, wild type mice are relatively resistant to atherosclerosis because they have a very different lipid profile compared to humans. Models, including genetically engineered ApoE^{-/-} mice fed a high fat diet (Nakashima et al., 1994), have been developed to overcome this problem but are unlikely to perfectly reflect the mechanisms which cause atherosclerosis in humans. Consequently, mice created to mimic human disease frequently have phenotypes that differ from their human counterparts (Perlman, 2016). Therefore, it is important to validate findings drawn from mouse models in human samples.

1.9.1 VSMC-specific conditional lineage tracing

VSMCs down regulate contractile VSMCs genes in response to injury and inflammation. Furthermore, many contractile VSMC markers are also expressed by other cell types (Gomez and Owens, 2012). Therefore, studying VSMC behavior in vascular disease is difficult. However, recent studies have overcome this problem by using transgenic mice expressing CreERT2 recombinase under the control of the Myh11 promoter (Figure 14A, B), regarded as a VSMC specific marker (Nguyen et al., 2013), with fluorescent Cre-dependent reporter genes. Such VSMC-specific conditional lineage tracing has proved to be extremely useful to efficiently and specifically identify VSMC and VSMC-derived cells and can therefore be used to test effects on VSMC and VSMC-derived cells *in vivo* (Albarrán-Juárez et al.; Chappell et al., 2016; Herring et al., 2014; Herring et al., 2017; Shankman et al., 2015).

The Cre recombinase used in this VSMC lineage tracing model is fused to a mutant form of the oestrogen receptor, which binds the synthetic oestrogen 4-hydroxytamoxifen instead of its natural ligand 17 β -estradiol. CreER(T2) resides within the cytoplasm and can only translocate to the nucleus following tamoxifen administration, allowing tight temporal control of recombination. The CreERT2 sequence was inserted into the ATG site of a bacterial artificial chromosome (BAC) carrying the Myh11 gene, the most specific marker of mature contractile VSMCs (Nguyen et al., 2013). The 180kb BAC was then injected into the pro-nuclei of mice oocytes. Myh11-CreER(T2) transgenic mice where the transgene had integrated into the Y chromosome were chosen for breeding onto the C57BL/6

background (Wirth et al., 2008), excluding its application in female mice. Gender has been identified as a risk factor for multiple vascular diseases (Mosca et al., 2011), therefore the use of only male mice in the studies described in this thesis is a limitation.

The multicolour Confetti (Figure 14A)/single colour EYFP (Figure 14B) reporter located within the ROSA26 *locus*, contains a CAG promoter, permitting high expression of the fluorescent transgene reporter, a loxP flanked stop cassette, ensuring the expression of the transgene is Cre-recombinase dependent and the reporter sequence (Livet et al., 2007; Snippert et al., 2010). The multicolour Confetti reporter sequence, Brainbow 2.1, contains floxed cDNA for green (GFP), yellow (YFP), red (RFP) and cyan (CFP) fluorescent proteins whereas the single colour EYFP reporter sequence contains floxed cDNA for enhanced yellow fluorescent protein (EYFP).

In Myh11-CreERT2, ROSA26-Confetti (Chappell et al., 2016)/EYFP (Gomez et al., 2013) mice, upon Cre driven recombination, the stop cassette is excised, allowing reporter genes to express specifically in Myh11-positive cells. For the Confetti construct, Cre driven recombination leads to the stochastic expression of one of the four fluorescent proteins described. GFP localises to the nucleus, YFP and RFP localise to the cytoplasm and CFP is recruited to the membrane (Livet et al., 2007; Snippert et al., 2010). Since removal of the stop cassette is permanent, the reporter genes are expressed in all the progeny produced by the initial cells where the Cre was once activated.

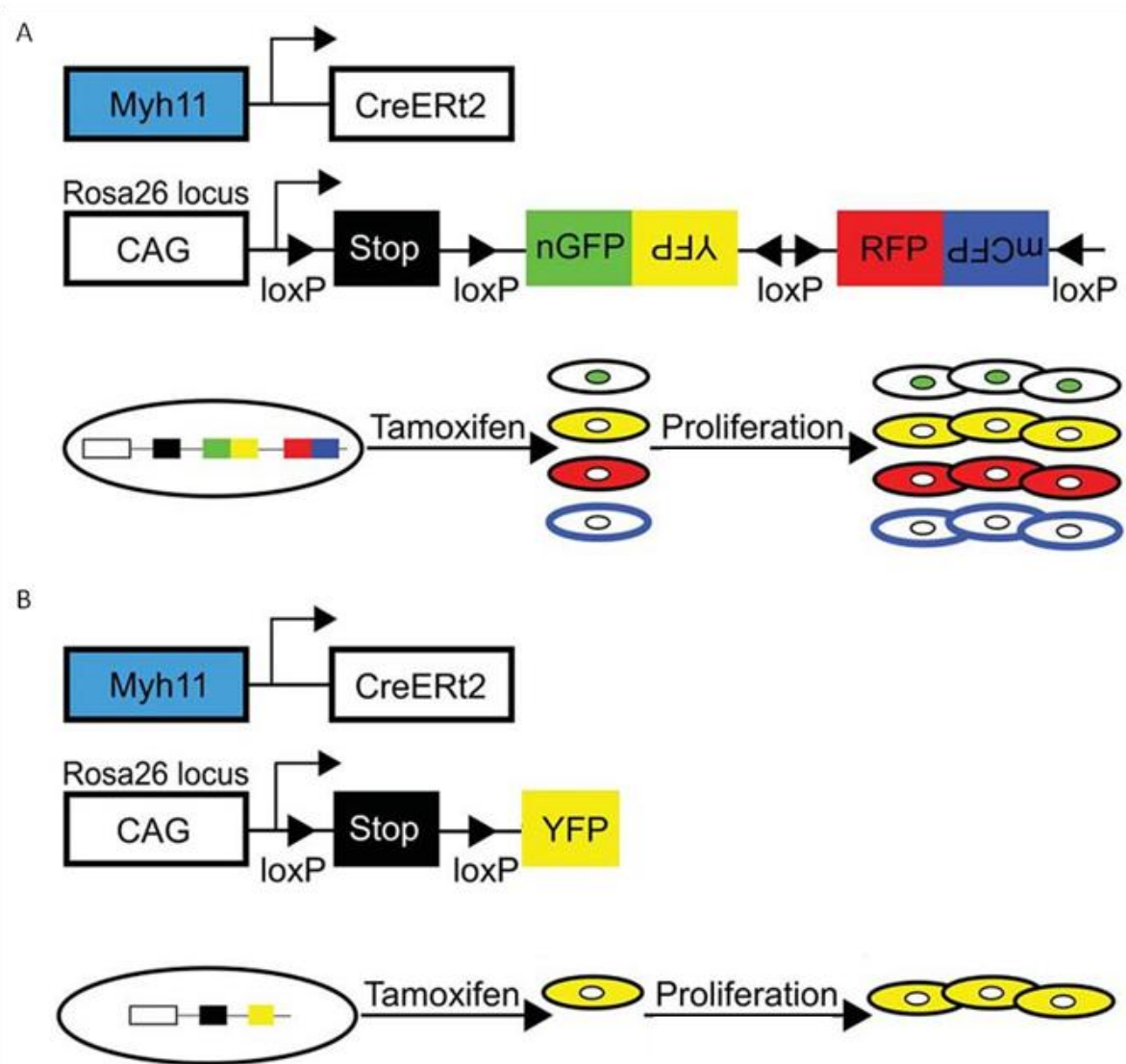


Figure 1.14: Schematic of 'Confetti' multi-colour and EYFP single-colour VSMC lineage tracing system. (A) Schematic of the Myh11-CreERT2 transgene (Wirth et al., 2008) and the ROSA26-Confetti reporter allele (Snippert et al., 2010). Tamoxifen-induced recombination at the ROSA26-Confetti *locus* results in the expression of one of four fluorescent proteins, which are stably propagated independent of Myh11 expression levels within progeny. (B) Schematic of the Myh11-CreERT2 transgene and the ROSA-EYFP reporter allele. Tamoxifen-induced recombination at the ROSA-EYFP *locus* results in the expression of EYFP protein, which is stably propagated independent of Myh11 expression levels within progeny (Adapted from Chappell et al., 2016).

1.9.2 Carotid ligation model

Vascular remodelling of the carotid artery, characterised by medial and intimal thickening, is a hallmark of many human CVDs (Davis et al., 2001) and can be mimicked using animal models (Emini Veseli et al., 2017). In mice, complete ligation of the left common carotid artery near the carotid bifurcation causes extensive vascular remodelling in the response to cessation of blood flow, leading

to neointima formation over time (Ali et al., 2013; Herring et al., 2017; Kumar and Lindner, 1997b). Carotid ligation rapidly elicits reproducible vessel growth and remodelling concomitant with changes in VSMC gene expression (Ali et al., 2013; Herring et al., 2014; Herring et al., 2017; Kumar and Lindner, 1997b). Analyses of the medial layer of carotid arteries, both 3 and 14 days post ligation, have revealed decreased expression of contractile VSMC genes accompanied by a significant increase in pro-inflammatory and MMP gene expression (Figure 1.15) (Ali et al., 2013; Herring et al., 2017). Furthermore, studies using lineage labelled adult VSMCs have shown that the neointima begins to develop between 7 and 14 days post ligation and that the neointimal cells mostly arise from medial VSMCs (Chappell et al., 2016; Herring et al., 2014).

A disadvantage of the mouse carotid ligation injury model is that it is performed on healthy blood vessels that lack pre-existing atherogenic or vasoproliferative pathologies (Baylis et al., 2017; Lee et al., 2017). Therefore, mechanisms underlying vascular remodelling due to arterial ligation may not recapitulate those involved in human disease. However, this model elicits an acute VSMC response to injury, which is quicker and more reproducible than many alternative models of vascular disease (Lee et al., 2017). Therefore, the carotid ligation model provides a good system to test effects on the early VSMC gene expression changes associated with vascular remodelling and disease.

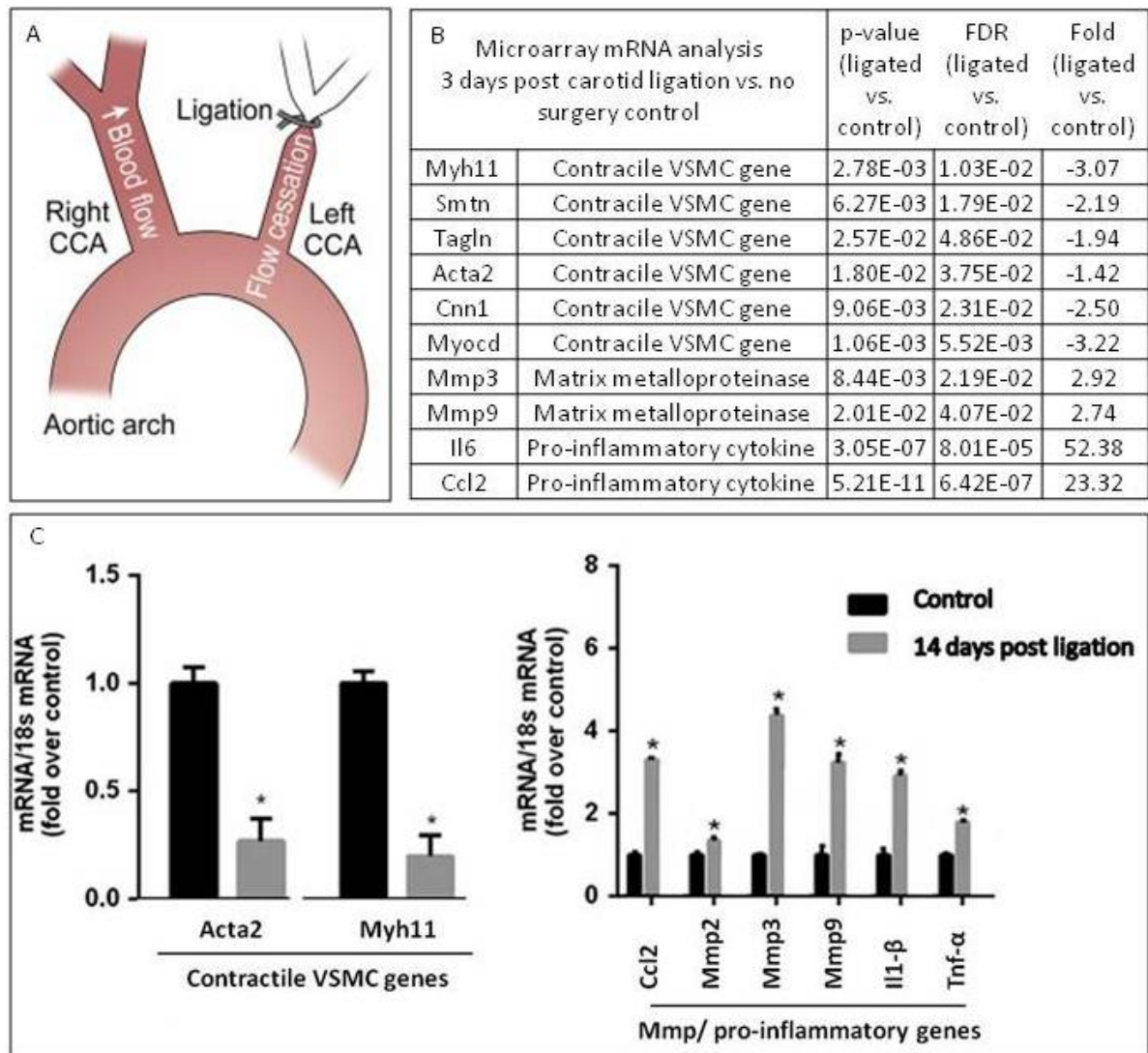


Figure 1.15: The carotid ligation-injury mouse model. (A) Schematic of carotid anatomy and left common carotid artery (Left CCA) ligation site. (B) Microarray analysis of mRNA levels from the medial layer of the left CCA 3 days after ligation relative to no surgery controls (Herring et al., 2017). (C) RT-qPCR analysis of mRNA levels from the medial layer of the left CCA 14 days after ligation relative to no surgery controls (Ali et al., 2013).

1.9.3 ApoE^{-/-}, high fat diet mouse model of atherosclerosis

In atherosclerotic plaque, VSMCs display significant plasticity; many VSMCs down regulate contractile markers and adopt a more proliferative, migratory and synthetic phenotype and can often acquire macrophage, osteo-chondrocytic and mesenchymal stem cell markers (Alexander and Owens, 2012; Bennett et al., 2016). Atherosclerosis can be induced in a reasonable time frame using mouse models. However, wild type mice are relatively resistant to atherosclerosis because they have a very different lipid profile compared to humans (Nakashima et al., 1994). Unlike humans, in mice

cholesterol is mostly transported in high density lipoprotein (HDL) like particles, which are less atherogenic compared to low density lipoprotein (LDL) and very low density lipoprotein (VLDL) (Nakashima et al., 1994). Therefore, genetic manipulation of the mouse's lipid metabolism is required to induce atherosclerosis. Genetic ablation of apolipoprotein E (ApoE), a glycoprotein involved in the clearance of lipoproteins and cholesterol from the body, elevates levels of atherogenic LDL, VLDL and plasma cholesterol (Nakashima et al., 1994). Consequently, atherosclerotic lesions develop in regions of the vasculature subject to flow disturbance, where shear stress is low and/or oscillatory, in a process similar to that observed in human disease (Figure 16). In ApoE^{-/-} mice, monocytes attach to endothelial cells from 6 weeks of age and foam cell lesions are detectable by 8 weeks. From 15 to 20 weeks of age atherosclerotic plaques consisting of VSMCs, ECM and a necrotic core covered with a fibrous plaque can be observed. When fed a high fat diet, atherosclerosis is greatly accelerated in ApoE^{-/-} mice (Emini Veseli et al., 2017; von Scheidt et al., 2017).

A caveat of the ApoE^{-/-} HFD mouse model is that plaques within these mice typically do not rupture and therefore fail to recapitulate the deadliest late stage events associated with atherosclerosis (Baylis et al., 2017). Furthermore, ApoE is known to play a role in inflammation, which may influence plaque development (Emini Veseli et al., 2017). However, the plaques within ApoE^{-/-} mice follow similar developmental steps observed within humans. The model is extensively used to study atherosclerosis and has greatly advanced our understanding of the disease (Lee et al., 2017; Meir and Leitersdorf, 2004; Nakashima et al., 1994).



Model	Lipid profile	Plaque distribution and characteristics (20 weeks WD)	Advantages & limitations
Disruption of the ApoE gene 	Plasma cholesterol: 400-600 mg/dl on ND >1000 mg/dl on WD Lipoproteins: ↑ VLDL ↑ LDL ↓ HDL	 Fibrous plaques: Smooth muscle cells Extracellular matrix Inflammatory cells Necrotic core	<ul style="list-style-type: none"> ➕ Develops atherosclerosis on ND ➖ No human-like lipid profile ➖ ApoE plays a role in inflammation → influence plaque development ➖ No spontaneous plaque rupture, thrombosis and complications

Figure 1.16: Overview of atherosclerosis model in ApoE-knockout mice fed on a high-fat diet.

The figure describes total plasma cholesterol levels on normal (ND) and high fat western-type diet (WD), lipoprotein profile, plaque characteristics and the advantages and limitations of the model. The distribution of the plaques in the thoracic aorta is shown for mice fed a WD for at least 20 weeks (from Emini Veseli et al., 2017).

1.10 Hypothesis and aims

VSMC phenotypic switching directly contributes to the development and progression of cardiovascular disease (CVD) (Herring et al., 2014; Nguyen et al., 2013), the leading cause of death worldwide (WHO, 2015). In response to inflammation and injury, VSMCs can reversibly change from their quiescent “contractile” phenotype to an active “synthetic” state (Owens et al., 2004). Synthetic VSMCs are characterised by the loss of contractile marker expression and the ability to upregulate selective gene sets in response to environmental stimuli. For example, stimulation of VSMCs with pro-inflammatory cytokines such as IL-1 α activates both NF κ B and AP-1 signalling associated transcription, inducing the expression of matrix metalloproteinases (MMPs), inflammatory cytokines (e.g. IL6) and chemokines (CCL2). Such inducible genes are essential for vascular repair and remodelling but can often become dysregulated and contribute to disease development.

The epigenetic mechanisms underlying phenotypic switch-associated changes in VSMC gene expression remain relatively unexplored. Interestingly, decreased levels of H3K9me2, a repressive mark associated with inactive gene promoters, have been observed in VSMCs derived from atherosclerotic plaques compared to healthy tissue in humans. Furthermore, H3K9me2 has been reported to affect the growth rate, migration and contractility of different smooth muscle cell types (Clifford et al., 2012; Yang et al., 2012) and numerous studies have found that H3K9me2 marks genes involved in processes that require tight and dynamic regulation, including those involved in cell fate switching (Chen et al., 2013; Chen et al., 2012) and the inflammatory response (Chen et al., 2009; Fang et al., 2012; Liu et al., 2014; Miao et al., 2007; Yoshida et al., 2015). Therefore, the experiments performed in this thesis attempt to assess the function and physiological importance of H3K9me2 in VSMCs.

Hypothesis: H3K9me2-mediated gene regulation is functionally important in VSMCs and influences their phenotypic plasticity.

Aims:

- (1) Use murine *in vitro* and *in vivo* models of VSMC phenotypic switching to:
 - a) assess global and local changes in H3K9me2 upon loss of the contractile state
 - b) and test the functional role of H3K9me2 on disease-associated VSMC gene expression.
- (2) Determine whether H3K9me2-mediated regulation of disease-associated VSMC genes is conserved in human VSMCs.

- (3) Investigate the mechanism underlying H3K9me2-mediated regulation of disease-associated VSMC gene expression.

CHAPTER 2 - METHODS

2.1 Mouse VSMC isolation

Whole aortas from C57BL/6J mice were dissected in PBS under an inverted Leica M80 microscope, applying aseptic technique. Fat and connective tissue were removed before the vessels were opened longitudinally to scrape off blood and endothelial cells. For primary mouse VSMC culture, each aorta was incubated in 1 ml of 1 mg/ml of collagenase II and 1 U/ml of elastase (Worthington) in DMEM at 37 °C, 5 % CO₂ for 10 minutes to peel off and remove the adventitia. Aortas intended for RNA extraction were stored in RNAlater (ThermoFisher) at -20 °C. Enzymatic digestion was not used to aid removal of the adventitia for *ex vivo* VSMC isolation intended for RNA extraction or CHIP; instead the adventitia was removed manually in PBS. The isolated medial layer of VSMCs was then washed in PBS before being snap frozen in liquid nitrogen or being further processed for culture.

2.2 Primary mouse VSMC culture

After isolating the medial layer of VSMCs, the tissue was further digested in 1 ml of 2.5 mg/ml of collagenase II (Invitrogen) and 2.5 U/ml of elastase (Worthington) in DMEM at 37 °C, 5 % CO₂ for approximately 2 hours, mixing every 20 minutes, until a single cell suspension was reached. The dissociated VSMCs were plated in VSMC growth medium (DMEM supplemented with 10 % (v/v) of FBS, 100 U/ml of penicillin, 100 mg/ml of streptomycin and 2 mM of glutamine). 1 well of a 12-well plate (Corning) was used per aorta. VSMCs were maintained at 37 °C, 5 % CO₂ in growth medium and split 1:2 every 5-7 days when approximately 90 % confluent. To split, the cells were washed in PBS and incubated in Trypsin-EDTA solution (T4049, Sigma-Aldrich) at 37 °C, 5 % CO₂ for approximately 5 minutes. Experiments were carried out using passage 4 VSMCs.

2.3 Derivation of human VSMCs

Human aortic VSMCs were isolated from patients undergoing aortic valve replacement surgery under informed consent with protocols approved by the Cambridge or Huntingdon Research Ethical Committee. Adventitia and endothelial cells were manually removed from aortic explants before being cut into ~2-3 mm² sections. The medial VSMC layer was either analysed directly or four ~2-3 mm² sections were placed in a 6-well plate with a cover slip placed on top and cultured in growth medium (DMEM supplemented with 10 % (v/v) of FBS, 100 U/ml of penicillin, 100 mg/ml of streptomycin and 2 mM of glutamine). VSMCs were cultured to approximately 90 % confluence before passaging. To split, the cells were washed in PBS and incubated in Trypsin-EDTA solution (T4049, Sigma-Aldrich) at 37 °C, 5 % CO₂ for ~5 minutes. The passage number of the VSMCs used is

indicated in the figure legends. Table 1 describes the age and sex of the donors from which the VSMCs were derived.

Table 1: Human donor information

Figure ID:	P#	Age:	Sex:
5.1	N/A	78	Male
5.1	N/A	65	Male
5.1	N/A	53	Female
5.1	7	36	Male
5.1	8	53	Male
5.1	7	59	Male
5.2	9	20	Male
5.2	8	33	Female
5.2	7	56	Male
5.2	11	64	Female
5.2	8	32	Male
5.2	13	44	Male
5.2	10	71	Female
5.2	11	77	Female
5.3	8	53	Male
5.3	6	64	Female
5.3	6	66	Male
5.3	6	78	Male
5.4	8	32	Male
5.4	13	44	Male
5.4	10	71	Female
5.4	11	77	Female

Figure ID:	P#	Age:	Sex:
5.5	9	20	Male
5.5	8	33	Female
5.5	7	56	Male
5.5	11	64	Female
6.1/6.4	6	41	Male
6.1/6.4	9	53	Female
6.1/6.4	7	45	Male
6.2/6.3	12	44	Male
6.2/6.3	7	69	Male
6.2/6.3	11	71	Female
6.2/6.3	9	77	Male
6.5	6	41	Male
6.5	11	45	Male
6.5	15	53	Female
6.5	11	71	Female
6.6/6.7	8	32	Male
6.6/6.7	13	44	Male
6.6/6.7	10	71	Female
6.6/6.7	11	77	Female
6.8	6	41	Male
6.8	11	45	Male
6.8	15	53	Female

P# = Passage number

2.4 Animal experiments

All experiments were carried out according to the UK Home Office regulations (PPL70/7565) and were approved by the local ethics committee. C57Bl/6 and *ApoE*^{-/-} mice were purchased from

Charles River. Myh11-CreERT2, ROSA26-Confetti and ROSA26-EYFP mice have all been previously described (Basak et al., 2014; Chappell et al., 2016; Majesky et al., 2017; Snippert et al., 2010; Wirth et al., 2007). Myh11-CreERT2/ROSA26-Confetti and Myh11-CreERT2/ROSA26-EYFP males (as the Myh11-CreERT2 transgene is Y linked) received intraperitoneal injections of tamoxifen at 3-8 weeks of age (10 injections of 1 mg/ml each) for lineage labelling.

For A366 treatment experiments, Myh11-CreERT2+, ROSA26-Confetti+ or Myh11-CreERT2, ROSA26-EYFP+ males were anaesthetised using 2.5-3% isoflurane (by inhalation) and given a pre-operative analgesic (Temgesic). Mini osmotic pumps filled with 30 mg/kg/day of A366 dissolved in 98:2 PEG 400/polysorbate 80 or 98:2 PEG 400/polysorbate 80 without active compound were then implanted subcutaneously (2002, Azlet). The aorta and right and left common carotid arteries were removed either 7- or 14-days post-surgery and processed for western blot or immunofluorescence to analyse global H3K9me2 levels in the VSMCs.

For A366 treatment plus carotid ligation experiments, 14 days after osmotic pump insertion carotid ligation surgery was performed. For carotid ligation experiments, Myh11-CreERT2+, ROSA26-Confetti+ or Myh11-CreERT2, ROSA26-EYFP+ males were anaesthetised using 2.5-3% isoflurane (by inhalation) and given a pre-operative analgesic (Temgesic). The left common carotid artery was tied firmly with one knot using 6-0 silk suture just below the bifurcation point. Both the right and left carotid arteries were removed 7 days post-surgery and processed for microscopy or FACS to isolate lineage labelled EYFP+ VSMCs.

2.4 Western blot

Cell pellets were lysed directly in 2X Laemmli sample buffer (20% glycerol, 4% SDS, 100 mM Tris HCl pH 6.8, 200 mM DTT), incubated at 98 °C for 5 minutes and sonicated for 1 minute at medium intensity using a standard Bioruptor (Diagenode). Total protein (10-30 µg) was resolved with SDS-PAGE and transferred to PVDF membranes. The membranes were incubated in blocking buffer (5% w/v non-fat dry milk in TBS (50 mM Tris-HCl, pH 7.5, 150 mM NaCl) for one hour at room temperature. The membranes were then probed with primary antibodies (Table 2) overnight at 4 °C followed by secondary antibodies conjugated to horseradish peroxidase (HRP) (Table 3) for 30-60 minutes at room temperature. All antibody incubation steps were done in blocking buffer. Protein was detected using the ECL system (GE Healthcare), following the manufacturer's instructions.

Table 2: Primary antibodies used for western blot

Protein	Size	Species [‡]	mg/ml	Dilution	Product ID
GLP	140, 165 kDa	Mouse mAb	1	1:1000	R&D Systems (#PP-B0422-00)
G9A	138 kDa	Mouse mAb	1	1:500	R&D Systems (#PP-A8620A-00)
H3K9me2	17 kDa	Mouse mAb	1	1:1000	Abcam (#ab1220)
NFkB-p65	64 kDa	Rabbit pAb	0.1	1:100	Santa Cruz (sc-372)
cJUN	43 kDa	Rabbit pAb	1	1:1000	Abcam (#ab31419)
p- cJUN (Ser63)	42 kDa	Rabbit mAb	0.1	1:1000	Abcam (#ab32385)
p-JNK (Thr183/Tyr185)	46, 54 kDa	Rabbit mAb	ND	1:1000	Cell Signaling (#4668)
p-ERK1/2 (Thr202/Tyr204)	42, 44 kDa	Rabbit pAb	ND	1:1000	Cell Signaling (#9101)
p-p38 (Thr180/Tyr182)	43 kDa	Rabbit pAb	ND	1:1000	Cell Signaling (#9211)
ACTB	45 kDa	Mouse mAb	1	1:10,000	Sigma-Aldrich (#A2228)
B-TUBULIN	55 kDa	Rabbit pAb	ND	1:1000	Cell Signaling (#2146)

[‡]mAb, monoclonal antibody; pAb, polyclonal antibody; ND, not determined; WB, western blot; p-, phosphorylated.

Table 3: Secondary antibodies used for western blot

Protein	Dilution	Product ID
Anti-rabbit IgG, HRP linked	1:5000	Cell Signaling (#7074)
Anti-mouse IgG, HRP linked	1:5000	Cell Signaling (#7076)

2.5 Quantitative Real Time-Polymerase Chain Reaction (RT-qPCR)

Total RNA was extracted with TRIzol (Life Technologies) and 0.4-1 µg was reverse transcribed using a QuantiTect Reverse Transcription kit (Qiagen), according to the manufacturer's directions.

For quantification, cDNA (diluted 1:5-1:10) or gDNA from CHIP was amplified, in technical duplicates, with a QuantiTect SYBR Green PCR kit (Qiagen) and primer pairs listed in Tables 4 to 7, using a Corbett Life Science Rotor Gene 6000 PCR system. RT-qPCR-obtained values were normalised to the average of two housekeeping genes (HMBS and YWHAZ or HPRT1).

2.5.1 Primer design and validation

Primers for RT-qPCR were designed as following: amplicon size of 100- 200bp, primer GC content of 45-55%, primer melting temperature 58-62°C, low 3' stability (no more than 2 C's and/or G's in the last 5bp of the primer) and primer size of 18-25 bp. For cDNA analysis primers were designed targeting different exons. Target sequences were obtained using the Ensembl genome browser and the primers were aligned to the genome using the NCBI BLAT function and checked using the UCSB In-Silico PCR tool. For each pair of primers designed, the efficiency in RT-qPCR was tested in 3-fold dilutions of gDNA/cDNA. Primers were chosen which yielded a good linear fit ($R^2 < 0.98$) in Ct vs. logarithm of the dilution factor plot and when the efficiency calculated was between 1.8 and 2.2 (Efficiency = $10^{(1/\text{slope})}$).

Table 4: Mouse RT-qPCR primer sequences

Gene	Species	Forward 5'-3'	Reverse 5'-3'	Type
<i>Hprt1</i>	Mouse	TGGATACAGGCC AGACTTTGTT	CAGATTCAACTTG CGCTCATC	Housekeeping
<i>Hmbs</i>	Mouse	ACTGGTGGAGTA TGGAGTCTCAGAT GGC	GCCAGGCTGATG CCCAGGTT	Housekeeping
<i>Ywhaz</i>	Mouse	CGTTGTAGGAGC CCGTAGGTCAT	TCTGGTTGCGAAG CATTGGG	Housekeeping
<i>Acta2</i>	Mouse	AGATCTGGCACCA CTCTTTC	GTGAGTCACACCA TCTCCAG	Contractile vSMC
<i>Myocd</i>	Mouse	ACTCCTGGATGTC CTCATTG	GTTGGCGTAGTG ATCGAAG	Contractile vSMC
<i>Tagln</i>	Mouse	AGTATGACGAGG AGCTGGAG	AAGAATTGAGCC ACCTGTTC	Contractile vSMC
<i>Cnn1</i>	Mouse	TCATCAAAGCCAT TACCAAG	TGCCTTCTCTCAA CTTCTCC	Contractile vSMC
<i>Smtn</i>	Mouse	GCAAGGCCATGA TTGAGAAG	CAGCAACATCTGC TTGATGC	Contractile vSMC
<i>Tagln</i>	Mouse	AGTATGACGAGG AGCTGGAG	AAGAATTGAGCC ACCTGTTC	Contractile vSMC
<i>Myh11</i>	Mouse	CTGAGGGAGCGA TACTTCTC	TGTAGCATGCTTC TGTAGGC	Contractile vSMC
<i>Mmp2</i>	Mouse	ACTACGATGATGA CCGGAAG	TCGGAAGTTCTTG GTGTAGG	MMP
<i>Mmp3</i>	Mouse	GGATTTGCCAAG ACAGAGTG	ATAGGCATGAGC CAAGACTG	MMP
<i>Mmp9</i>	Mouse	CTCAAGTGGGAC CATCATAAC	CGACACCAAAC TG GATGAC	MMP
<i>Mmp12</i>	Mouse	AGCCACACATATC CCAGGAGCA	TCCTGCCTCACAT CATACTCCA	MMP
<i>Il6</i>	Mouse	TCAATTCCAGAAA CCGCTATG	GTCTCCTCTCCGG ACTTGTG	Inflammatory
<i>Ccl2</i>	Mouse	GGCTCAGCCAGA TGCAGTTA	CTTCTTTGGGACA CCTGCTG	Inflammatory
<i>Cd34</i>	Mouse	AGGCTGATGCTG GTGCTAG	AGTCTTTCGGGAA TAGCTCTG	Vascular progenitor
<i>Cd45</i>	Mouse	GAGGTGTCTGAT GGTGCAAG	TGTATTCCACTAA AGCCTGATGAA	Bone marrow derived
<i>Pdgfra</i>	Mouse	GGTCCCAACCTGT AATGAAG	GTAAATGGGACC TGACTTGG	Adventitial fibroblast
<i>Cd31</i>	Mouse	GTCATGGCCATG GTCGAGTA	CTCCTCGGCATCT TGCTGAA	Endothelial

Table 5: Human RT-qPCR primer sequences

Gene	Species	Forward 5'-3'	Reverse 5'-3'	Type
<i>HMBS</i>	Human	GGTTGTTCACTCC TTGAAGG	TTCTCTGGCAGGG TTTCTAG	Housekeeping
<i>YWHAZ</i>	Human	CGTTGTAGGAGC CCGTAGGTCAT	TCTGGTTGCGAAG CATTGGG	Housekeeping
<i>HPRT1</i>	Human	GTAATTGGTGGGA GATGATCTCTCAA CT	TGTTTTGCCAGTG TCAATTATATCTTC	Housekeeping
<i>ACTA2</i>	Human	AGATCTGGCACCA CTCTTTC	GTGAGTCACACCA TCTCCAG	Contractile vSMC
<i>MYOCD</i>	Human	CCAACAACCTCA CTTTCTG	AGAATGGGGAGA GAAGCTTG	Contractile vSMC
<i>TAGLN</i>	Human	TCTTTGAAGGCAA AGACATGG	TTATGCTCCTGCG CTTTCTT	Contractile vSMC
<i>CNN1</i>	Human	GTCCACCCTCCTG GCTTT	AAACTTGTTGGTG CCCATCT	Contractile vSMC
<i>SMTN</i>	Human	GGCAGTATGAAG ACCACATTC	CACTACTGGTGCT GAGTAGGG	Contractile vSMC
<i>MMP2</i>	Human	ACTACGATGATGA CCGGAAG	TCGGAAGTTCTTG GTGTAGG	MMP
<i>MMP3</i>	Human	CTGGGCTATCAGA GGAAATG	CTTATCAGAAATG GCTGCATC	MMP
<i>MMP9</i>	Human	TTGACAGCGACA AGAAGTGG	GCCATTCACGTCG TCCTTAT	MMP
<i>MMP12</i>	Human	CACACCTGACATG AACCGTG	ATGCCAGATCCAG GTCCAAA	MMP
<i>IL6</i>	Human	GGTACATCCTCGA CGGCATCT	GTGCCTCTTTGCT GCTTTCAC	Inflammatory
<i>CCL2</i>	Human	AAGATCTCAGTGC AGAGGCTCG	TTGCTTGCCAGG TGGTCCAT	Inflammatory
<i>JUN</i>	Human	ATCAAGGCGGAG AGGAAGCG	TGAGCATGTTGGC CGTGGAC	AP-1 TF
<i>P65</i>	Human	ATCCCATCTTTGA CAATCGTGC	CTGGTCCCGTGAA ATACACCTC	NFkB TF
<i>G6PD</i>	Human	GCCAACCGCTCT TCTACCT	GATGATGCGGTTT CAGCCTA	Negative regulator of contractile VSMC genes
<i>KLF4</i>	Human	ATCTTTCTCCACG TTCGCTCTG	AAGCACTGGGGG AAGTCGCTTC	Negative regulator of contractile VSMC genes
<i>IL1R1</i>	Human	CCTGCTATGATTT TCTCCCAATAAA	AACACAAAAATAT CACAGTCAGAGG TAGAC	IL-1 α receptor

Table 6: Mouse ChIP-qPCR Primers

Gene	Species	Forward 5'-3'	Reverse 5'-3'	Region
<i>Magea2</i>	mouse	TTGGTGGACAGG GAAGCTAGGGGA	CGCTCCAGAACAA AATGGCGCAGA	Promoter
<i>ActB</i>	mouse	CCACATAGGAGTC CTTCTG	ACCTGTTACTTTG GGAGTGG	Promoter
<i>Acta2</i>	mouse	TATAACCC TTCAG CGTTCAG	TCATTCAGATTCC CACAGAC	Promoter
<i>Tagln</i>	mouse	TGCCATAAAAG GTTTTTCC	GAAGTCTGCTTGG CTCACC	Promoter
<i>Cnn1</i>	mouse	GTCTGTGTCATCT GCACCTC	CACAGGTAGGAG GGATTTTG	Promoter
<i>Myocd</i>	mouse	CCGGCTGTTAAGA CTCCTG	TTCCTGGCTGATG TCATAGG	Promoter
<i>Smtn</i>	mouse	AGAGAATTGGCT GGGACAG	GACCCGGTAGAT GCAGTAGAG	Promoter
<i>Mmp2</i>	mouse	AGTATCCCTCCAA AGGCAAG	TTCTTCCCACCTCT TCTTCC	Promoter
<i>Mmp3</i>	mouse	AAGAAGGTGGAC CTAGAAGGAG	CACTGTCATGCAA TGGGTAG	Promoter
<i>Mmp9</i>	mouse	AAGGCTGAGACC ACTGAATG	GTGATTCCATGGT TTGGTG	Promoter
<i>Mmp12</i>	mouse	GGCTTTAAGGGA ACTTG CAG	ACTGTCATTCATG GGAGCAG	Promoter
<i>Il6</i>	mouse	CCCACCCTCCAAC AAAGATT	GCTCCAGAGCAG AATGAGCTA	Promoter
<i>Ccl2</i>	mouse	CTTCCACTTCCTG GAAACAC	GGCAGCCTTTTAT TGTAAGC	Promoter

Promoter = within 500bp of transcriptional start site.

Table 7: Human ChIP-qPCR primer sequences

Gene	Species	Forward 5'-3'	Reverse 5'-3'	Region
<i>MAGEA2</i>	Human	CCTACACCAACAC CATCTTC	AGAATCTCGCTGT CCTCTG	Promoter
<i>ACTB</i>	Human	CCATTGGCAAGA GCCCGGCT	GACACCCACGCC AGTTCCG	Promoter
<i>ACTA2</i>	Human	CCAGTGGAAATGC AGTGGAAAGAGA	AGGGAAGCTGAA AGCTGAAGGGTT	Promoter
<i>TAGLN</i>	Human	TAGGTCCTCAGGA AAGGTTG	AATAGAGTCTGG CTGGAGAGAG	Promoter
<i>CNN1</i>	Human	TGCTTCAAGACTC CAGAGAG	GACAGAGACCAG CCTTCTTC	Promoter
<i>MYOCD</i>	Human	TCTCCAGATGCGC CGTGTCA	TCAGGGCACTGG CAGAGACGA	Promoter
<i>SMTN</i>	Human	GTATGAATTGGCA GGAGGTG	TGTCATTCCCCCA GGTATAG	Promoter
<i>MMP2</i>	Human	ACGTAGAGGCCA GGAGTAGC	GCCTGAGGAAGT CTGGATG	Promoter
<i>MMP3</i>	Human	GCAAGGATGAGT CAAGCTG	TGTCTCTATGCCT TGCTGTC	Promoter (IL-1- responsive element (Quinones et al., 1994), cJUN bs (Clark et al., 2008))
<i>MMP9</i>	Human	AGAGAGGAGGAG GTGGTGTAAAGC	ACCCACCCCTCC TTGAC	Promoter
<i>MMP12</i>	Human	CAGACGACATGG ATCAATTAGC	GTAGGATAGGTG GACGTAGAGGC	Promoter
<i>IL6</i>	Human	CGTGCATGACTTC AGCTTTAC	TGCAGCTTAGGTC GTCATTG	Promoter
<i>CCL2</i>	Human	CCGAGAGGCTGA GACTAACC	CTATGAGCAGCA GGCACAGA	Promoter
<i>IL6</i>	Human	TAGAGCTTCTCTT TCGTTCCCGGT	TGTGTCTTGCGAT GCTAAAGGACG	NFkB, cJUN bs (Gomard et al., 2010).
<i>CCL2</i>	Human	CCTGGAAATCCAC AGGATGC	CGAGAGTGCAG CTTCAG	NFkB, cJUN bs (Sutcliffe et al., 2009).
<i>MMP3</i>	Human	CATCAAAGGAAT GGAGAACC	GACAGAGGTTTC ACTATGTTGC	NFkB bs (Borghaei et al., 2004).

[‡]bs, binding site. Promoter = within 500bp of transcriptional start site.

2.6 ChIP for histone modifications

Cultured VSMCs and *ex vivo* tissue from the medial layer of the aorta were washed in PBS and fixed in 1% formaldehyde in PBS for 10 minutes at room temperature before quenching with 0.125 mM glycine for 5 minutes. Subsequently, the cells/tissue were washed three times in PBS. *Ex vivo* tissue was snap frozen and homogenised using a metal mortar. The cells/homogenised tissue were resuspended in nuclear lysis buffer (50 mM Tris-HCl pH 8.1, 10 mM EDTA pH 8.0, 1% SDS) supplemented with protease inhibitors (Roche) and incubated on ice for a minimum of 5 minutes.

A Bioruptor Pico sonication device (Diagenode) set at high power, 30 seconds on and 30 seconds off for 15 to 20 cycles, was used to fragment the chromatin to approximately 0.2-1 kb. The sonicated chromatin was centrifuged at 12,000 g at 4 °C for 15 minutes to remove insoluble debris. The DNA concentration was determined using a Nanodrop ND-1000 spectrometer. Fragmentation of chromatin was confirmed by Bioanalyzer analysis (DNA High Sensitivity Analysis Kit, Agilent Technologies) of a 0.5 µg aliquot after de-cross-linking. To de-cross link, the 0.5 µg aliquots were incubated in elution buffer (20 mM Tris-HCl pH8.0, 5mM EDTA pH 8.0, 50 mM NaCl, 1% SDS, 50 µg/ml Proteinase K, 100 µg/ml RNase A) at 37 °C for an hour and then at 68 °C overnight.

Sonicated chromatin (2-20 µg) was incubated with the appropriate antibodies (Table 8) or control IgG (IgG of the same species as the primary antibody) with BSA (100 µg/ml) and yeast tRNA (20 µg/ml), diluted 10x in RIPA-140 (10 mM Tris-HCl pH 7.5, 1 mM EDTA pH 8.0, 0.5 mM EGTA, 1% Triton X-100, 0.10% SDS, 0.10% sodium deoxycholate, 140 mM NaCl) supplemented with protease inhibitors (Roche), overnight at 4 °C. 10% of the chromatin used for each ChIP was directly de-cross-linked as described above. 600 µg of protein A and protein G magnetic beads (Life Technologies), washed twice in RIPA-140 buffer were added to the samples and incubated at 4 °C on a rotating wheel for 2 hours. Samples were then washed twice in RIPA-140, twice in RIPA-500 (10 mM Tris-HCl pH 7.5, 1 mM EDTA pH 8.0, 0.5 mM EGTA, 1% Triton X-100, 0.10% SDS, 0.10% sodium deoxycholate, 500 mM NaCl), RIPA-LiCl (10 mM Tris-HCl pH 7.5, 1 mM EDTA pH 8.0, 0.5 mM EGTA, 1% Triton X-100, 0.10% SDS, 0.10% sodium deoxycholate, 250 mM LiCl) and twice in TE (10 mM Tris-HCl pH 8.1, 1 mM EDTA pH 8.0) before being resuspended in 200 µl of elution buffer. Samples were incubated in elution buffer at 37 °C for an hour and then 68 °C overnight. The gDNA samples were purified using a gel extraction kit (Qiagen) following the manufacturer's protocol and eluted in 50-100 µl of TE. The purified gDNA was analysed by RT-qPCR as described in section 2.5.

Table 8: Antibodies used for ChIP of histone modifications

Protein	Size	Species [‡]	mg/ml	Dilution	Product ID
H3K9me2	17 kDa	Mouse mAb	1	1:150	Abcam (#ab1220)
H3K4me3	17 kDa	Rabbit pAb	1	1:300	Abcam (#ab8580)
H3K27me2/3	17 kDa	Mouse mAb	1	1:150	Active Motif (#39535)

[‡]mAb, monoclonal antibody; pAb, polyclonal antibody.

2.7 UNC0638 (UNC)/SP600125/IL-1 α /TNF α treatment

Mouse and human VSMCs were seeded in 12-well plates in growth medium at a ratio of 1:2. When the cells became 70 % confluent the medium was changed to chemically defined medium (CDM; 1:1 mixture of Iscove's modified Dulbecco's medium plus Ham's F-12 medium, both supplemented with GlutaMAX (Gibco, Life technologies), 5 mg/ml bovine serum albumin, 450 μ M monothioglycerol, 15 mg/ml Transferrin, 7 mg/ml Insulin, 1 x lipids (100 x chemically defined lipid concentrate, Gibco Life Technologies), 1 x penicillin/streptomycin (100 x penicillin/streptomycin, Gibco Life Technologies). 24 hours later the medium was replaced with CDM with 1 μ M UNC0638 (Tocris) and/or 10 μ M SP600125 (Abcam) or vehicle control DMSO, a further 24 hours later this was refreshed. After 48 hours of UNC0638/SP600125/UNC0638+SP600125/DMSO treatment, 2 ng/ml of human recombinant IL-1 α (Peprotech) or 90 ng/ml of human recombinant TNF α (Peprotech) was added to the appropriate wells. After 6 hours of IL-1 α or TNF α stimulation, unless otherwise indicated in the figure legends, the cells were washed twice with PBS before harvest. To harvest, cells were dissociated with Trypsin (Sigma Aldrich) and washed twice with PBS. Cell pellets were frozen at -80°C.

Cytotoxicity of small molecule inhibitors (UNC0638, SP600125) was assessed after VSMCs were treated as described above with a hemocytometer and Trypan Blue staining (T8154, Sigma Aldrich) or MTT cell viability assay (V13154, ThermoFisher Scientific). Neither UNC0638 and SP600125 alone or in combination led to significant loss of cell viability compared to vehicle control.

2.8 DQ-gelatin ECM degradation assay

Immediately after UNC0638 and/or IL-1 α treatment of primary mouse VSMCs, 1 ml of 50 μ g/ml of DQ-gelatin (ThermoFisher Scientific), dissolved in CDM, was added per 9.5 cm² well. After 2 hours of DQ-gelatin treatment the cells were washed twice in CDM before incubating with 300 nM of DAPI in PBS for 2 minutes. The cells were then washed once with PBS and mounted in VECTASHIELD Antifade mounting medium (Vector laboratories).

Degradation-induced fluorescence was used to measure MMP activity. The DQ-gelatin treated VSMCs were imaged using a 20x objective with a fluorescence microscope (ZEISS Axio Vert A.1). The corrected total fluorescence (CTF) was quantified using ImageJ software as follows; CTF = [(area x mean pixel intensity) - (area x mean pixel intensity of 5 background readings)]/ cell number. Cell numbers were determined by counting DAPI stained nuclei. The average CTF of 5 fields of view was used to quantify the MMP activity of each sample to limit variability.

2.9 FACS of lineage labelled VSMCs

Labelled tamoxifen injected Myh11-CreERT2, ROSA26-EYFP+ male mice were culled by CO₂ asphyxiation. Carotid arteries were removed, dissected free from adipose and connective tissue and digested in 2.5 mg/ml of Collagenase Type IV (Life Technologies) and 2.5 U/ml of porcine pancreatic elastase (Worthington) in DMEM at 37 °C, 5 % CO₂ (0.5 ml per carotid artery) for approximately 2 hours, mixing every 20 minutes, until a single cell suspension was reached. The dissociated cells were washed once in PBS, resuspended in 1 % BSA in PBS, filtered through a 40 μ m cell strainer and index-sorted on an Aria-fusion flow cytometry-assisted cell sorter (BD Bioscience) with help from the NIHR Cambridge BRC Cell Phenotyping Hub. Isolated EYFP+ cell pellets were resuspended in 500 μ l of TRIzol and stored at -80°C.

2.10 RT-qPCR analysis of mRNA levels from lineage labelled YFP+ VSMCs isolated by FACS

Total RNA was extracted with TRIzol and cleaned using a RNeasy Micro Kit (Qiagen) following the manufacturer's instructions. RNA integrity was analysed using an Agilent 2100 Bioanalyzer and RNA 6000 Pico Kit (Agilent Technologies). 2.5 ng of total RNA with a RIN value >8 was reverse transcribed using a QuantiTect Reverse Transcription kit (Qiagen), according to the manufacturer's directions. For quantification, cDNA (diluted 1:4) was amplified, in technical duplicates, with a QuantiTect SYBR Green PCR kit (Qiagen) and primer pairs listed in Table 4, using a Corbett Life Science Rotor Gene

6000 PCR system. RT-qPCR-obtained values were normalised to the average of two housekeeping genes (HMBS and YWHAZ or HPRT1).

2.11 Tissue processing for immunofluorescent staining

Mice were culled by CO₂ asphyxiation. The arteries were removed and dissected free from adipose and connective tissue, fixed with 4% (v/w) paraformaldehyde (Sigma-Aldrich) in PBS for 20 minutes at room temperature, washed for 5 minutes in PBS, incubated in 30% sucrose in PBS at 4 °C overnight. Tissue was then transferred to a 50:50 solution of 30% sucrose in PBS: O.C.T (VWR) for one hour at room temperature before a final incubation of 1 hour in O.C.T. Samples were then embedded in O.C.T using plastic molds and frozen using dry ice before storage at -80 °C. The arteries were then cut transversely into 14 µm thick sections, mounted on SuperFrost Plus Adhesion microscope slides (Thermo Scientific) and stored at -80 °C.

2.12 Immunofluorescent staining of cryosections

Serial cryosections were rinsed in PBS, permeabilised in 0.5 % Triton x-100 in PBS for 30 minutes at room temperature and blocked for 1 hour at room temperature in 1% BSA, 10 % normal goat serum, 0.1 % Triton x-100 in PBS. Sections were then incubated with anti-H3K9me2 antibody conjugated to Alexa Fluor-647 (1:100 ab203851, Abcam) in blocking buffer overnight at 4 °C. The sections were then washed twice for 5 minutes in PBS before staining the nuclei with 300 nM of DAPI in PBS for 10 minutes. The sections were then washed twice in PBS and mounted in RapiClear 1.52 (Sunjinlab).

2.13 Imaging and image processing of immunofluorescent stained cryosections

Immunofluorescent stained cryosections were imaged using confocal laser scanning microscopy (Leica SP5 or SP8) with laser lines and detectors set for maximal sensitivity without spectral overlap for DAPI (405 laser, 417-508 nm), CFP (458 laser, 454-502 nm), GFP (488 laser, 498-506 nm), YFP (514 laser, 525-560 nm), RFP (561 laser, 565-650 nm) and Alexa Fluor 647 (633 laser, 650-700 nm). Cryosections were imaged using a 20x oil objective, and data were acquired at an optical section resolution of 1024 x 1024. Image stacks were collected over a 12 µm stack thickness with 1 µm z-steps.

VSMCs were identified by fluorescent Myh11-lineage labelling and their nuclei defined by DAPI staining. Ten individual Myh11-lineage labelled nuclei were chosen per cryosection with Alexa Fluor 647 omitted to eliminate bias. Three cryosections per CCA were analysed to limit variability due to

the immunofluorescent staining protocol itself. ImageJ software was used to measure the mean pixel intensity of H3K9me2-Alexa Fluor 647 staining of each Myh11-lineage labelled nuclei to denote H3K9me2 signal. H3K9me2 signal of each Confetti+ or EYFP+ nucleus is relative to the average Confetti+ or EYFP+ nuclear mean H3K9me2 signal of the control samples.

2.14 G9A siRNA knock down

300,000 cultured human VSMCs were plated per well of a 6-well plate in VSMC growth medium. 8 hours after plating the medium was changed to CDM BSA without penicillin/streptomycin. 24 hours after plating, the cells were transfected with either a 100 nM pool of siRNA targeted against G9A (sc-43777, Santa Cruz) or a 100 nM pool of control scrambled siRNA (sc-37007, Santa Cruz) using HiPerfect transfection reagent (Qiagen), following the manufacturer's protocol (12 μ l of HiPerfect was used per transfection). 48 hours after transfection the cells were treated with or without 2ng/ml of human recombinant IL-1 α (Peprotech) before harvest 6 hours later. To harvest, cells were dissociated with Trypsin (Sigma) and washed twice with PBS. Cell pellets were frozen at -80 $^{\circ}$ C.

2.15 ChIP for NFkB-p65 and AP-1-cJUN

3 to 4 million cultured human VSMCs were used per ChIP. Human VSMCs were washed in PBS and fixed with 1% formaldehyde and Cross-link gold (Diagenode) following the manufacturers protocol. Fixed cells were incubated at room temperature for 30 minutes, then quenched with 0.125 M glycine for 15 min at room temperature. The cells were then lysed using buffers from the iDeal ChIP-seq Kit for Transcription Factors (Diagenode), following the manufacturer's instructions. The chromatin was sheared using a Bioruptor Pico sonication device (Diagenode) set at high power, 30 seconds on and 30 seconds off for 20 cycles, to fragment the chromatin to approximately 0.2-1 kb. Fragmentation of chromatin was confirmed by Bioanalyzer analysis (DNA High Sensitivity Analysis Kit, Agilent Technologies) of a 0.5 μ g aliquot after de-cross-linking. To de-cross-link, the 0.5 μ g aliquots were incubated in elution buffer (20 mM Tris-HCl pH8.0, 5mM EDTA pH 8.0, 50 mM NaCl, 1% SDS, 50 μ g/ml Proteinase K, 100 μ g/ml RNase A) at 37 $^{\circ}$ C for an hour and then at 68 $^{\circ}$ C overnight. Chromatin immunoprecipitation was carried out using an iDeal ChIP-seq Kit for Transcription Factors (Diagenode), using the appropriate antibodies (Table 9) or control IgG, according to the manufacturer's protocol. The gDNA samples were purified using iPure magnetic beads (Diagenode) and eluted in 40 μ l of the elution buffer provided in the iDeal ChIP-seq Kit for Transcription Factors. The purified gDNA was analysed by RT-qPCR as described in section 2.5.

Table 9: Antibodies used for ChIP for NFkB-p65 and AP1-cJUN

Protein	Size	Species [‡]	mg/ml	Dilution	Product ID
NFkB-p65	64 kDa	Rabbit pAb	ND	1ul per IP	Diagenode (#C15310256)
cJUN	43 kDa	Rabbit pAb	1	5µg per IP	Abcam (#ab31419)

[‡] pAb, polyclonal antibody; ND, not determined.

2.16 NFkB-p65 immunofluorescent staining of cultured VSMCs

Primary human VSMCs were treated with 1 µM UNC0638 or vehicle control DMSO for 48 hours as previously described before being stimulated with 2 ng/ml of IL-1α or 90 ng/ml of TNFα for one hour. The cells were then washed twice with PBS and fixed with 4 % paraformaldehyde for 10 minutes at room temperature. Cells were subsequently incubated with 0.5 % Triton-X100 (Sigma) for 20 minutes at room temperature before being washed three times with PBS and blocked with 10% normal goat serum (Dako) in PBS for 1 hour at room temperature. Cells were then incubated with NF-kB p65 antibody diluted 1:100 in blocking buffer (sc-372, Santa Cruz) for 2 hours at room temperature before being washed three times with blocking buffer. The cells were then incubated with Alexa-Fluor488-conjugated goat anti-rabbit IgG (ab150077, Abcam) diluted 1:1000 in blocking buffer at room temperature for 1 hour and washed twice with PBS. After incubating the cells with 300 nM of DAPI in PBS for 2 minutes, the cells were washed once with PBS and mounted in VECTASHIELD Antifade mounting medium (Vector laboratories).

The staining specificity was determined by omitting the primary antibody. The cells were imaged using a 10 x objective with a fluorescent microscope (ZEISS Axio Vert A.1). The nuclear/cytoplasmic ratio of p65 was measured using ImageJ software (http://dev.mri.cnrs.fr/projects/imagej-macros/wiki/Intensity_Ratio_Nuclei_Cytoplasm_Tool). The nuclear/cytoplasmic ratio measures the mean grey value of nuclear area defined by DAPI divided by the mean grey value of the cytoplasmic area. The average nuclear/cytoplasmic p65 ratio of 3 fields of view was used to calculate the nuclear/cytoplasmic ratio of p65 of each sample to limit variability.

2.17 Statistics.

Data are expressed as mean ± SEM of ≥3 independent experiments (indicated in figure legends). unpaired student t-tests or, if groups were larger than two, one-way ANOVA with *Bonferroni* correction were performed to determine significance using GraphPad Prism 4.02 (GraphPad Software, Inc., La Jolla, CA, USA). Nested ANOVA was applied to immunofluorescence data sets

where multiple measurements per sample were available. Changes were accepted to be significant when the P-value was below 0.05.

**CHAPTER 3 - RESULTS: Assessing the role of
H3K9me2 in maintaining the contractile VSMC state.**

3.1 Introduction

VSMCs are highly differentiated and specialised yet retain the capacity to undergo profound and reversible changes in phenotype. Such VSMC phenotypic switching directly contributes to the development and progression of cardiovascular disease, the leading cause of death worldwide. In response to injury or inflammation, VSMCs downregulate contractile proteins and upregulate genes associated with vascular remodelling, including matrix metalloproteinases (MMPs) and pro-inflammatory cytokines. However, the epigenetic mechanisms which regulate these changes in gene expression remain unclear.

H3K9me2, an epigenetic mark associated with transcriptional repression (Hublitz et al., 2009; Peters et al., 2003; Tachibana et al., 2005; Wen et al., 2009), has been reported to influence smooth muscle cell behaviour (Yang et al., 2012), cell fate commitment (Cloos et al., 2008) and cell reprogramming (Chen et al., 2013). H3K9me2 is found both at isolated regions near genes and in large megabase blocks, termed Large Organised Chromatin K9 domains. These H3K9me2-marked domains cover up to 46% of the genome in terminally differentiated cell types compared to only 4% in embryonic stem cells (Wen et al., 2009), prompting speculation over the role of H3K9me2 in maintaining cell identity. In support of this theory, bulk levels of H3K9me2 appear to diminish during epithelial-mesenchymal transition, a process in which cells acquire stem cell like properties (McDonald et al., 2011). Furthermore, hematopoietic stem and progenitor cells display lower global H3K9me2 levels compared to mature bone marrow cells (Li et al., 2018). These observations suggest that H3K9me2 deposition is patterned according to cell identity and must be reset to specify new fates. In support of this notion, global loss of H3K9me2 has been shown to improve the reprogramming efficiency of human cells by heterochromatin relaxation and facilitating transcription factor binding (Chen et al., 2013; Rodriguez-Madoz et al., 2017).

Interestingly, H3K9me2 inhibition attenuates the contractility of different smooth muscle cell types (Yang et al., 2012) and reduced levels of H3K9me2 have been observed in VSMCs from human atherosclerotic lesions compared to healthy aortic tissue in patients (Greißel et al., 2015). Collectively, these findings indicate H3K9me2 could be involved in maintaining the contractile VSMC state, a role that has not been explored. Expression levels of contractile marker genes gradually decrease when VSMCs are cultured (Rensen et al., 2007). Therefore, I will compare H3K9me2 levels in *ex vivo* VSMCs directly isolated from mouse aorta to cultured murine VSMCs. VSMCs are also known to downregulate contractile genes in response to inflammation and/or injury (Rensen et al., 2007). Therefore, I will use VSMC-lineage labelled mice, as described in section 1.9.1, to assess global

levels of H3K9me2 in VSMCs within ligated and atherosclerotic common carotid arteries (CCAs) compared to those within control tissue.

Aims:

1. Assess global changes in H3K9me2 upon loss of the contractile VSMC state using *in vitro* and *in vivo* models of VSMC phenotypic switching.
2. Assess local levels of H3K9me2 at contractile VSMC genes upon loss of the contractile VSMC state using an *in vitro* model of VSMC phenotypic switching and chromatin immunoprecipitation.
3. Test the functional role of H3K9me2 on contractile VSMC gene expression *in vitro* using small molecule inhibition of the main H3K9 di-methyltransferases G9A/GLP.

3.2 Results

3.2.1 Global levels of H3K9me2, and the associated histone methyltransferase GLP, are reduced in cultured relative to ex vivo VSMCs, concomitant with loss of the contractile state.

To test whether global levels of H3K9me2 are affected by VSMC state, mouse VSMCs (mVSMCs) freshly isolated from the aortic media (*ex vivo*) were compared to those cultured for four passages (Figure 3.1).

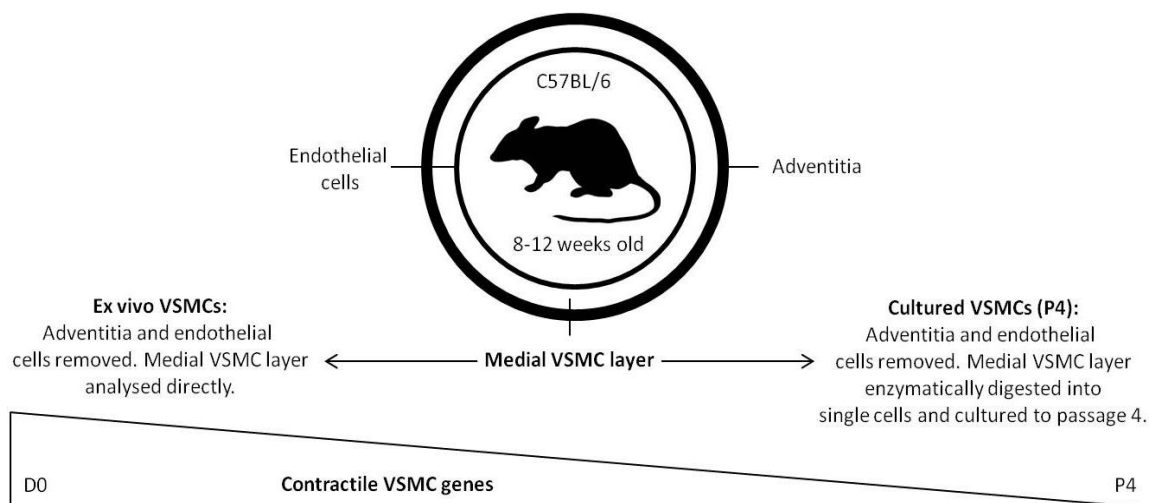


Figure 3.1: Schematic of *in vitro* model of VSMC phenotypic switching. The medial VSMC layer from 8-12 week old C57BL/6 mice was freshly isolated from the aortic media (*ex vivo*) and compared to enzymatically digested medial VSMC layer cultured to passage 4. The triangle represents loss of contractile VSMC gene expression upon culture.

Upon culture, mVSMCs downregulate contractile VSMC genes encoding structural (*Cnn1*, *Tagln*, *Acta2* and *Smtn*) and regulatory proteins (*Myocd*) (Figure 3.2 A). Interestingly, western blot analysis revealed a 5-fold reduction of H3K9me2 in cultured compared to *ex vivo* mVSMCs (Figure Figure 3.2 B, C). H3K9me2 is catalyzed by the G9A/GLP enzymatic complex (Shinkai and Tachibana, 2011). Loss of H3K9me2 was accompanied by a decrease in GLP at both the protein (98-fold) (Figure 3.2 B-D) and mRNA level (2.4-fold) (Figure 3.2 D). In contrast, *G9a* mRNA showed a modest increase in cultured compared to *ex vivo* mVSMCs (1.6-fold) (Figure 3.2 D), and no difference in G9A protein levels was observed (Figure 3.2 B, C). RT-qPCR analysis revealed that histone demethylases (HDMs) targeting H3K9me2 were either downregulated upon mVSMC culture or not expressed in *ex vivo* or cultured mVSMCs (Figure 3.2 D). Taken together, these results imply that H3K9me2 is reduced upon loss of the contractile VSMC state, which is perhaps explained by repression of GLP, suggesting H3K9me2 is involved in regulating VSMC-phenotype.

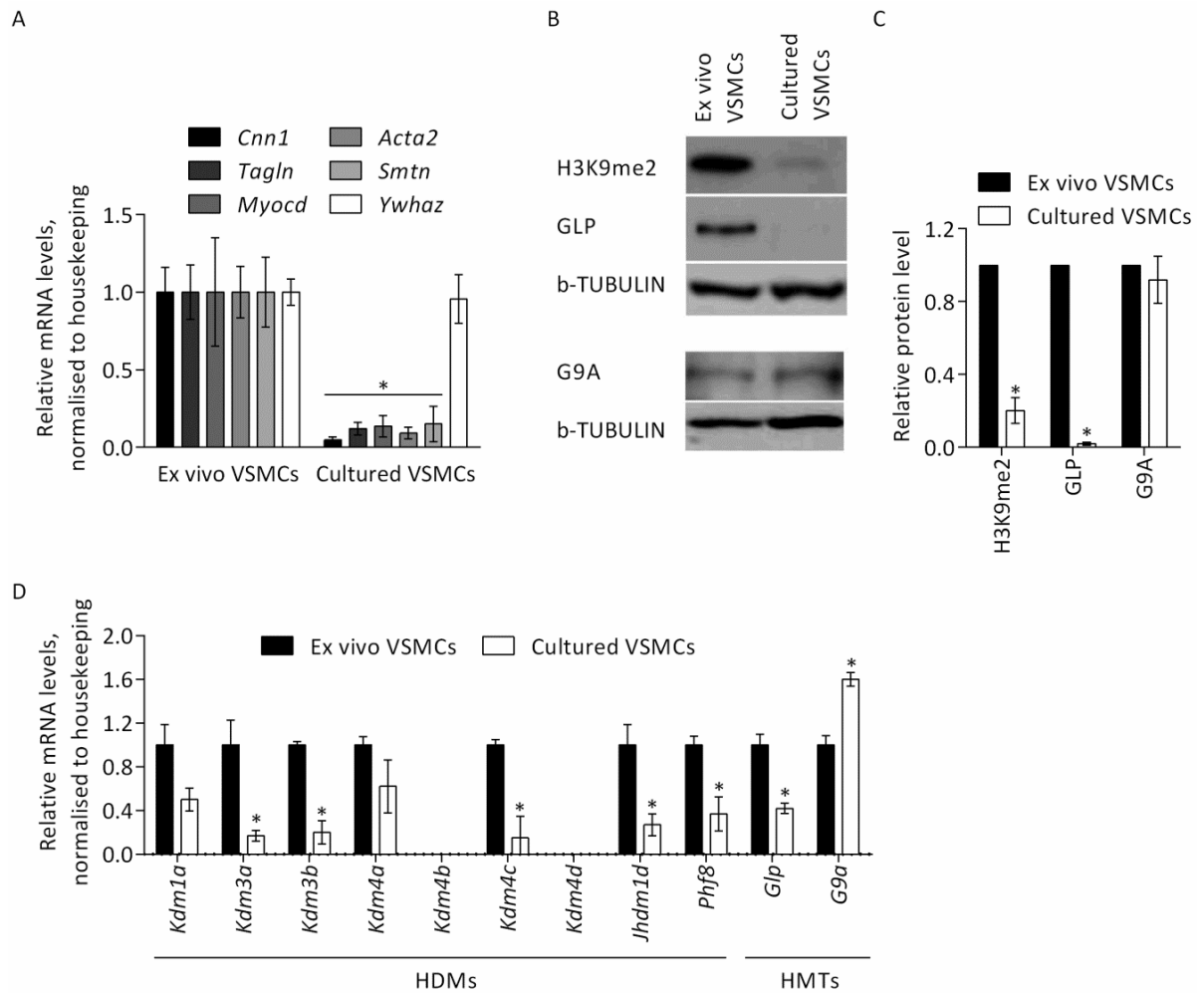


Figure 3.2: Global levels of H3K9me2 are reduced upon culture-induced VSMC phenotypic switching. (A) RT-qPCR analysis of contractile VSMC gene expression in *ex vivo* compared to cultured mVSMCs. Data are relative to *ex vivo* mVSMCs and normalised to the average of two housekeeping genes (*Hprt1* and *Ywhaz*). Data represent means \pm SEM of 4 biological replicates. Asterisks indicate significant differences ($P < 0.05$) in expression level in cultured versus *ex vivo* mVSMCs by unpaired student's t test. (B, C) Representative western blot (B) and densitometric analysis (C) of H3K9me2, GLP and G9A in *ex vivo* and cultured mVSMCs. Data are relative to *ex vivo* mVSMCs and normalised to b-TUBULIN. Data represent means \pm SEM of 4 biological replicates. Asterisks indicate significant differences ($P < 0.05$) in protein level in cultured versus *ex vivo* mVSMCs by unpaired student's t test. (D) RT-qPCR analysis of known histone demethylases (HDMs) and histone methyltransferases (HMT) which target H3K9me2 in *ex vivo* and cultured mVSMCs. Data are relative to *ex vivo* mVSMCs and normalised to the average of two housekeeping genes (*Hprt1* and *Ywhaz*). Data represent means \pm SEM of 3 to 7 biological replicates. $n = 4$ for *Kdm1a*, *Kdm3a*, *Kdm3b*, *Kdm4a*, *Kdm4b*, *Kdm4c*, *Kdm4d*, *Jhdm1d* and *Phf8* $n = 4$, $n = 7$ for *Glp* and $n = 3$ for *G9a*. Asterisks indicate significant differences ($P < 0.05$) in expression level in cultured versus *ex vivo* mVSMCs by unpaired student's t test.

3.2.2 Assessing the role of H3K9me2 in VSMC phenotypic switching using *in vivo* mouse models of CVD.

In vivo models of cardiovascular disease were used to investigate the role of H3K9me2 in VSMC phenotypic switching. VSMCs were genetically labelled by combining the Myh11-CreERT2 transgene (Wirth et al., 2008), which is specifically expressed by mature VSMCs, with the multi-colour ROSA26-Confetti or single colour ROSA26-EYFP reporter (Gomez and Owens, 2012). Both Myh11-CreERT2/ROSA26-Confetti and Myh11-CreERT2/ROSA26-EYFP mice were used to make use of extra tissue generated by Dr Joel Chappell from previous experiments and comply with the 3R's of animal research. Recombination was induced in healthy mice with a pulse of tamoxifen, which results in stable fluorescent protein expression (Nemenoff et al., 2011; Wirth et al., 2008). Expression of the lineage reporter was specific to cells in the medial layer of the vasculature (Chappell et al., 2016; Gomez and Owens, 2012), where the recombination efficiency was 70-95% for the Confetti reporter (Chappell et al., 2016) and 40-60% for the EYFP reporter (Dobnikar et al., 2018). Importantly, the specific fluorescent label was stably transferred to all progeny after VSMC proliferation independent of the expression status of the Myh11-CreERT2 transgene (Chappell et al., 2016).

3.2.2.1 Global levels of H3K9me2 are reduced in VSMCs upon vascular injury, concomitant with loss of the contractile state.

The carotid ligation-injury mouse model of CVD rapidly elicits vessel growth and remodelling concomitant with changes in VSMC gene expression, including decreased expression of contractile VSMC genes (Ali et al., 2013; Herring et al., 2017; Kumar and Lindner, 1997a). Therefore, this method was used to explore whether global levels of H3K9me2 are reduced upon loss of the contractile VSMC state. After tamoxifen labelling Myh11-CreERT2/ROSA26-Confetti or Myh11-CreERT2/ROSA26-EYFP animals, the left common carotid artery (CCA) was ligated and tissues were harvested 1, 3, 5, 7 and 28 days later (Figure 3.3).

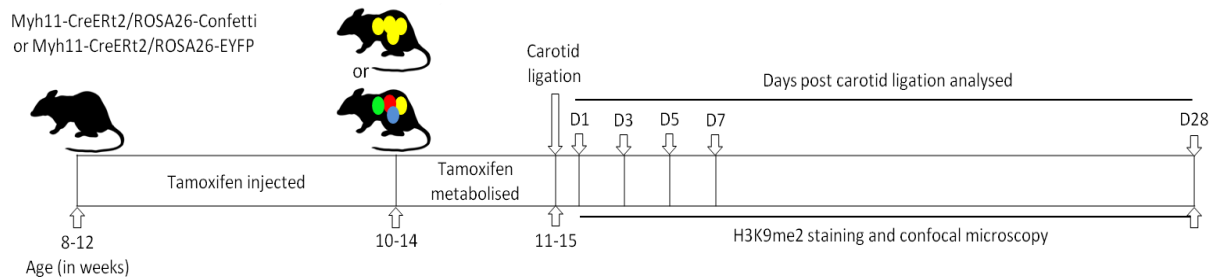


Figure 3.3: Schematic of the mouse carotid ligation model of vascular injury. The left common carotid artery (CCA) was ligated in tamoxifen labelled 10-14-week-old male Myh11-CreErt2+/ROSA26-Confetti+ (CFP, YFP, RFP, GFP) or Myh11-CreErt2+/ROSA26-EYFP+ mice, and tissues were harvested 1, 3, 5, 7 or 28 days later (D1-28).

Immunofluorescence staining of CCA cryosections revealed global levels of H3K9me2 were significantly reduced in the nuclei of cells expressing the Confetti (Confetti+) or EYFP reporter, which are derived from Myh11-expressing VSMCs, seven days following carotid ligation injury compared to no surgery controls (Figure 3.4 A, B). To assess the timing of this vascular injury-induced downregulation of H3K9me2 in VSMCs, H3K9me2 signal in Confetti+ or EYFP+ nuclei were also analysed 1, 3, 5 and 28 days post carotid ligation. Both 1- and 3-days post ligation, H3K9me2 levels in Confetti+ and EYFP+ nuclei from ligated CCAs appeared unchanged compared to those within non-ligated internal control CCAs (Figure 3.4 C). However, levels of H3K9me2 in Confetti+ and EYFP+ nuclei began to fall 5 days post ligation (Figure 3.4 C) and were significantly reduced 7 days post surgery (Figure 3.4 B). Levels of H3K9me2 in Confetti+ and EYFP+ nuclei appeared downregulated to the same level 28 days post surgery as those within 7 day post carotid ligation CCAs compared to non-ligated controls (Figure 3.4 C). Previous studies have shown that contractile VSMC genes are rapidly downregulated upon vascular injury and are dramatically reduced 7 days post carotid ligation compared to non-ligated controls (Herring et al., 2014; Herring et al., 2017; Sayers et al., 2008; Shi et al., 2013). However, studies have reported that contractile VSMC genes become upregulated again around 9 to 28 days post carotid ligation surgery (Allagnat et al., 2016; Shi et al., 2013). Therefore, even though H3K9me2 levels appear reduced upon loss of the contractile VSMC state but H3K9me2 may not directly influence the expression of contractile VSMC genes.

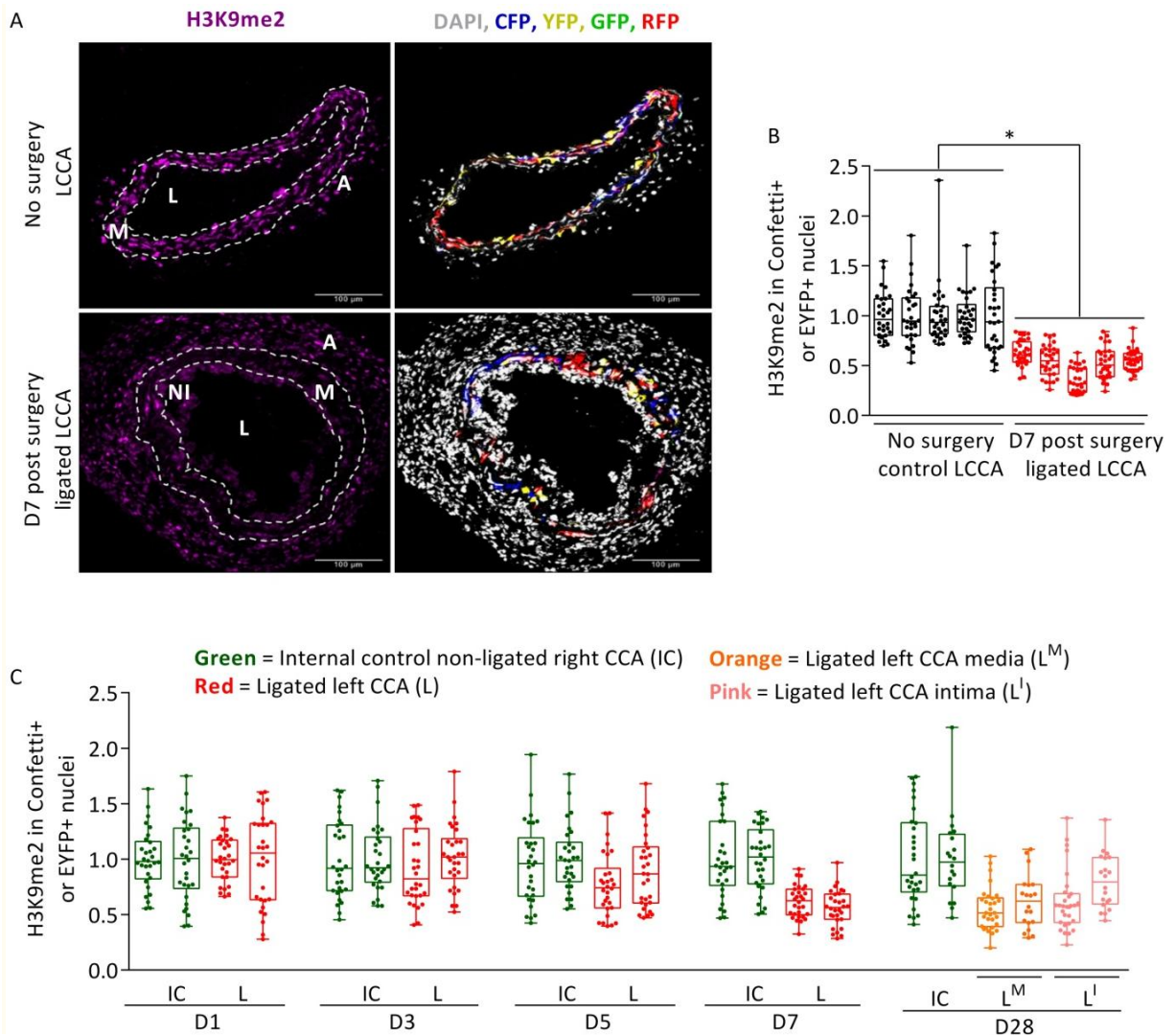


Figure 3.4: Global levels of H3K9me2 are reduced in VSMCs upon vascular injury. (A) Immunofluorescence staining for H3K9me2 in representative 12 μm LCCA cryosections from ligated (D7 post surgery) and non-ligated control mice. Signals for H3K9me2-Alexa Fluor 647 (magenta), Confetti reporter proteins (red, blue, yellow, green) and nuclei counter stained with DAPI (white) are shown. Scale bars, 100 μm . A, adventitia; NI, neo-intima; M, media; L, Lumen. White dashed lines outline the media as determined by auto-fluorescence of the inner and outer elastic lamina. **(B)** Box plot showing H3K9me2 signal in Confetti+ or EYFP+ VSMC nuclei as determined by immunofluorescence analysis of LCCAs from ligated (D7 post surgery) and non-ligated control mice. $n = 5$ animals per group. The asterisk indicates significant difference ($P < 0.05$) in H3K9me2 levels in ligated versus no surgery control by nested ANOVA testing. **(C)** Box plot showing H3K9me2 signal in Confetti+ or EYFP+ VSMC nuclei as determined by immunofluorescence analysis of ligated left (L) and non-ligated right internal control (IC) CCAs. At D28, the HK9me2 signal was quantified separately for the media (L^M) and intima (L^I). $n = 2$ animals per group. For immunofluorescence analyses, each dot shows H3K9me2 signal intensity in one Confetti+ or EYFP+ nucleus.

3.2.2.2 Global levels of H3K9me2 are reduced in VSMCs within atherosclerotic plaque compared to healthy vascular tissue, concomitant with loss of the contractile state.

H3K9me2 levels in VSMCs were further analysed using a mouse model of atherosclerosis. Myh11-CreERT2/ROSA26-Confetti animals were crossed onto an ApoE^{-/-} background. Recombination was induced in 8-12-week-old animals prior to feeding them either an atherosclerosis-inducing high fat diet (HFD) (21% fat, 0.2% cholesterol) or control safe diet (SD) for 3.5 to 7 months (Figure 3.5).

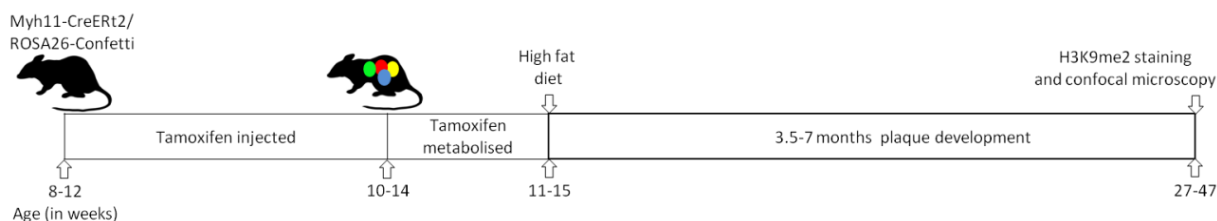


Figure 3.5: Schematic of the mouse model of atherosclerosis. 8-12-week-old Myh11-CreERT2+/ROSA26-Confetti, ApoE^{-/-} male mice were labelled using tamoxifen prior being fed either a safe (SD) or high fat diet (HFD) for 3.5-7 months before the CCAs were harvested.

Western blot analysis comparing the aorta from mice fed a HFD, which contained many visible atherosclerotic lesions, to those from mice fed a SD, which contained little or no plaque, revealed that loss of H3K9me2 upon HFD correlates with reduced expression of MYH11 (Figure 3.6 A, B). Immunofluorescence staining of their LCCAs demonstrated VSMC nuclei within plaque from mice fed a HFD exhibited decreased levels of H3K9me2 compared to medial contractile VSMCs from mice fed a SD (Figures 3.6 C, D). VSMCs within different regions of atherosclerotic plaque are known to express different levels of contractile VSMC genes. For instance, VSMCs within the plaque core express lower levels of contractile VSMC genes compared to those within the media or cap (Bennett et al., 2016; Chappell et al., 2016). Therefore, levels of H3K9me2 in Confetti+ nuclei within the plaque media, core and cap were compared but no significant differences were observed (Figure 3.6 C, D).

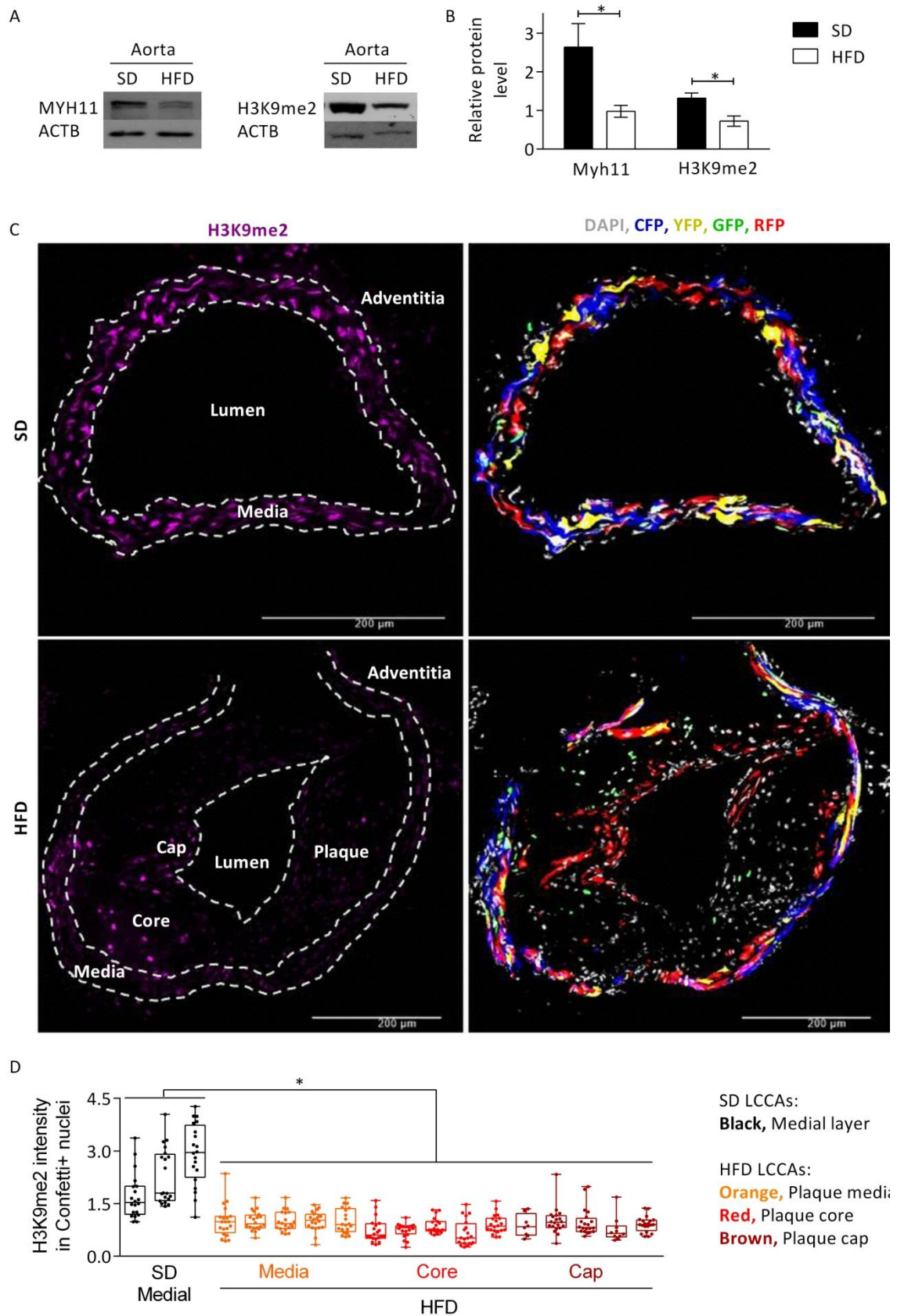


Figure 3.6: Global levels of H3K9me2 are reduced in VSMCs within atherosclerotic lesions compared to healthy vessels. (A, B) Representative western blots (A) and densitometric analysis (B) for MYH11 and H3K9me2 in whole aorta's, with adventitia and endothelial cells removed, from mice either fed a SD (black

bars) or HFD (white bars). Data are normalised to ACTB. Data represent means \pm SEM of 3 biological replicates. The asterisk indicates significant difference ($P < 0.05$) in protein level in HFD versus SD by unpaired student's t test. **(C)** Immunofluorescence staining for H3K9me2 in representative 12 μ m LCCA cryosections from mice fed either a SD or HFD. Signals for H3K9me2-Alexa Fluor 647 (magenta), Confetti reporter proteins (red, blue, yellow, green) and nuclei counter stained with DAPI (white) are shown. Scale bars, 200 μ m. The two outer white dashed lines outline the media as determined by auto-fluorescence of the inner and outer elastic lamina, the third inner dashed lined outlines the DAPI positive plaque. **(D)** Box plot shows H3K9me2 signal in Confetti+ VSMC nuclei as determined by immunofluorescence analysis of LCCAs from mice either fed a SD or HFD. For mice fed a HFD, the HK9me2 signal was quantified separately for the plaque media (orange dots), core (red dots) and cap (brown dots). $n = 3$ animals for SD, $n = 5$ animals for HFD. The asterisks indicate significant differences ($P < 0.05$) in H3K9me2 levels versus SD Medial (black dots) by nested ANOVA testing. Each dot shows H3K9me2 signal intensity in one Confetti+ or EYFP+ nucleus.

3.2.3 H3K9me2 is enriched at contractile VSMC gene promoters upon culture-induced phenotypic switching.

Chromatin Immunoprecipitation (ChIP) was used to analyse local levels of H3K9me2 at contractile VSMC gene promoters in *ex vivo* contractile mVSMCs compared to culture-induced phenotypically switched mVSMCs. H3K9me2 was not present at any of the contractile VSMC gene promoters analysed in *ex vivo* cells (Figure 3.7 A) but was recruited to *Cnn1* and *Myocd* upon culture (Figure 3.7 B), concomitant with their repression (Figure 3.2 A). These findings suggest H3K9me2 enrichment at the promoters of *Cnn1* and *Myocd* could be responsible for the culture-induced repression of these genes. H3K4me3, a mark widely used to identify active gene promoters, was present at contractile VSMC gene promoters in both *ex vivo* and cultured VSMCS albeit at reduced levels (Figure 3.7 C, D), independent of their transcriptional state (Figure 3.2 A). Therefore, H3K4me3 may serve as a mechanism for epigenetic cell lineage memory to enable phenotypically modulated VSMCs to switch back to their contractile state.

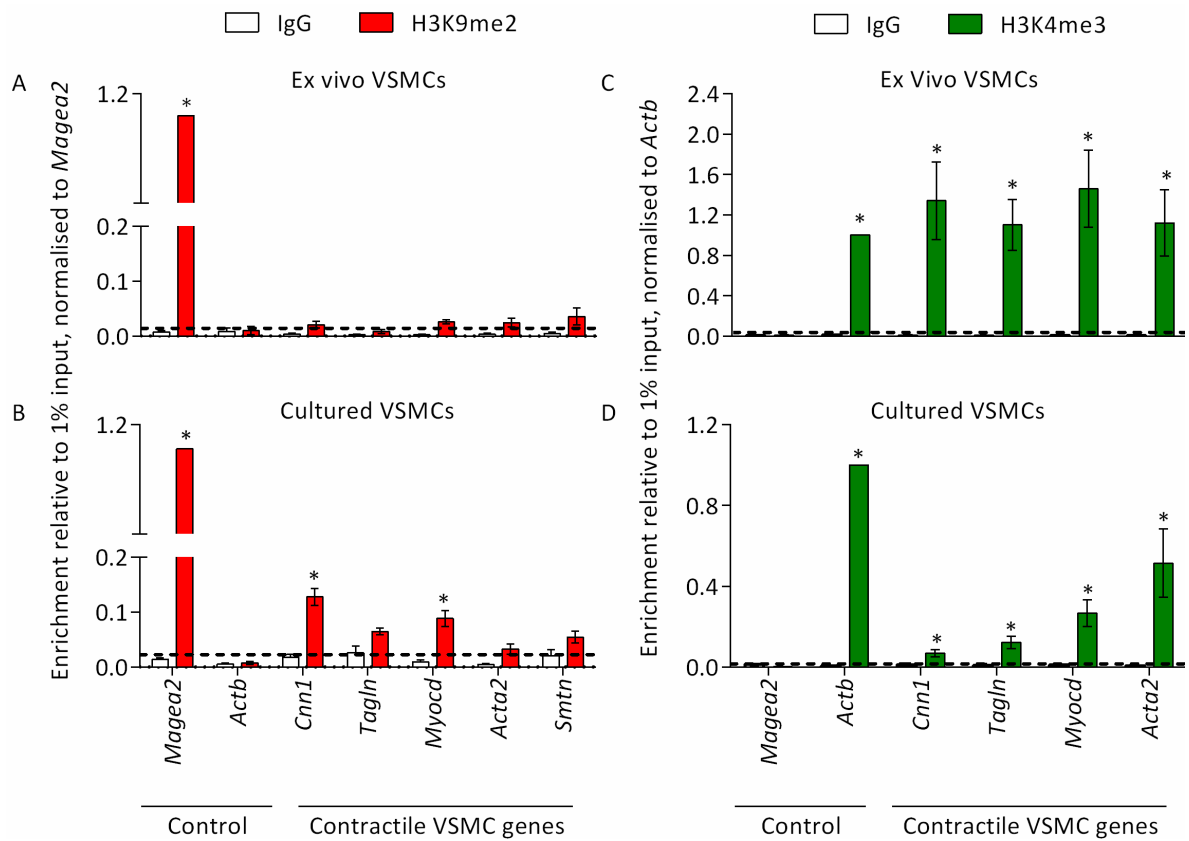


Figure 3.7: Local levels of histone modifications at contractile VSMC gene promoters in *ex vivo* and cultured murine VSMCs. (A, B) ChIP-qPCR analysis for H3K9me2 (red bars) and negative control IgG (white bars) in *ex vivo* (A) and cultured mVSMCs (B) showing levels of enrichment at control *loci* (*Magea2*, positive and *Actb*, negative) and contractile VSMC genes. Data are relative to 1% input and normalised to enrichment at *Magea2* (red bar). Data represent means \pm SEM of 3 to 10 biological replicates. *Ex vivo* mVSMCs: *Magea2* $n = 7$, *Actb* $n = 7$, *Cnn1* $n = 5$, *Tagln* $n = 4$, *Myocd* $n = 7$, *Acta2* $n = 5$, *Smtn* $n = 3$. Cultured mVSMCs: *Magea2* $n = 10$, *Actb* $n = 10$, *Cnn1* $n = 10$, *Tagln* $n = 3$, *Myocd* $n = 10$, *Acta2* $n = 10$, *Smtn* $n = 10$. Background levels of H3K9me2 are based on enrichment in negative control IgG samples and are indicated by a dashed line. Asterisks indicate significant differences ($p < 0.05$) in H3K9me2 levels versus IgG negative control samples by unpaired student's t test. Amanda Dalby performed 4 of these *ex vivo* mVSMC ChIP experiments. (C, D) ChIP qPCR analysis for H3K4me3 (green bars) and negative control IgG (white bars) in *ex vivo* (C) and cultured mVSMCs (D) showing levels of enrichment at control *loci* (*Magea2*, negative and *Actb*, positive) and contractile VSMC genes. Data are relative to 1% input and normalised to enrichment at *Actb* (green bar). Data represent means \pm SEM of 3 biological replicates. Background levels of H3K4me3 are based on enrichment at the *Magea2* negative control *locus* and are indicated by a dashed line. Asterisks indicate significant differences ($P < 0.05$) in enrichment versus IgG negative control samples by unpaired student's t test.

3.2.4 Loss of H3K9me2 accelerates downregulation of contractile VSMC marker genes upon culture.

To assess whether local enrichment of H3K9me2 at the *Cnn1* and *Myocd* promoters regulates the expression of these genes, cultured mVSMCs were treated with UNC0638 (UNC), a small molecule inhibitor of the G9A/GLP methyltransferase, to reduce H3K9me2. UNC treatment resulted in a 4-fold reduction of global H3K9me2 levels (Figure 3.8 A, B) and effectively eliminated H3K9me2 levels locally at contractile VSMC gene promoters (Figure 3.8 C). Compared to mVSMCs directly isolated from tissue, initial culture of mVSMCs in serum (P0) resulted in a marked reduction in expression of contractile genes, with a further reduction on subsequent passage (Figure 3.8 D). Interestingly, loss of H3K9me2 did not relieve repression of *Cnn1*, *Myocd* and other contractile VSMC genes in freshly cultured cells (P0) or after prolonged culture (P4), but instead exacerbated the culture-induced decrease in expression levels (Figure 3.8 D).

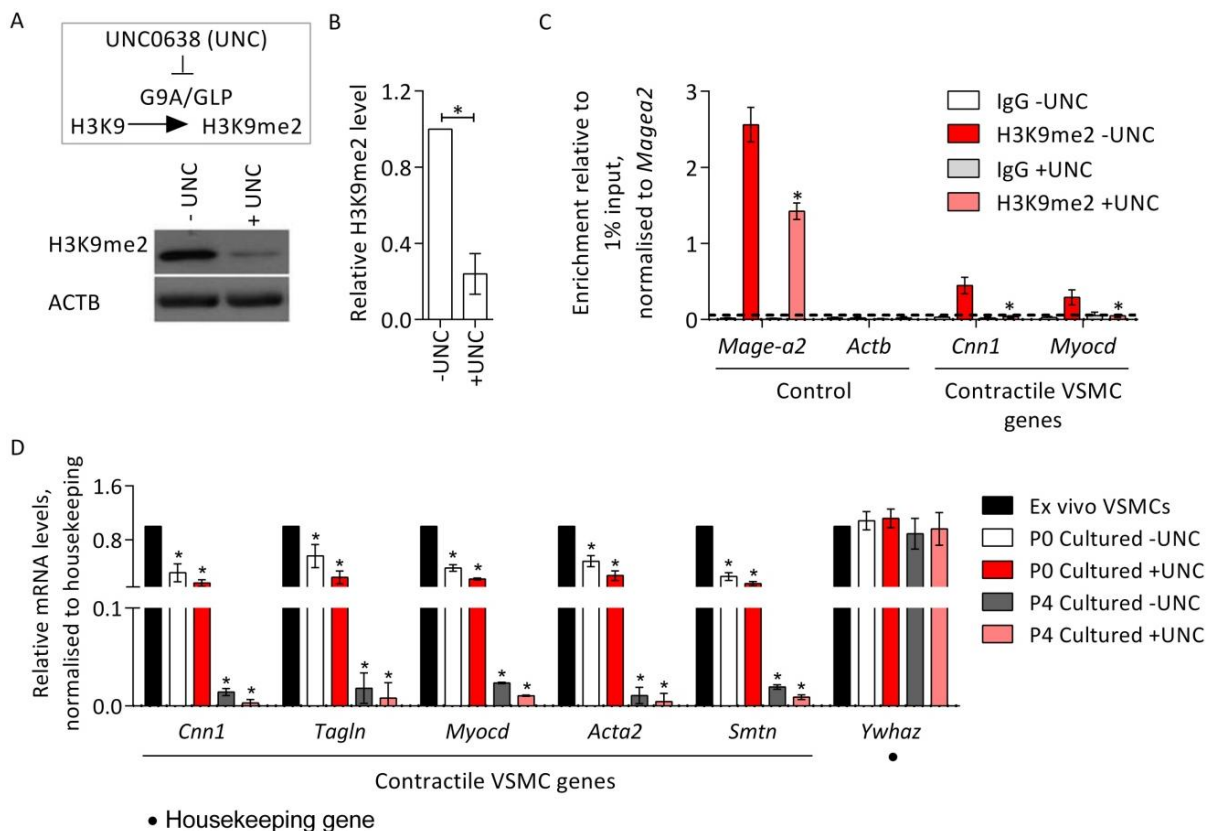


Figure 3.8: Loss of H3K9me2 accelerates downregulation of contractile VSMC marker genes. (A, B) Representative western blot (A) and densitometric analysis (B) of H3K9me2 levels in untreated control (-UNC) and UNC0638 treated (+UNC) mVSMCs cultured to passage 4 (p4). Data are relative to untreated control (-UNC) mVSMCs and normalised to ACTB. Data represent means \pm SEM of 3 biological replicates. The asterisk indicates significant difference (P<0.05) in H3K9me2 levels in UNC treated (+UNC) versus untreated control (-UNC) mVSMCs by unpaired student's t test. (C) ChIP-qPCR analysis for H3K9me2 in untreated control (-UNC, red bars) and UNC0638 treated (+UNC, pink bars) mVSMCs cultured to passage 4 (p4) showing levels of enrichment at

control *loci* (*Magea2*, positive and *Actb*, negative) and the promoters of contractile VSMC genes compared with enrichment observed using negative control IgG (white and grey bars). Background levels of H3K9me2 are based on enrichment at the *Actb* negative control *locus* and are indicated by a dashed line. Data represent means \pm SEM of 3 biological replicates. Asterisks indicate significant differences ($P < 0.05$) in H3K9me2 levels in UNC treated (+UNC, pink bars) versus untreated control (-UNC, red bars) mVSMCs by one-way ANOVA with *Bonferroni* correction. **(D)** RT-qPCR analysis of *Cnn1*, *Tagln*, *Myocd*, *Acta2*, *Smtn* and *Ywhaz* transcript levels in *ex vivo* mVSMCs (black bars), untreated control mVSMCs cultured to passage 0 (P0 Cultured -UNC, white bars), UNC treated mVSMCs cultured to passage 0 (P0 Cultured +UNC, red bars), untreated control mVSMCs cultured to passage 4 (P4 Cultured -UNC, grey bars) and UNC treated mVSMCs cultured to passage 4 (P4 Cultured +UNC, pink bars). Data are relative to *ex vivo* mVSMCs and normalised to the average of two housekeeping genes (*Hmbs* and *Ywhaz*). Data represent means \pm SEM of 3 biological replicates. Asterisks indicate significant differences ($P < 0.05$) versus *ex vivo* VSMCs (black bars) as determined by one-way ANOVA with *Bonferroni* correction.

These results suggest that although H3K9me2 is recruited to VSMC contractile gene promoters in cultured cells, H3K9me2 at these promoters is not required for their repression. Rather, the accelerated downregulation of contractile VSMC gene expression upon global loss of H3K9me2 suggests that the modification indirectly regulates these genes to maintain VSMCs in a contractile state.

3.3 Summary and Conclusions

In summary, the results described in this chapter point towards a role for H3K9me2 in the regulation of VSMC phenotype. Global levels of H3K9me2 were reduced in phenotypically switched VSMCs *in vitro* and *in vivo*, concomitant with decreased levels of contractile VSMC gene expression. In agreement with our findings, work by Yang and colleagues showed that global loss of H3K9me2, by pharmacological inhibition of G9A/GLP using BIX01294, blocks the expression of CNN1 and contractility in ovine fetal pulmonary artery SMCs (Yang et al., 2012). Furthermore, compared to VSMCs from healthy aortic tissue, global levels of H3K9me2 are reduced in human VSMCs from atherosclerotic lesions, suggesting H3K9me2 may contribute to VSMC phenotypic switching observed in human disease (Greissel et al., 2015). Interestingly, loss of H3K9me2 upon VSMC culture correlated with reduced GLP expression (Figure 3.2). Therefore, it is tempting to speculate that GLP may regulate H3K9me2 to facilitate VSMC phenotypic switching.

Like human VSMCs, mouse VSMCs within atherosclerotic plaque displayed reduced levels of H3K9me2 compared to healthy tissue (Figure 3.6). However, levels of H3K9me2 in VSMC nuclei did not fluctuate between the media, core or cap of atherosclerotic plaque, which are known to express

different levels of contractile VSMC genes (Figure 3.6). Furthermore, H3K9me2 levels in LCCA VSMC nuclei were not significantly reduced until 7 days post carotid ligation compared to non-ligated controls (Figure 3.6) whereas contractile VSMC genes have been reported to be significantly reduced as soon as 1 day post ligation (Shi et al., 2013). Moreover, I observed the same downregulated levels of H3K9me2 in LCCA VSMC nuclei 28 days post ligation compared to 7 days post surgery while contractile VSMC genes have been shown to become upregulated around 9 to 28 days post carotid ligation (Allagnat et al., 2016; Shi et al., 2013). These observations imply H3K9me2 does not directly regulate VSMC contractility. Perhaps, H3K9me2 instead regulates the VSMC response to stimuli such as injury or inflammation, which indirectly influences the expression of contractile VSMC genes.

H3K4me3, a mark associated with active gene promoters, was observed at contractile VSMC genes in both *ex vivo* and cultured VSMCs (figure 3.7 C, D), despite downregulation of their expression upon culture (Figure 3.2). Similar to this observation, H3K4me2, a mark linked to active and poised gene promoters, has been shown to persist at contractile VSMC genes after phenotypic switching, independent of their transcriptional state (Alexander and Owens, 2012). These findings suggest H3K4me2/3 may serve as a mechanism for epigenetic cell lineage memory to enable phenotypically modulated VSMCs to switch back to their contractile state.

Intriguingly, local H3K9me2 was recruited to a subset of contractile VSMC gene promoters upon culture (Figure 3.7 A, B), concomitant with their repression (Figure 3.2). However, global loss of H3K9me2 by inhibiting the methyltransferase activity of G9A/GLP, did not upregulate but further attenuated contractile VSMC gene expression (Figure 3.8). This finding implies reduced levels of H3K9me2 may be causally related to loss of the contractile VSMC state. G9A and GLP are both known to have methyltransferase-independent activity and can methylate a range of non-histone proteins as discussed in the introduction of this thesis (Shinkai and Tachibana, 2011). For example, G9A can act as a positive regulator of transcription by binding to co-activators (Bittencourt et al., 2012). Therefore, it is possible that G9A/GLP indirectly act to maintain the expression of contractile VSMC genes by altering the activity of a transcriptional activator or repressor at the transcriptional or post transcriptional level.

CHAPTER 4 - RESULTS: H3K9me2 plays a functional role in regulating inflammation/injury-induced gene expression in VSMCs.

4.1 Introduction

Experiments described in Chapter 3 demonstrate that H3K9me2 is reduced in phenotypically switched VSMCs associated with vascular disease. Interestingly, it has been reported that phosphorylated p65 (Serine 536), a marker of vascular inflammation, is markedly increased seven days post carotid ligation in mice (Song et al., 2011). Furthermore, in ApoE^{-/-} mice, mRNA levels of numerous pro-inflammatory cytokines known to elicit the VSMC inflammatory response including *IL1A*, *IL1B* and *TNFA*, peak seven days post carotid ligation (Alberts-Grill et al., 2012). With these observations in mind, it is tempting to speculate that loss of H3K9me2 in VSMCs seven days post carotid ligation (Figure 3.4) is concomitant with vascular inflammation. H3K9me2 often marks genes involved in processes that require tight and dynamic regulation, including those involved in the inflammatory response (Chen et al., 2009; Fang et al., 2012; Liu et al., 2014; Miao et al., 2007; Yoshida et al., 2015). In various cell types, altered levels of H3K9me2 at MMP and inflammatory gene promoters have been linked to inflammatory and autoimmune diseases (Chen et al., 2017; El Mansouri et al., 2014; Zhong and Kowluru, 2013b). Together, these findings suggest H3K9me2 may play a functional role in regulating the inflammatory activation of VSMCs.

The vascular inflammatory response requires bidirectional interaction between resident vascular cells and inflammatory cells, which is governed in part by pro-inflammatory cytokines. Bone marrow-derived, adventitial, endothelial and VSMCs are all able to produce and respond to pro-inflammatory cytokines, which stimulate NFκB, AP-1, JAK-STAT and Smad signalling pathways (Schober, 2008; Sprague and Khalil, 2009). Activation of such signalling pathways regulate the VSMC inflammatory response, prompting VSMCs to secrete a diverse range of pro-inflammatory mediators including MMPs, cytokines, chemokines and adhesion molecules. For example, the pro-inflammatory cytokines IL-1α and IL-1β induce VSMCs to switch from a contractile to a synthetic phenotype, stimulating NFκB and AP-1-dependent transcription of cytokines (e.g. *IL6*), chemokines (e.g. *CCL2*) and MMPs (Lim and Park, 2014; Nagase et al., 2006).

MMPs comprise a family of proteases capable of degrading major components of the ECM and processing a variety of signalling molecules including cytokines and cell surface receptors (Fanjul-Fernández et al., 2010). MMPs are important for the migration and proliferation of VSMCs, infiltration of inflammatory cells and the stability of atherosclerotic plaque (Galis and Khatri, 2002; Johnson, 2014; Nagase et al., 2006). For instance, MMP3 and MMP9 promote VSMC migration and neointima formation after carotid ligation in mice (Johnson et al., 2011b) and numerous animal atherosclerosis studies implicate MMP12 in plaque development and instability (Johnson et al., 2005b; Liang et al., 2006; Yamada et al., 2008). Interestingly, increased MMP3, MMP9 and MMP12

expression has been observed in vulnerable compared to stable human atherosclerotic lesions (Galis et al., 1994b; Halpert et al., 1996; Muller et al., 2014; Thomas et al., 2007).

IL6 and CCL2 are also implicated in the progression of CVD (Schober, 2008; Stoner et al., 2013; Tousoulis et al., 2016). IL6 attenuates VSMC contractility while promoting VSMC migration, proliferation and vascular calcification (Kurozumi et al., 2016; Lee et al., 2016; Watanabe et al., 2004) whereas CCL2 recruits leukocytes to the vessel wall and stimulates VSMC migration and proliferation (Schober, 2008; Selzman et al., 2002). Human studies have revealed that elevated serum levels of IL6 and CCL2 are associated with greater CVD risk (Anderson et al., 2013; Biasucci et al., 1999; Piemonti et al., 2009; Tousoulis et al., 2016).

The VSMC inflammatory response is associated with the initiation and progression of vascular dysfunction and adverse clinical outcome (Schober, 2008; Sprague and Khalil, 2009). Indeed, directly reducing inflammation with Canakinumab, an IL-1 β neutralising antibody, significantly lowered the rate of cardiovascular events compared to placebo in patients (Ridker et al., 2017; Weber and von Hundelshausen, 2017). Identification of mechanisms that regulate inflammation-associated changes in VSMC gene expression is therefore of considerable therapeutic importance. This chapter investigates the role of H3K9me2 in regulating the VSMC inflammatory response using an *in vitro* and *in vivo* model of VSMC inflammatory activation.

Aims:

1. Assess levels of H3K9me2 at MMP and pro-inflammatory VSMC gene promoters, which are strongly associated with CVD, using chromatin immunoprecipitation.
2. Test the functional role of H3K9me2 on MMP and pro-inflammatory VSMC gene expression *in vitro* using small molecule inhibition of the main H3K9 di-methyltransferases G9A/GLP prior to IL-1 α stimulation.
3. Test the functional role of H3K9me2 on MMP and pro-inflammatory VSMC gene expression *in vivo* using VSMC-lineage labelled mice and small molecule inhibition of the main H3K9 di-methyltransferases G9A/GLP prior to carotid ligation injury.

4.2 Results

4.2.1 H3K9me2 marks IL-1 α -responsive gene promoters in mVSMCs.

ChIP was performed to investigate local levels of H3K9me2 at specific gene promoters implicated in the inflammatory activation of VSMCs. Intriguingly, ChIP revealed high levels of H3K9me2 locally at a subset of IL-1 α -induced genes including *Mmp3*, *Mmp9* and *Mmp12* in both *ex vivo* (Figure 4.1 A) and cultured murine VSMCs (mVSMCs) (Figure 4.1 B) compared to the *Actb* negative control *locus*, which persisted after IL-1 α stimulation in cultured mVSMCs (Figure 4.1 C, D). Unlike cultured mVSMCs, *ex vivo* mVSMCs also displayed modest enrichment of the H3K9me2 mark at the promoters of *Il6* and *Ccl2* (Figure 4.1 A, B), which are also induced by IL-1 α treatment (Figure 4.1 C). The *Mmp2* promoter, a gene constitutively expressed by VSMCs and unaffected by IL-1 α treatment (Figure 4.1 C), also displayed modest levels of H3K9me2 in both *ex vivo* and cultured mVSMCs (Figure 4.1 A, B). Aberrant expression of a number of MMP genes is associated with H3K9me2 depletion at their promoter (Miao et al., 2007; Zhong and Kowluru, 2013a). Therefore, we decided to investigate whether H3K9me2 plays a role in controlling the level of IL-1 α -induced MMP gene expression in cultured mVSMCs.

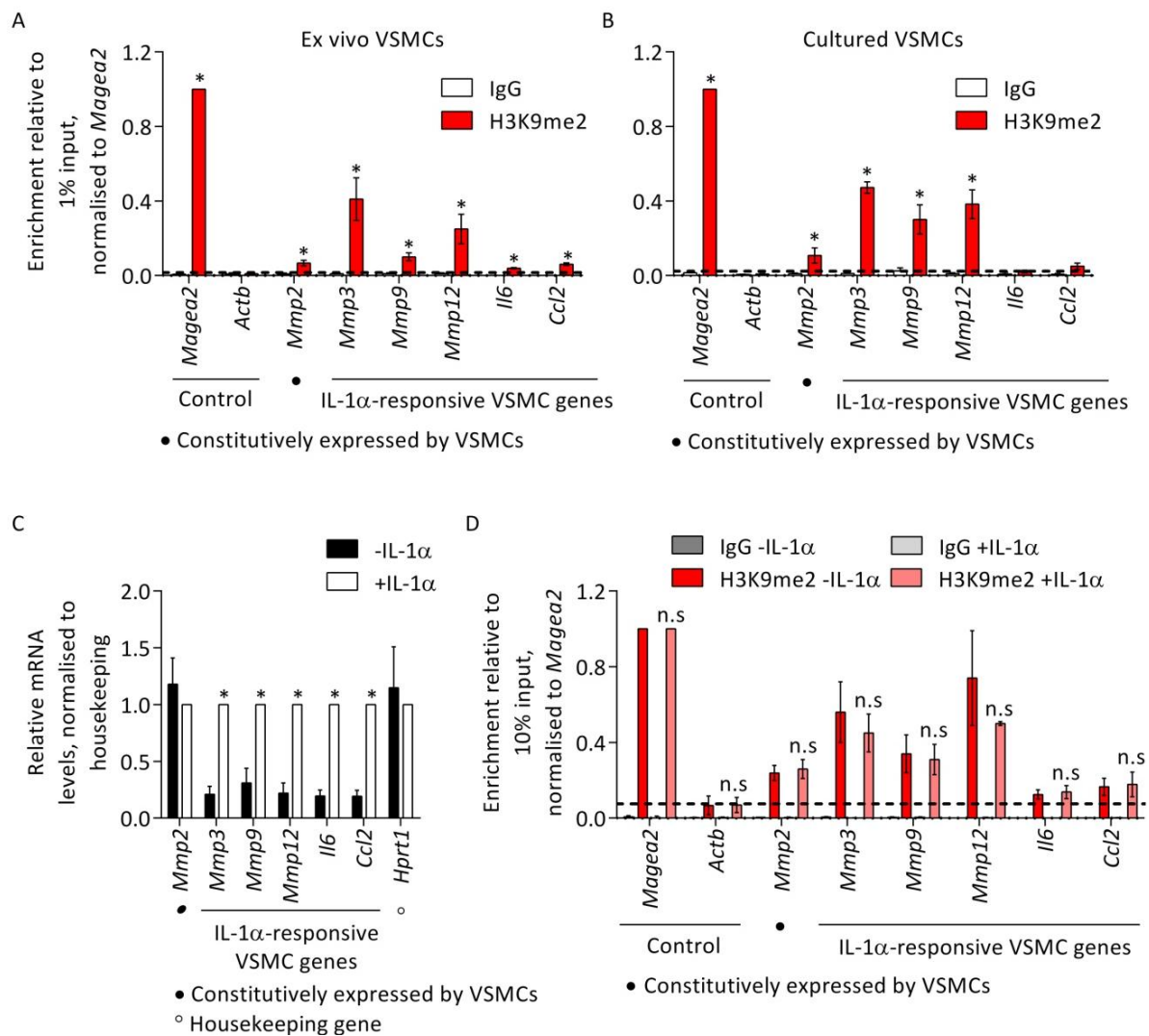


Figure 4.1: IL-1 α -responsive MMP gene promoters are highly enriched for H3K9me2 in both *ex vivo* and cultured mVSMCs. (A, B) ChIP-qPCR analysis for H3K9me2 (red bars) and negative control IgG (white bars) in *ex vivo* (A) and cultured (B) mVSMCs, showing levels of enrichment at control *loci* (*Magea2*, positive and *Actb*, negative) and the promoters of *Mmp2*, *Mmp3*, *Mmp9*, *Mmp12*, *Il6* and *Ccl2*. Background levels of H3K9me2 are based on enrichment at the *Actb* negative control *locus* and are indicated by a dashed line. Data represent means \pm SEM of 3-10 biological replicates (*Ex vivo* samples: n=3 for *Mmp2*, *Mmp9*, *Il6*, *Ccl2*; n=4 for *Mmp12*; n=7 for *Magea2*, *Actb*, *Mmp3*. Cultured samples: n=3 for *Il6*, *Ccl2*; n=10 for *Magea2*, *Actb*, *Mmp2*, *Mmp3*, *Mmp9*, *Mmp12*). Asterisks indicate significant differences ($p < 0.05$) in H3K9me2 levels versus IgG negative control by unpaired student's t test. (C) RT-qPCR analysis of *Mmp2*, *Mmp3*, *Mmp9* and *Mmp12* transcript levels in untreated control (black bars) and IL-1 α -treated (white bars) cultured mVSMCs. Data are relative to IL-1 α -treated cultured VSMCs (white bars) and normalised to two housekeeping genes (*Hprt1* and *Ywhaz*). Data represent means \pm SEM of 6 biological replicates. Asterisks indicate significant differences ($p < 0.05$) in expression level in IL-1 α -treated (+IL-1 α , white bars) versus untreated control (-IL-1 α , black bars) cultured mVSMCs by unpaired student's t test. (D) ChIP-qPCR analysis for H3K9me2 in untreated control (-IL-1 α , red bars) and IL-1 α treated (+IL-1 α , pink bars) cultured mVSMCs showing levels of enrichment at control *loci* (*Magea2*, positive and *Actb*, negative) and the promoters of *Mmp2*, *Mmp3*, *Mmp9*, *Mmp12*, *Il6* and *Ccl2*

compared with enrichment observed using negative control IgG (grey bars). Background levels of H3K9me2 are based on enrichment at the *Actb* negative control *locus* and are indicated by a dashed line. Data represent means \pm SEM of 3 biological replicates. n.s indicates no significant differences ($P < 0.05$) in H3K9me2 levels in IL-1 α treated (+IL-1 α , pink bars) versus untreated control (-IL-1 α , red bars) cultured mVSMCs by one-way ANOVA with *Bonferroni* correction.

4.2.2 Loss of H3K9me2, by pharmacological inhibition of G9A/GLP (UNC0638), potentiates MMP gene expression in cultured mVSMCs.

To test the functional importance of H3K9me2 at the MMP gene promoters, cultured VSMCs were pretreated with UNC0638 (UNC), a G9A/GLP inhibitor, prior to IL-1 α stimulation. UNC treatment significantly reduced H3K9me2 levels both globally (Figure 4.2 A, B) and locally at the MMP promoters (Figure 4.2 C). The reduced level of H3K9me2 did not directly affect MMP gene expression, but significantly potentiated IL-1 α -mediated upregulation of *Mmp3* (3.2 fold), *Mmp9* (1.8 fold) and *Mmp12* (7.1 fold) relative to cells treated with IL-1 α alone (Figure 4.2 D). Neither IL-1 α nor UNC treatment alone, or in combination, affected the expression of *Mmp2* (Figure 4.2 D). To test whether the effect of UNC on MMP expression is due to a general upregulation of the inflammatory response, we analysed expression of the pro-inflammatory cytokines *Il6* and *Ccl2*, which showed no H3K9me2 enrichment in cultured VSMCs (Figure 4.2 C). IL-1 α treatment induced the expression of both *Il6* and *Ccl2*, whereas UNC alone or in combination with IL-1 α had no effect (Figure 4.2 D). These results imply that H3K9me2 acts to repress specific MMP promoters, possibly to prevent spurious induction of their expression.

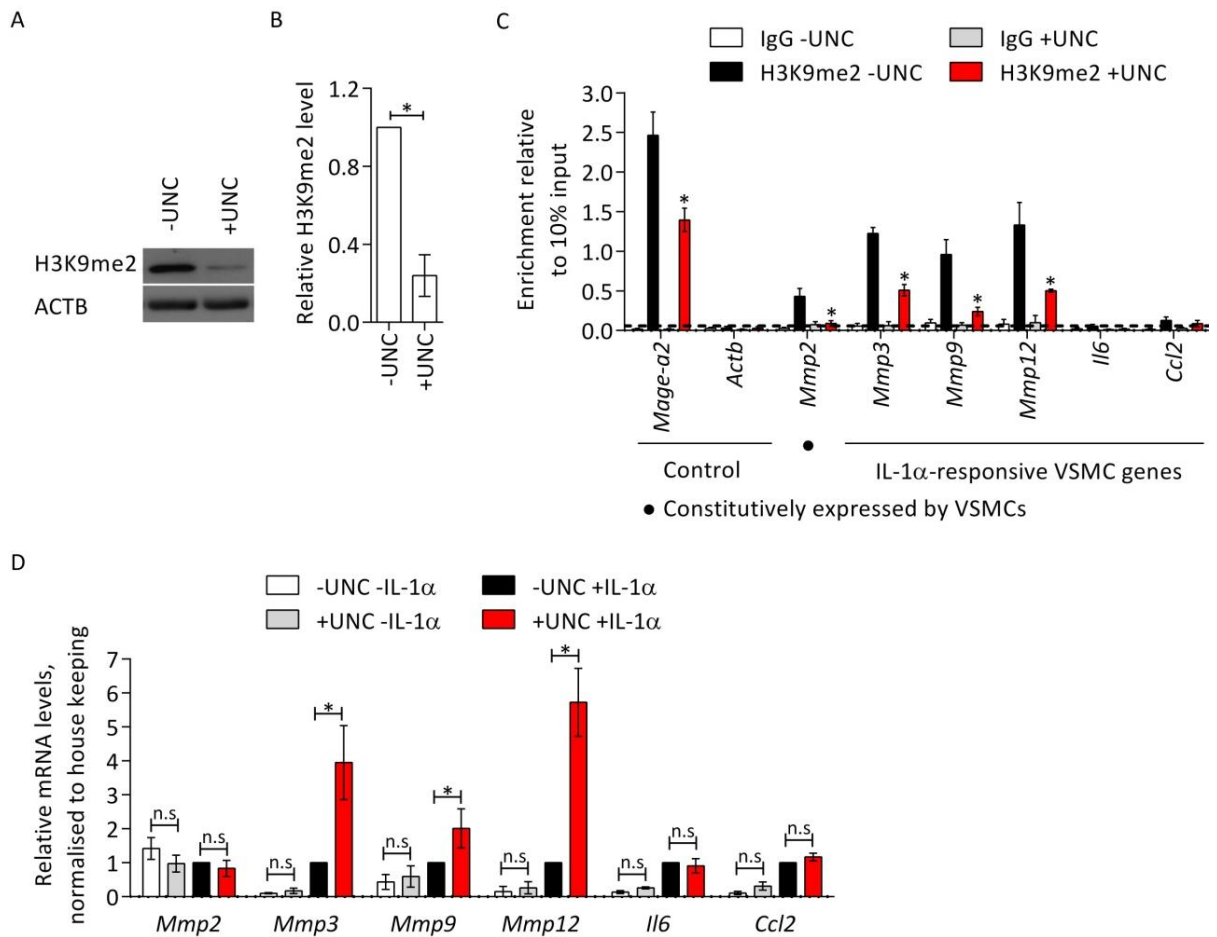


Figure 4.2: Global reduction of H3K9me2, by pharmacological inhibition of G9A/GLP, significantly potentiates IL-1 α -mediated MMP gene induction in cultured mVSMCs. (A, B) Representative western blot (A) and densitometric analysis (B) of H3K9me2 in UNC0638 (+UNC) treated cultured mVSMCs relative to untreated controls (-UNC), normalised to ACTB. Data represent means \pm SEM of 3 biological replicates. The Asterisk indicates significant difference ($p < 0.05$) in H3K9me2 levels in untreated (-UNC) versus UNC treated (+UNC) cultured mVSMCs by unpaired student's t test. (C) ChIP-qPCR analysis for H3K9me2 in untreated control (black bars) and UNC0638 (UNC) treated cultured mVSMCs (red bars) showing levels of enrichment at control *loci* (*Magea2*, positive and *Actb*, negative) and the promoters of *Mmp2*, *Mmp3*, *Mmp9*, *Mmp12*, *Il6* and *Ccl2* compared with enrichment observed using negative control IgG (white and grey bars). Background levels of H3K9me2 are based on enrichment at the *Actb* negative control *locus* and are indicated by a dashed line. Data represent means \pm SEM of 3 biological replicates. Asterisks indicate significant differences ($p < 0.05$) in H3K9me2 levels in UNC treated (+UNC, red bars) versus untreated control (-UNC, black bars) cultured mVSMCs by one-way ANOVA with *Bonferroni* correction. (D) RT-qPCR analysis of *Mmp2*, *Mmp3*, *Mmp9*, *Mmp12*, *Il6* and *Ccl2* transcript levels in untreated control (white bars), IL-1 α (black bars), UNC (grey bars) and IL-1 α plus UNC-treated (red bars) cultured mVSMCs. Data are relative to UNC plus IL-1 α -treated cultured mVSMCs (+UNC +IL-1 α , red bars) and normalised to two housekeeping genes (*Hmbs* and *Ywhaz*). Data represent means \pm SEM of 3 biological replicates. Asterisks indicate significant differences ($p < 0.05$) in expression level by one-way ANOVA with *Bonferroni* correction.

4.2.3 Loss of H3K9me2, by pharmacological inhibition of G9A/GLP (UNC0638), potentiates IL-1 α -induced ECM degradation of gelatin by cultured mVSMCs.

MMPs govern vascular remodelling by degradation of the ECM. Vascular remodelling and degradation of the ECM is associated with the development of vascular disease, including atherosclerosis (Johnson, 2017; Xu and Shi, 2014). To investigate whether enhanced IL-1 α -induced MMP expression by H3K9me2 inhibition increased proteolytic activity, cultured mVSMCs were pre-treated with IL-1 α and/or UNC prior to incubation with dye quenched (DQ) gelatin, which, upon digestion, is converted into fluorescent fluorescein-labelled peptides. The fluorescent fluorescein signal was quantified (CTF) to measure ECM degradation and denote levels of MMP activity. As shown in Figure 4.3, inhibition of H3K9me2 by UNC further increased IL-1 α -induced digestion of the DQ gelatin by 1.5-fold compared to VSMCs treated with IL-1 α alone. These results provide additional evidence to support the role of H3K9me2 in the negative regulation of MMP activity in VSMCs.

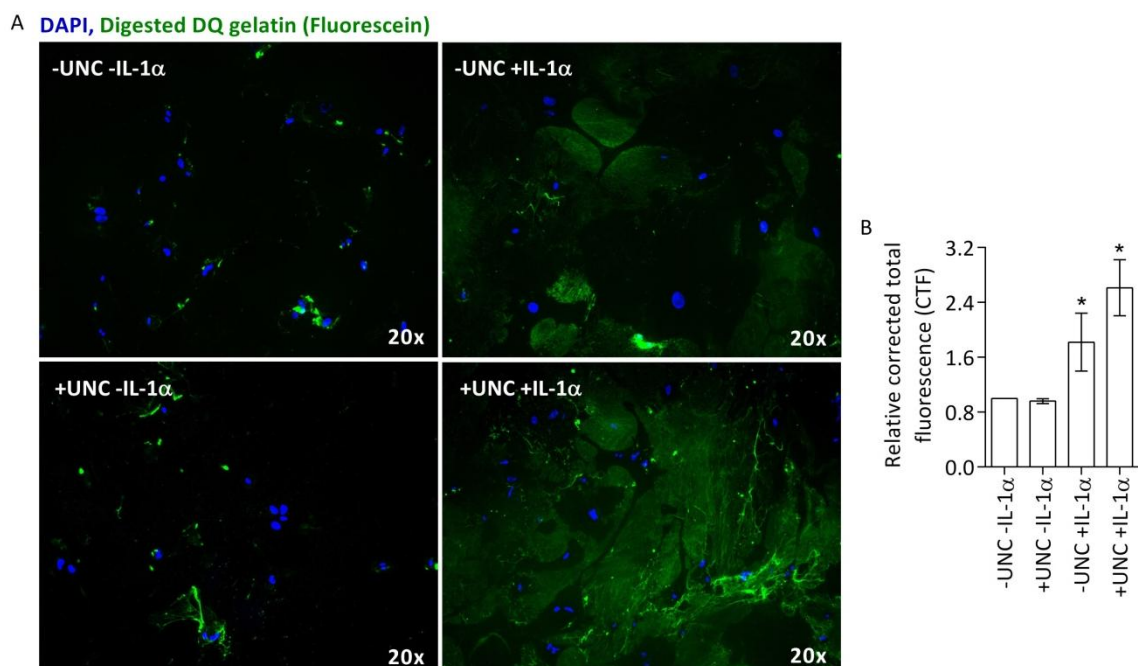


Figure 4.3: In cultured mVSMCs, H3K9me2 protects against IL-1 α -induced extra cellular matrix (ECM) degradation. (A) Representative immunofluorescence images showing cultured mVSMCs treated with vehicle control or UNC0638 (UNC) and/ or IL-1 α prior to incubation with dye-quenched (DQ) gelatin. Upon digestion, DQ gelatin releases a fluorescent fluorescein signal represented in green. Nuclei were counterstained with DAPI (blue). Images were taken using a 20x objective with a fluorescence microscope (ZEISS Axio Vert A.1). **(B)** Bar plot shows levels of DQ gelatin digestion, as represented by the corrected total fluorescence (CTF), by cultured mVSMCs treated with vehicle control or UNC and/ or IL-1 α . The CTF was quantified using ImageJ software as follows; $CTF = [(area \times mean \text{ pixel intensity}) - (area \times mean \text{ pixel intensity of } 5 \text{ background readings})] / \text{cell number}$. Cell numbers were determined by counting DAPI stained nuclei (blue). Data represent the average CTF

of 5 fields of view per group and are normalised to untreated control (-UNC -IL-1 α) cultured mVSMCs. Data represent means \pm SEM of 3 biological replicates. Asterisks indicate significant differences ($p < 0.05$) in CTF compared to vehicle control (-UNC -IL-1 α) cultured mVSMCs by one-way ANOVA with *Bonferroni* correction.

4.2.4 Loss of H3K9me2, by pharmacological inhibition of G9A/GLP (A366), significantly potentiates injury-induced Mmp3, Mmp12 and Il6 gene expression in the VSMCs *in vivo*.

The vasculature is comprised of multiple cell types, which are influenced by a variety of signals in the surrounding milieu including shear stress, circulating blood cells and cytokines. *In vitro* studies fail to mimic this complex environment. Therefore, to validate and substantiate the *in vitro* findings, the impact of G9A/GLP inhibition on injury-induced MMP expression was next explored *in vivo*. To determine whether a pharmacological model could be used to reduce H3K9me2 in VSMCs *in vivo*, non-labelled Myh11-CreERT2/ROSA26-EYFP mice were implanted with osmotic pumps delivering either vehicle control or A366 (30 mg/kg body weight (BW)/day) (Figure 4.4), a small molecule inhibitor which has potent and specific inhibitory effects on the enzymatic activity of G9A/GLP without cytotoxicity (Sweis et al., 2014; Thienpont et al., 2017). A366 has better pharmacokinetics compared to UNC for *in vivo* use (Sweis et al., 2014). Non-labelled rather than tamoxifen-labelled Myh11-CreERT2/ROSA-EYFP mice were used to comply with the 3R's of animal research. The medial layer of blood vessels, which predominantly contains VSMCs, can be easily defined by the elastic lamina. Therefore, it is possible to assess the effect of A366 on H3K9me2 in VSMCs *in vivo* without labelling VSMCs with a fluorescent reporter, which would cause unnecessary pain due to the administration of tamoxifen intra-peritoneal injections.

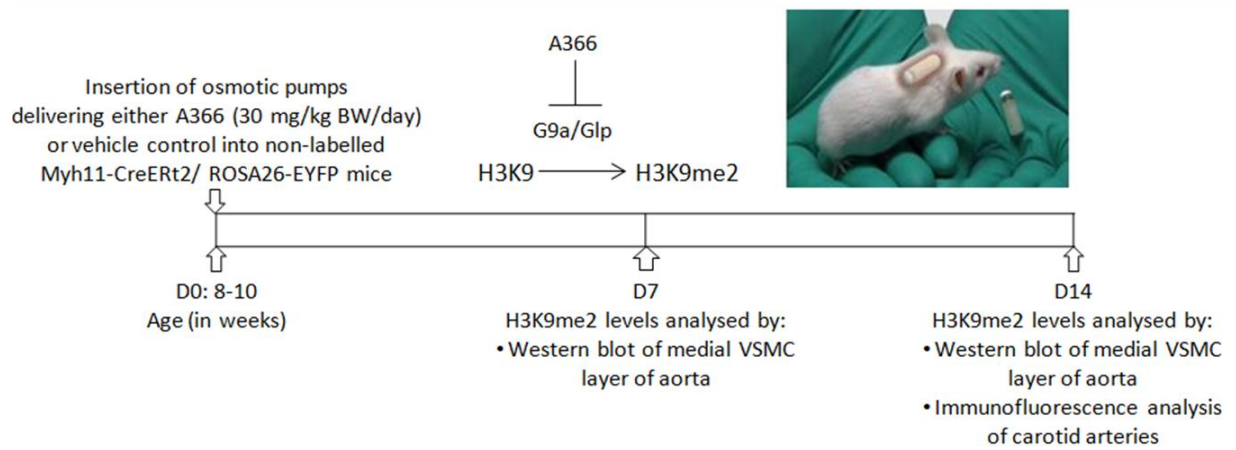


Figure 4.4: Experimental protocol to test the effect of A366, a small molecule inhibitor of G9A/GLP, on H3K9me2 levels in mVSMCs *in vivo*. Osmotic pumps delivering either A366 or vehicle control were inserted into 8-10 weeks old non-labelled Myh11-CreERT2/ ROSA26-EYFP male mice for 7 or 14 days. H3K9me2 levels within the aortic medial cell layer were analysed by western blot and H3K9me2 levels in VSMCs within the LCCA were analysed by immunofluorescence staining.

Western blot analysis revealed that 7 days post osmotic pump insertion, H3K9me2 levels were not significantly different within the aortic medial VSMC layer from mice administered A366 compared to vehicle controls (Figure 4.5 A, B). However, by 14 days post osmotic pump insertion, H3K9me2 levels were significantly downregulated by approximately 40% within the aortic medial VSMC layer from mice administered A366 compared to vehicle controls (Figure 4.5 A, B). This loss of H3K9me2 was also evident in cells within the medial VSMC layer of the left common carotid artery (LCCA) by immunofluorescence analysis (Figure 4.5 C, D).

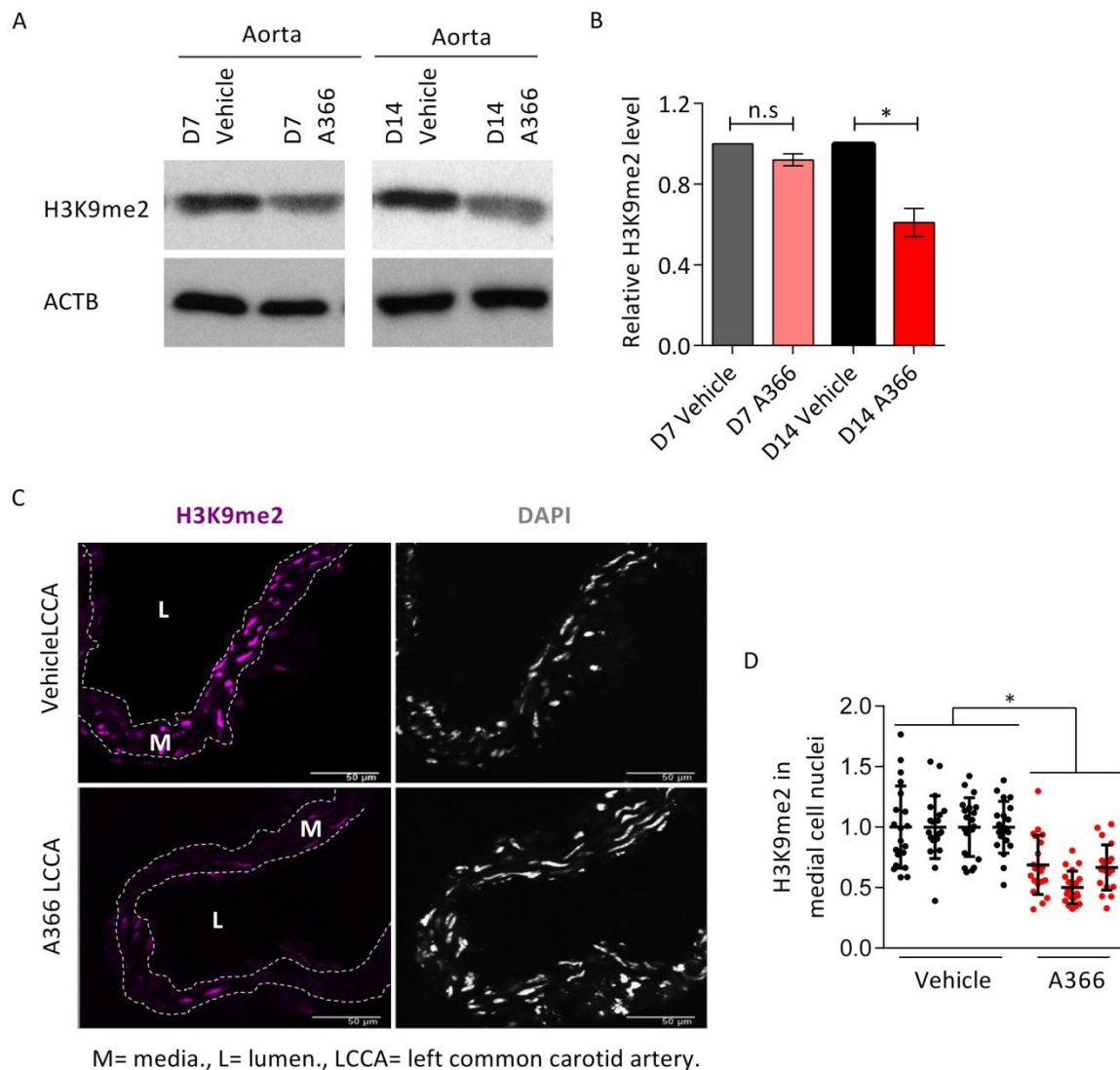


Figure 4.5: A366, a small molecule inhibitor of G9A/GLP, reduces H3K9me2 in VSMCs *in vivo*.

(A, B) Representative western blot **(A)** and densitometric analysis **(B)** of H3K9me2 levels in the aortic medial VSMC layer of mice administered vehicle control (grey and black bars) or A366 (pink and red bars) for 7 (grey and pink bars) or 14 (black and red bars) days. Data are relative to vehicle control treated mice (grey and black bars) and normalised to ACTB. Data represent means \pm SEM of 3 biological replicates from 3 animals. The asterisk indicates significant difference ($p < 0.05$) in H3K9me2 levels in the aortic medial VSMC layer from A366 (pink and red) versus vehicle control (grey and black) treated mice by unpaired student's t test. **(C)** Immunofluorescence staining for H3K9me2 in representative 12 μ m LCCA cryosections from mice administered vehicle control or A366 for 14 days. Signals for H3K9me2-Alexa Fluor 647 (magenta, right panels) and nuclei counter stained with DAPI (white, left panels) are shown. Scale bars, 50 μ m. M, media; L, Lumen. White dashed lines outline the media as determined by auto-fluorescence of the inner and outer elastic lamina. **(D)** Dot plot shows H3K9me2 signal in medial cell nuclei, defined by their location between elastic lamina, as determined by immunofluorescence analysis of LCCAs from mice administered vehicle control (black dots) or A366 (red dots) for 14 days. Each dot shows H3K9me2 signal intensity in one LCCA medial cell nucleus. $n = 4$ animals for vehicle, $n = 3$ animals for A366. The analysis was performed blindly. The asterisk indicates significant difference ($p < 0.05$)

in H3K9me2 levels in LCCA medial cell nuclei from mice treated with A366 (red dots) versus mice treated with vehicle control (black dots) by nested ANOVA testing.

To test whether H3K9me2-mediated regulation of VSMC gene expression is functional *in vivo*, VSMCs were genetically labelled by combining the Myh11-CreERT2 transgene (Wirth et al., 2008), which is specifically expressed by mature VSMCs, with the ROSA26-EYFP reporter allele (Gomez and Owens, 2012). Recombination was induced in healthy mice with a pulse of tamoxifen, which resulted in stable fluorescent protein (EYFP) expression. As demonstrated previously, expression of the lineage reporter is specific to cells in the medial layer of the vasculature where the recombination efficiency is 40-60% (Dobnikar et al., 2018). Carotid ligation was performed 14 days after mice received osmotic pumps delivering either vehicle or A366 (30 mg/kg BW/day), when H3K9me2 levels in cells within the medial VSMC layer were reduced by 40% in mice administered A366 compared to vehicle controls (Figure 4.5). Common carotid arteries (CCAs) were harvested 7 days following carotid ligation surgery and cells expressing the EYFP reporter, which are derived from Myh11-expressing VSMCs, were isolated by FACS allowing analysis of VSMC mRNA levels via RT-qPCR (Figure 4.6).

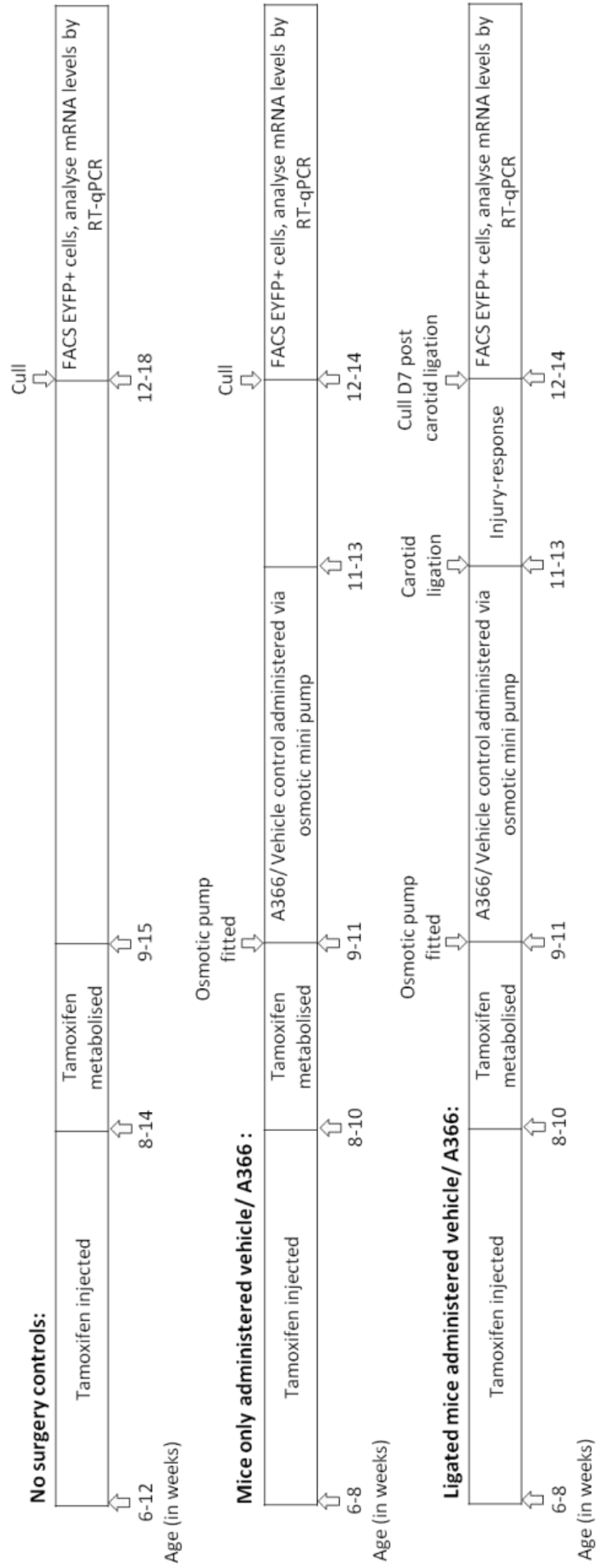
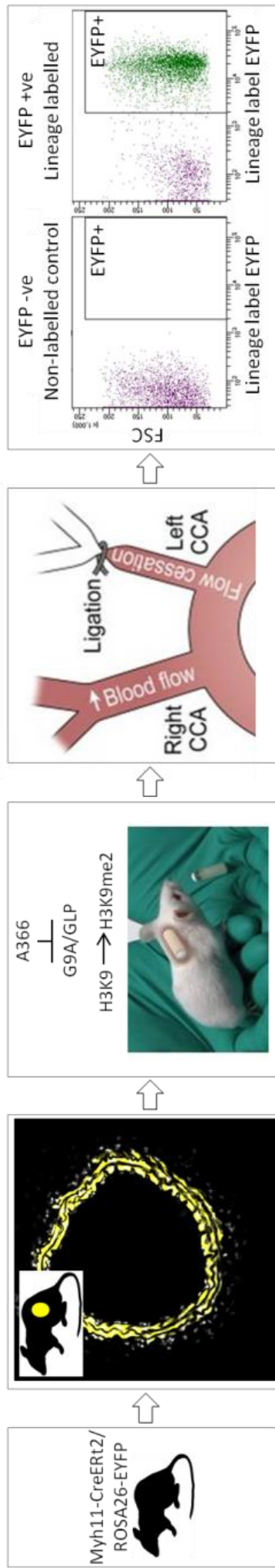
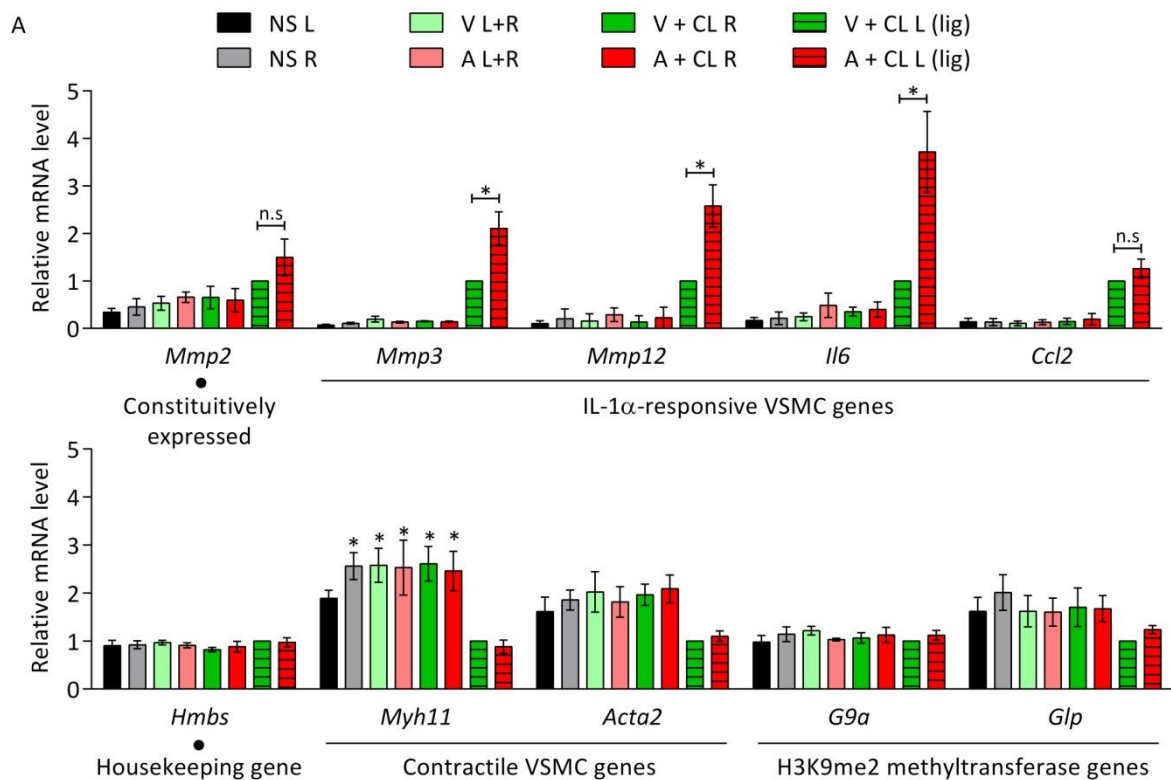


Figure 4.6: Schematic of pharmacological model to test whether H3K9me2-mediated regulation of VSMC gene expression is functional in vivo. 6-8 week old Myh11-CreERT2/ ROSA-EYFP mice were labelled by intraperitoneal tamoxifen injections (10x 1mg) prior to subcutaneous osmotic pump insertion delivering either A366 (30 mg/kg BW/day) or vehicle and ligation surgery of the left common carotid artery (CCA).

Seven days after ligation, *Myh11* and *Acta2* mRNA levels are downregulated whereas *Mmp3*, *Il6* and *Ccl2* mRNA levels are upregulated in EYFP+ cells from the ligated CCAs compared to all the controls (Figure 4.7 A). Interestingly, like culture-induced phenotypically switched VSMCs (Figure 3.2 D), EYFP+ cells from ligated left CCAs (green and red striped bars) displayed a trend towards lower levels of *Glp* mRNA compared to those from non-ligated right CCA (green and red bar) and no ligation surgery CCA (black, grey, light green and pink bars) controls (Figure 4.7 A), although this did not reach statistical significance. *G9a* mRNA levels in EYFP+ cells were not influenced by carotid ligation injury (Figure 4.7 A). The reduced level of H3K9me2 in EYFP+ cells by A366 (pink bars) treatment (Figure 4.5) did not directly affect the expression of any of the genes analysed (Figure 4.7 A). A366 treatment (red striped bars) also did not influence ligation injury-induced downregulation of *Myh11* or *Acta2* in EYFP+ cells (Figure 4.7 A). However, the reduced level of H3K9me2 in EYFP+ cells by A366 treatment (red striped bars) significantly potentiated ligation injury-induced upregulation of *Mmp3* (2.1 fold), *Mmp12* (2.6 fold) and *Il6* (3.8 fold) (Figure 4.7 A). This observation correlates with what appears to be reduced levels of H3K9me2 at the promoters of *Mmp3*, *Il6* and *Ccl2* in the medial cell layer of aortas derived from mice administered A366 (red bars) for 21 days compared to vehicle controls (green bars) (Figure 4.7 B). A366 treatment (red striped bars) did not significantly influence ligation injury-induced upregulation of *Mmp2* or *Ccl2* (Figure 4.7 A).



n= 4 experiments		
	# mice	# CCAs pooled per experiment
■ NS L	12	3
■ NS R	12	3
■ V L+R	4	2
■ A L+R	4	2
■ V + CL R	12	3
■ A + CL R	12	3
■ V + CL L (lig)	12	3
■ A + CL L (lig)	12	3

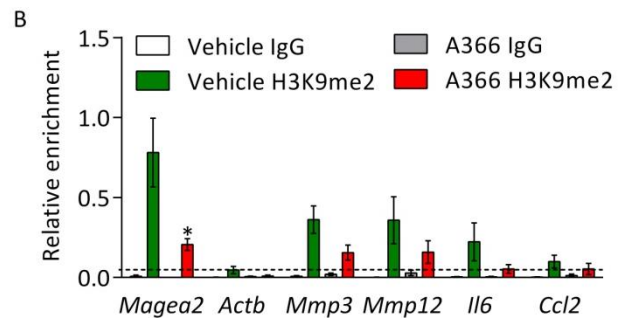


Figure 4.7: Global reduction of H3K9me2, by pharmacological inhibition of G9A/GLP (A366), significantly potentiates injury-mediated *Mmp3*, *Mmp12* and *Il6* gene induction in mVSMCs *in vivo*. (A) RT-qPCR analysis of *Hmbs*, *Myh11*, *Acta2*, *G9a*, *Glp*, *Mmp2*, *Mmp3*, *Mmp12*, *Il6* and *Ccl2* transcript levels in EYFP+ cells within common carotid arteries (CCAs). NS L/R (black/ grey bars) = left/right CCAs from mice which had not undergone surgery. V/A L+R (light green/ pink bars) = left plus right CCAs from mice administered an osmotic pump delivering vehicle/A366. V/A + CL R (green/ red bars) = right non-ligated CCAs from mice administered an osmotic pump delivering vehicle/A366 and subjected to left CCA ligation surgery. V/A + CL L (green striped/ red striped bars) = left ligated CCAs from mice administered an osmotic pump delivering vehicle/A366 and subjected to left CCA ligation surgery. Data are relative to [V+CL L (lig)] samples and normalised to two housekeeping genes (*Hprt1* and *Hmbs*). Data represent means \pm SEM of 4 experiments as detailed in the figure. Asterisks indicate significant differences (p < 0.05) in expression versus [V + CL L (lig)] samples (green striped bars) by one-way ANOVA with *Bonferroni* correction. (B) ChIP-qPCR analysis for H3K9me2 in the aortic medial

cell layer, with adventitial and endothelial cells removed, from mice administered either vehicle control (V L+R, green bars) or A366 (A L+R, red bars) showing levels of enrichment at control *loci* (*Magea2*, positive and *Actb*, negative) and the promoters of *Mmp3*, *Mmp12*, *Il6* and *Ccl2* compared with enrichment observed using negative control IgG (white and grey bars). Background levels of H3K9me2 are based on enrichment at the *Actb* negative control *locus* and are indicated by a dashed line. Data represent means \pm SEM of 3 biological replicates from 3 mice. Asterisks indicate significant differences ($p < 0.05$) versus vehicle control (Vehicle H3K9me2, green bars) by one-way ANOVA with *Bonferroni* correction.

RT-qPCR analysis revealed no significant differences in expression levels of bone marrow-derived (*Cd45*), endothelial (*Cd31*) and adventitial fibroblast cell (*Pdgfra*) markers between treatment groups, which suggests that differences in transcript levels in EYFP+ cells between treatment groups is not due to contamination by these cell types (Figure 4.8). These results confirm H3K9me2 plays a functional role in regulating the expression of *Mmp3*, *Mmp12* and *Il6* *in vivo* and may therefore be relevant in the context of human CVD.

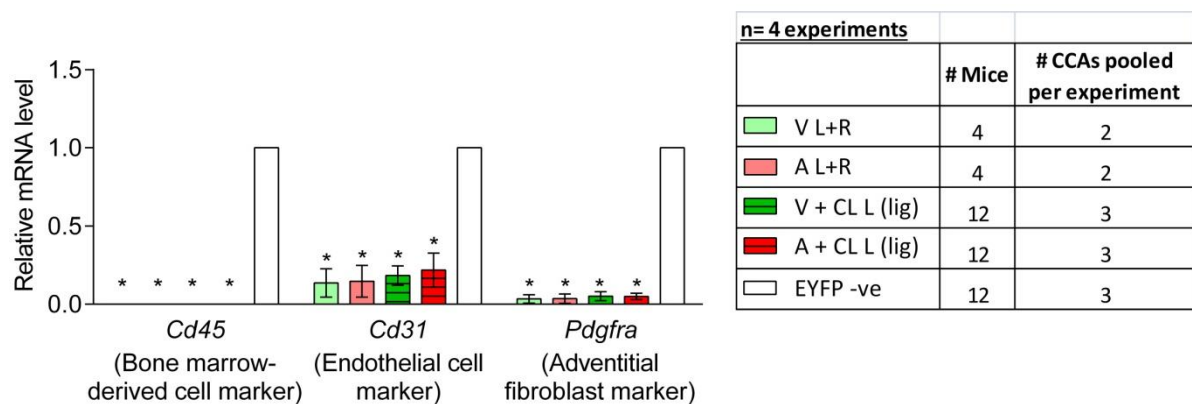


Figure 4.8: Levels of bone marrow-derived endothelial and adventitial cell marker gene expression is independent of sample treatment. RT-qPCR analysis of *Cd45* (a bone marrow-derived cell marker), *Cd31* (a endothelial cell marker) and *Pdgfra* (a adventitial fibroblast cell marker) transcript levels in EYFP+ cells within CCAs. V/A L+R (light green/ pink bars) = left plus right CCAs from mice administered an osmotic pump delivering vehicle/A366. V/A + CL L (green striped/ red striped bars) = left ligated CCAs from mice administered an osmotic pump delivering vehicle/A366 and subjected to left CCA ligation surgery. Data are relative to EYFP -ve cells, from no surgery control left CCAs, and normalised to two housekeeping genes (*Hprt1* and *Hmbs*). Data represent means \pm SEM of 4 experiments as described in the figure. Asterisks indicate significant differences ($p < 0.05$) in expression versus EYFP -ve cells (white bars) by one-way ANOVA with *Bonferroni* correction.

4.3 Summary and conclusions

Chromatin immunoprecipitation revealed high levels of H3K9me2 at a subset of IL-1 α -mediated gene promoters, including *Mmp3*, *Mmp9* and *Mmp12*, in both *ex vivo* and cultured mVSMCs (Figure 4.1 A, B). H3K9me2 was also observed at the promoters of *Il6* and *Ccl2* in *ex vivo* mVSMCs, albeit at modest levels, while the mark was absent in cultured mVSMCs (Figure 4.2 A, B). Upon culture, VSMCs alter their phenotype and downregulate the expression of contractile genes (Figure 3.2 A) and become more proliferative (Metz et al., 2012). Both IL6 and CCL2 are known to upregulate VSMC proliferation (Lee et al., 2016; Schober, 2008). Perhaps, loss of H3K9me2 at the *Il6* and *Ccl2* promoter upon culture reflects induction of their expression. Therefore, it would be interesting to compare *Il6* and *Ccl2* transcript levels in *ex vivo* compared to cultured VSMCs.

Interestingly, in cultured mVSMCs, IL-1 α -responsive MMP gene promoters retained high levels of H3K9me2 after IL-1 α stimulation (Figure 4.1 D). Perhaps, H3K9me2 blocks spurious expression of these genes under inflammatory conditions. Indeed, reduction of H3K9me2, by pharmacological inhibition of G9A/GLP using UNC, potentiated IL-1 α -mediated upregulation of MMP gene expression and activity in cultured mVSMCs (Figure 4.2). However, there is a possibility that UNC has off-target effects (Pappano et al., 2015), which could be responsible for this observation. Therefore, it is important to validate these results via an alternative method such as siRNA knock down of G9A. Importantly, the mouse carotid ligation injury model of vascular disease demonstrates that loss of H3K9me2, by pharmacological inhibition of G9A/GLP, also potentiates injury-induced expression of MMP and pro-inflammatory VSMC genes *in vivo* (Figure 4.7). However, A366 is also likely to inhibit G9A/GLP in other cell types, which influence VSMC gene expression. Therefore, the differences in transcript levels in VSMCs between treatment groups may be due to the effects of A366 on other cell types, such as bone marrow-derived cells. Furthermore, like UNC, A366 may have off target effects. Therefore, it would be interesting to delete G9A or GLP specifically in VSMCs, by introducing the appropriate Cre-deleter transgene onto Flox/Flox mice, to substantiate these findings.

In accordance with our data, several studies report an inverse correlation between H3K9me2 occupancy at MMP and other inflammatory gene promoters and the ability of other cell types to express these genes (Fang et al., 2012; Gesumaria et al., 2015; Liu et al., 2014; Zhong and Kowluru, 2013b). For example, H3K9me2 depletion at the *Mmp9* promoter correlates with elevated *Mmp9* expression in retinal endothelial cells from diabetic rats compared to controls (Zhong and Kowluru, 2013b). Furthermore, solar-stimulated ultraviolet radiation (ssUVR) induces loss of H3K9me2 at the MMP3 promoter in primary human dermal fibroblasts, correlating with enhanced MMP3 mRNA levels following ssUVR exposure (Gesumaria et al., 2015). In addition, genetic ablation or pharmacological inhibition of G9A/GLP stimulates the expression of inflammatory genes in mouse embryonic fibroblasts (MEFs) (Fang et al., 2012). Similar to what is reported here, reduction of

H3K9me2 levels in MEFs, further potentiated poly(I:C)-induced upregulation of inflammatory genes (Fang et al., 2012). These observations support the conclusion that H3K9me2 is functionally important to block excessive inflammation-induced VSMC gene expression.

MMPs play a central role in many CVDs which are associated with structural changes in blood vessels (Galis and Khatri, 2002; Johnson, 2014). MMPs are known to influence the migration and proliferation of VSMCs, infiltration of inflammatory cells into tissue and the stability of atherosclerotic plaques (Figure 1.6) (Galis and Khatri, 2002; Johnson, 2014; Nagase et al., 2006). For instance, MMP3 and MMP9 promote VSMC migration and neointima formation after carotid ligation in mice (Johnson et al., 2011b) and numerous animal atherosclerosis studies implicate MMP12 in plaque development and instability (Johnson et al., 2005b; Liang et al., 2006; Yamada et al., 2008). Interestingly, increased MMP3, MMP9 and MMP12 expression have been observed in vulnerable compared to stable human atherosclerotic lesions. IL6 is also involved in vascular dysfunction and elevated serum levels of IL6 associated with greater cardiovascular disease risk (Anderson et al., 2013; Biasucci et al., 1999; Piemonti et al., 2009; Tousoulis et al., 2016). IL6 has been shown to upregulate VSMC migration, proliferation and vascular calcification whilst attenuating VSMC contraction (Kurozumi et al., 2016; Lee et al., 2016; Watanabe et al., 2004).

The experiments described in this chapter suggest H3K9me2 is functionally required for correct regulation of MMP and IL6 gene expression under inflammatory conditions. Interestingly, the recent CANTOS (Canakinumab Anti-Inflammatory Thrombosis Outcome Study) trial demonstrates diverse clinical benefits to inhibiting IL-1 β for cardiovascular events (Ridker et al., 2017; Weber and von Hundelshausen, 2017). IL-1 β has distinct properties from IL-1 α but shares many pro-inflammatory actions and can also induce VSMCs to express MMP3, MMP9, MMP12 and IL6 (Libby, 2017; Rader, 2012). Antibody reagents that neutralize IL-1 α have entered clinical trials and hold potential for the treatment of CVD (Libby, 2017; Pradère et al., 2016). Enzymes that regulate epigenetic mechanisms have been successfully targeted in cancer treatments (Song et al., 2016). Perhaps, manipulation of the expression of IL-1 α -responsive genes by interfering with the H3K9me2 pathway provides an alternative strategy to the development of IL-1 α inhibitors.

**CHAPTER 5 - RESULTS: The functional role of
H3K9me2 in regulating VSMC gene expression
changes associated with vascular disease is
conserved in human**

5.1 Introduction

Mouse models have greatly developed our understanding of human CVD and have been instrumental in evaluating the effectiveness of new therapies. Strikingly, we share 95% of our protein encoding genes with mice (von Scheidt et al., 2017) and regulatory elements are often marked by evolutionarily conserved histone modifications which signify their function (Diehl and Boyle, 2018). Indeed, out of 46 genes with strong association signals in human coronary artery disease-genome wide association studies that were studied in mice, 45 significantly affected atherosclerosis (von Scheidt et al., 2017). The murine findings discussed in Chapters 3 and 4 suggest that H3K9me2 plays an indirect role in maintaining the contractile VSMC state and acts directly at IL-1 α -responsive gene promoters to block spurious induction of a pro-inflammatory state.

However, despite phylogenetic similarities between mice and humans there are still many differences between the two species and conserved chromatin signatures do not always equate to conserved regulatory functions (Diehl and Boyle, 2018; von Scheidt et al., 2017). In contrast to mice, within human vasculature, a significant number of VSMCs exist within the intima in conserved locations, including branch sites and areas of turbulent blood flow, prior to disease (Doran et al., 2008). Furthermore, as wild-type mice are resistant to plaque development, mouse models of atherosclerosis are based on genetic modifications of lipid metabolism with additional dietary changes and are therefore unlikely to perfectly reflect the mechanisms which underlie human disease. For example, a disadvantage of the ApoE^{-/-} high fat diet mouse model of atherosclerosis is lack of plaque rupture (Emini Veseli et al., 2017). In addition, ApoE is known to play a role in inflammation, which may influence plaque development (Emini Veseli et al., 2017). Consequently, mice created to mimic human disease frequently have phenotypes that differ from their human counterparts (Perlman, 2016). Perhaps, the lack of success of CVD clinical trials can, in part, be attributed to differences between mice and humans (Baylis et al., 2017). Therefore, whether the functional role of H3K9me2 in the regulation of vascular disease associated gene expression is conserved in human VSMCs (hVSMCs) and could therefore be relevant in the context of human CVD was explored.

Aims:

Use human VSMCs to:

1. Assess local levels of H3K9me2 at contractile VSMC genes upon loss of the contractile VSMC state using an *in vitro* model of VSMC phenotypic switching and chromatin immunoprecipitation.
2. Test the functional role of H3K9me2 on contractile VSMC gene expression *in vitro* using small molecule inhibition and siRNA knock down of the main H3K9 di-methyltransferases G9A/GLP.
3. Assess local levels of H3K9me2 at MMP and pro-inflammatory VSMC gene promoters, which are strongly associated with CVD, by chromatin immunoprecipitation.
4. Test the functional role of H3K9me2 on MMP and pro-inflammatory VSMC gene expression *in vitro* using small molecule inhibition or siRNA knock down of the main H3K9 di-methyltransferases G9A/GLP prior to IL-1 α stimulation.

5.2 Results

5.2.1 Global levels of H3K9me2 are reduced in cultured relative to ex vivo human VSMCs, concomitant with loss of the contractile state.

To explore whether the functional role of H3K9me2 in the regulation of VSMC gene expression is conserved in human, hVSMCs were derived from explant cultures from patients undergoing aortic valve replacement surgery. Similar to mouse, cultured hVSMCs display absent or low levels of H3K9me2 at contractile VSMC gene promoters compared to the *ACTB* negative control *locus* (Figure 5.1 A). Furthermore, contractile VSMC genes (*CNN1*, *TAGLN*, *MYOCD*, *ACTA2*, *STMN*) retained the active H3K4me3 chromatin mark (Figure 5.1 B) but were 20-100-fold downregulated in cultured compared to *ex vivo* tissue samples (Figure 5.1 C). Retention of H3K4me3 is commonly used to identify active gene promoters and does not normally mark repressed gene promoters. Therefore, like H3K4me2, if H3K4me3 marks contractile gene promoters specifically in VSMCs, the H3K4me3 mark could be used for VSMC lineage tracing in human tissue using *in situ* hybridisation proximity ligation (Shankman et al., 2015). Furthermore, this finding supports the theory that H3K4me2/3 may serve as a mechanism for epigenetic cell lineage memory to enable phenotypically modulated VSMCs to switch back to their contractile state.

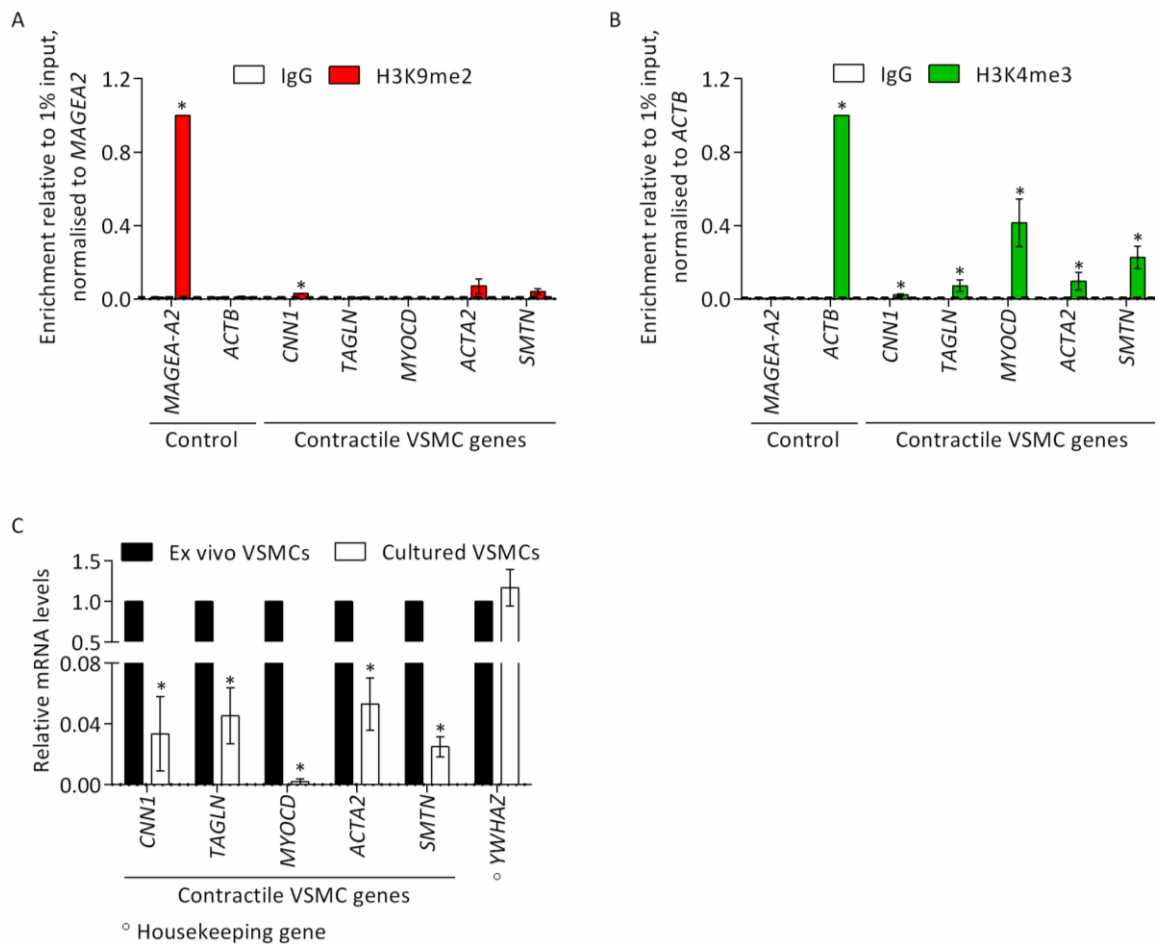


Figure 5.1: The repressive H3K9me2 mark is absent while the active H3K4me3 mark is retained at contractile VSMC gene promoters in cultured human VSMCs, despite their transcriptional silencing. (A) ChIP-qPCR analysis for H3K9me2 (red bars) and negative control IgG (white bars) in hVSMCs cultured to passage 7-8 showing levels of enrichment at control *loci* (*MAGEA2*, positive and *ACTB*, negative) and contractile VSMC genes. Data are relative to 1% input and normalised to enrichment at *MAGEA2* (red bar). Data represent means \pm SEM of 3 biological replicates using VSMCs derived from independent biopsies. Background levels of H3K9me2 are based on enrichment at the *ACTB* negative control *locus* and are indicated by a dashed line. Asterisks indicate significant differences (P<0.05) in enrichment versus IgG negative control by unpaired student's t test. **(B)** ChIP qPCR analysis for H3K4me3 (green bars) and negative control IgG (white bars) in hVSMCs cultured to passage 7-8 showing levels of enrichment at control *loci* (*MAGEA2*, negative and *ACTB*, positive) and contractile VSMC genes. Data are relative to 1% input and normalised to enrichment at *ACTB* (green bar). Data represent means \pm SEM of 3 biological replicates using VSMCs derived from independent biopsies. Background levels of H3K4me3 are based on enrichment at the *MAGEA2* negative control *locus* and are indicated by a dashed line. Asterisks indicate significant differences (P<0.05) in enrichment versus IgG negative control by unpaired student's t test. **(C)** RT-qPCR analysis of *CNN1*, *TAGLN*, *MYOCD*, *ACTA2*, *SMTN* and *YWHAZ* transcript levels in *ex vivo* hVSMCs and hVSMCs cultured to passage 7-8. Data are relative to *ex vivo* hVSMCs from different biopsies and normalised to two housekeeping genes (*HMBS* and *YWHAZ*). Data represent means \pm SEM of 3 biological replicates using VSMCs derived from independent biopsies. Asterisks

indicate significant differences ($P < 0.05$) in expression level in cultured versus *ex vivo* hVSMCs by unpaired student's t test.

To investigate whether H3K9me2 also influences the expression of contractile markers in cultured hVSMCs, the methyltransferases G9A/GLP were pharmacologically inhibited by UNC treatment. Consistent with how UNC affects mouse VSMCs, the resulting global loss of H3K9me2 (Figure 5.2 A, B) further attenuated the expression of *MYOCD* and *MYOCD*-dependent contractile VSMC genes including *CNN1*, *TAGLN*, *ACTA2* (Figure 5.2 C). However, *SMTN*, a *MYOCD*-independent contractile VSMC gene, was not influenced by UNC treatment (Figure 5.2 C). I therefore hypothesised that, in hVSMCs, H3K9me2 acts to inhibit a negative regulator of *MYOCD* and therefore *MYOCD*-dependent genes. Potent repressors of *MYOCD* and *MYOCD*-dependent genes include *KLF4*, *P65* and *G6PD* (Chettimada et al., 2016; Dhagia et al., 2014; Herring et al., 2017; Liu et al., 2005; Turner et al., 2013; Yoshida et al., 2013). Inhibition of H3K9me2 in cultured human VSMCs did not influence the expression of *KLF4* or *P65* but upregulated levels of *G6PD* by 1.6-fold compared to untreated VSMCs (Figure 5.2 C).

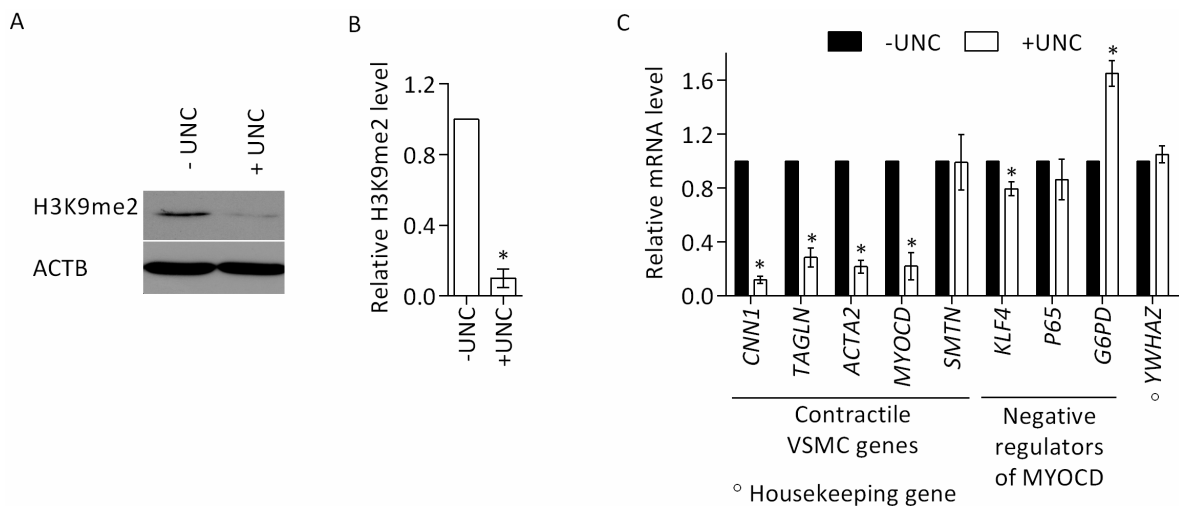


Figure 5.2: Loss of H3K9me2 correlates with the downregulation of contractile genes in human VSMCs. (A, B) Representative western blot (A) and densitometric analysis (B) of H3K9me2 levels in untreated control (-UNC) and UNC treated (+UNC) hVSMCs. hVSMCs were treated after 7-13 passages of culture. Data are relative to untreated control (-UNC) hVSMCs and normalised to ACTB. Data represent means \pm SEM of 3 biological replicates using VSMCs derived from independent biopsies. The asterisk indicates significant difference ($P < 0.05$) in H3K9me2 levels in UNC treated (+UNC) versus untreated control (-UNC) hVSMCs by unpaired student's t test. (C) RT-qPCR analysis of *CNN1*, *TAGLN*, *ACTA2*, *MYOCD*, *SMTN*, *KLF4*, *P65*, *G6PD* and *YWHAZ* transcript levels in untreated control (-UNC, black bars) and UNC treated (+UNC, white bars) hVSMCs. hVSMCs were treated after 7-13 passages of culture. Data are relative to untreated control (-UNC, black bars) hVSMCs and normalised to the average of two housekeeping genes (*HPRT1* and *YWHAZ*). Data represent means \pm SEM

of 3-8 biological replicates using VSMCs derived from independent biopsies (n= 3 for *P65* and *TAGLN*, n= 4 for *CNN1* and *KLF4*, n= 5 for *MYOCD* and *SMTN*, n= 6 for *ACTA2* and n= 8 for *G6PD* and *YWHAZ*). Asterisks indicate significant differences ($P < 0.05$) in expression level in UNC treated (+UNC, white bars) versus untreated control (-UNC, black bars) hVSMCs by unpaired student's t test.

In summary, reduced levels of H3K9me2 correlate with increased expression of G6PD, a potent repressor of MYOCD (Chettimada et al., 2016; Dhagia et al., 2014; Gupte et al., 2011). Interestingly, a study has found that G6PD activity is increased, while expression of MYOCD and MYOCD-dependent genes is decreased, in large blood vessels from obese-diabetic compared to non-obese-diabetic patients and that MYOCD downregulation is blocked by G6PD inhibition or knockdown (Dhagia et al., 2014). Furthermore, it has been reported that compared to VSMCs from healthy aortic tissue, global levels of H3K9me2 are reduced in human VSMCs from atherosclerotic lesions (Greiβel et al., 2015). Therefore, it is interesting that inhibition of H3K9me2 by UNC treatment upregulated G6PD transcript levels, whilst attenuating the expression of MYOCD and MYOCD-dependent contractile VSMC gene expression. Based on these observations, it is tempting to speculate that H3K9me2 inhibits the expression of G6PD, which could explain the reduced level of MYOCD and MYOCD-dependent contractile VSMC gene expression upon UNC treatment.

5.2.2 H3K9me2 marks IL-1 α -responsive gene promoters in human VSMCs.

Consistent with findings using mouse VSMCs, ChIP revealed high levels of H3K9me2 locally at a subset of IL-1 α -induced genes including *MMP3*, *MMP9* and *IL6* in cultured hVSMCs (Figure 5.3 A, B) compared to the *ACTB* negative control *locus*, which persisted after IL-1 α stimulation (Figure 5.3 B). However, the *MMP2* promoter, a gene constitutively expressed by VSMCs and uninfluenced by IL-1 α treatment (Figure 5.3 A), did not display H3K9me2 (Figure 5.3 B). Like in mouse, H3K9me2 was not observed at the *CCL2* promoter, a IL-1 α -induced gene, in cultured hVSMCs with or without IL-1 α stimulation (Figure 5.3 A, B).

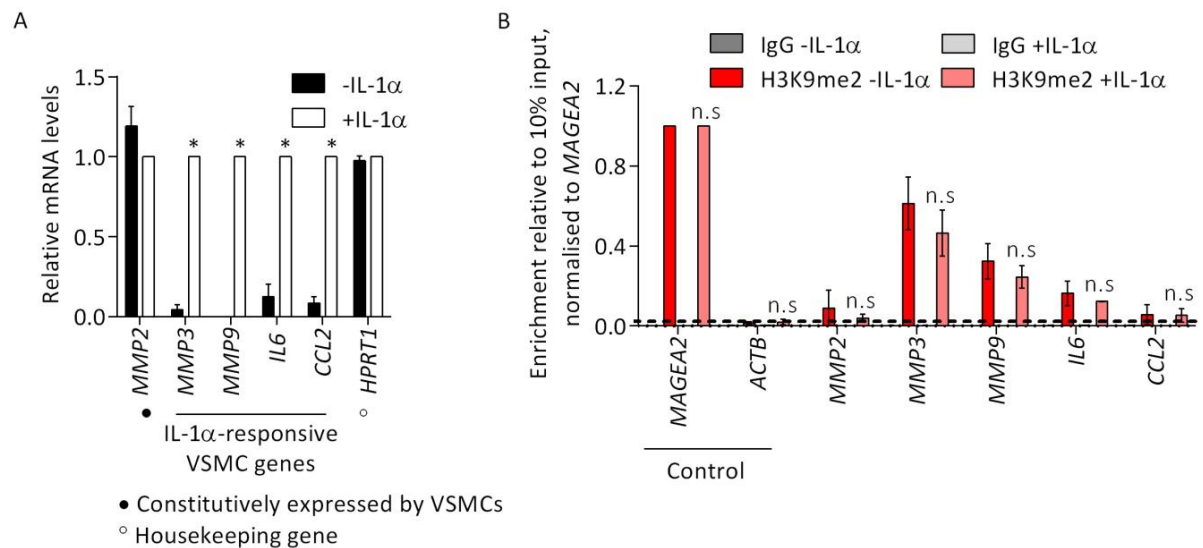


Figure 5.3: A subset of IL-1 α -responsive gene promoters, including *MMP3*, *MMP9* and *IL6*, are highly enriched for H3K9me2 in cultured hVSMCs. (A) RT-qPCR analysis of *MMP2*, *MMP3*, *MMP9*, *IL6*, *CCL2* and *HPRT1* transcript levels in untreated control (-IL-1 α , black bars) and IL-1 α -treated (+IL-1 α , white bars) cultured hVSMCs. hVSMCs were treated at passage 6-8. Data are relative to IL-1 α -treated (+IL-1 α , white bars) cultured hVSMCs and normalised to two housekeeping genes (*HPRT1* and *YWHAZ*). Data represent means \pm SEM of 4 biological replicates using hVSMCs derived from independent biopsies. Asterisks indicate significant differences in expression level in IL-1 α -treated (+IL-1 α , white bars) versus untreated control (-IL-1 α , black bars) hVSMCs by unpaired student's t test. **(B)** CHIP-qPCR analysis for H3K9me2 in untreated control (-IL-1 α , red bars) and IL-1 α -treated (+IL-1 α , pink bars) cultured hVSMCs (treated at passage 6-8), showing levels of enrichment at control loci (*MAGEA2*, positive and *ACTB*, negative) and the promoters of *MMP2*, *MMP3*, *MMP9*, *IL6* and *CCL2* compared with enrichment observed using negative control IgG (grey bars). Background levels of H3K9me2 are based on enrichment at the *ACTB* negative control locus and are indicated by a dashed line. Data represent means \pm SEM of 4 biological replicates using hVSMCs derived from independent biopsies. n.s indicates no significant differences in H3K9me2 levels in IL-1 α -treated (+IL-1 α , pink bars) versus untreated control (-IL-1 α , red bars) cultured hVSMCs by one-way ANOVA with *Bonferroni* correction.

5.2.3 Inhibition of H3K9me2 potentiates *IL6* and *MMP* gene expression in human VSMCs

To explore whether the levels and/or kinetics of IL-1 α -induced VSMC gene expression are altered by H3K9me2 inhibition we analysed cultured hVSMCs at numerous time points following IL-1 α stimulation with or without prior UNCO638 (UNC) treatment. UNC treatment significantly reduced global levels of H3K9me2 by 12.5-fold (Figure 5.2 A, B). Consistent with how UNC affects mouse VSMCs, the reduced level of H3K9me2 did not directly affect *IL6* or *MMP* gene expression, but significantly potentiated IL-1 α -mediated upregulation of *MMP3*, *MMP9* and *IL6* without influencing the timing of their induction (Figure 5.4 A-D). Interestingly, *MMP3*, *IL6* and *CCL2* became significantly

upregulated following 1.5 hours of IL-1 α stimulation (Figure 5.4 A, B D, E), whereas *MMP9* did not become significantly upregulated until 6 hours post IL-1 α treatment (Figure 5.4 C). Neither IL-1 α nor UNC treatment alone, or in combination, affected the expression of *MMP2* (Figure 5.4 F). To test whether the effect of UNC on MMP expression is due to a general upregulation of the inflammatory response, we analysed expression of the pro-inflammatory cytokine *CCL2*, that showed no H3K9me2 enrichment (Figure 5.3 B). IL-1 α treatment induced the expression of *CCL2*, whereas UNC alone or in combination with IL-1 α had no effect (Figure 5.4 E) demonstrating the specific effect of UNC-mediated reduction of H3K9me2 on genes showing enrichment for this mark. Together, these results suggest that in human VSMCs, H3K9me2 acts directly at the promoters of *MMP3*, *MMP9* and *IL6* to prevent excessive levels of expression without influencing the timing of their induction.

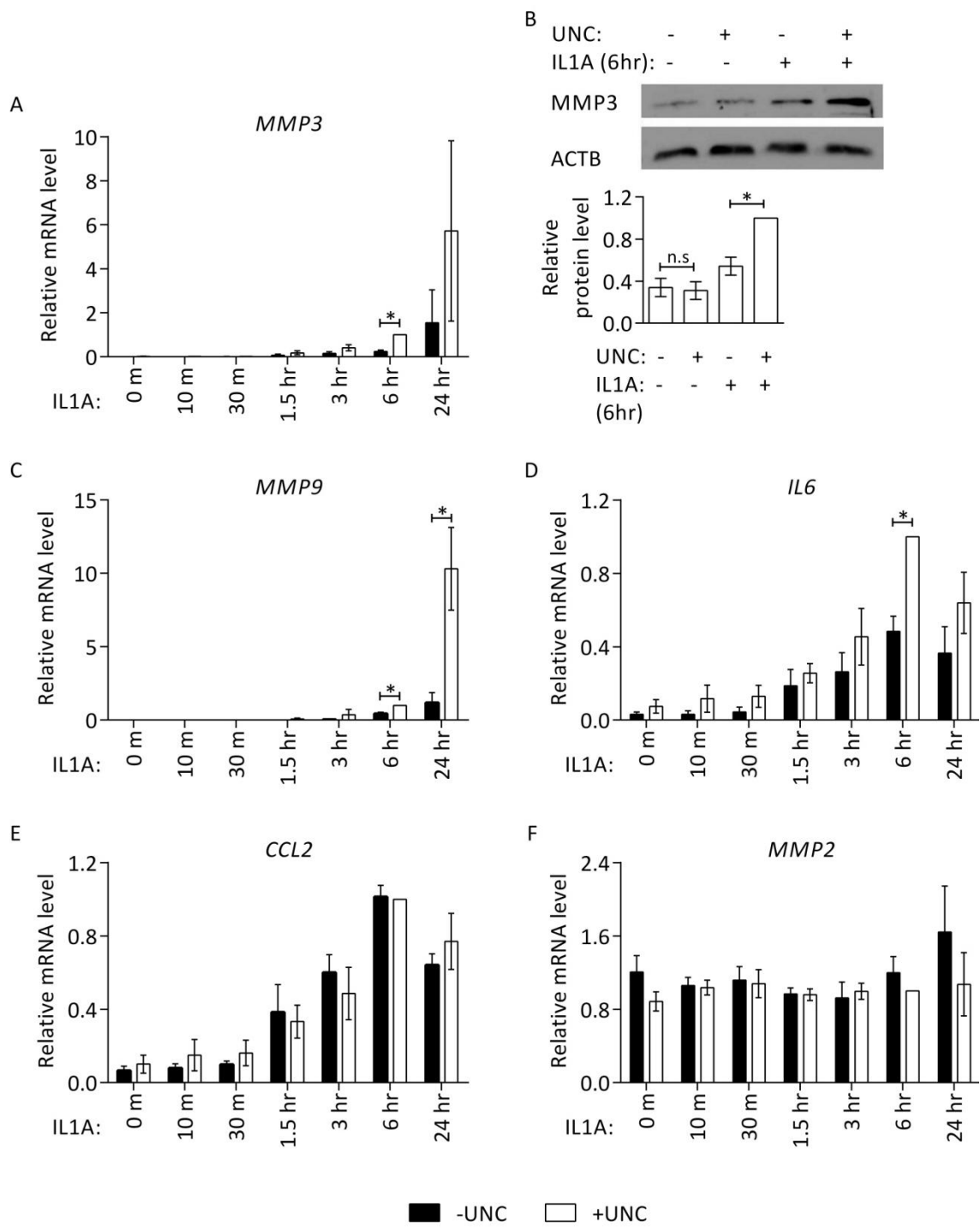


Figure 5.4: H3K9me2 regulates IL-1 α -responsive genes in cultured hVSMCs. (A, C-F) RT-qPCR analysis of *MMP3* (A), *MMP9* (C), *IL6* (D), *CCL2* (E) and *MMP2* (F) transcript levels in untreated control and IL-1 α -treated (for 10 mins, 30 mins, 1.5 hr, 3 hr, 6 hr or 24 hr) cultured hVSMCs, without (-UNC, black bars) and with (+UNC, white bars) prior UNC0638 treatment. hVSMCs were treated after 8-13 passages of culture. Data are relative to UNC plus IL-1 α (6hrs) treated hVSMCs and normalised to the average of two housekeeping genes (HMBS and YWHAZ). Data represent means \pm SEM of 4 biological replicates using VSMCs derived from independent biopsies. Asterisks indicate significant differences ($P < 0.05$) by one-way ANOVA with *Bonferroni* correction. (B) Representative western blot and densitometric analysis of MMP3 protein levels in untreated control (-UNC -IL-1 α), UNC (+UNC -IL-1 α), IL-1 α (-UNC, +IL-1 α) and IL-1 α plus UNC (+UNC +IL-1 α) treated hVSMCs. hVSMCs were

treated after 8-13 passages of culture. Data are relative to +UNC +IL-1 α and normalised to ACTB levels. Data represent means \pm SEM of 3 biological replicates using VSMCs derived from independent biopsies. Asterisks indicate significant differences ($P < 0.05$) by one-way ANOVA with *Bonferroni* correction.

5.2.4 siRNA knockdown of G9A attenuates the expression of contractile VSMC genes.

Reduction of H3K9me2, by pharmacological inhibition of G9A/GLP using UNC, potentiated IL-1 α -mediated upregulation of MMP gene expression in both mouse (Figure 4.2 D) and human cultured VSMCs (Figure 5.4). However, there is a possibility that UNC has off-target effects (Pappano et al., 2015), which are perhaps responsible for this observation. Therefore, to validate these results I knocked down G9A in cultured human VSMCs using siRNA. G9A knockdown resulted in a 15.8-fold reduction in G9A at the protein level (Figure 5.5 A, B) and a 70% reduction of G9A at the mRNA level compared to control cells treated with scrambled non-targeting siRNA (Figure 5.5 D). This reduction in G9A led to a 3.3-fold reduction in global levels of H3K9me2 (Figure 5.5 A, C). Similar to what was observed using G9A/GLP inhibition, G9A knockdown attenuated the expression of a subset of VSMC genes, including *ACTA2*, *TAGLN* and *CNN1* (Figure 5.5 D). However, in contrast to UNC treatment, G9A knockdown by siRNA did not influence *MYOCD* or *G6PD* expression (Figure 5.5 D). Consistent with the effect of UNC treatment, G9A knockdown alone did not significantly influence the expression of *MMP3* or *IL6*, but further potentiated IL-1 α -induced *MMP3* and *IL6* expression (Figure 5.5 E). Neither IL-1 α treatment nor G9A knockdown alone, or in combination, affected the expression of *MMP2* (Figure 5.5 E). IL-1 α treatment induced the expression of *CCL2*, whereas G9A knockdown alone or in combination with IL-1 α had no effect (Figure 5.5 E). These results confirm that the functional role of H3K9me2 in blocking IL-1 α -mediated induction of target gene expression is not due to an off-target effect of UNC.

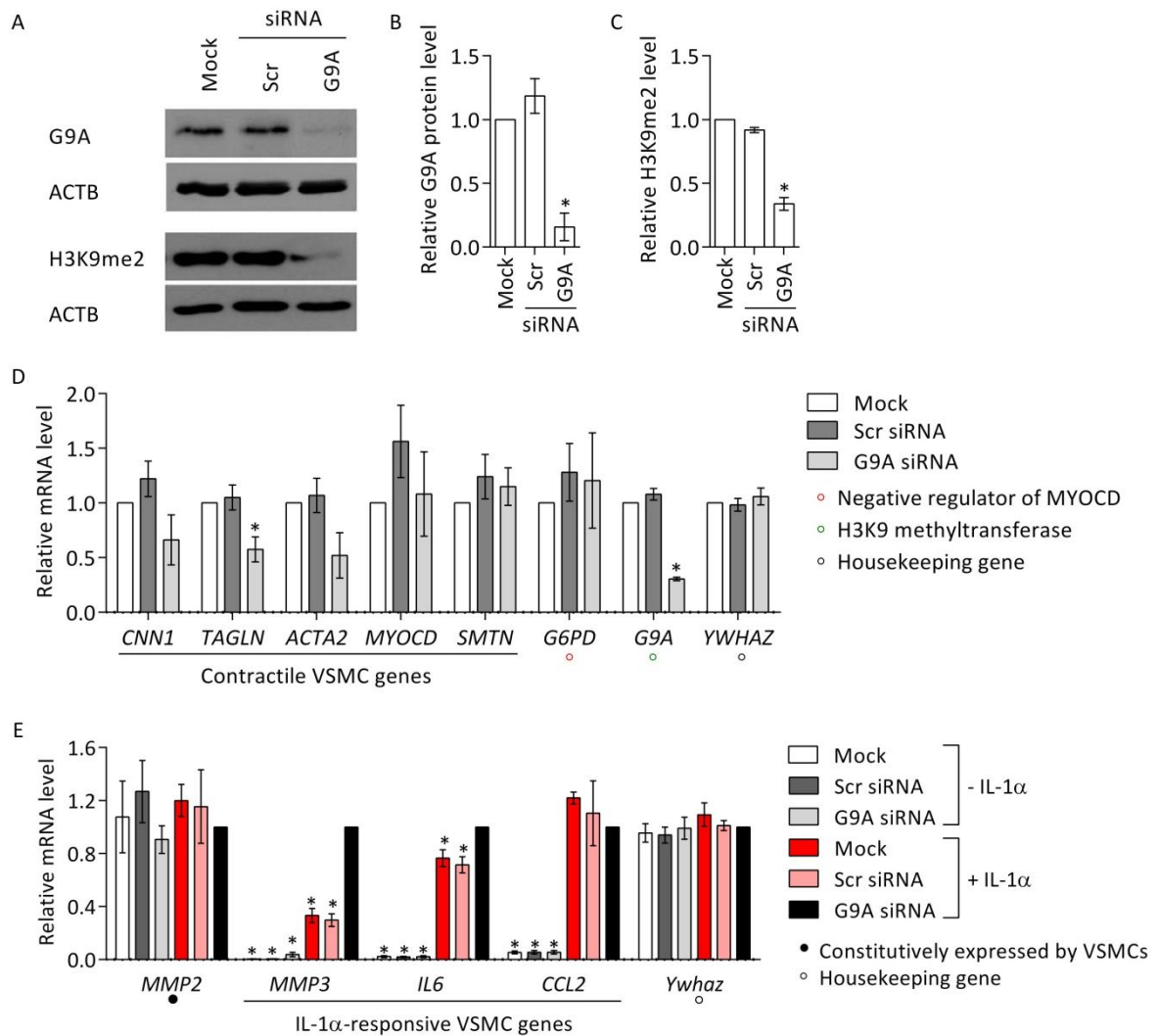


Figure 5.5: SiRNA knock down of G9A reduced global H3K9me2 levels, attenuated contractile VSMC gene expression and potentiated IL-1 α -induced *MMP3* and *IL6* expression in cultured hVSMCs. (A-C) Representative western blot **(A)** and densitometric analysis of G9A **(B)** and H3K9me2 **(C)** levels in mock, scrambled (Scr) siRNA and G9A siRNA transfected cultured hVSMCs. hVSMCs were treated after 7-11 passages of culture. Data are relative to mock transfected hVSMCs and normalised to ACTB. Data represent means \pm SEM of 4 biological replicates using VSMCs derived from independent biopsies. Asterisks indicate significant difference ($P < 0.05$) in protein level versus mock transfected hVSMCs by one-way ANOVA with *Bonferroni* correction. **(D)** RT-qPCR analysis of *CNN1*, *TAGLN*, *ACTA2*, *MYOCD*, *SMTN*, *G6PD*, *G9A* and *YWHAZ* transcript levels in mock, Scr siRNA and G9A siRNA transfected cultured hVSMCs. hVSMCs were transfected after 7-11 passages of culture. Data are relative to mock (white bars) transfected hVSMCs and normalised to two housekeeping genes (*HPRT1* and *YWHAZ*). Data represent means \pm SEM of 4 biological replicates using VSMCs derived from independent biopsies. Asterisks indicate significant differences ($P < 0.05$) versus mock transfected hVSMCs (white bars) by one-way ANOVA with *Bonferroni* correction. **(E)** RT-qPCR analysis of *MMP2*, *MMP3*, *IL6*, *CCL2* and *Ywhaz* transcript levels in mock, Scr siRNA and G9A siRNA transfected cultured hVSMCs. hVSMCs were transfected/ treated after 7-11 passages of culture. Data are relative to G9a siRNA + IL-1 α (black bars) treated hVSMCs and normalised to two housekeeping genes (*HPRT1* and *YWHAZ*). Data represent means \pm SEM

of 4 biological replicates using VSMCs derived from independent biopsies. Asterisks indicate significant differences ($P < 0.05$) in expression level versus G9A siRNA +IL-1 α (black bars) treated hVSMCs by one-way ANOVA with *Bonferroni* correction.

5.3 Summary and Conclusions

Together, the results presented in this chapter show that H3K9me2 plays a role in regulating the expression of human VSMC genes associated with vascular disease. Consistent with how UNC affects mouse VSMCs, loss of H3K9me2 by pharmacological inhibition of the associated methyltransferase G9A (Figure 5.2 A, B) attenuates the expression of *MYOCD* and *MYOCD*-dependent contractile hVSMC genes including *CNN1*, *TAGLN*, *ACTA2* (Figure 5.2 C). However, in contrast to mouse, *SMTN*, a *MYOCD*-independent contractile VSMC gene, was not influenced by UNC treatment (Figure 5.2 C). I therefore hypothesised that H3K9me2 acts to inhibit a negative regulator of *MYOCD* and therefore *MYOCD*-dependent genes in human VSMCs. Interestingly, global loss of H3K9me2 upregulated mRNA levels of *G6PD* (Figure 5.2 C), a potent repressor of *MYOCD* (Chettimada et al., 2016; Dhagia et al., 2014; Gupte et al., 2011).

G6PD is the rate-limiting enzyme that commits glucose to the pentose phosphate pathway (Gupte et al., 2011). It is responsible for the generation of nicotinamide adenine dinucleotide phosphate reduced (NADPH), a key cofactor in various redox and antioxidant systems, and ribose 5-phosphate, an essential precursor for the *de novo* synthesis of RNA and DNA (Gupte et al., 2011). Researchers have shown that G6PD inhibition in cultured rat aortic SMCs increases the expression of *MYOCD* and *MYOCD*-dependent genes (Chettimada et al., 2016). Another study has also found that G6PD activity is increased, while expression of *MYOCD* and *MYOCD*-dependent genes is decreased, in large blood vessels from obese-diabetic compared to non-obese-diabetic patients and that *MYOCD* downregulation is blocked by G6PD inhibition or knockdown (Dhagia et al., 2014). Furthermore, compared to VSMCs from healthy aortic tissue, global levels of H3K9me2 are reduced in human VSMCs from atherosclerotic lesions (Greißel et al., 2015). Therefore, it is interesting that inhibition of H3K9me2 by UNC treatment upregulated G6PD transcript levels, whilst attenuating the expression of *MYOCD* and *MYOCD*-dependent contractile VSMC gene expression. Perhaps, H3K9me2 inhibits the expression of G6PD to maintain the contractile VSMC state. It would be interesting to investigate whether levels of H3K9me2 specifically at the G6PD promoter influence the expression of *MYOCD* and *MYOCD*-dependent genes in human VSMCs. This could be achieved using CRISPR/dCas9 technology to recruit the enzymatic activity of a H3K9me2 demethylase or methyltransferase specifically to the G6PD promoter.

In further agreement with our murine studies, IL-1 α -responsive genes including *IL6*, *MMP3* and *MMP9* are enriched for H3K9me2 in cultured hVSMCs (Figure 5.3) and global loss of H3K9me2 by pharmacological inhibition (Figure 5.4) or siRNA mediated knock-down of G9A (Figure 5.5) potentiates the IL-1 α -induced expression of these genes. To explore whether loss of H3K9me2 alters the kinetics of IL-1 α -induced gene expression we analysed a number of time points after stimulating cultured hVSMCs with IL-1 α with and without prior UNC treatment (Figure 5.4). Loss of H3K9me2 did not alter the timing of IL-1 α -induced expression of the H3K9me2 marked genes analysed (*MMP3*, *MMP9* and *IL6*) but did potentiate the level of their expression (Figure 5.4). In contrast to mouse, IL-1 α -induced *IL6* expression was significantly higher after H3K9me2 inhibition (Figure 5.4), corresponding with H3K9me2 enrichment at the *IL6* promoter (Figure 5.3 B). Intriguingly *MMP3*, *IL6* and *CCL2* became significantly upregulated 1.5 hours after IL-1 α stimulation, whereas *MMP9* did not become significantly upregulated until 6 hours after IL-1 α treatment (Figure 5.4) suggesting *MMP9* is regulated by a different mechanism. In agreement with this finding, researchers have shown that *Mmp3* expression precedes *Mmp9* expression after balloon angioplasty of the rat carotid artery (Webb et al., 1997). Interestingly, Johnson and colleagues demonstrated that MMP3 is required to activate MMP9 mediated VSMC migration and neointima formation using a mouse carotid ligation injury model (Johnson et al., 2011b).

Discrepancies in the regulation of *SMTN* and *IL6* could be due to species-specific targeting of H3K9me2 in VSMCs or derived from technical or biological differences between human and murine VSMC cultures. Murine VSMCs were derived from young male mice while human VSMCs were sourced from male and female patients ranging from 20 to 78 years old. As sex and age are known to influence VSMC gene expression (Bennett et al., 2016; Mosca et al., 2011), this could explain the observed differences between species. Furthermore, human VSMCs were derived from patients undergoing aortic valve replacement surgery and are therefore likely to be from the aortic root, whereas mVSMCs were derived from the whole aorta. The difference in *SMTN* and *IL6* regulation between mouse and human VSMCs could therefore be due to regional differences in VSMC physiology and disease response (Sinha et al., 2014). Moreover, human VSMC cultures were derived using the explant method, which may have selected for migratory and proliferative cells, whereas mouse VSMC cultures were derived from dissociated aortic medial cell layers. Therefore, technical differences between human and mouse VSMC cultures could also contribute to the observed discrepancies in the regulation of *SMTN* and *IL6* between species.

To explore whether UNC was exerting its effects independently from G9A inhibition we knocked down G9A in cultured human VSMCs using siRNA (Figure 5.5). G9A siRNA knock down reduced global levels of H3K9me2, attenuated contractile VSMC gene expression and potentiated IL-1 α -induced

MMP3, *MMP9* and *IL6* expression in cultured hVSMCs but did not influence the expression of *MYOCD* and *G6PD* (Figure 5.5). Furthermore, although G9A siRNA knockdown (Figure 5.5) did significantly potentiate IL-1 α -induced expression of *MMP3* and *IL6*, it wasn't to as great an extent as pharmacological inhibition (Figure 5.4). G9A knockdown did not reduce global levels of H3K9me2 (3.3-fold reduction) (Figure 5.5 A, C) to as great a level as pharmacological inhibition (9.9-fold reduction) (Figure 5.2 A, B), which could explain these inconsistencies.

To conclude, our results show a specific, evolutionary conserved function of H3K9me2 to maintain contractile VSMC gene expression and block excessive expression of a subset of IL-1 α -responsive genes. Since decreased contractile VSMC gene expression and increased MMP and IL6 activity are features of vascular disease, H3K9me2-regulation may be a novel target for clinical intervention.

**CHAPTER 6 - RESULTS: Investigating the mechanism
behind G9A/GLP -mediated regulation of IL-1 α -
responsive VSMC genes**

6.1 Introduction

Pro-inflammatory cytokines activate NF κ B and MAPK-AP-1 signalling pathways leading to VSMC inflammatory activation. Dysregulation of these pathways is often linked to vascular disease, including atherosclerosis (Meijer et al., 2012; Ridker et al., 2017; van der Heiden et al., 2010; Weber and von Hundelshausen, 2017). IL-1 α activates translocation of the NF κ B mediated transcription factor p65, which contains the transactivation domain necessary for gene induction (Bhatt and Ghosh, 2014; Tak and Firestein, 2001), from the cytoplasm to the nucleus (Figure 6.1 A). IL-1 α also induces phosphorylation of MAPKs at specific residues, which ultimately leads to phosphorylation and binding of AP-1 transcription factors, such as cJUN, to target genes (Kim and Choi, 2015; Sun et al., 2015; Yang et al., 2013) (Figure 6.1 A).

In the literature, p65 and cJUN are reported as necessary to induce the expression of *MMP3* (Borghaei et al., 2004; Clark et al., 2008; Fleenor et al., 2003; Huang et al., 2012; Lu et al., 2016), *MMP9* (Chen and Chang, 2015; Clark et al., 2008), *MMP12* (Clark et al., 2008; Xie et al., 2005) (Huang et al., 2012; Park et al., 2015) and *IL6* (Faggioli et al., 2004). Furthermore, p65 and cJUN binding sites have been reported within 2 kb of the transcriptional start site (TSS) of *MMP3* (Borghaei et al., 2004; Clark et al., 2008; Fanjul-Fernández et al., 2010), *MMP9* (Chen and Chang, 2015; Clark et al., 2008; Fanjul-Fernández et al., 2010; Mishra et al., 2016), *MMP12* (Clark et al., 2008) and *IL6* (Faggioli et al., 2004; Gomard et al., 2010; Ndlovu et al., 2009).

Genome wide mapping has shown that H3K9me2 is broadly distributed (Wen et al., 2009) and may therefore influence numerous genes associated with NF κ B and MAPK-mediated pathways. Moreover, in addition to their role as histone lysine methyltransferases, G9A/GLP also have non-histone substrates, which may influence protein stability (Lee et al., 2015), protein-protein interactions (Lee et al., 2010; Ling et al., 2012) and regulate cellular signalling pathways (Biggar and Li, 2015; Pless et al., 2008). Therefore, G9A/GLP may influence IL-1 α -induced signalling, including NF κ B and MAPK-AP-1-mediated pathways, upstream of MMP and pro-inflammatory VSMC gene promoters. This chapter investigates how abolishing GLP/G9A activity affects IL-1 α signalling in cultured hVSMCs.

Aims:

To test whether G9A/GLP regulates inflammation-induced:

1. NFkB activity,
2. MAPK phosphorylation
3. and transcription factor binding to H3K9me2-target genes

in cultured hVSMCs by small molecule inhibition of G9A/GLP prior to IL-1 α stimulation.

6.2 Results

6.2.1 Loss of H3K9me2, by pharmacological inhibition of G9A/GLP, does not influence the upstream NFkB signalling pathway.

IL-1 α signals via the cell surface receptor IL1R1 (Garlanda et al., 2013), therefore I first examined whether pharmacological inhibition of G9A/GLP directly influences the expression of IL1R1. Cultured hVSMCs were pre-treated with UNC, a G9A/GLP inhibitor, prior to IL-1 α stimulation. UNC treatment significantly reduced H3K9me2 levels globally (Figure 5.2 A, B) but did not alter basal or IL-1 α -induced upregulation of *IL1R1* transcript levels (Figure 6.1 B). TNF α is also known to activate the transcription of MMP and pro-inflammatory genes via NFkB and AP-1 signalling pathways (Figure 6.1 A). However, TNF α signals via different membrane bound cytokine receptors (Sedger and McDermott, 2014). Therefore, cultured hVSMCs were pre-treated with UNC prior to TNF α treatment to further explore the mechanism by which G9A/GLP regulates the expression of IL-1 α -responsive genes. Consistent with results from hVSMCs treated with IL-1 α , the reduced level of H3K9me2 did not directly affect *IL6* or *MMP* gene expression, but significantly potentiated TNF α -mediated upregulation of *MMP3*, *MMP9* and *IL6* (Figure 6.1 C). Neither TNF α nor UNC treatment alone, or in combination, affected the expression of *MMP2* (Figure 6.1 C). Furthermore, UNC treatment did not alter basal or TNF α -induced upregulation of *CCL2* (Figure 6.1 C). Together, these results suggest that pharmacological inhibition of G9A/GLP mediates a feature common to both IL-1 α and TNF α signalling pathways in hVSMCs.

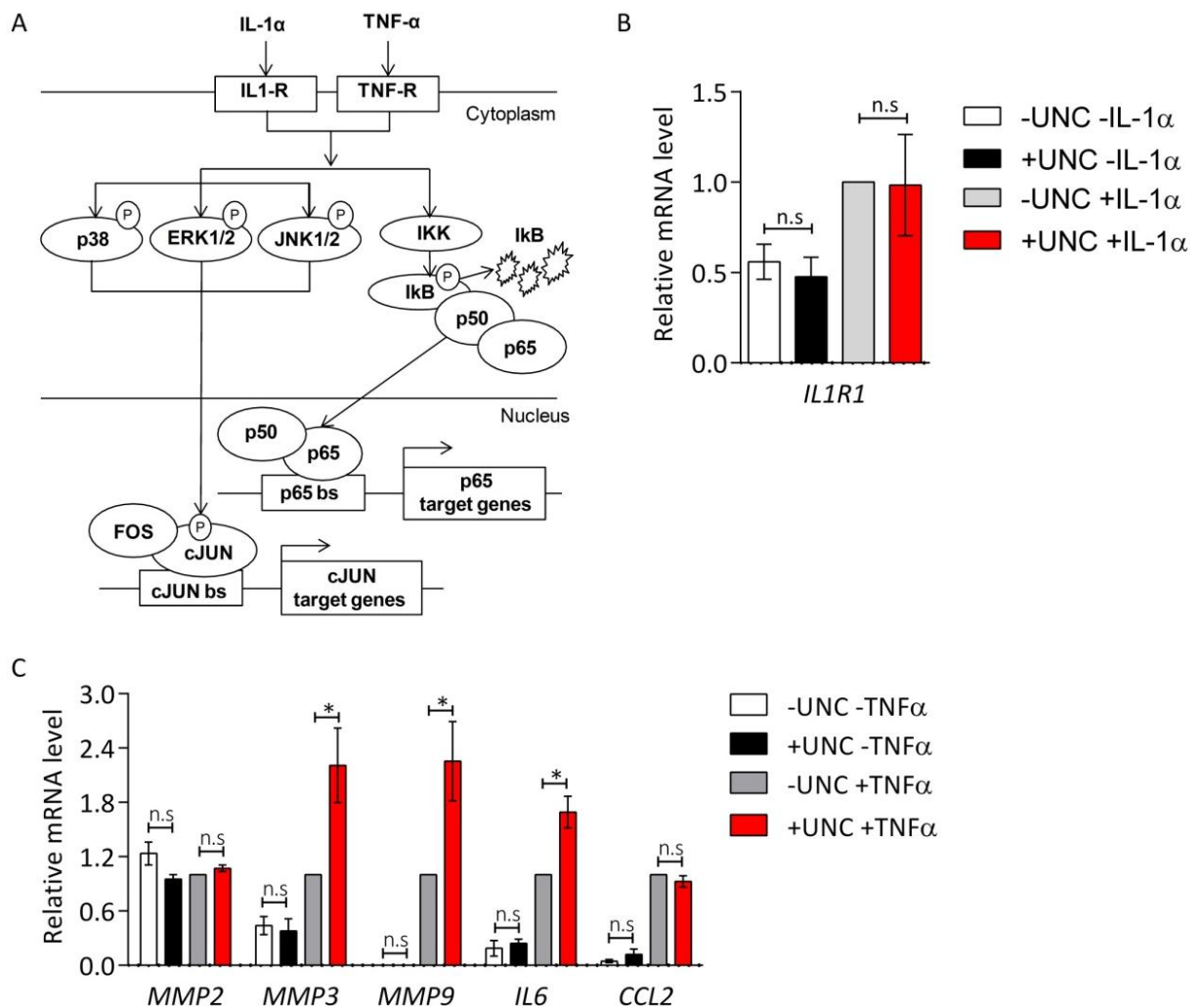


Figure 6.1: Loss of H3K9me2, by pharmacological inhibition of G9A/GLP (UNC), influences a feature common to both IL-1 α and TNF α signalling pathways in cultured hVSMCs. (A) Schematic of IL-1 α /TNF α -induced MAPK/NF κ B signalling pathways. **(B)** RT-qPCR analysis of *IL1R1* transcript levels in untreated control (-UNC -IL-1 α , white bars), UNC (+UNC -IL-1 α , black bars), IL-1 α (-UNC +IL-1 α , grey bars) and IL-1 α plus UNC (+UNC +IL-1 α , red bars) treated cultured hVSMCs. hVSMCs were treated after 6-9 passages of culture. Data are relative to IL-1 α treated hVSMCs (-UNC +IL-1 α , grey bars) and normalised to the average of two housekeeping genes (*HPRT1* and *HMBS*). Data represent means \pm SEM of 3 experiments using hVSMCs from independent biopsies. Asterisks indicate significant differences (p < 0.05) in expression level by one-way ANOVA with *Bonferroni* correction. **(C)** RT-qPCR analysis of *MMP2*, *MMP3*, *MMP9*, *IL6* and *CCL2* transcript levels in untreated control (-UNC -TNF α , white bars), UNC (+UNC -TNF α , black bars), TNF α (-UNC +TNF α , grey bars) and TNF α plus UNC (+UNC +TNF α , red bars) treated cultured hVSMCs. hVSMCs were treated after 6-9 passages of culture. Data are relative to TNF α treated hVSMCs (-UNC +TNF α , grey bars) and normalised to the average of two housekeeping genes (*HPRT1* and *HMBS*). Data represent means \pm SEM of 3 experiments using VSMCs isolated from independent biopsies. Asterisks indicate significant differences (p < 0.05) in expression level by one-way ANOVA with *Bonferroni* correction.

IL-1 α and TNF α both activate the NF κ B signalling pathway. Ligand binding to a cell surface receptor activates the IKK complex which phosphorylates I κ B and triggers ubiquitin-dependent proteosomal degradation of I κ B. NF κ B dimers are then released and translocate from the cytoplasm to the nucleus to bind to target gene promoters (Figure 6.1 A). The most prevalent activated form of NF κ B dimer includes a p65 subunit, which contains the transactivation domain necessary for gene induction (Bhatt and Ghosh, 2014; Tak and Firestein, 2001). Binding of p65 to a number of MMP and pro-inflammatory gene promoters, including *MMP3* (Borghaei et al., 2004; Clark et al., 2008; Fleenor et al., 2003; Huang et al., 2012; Lu et al., 2016), *MMP9* (Chen and Chang, 2015; Clark et al., 2008), *MMP12* (Clark et al., 2008; Xie et al., 2005) (Huang et al., 2012; Park et al., 2015) and *IL6* (Faggioli et al., 2004), has been reported as necessary to induce their expression.

To investigate whether G9A/GLP regulates inflammation-induced NF κ B activity, cultured VSMCs were pre-treated with UNC, a G9A/GLP inhibitor, prior to IL-1 α or TNF α stimulation. UNC treatment significantly reduced global levels of H3K9me2 (Figure 5.2 A, B). G9A/GLP inhibition did not change I κ B α levels upon IL-1 α stimulation, suggesting that I κ B α degradation is not affected (Figure 6.2 A, B). G9A/GLP inhibition also did not significantly alter the IL-1 α -induced upregulation of p65 (Figure 6.2 C, D).

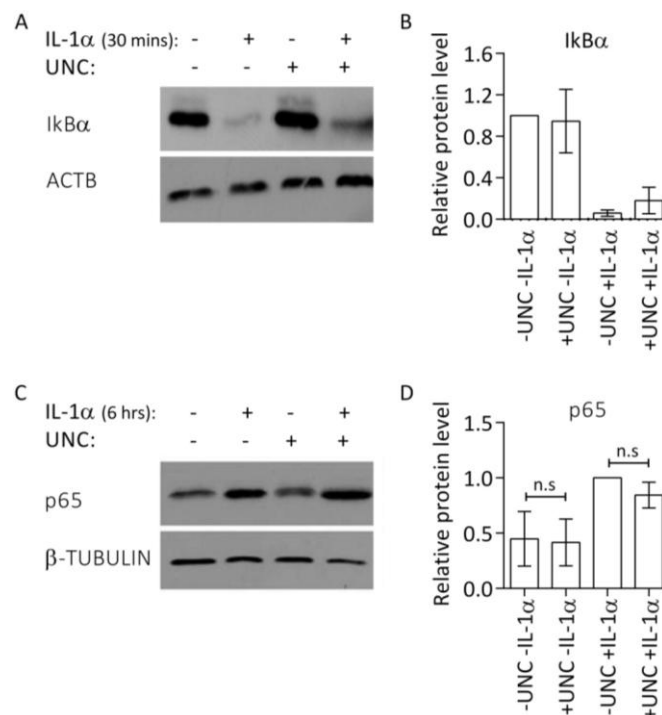


Figure 6.2: Pharmacological inhibition of G9A/GLP does not influence I κ B α levels upon IL-1 α stimulation or alter IL-1 α -induced upregulation of p65. (A, B) Representative western blot and densitometric analysis (B) of I κ B α protein and ACTB (control) in untreated control (-UNC -IL-1 α), IL-1 α -UNC +IL-1 α (for 30 mins), UNC (+UNC -IL-1 α), and UNC plus IL-1 α (+UNC +IL-1 α) treated cultured hVSMCs. hVSMCs were treated after 7-12 passages

of culture. **(B)** Bar plot showing I κ B α protein levels in untreated control (-UNC -IL-1 α), UNC (+UNC -IL-1 α), IL-1 α (-UNC +IL-1 α) and UNC plus IL-1 α (+UNC +IL-1 α) treated cultured hVSMCs. Data are relative to untreated control (-UNC -IL-1 α) cultured hVSMCs and normalised to ACTB levels. Data represent means \pm STDEV of 2 experiments using VSMCs derived from independent biopsies. **(C, D)** Representative western blot and densitometric analysis **(D)** of p65 protein and β -TUBULIN in untreated control (-UNC -IL-1 α), IL-1 α (-UNC +IL-1 α), UNC (+UNC-IL-1 α), and UNC plus IL-1 α (+UNC +IL-1 α) treated cultured hVSMCs. hVSMCs were treated after 7-12 passages of culture. **(D)** Bar plot showing p65 protein levels in untreated control (-UNC -IL-1 α), UNC (+UNC- IL-1 α), IL-1 α (-UNC + IL-1 α) and UNC plus IL-1 α (+UNC + IL-1 α) treated cultured hVSMCs. Data are relative to IL-1 α treated hVSMCs (-UNC +IL-1 α) and normalised to β -TUBULIN levels. Data represent means \pm SEM of 4 experiments using VSMCs derived from independent biopsies. n.s. = no significant difference by one-way ANOVA with *Bonferroni* correction. The IL-1 α treatment times are indicated in the figure (30 mins or 6 hrs).

Immunofluorescence staining revealed the reduced level of G9A/GLP activity did not directly affect the nuclear to cytoplasmic ratio of p65 under basal conditions nor the translocation of p65 from the cytoplasm to the nucleus upon IL-1 α (Figure 6.3 A, B) or TNF α stimulation (Figure 6.4 A, B). These results suggest that the potentiation of IL-1 α / TNF α -induced expression of *IL6* and *MMP* genes by pharmacological inhibition of G9A/GLP is not due to increased upstream NF κ B signalling.

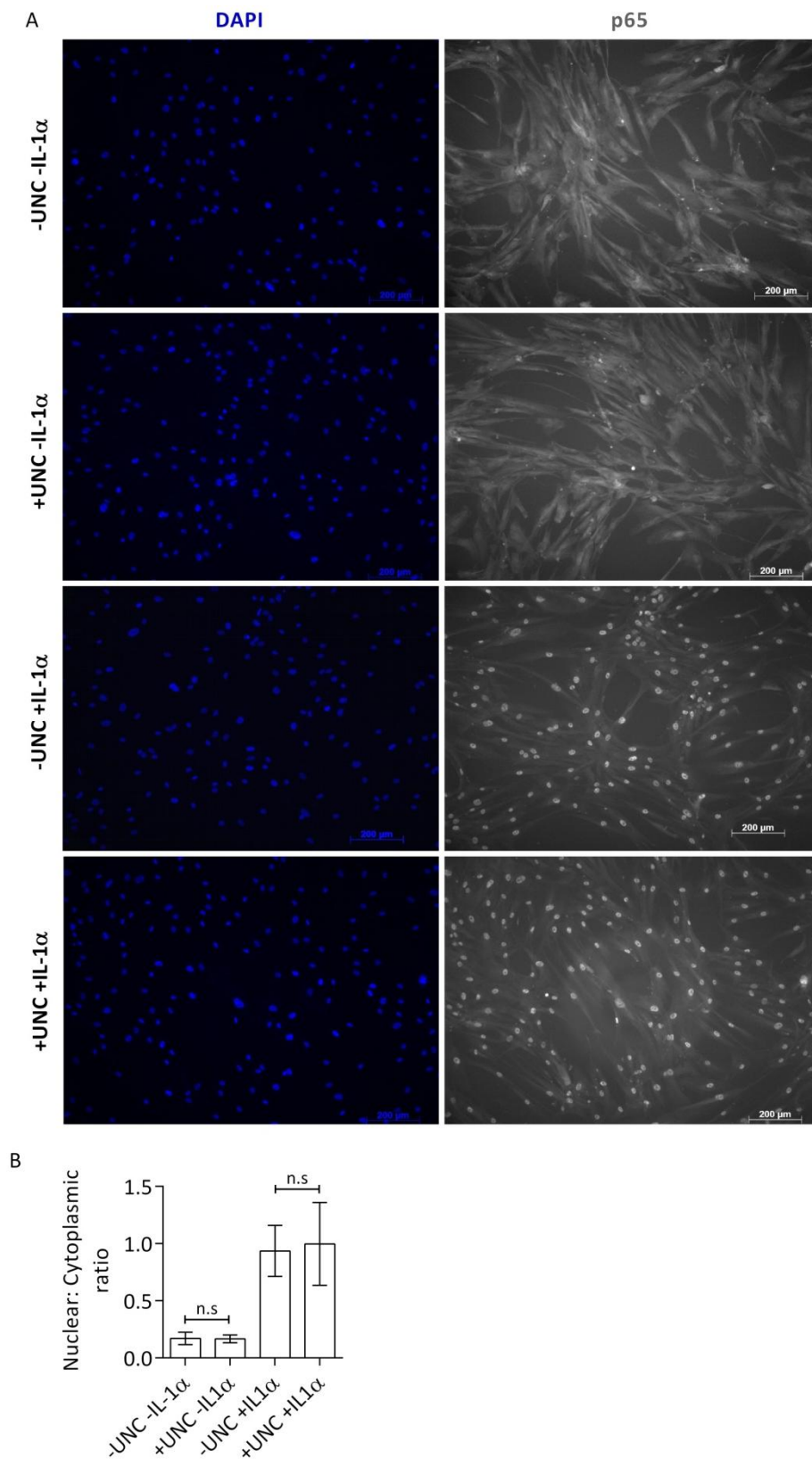


Figure 6.3: Pharmacological inhibition of G9A/GLP does not influence IL-1 α -mediated nuclear translocation of p65. (A) Immunofluorescence staining for p65 in untreated control (-UNC -IL-1 α), UNC (+UNC-IL-1 α), IL-1 α (-UNC +IL-1 α) and UNC plus IL-1 α (+UNC +IL-1 α) treated cultured hVSMCs. hVSMCs were treated after 7-12 passages of culture. Signals for p65 (Alexa Fluor 488, white) and DAPI counter-stained nuclei (blue) are shown.

Scale bars, 200 μm . **(B)** Bar plot showing the nuclear: cytoplasmic ratios of p65 staining in untreated control (-UNC -IL-1 α), UNC (+UNC -IL-1 α), IL-1 α (-UNC +IL-1 α) and UNC plus IL-1 α (+UNC +IL-1 α) treated cultured hVSMCs. hVSMCs were treated after 7-12 passages of culture. Data represent means \pm SEM of 4 experiments using VSMCs derived from independent biopsies. n.s. = no significant difference by one-way ANOVA with *Bonferroni* correction.

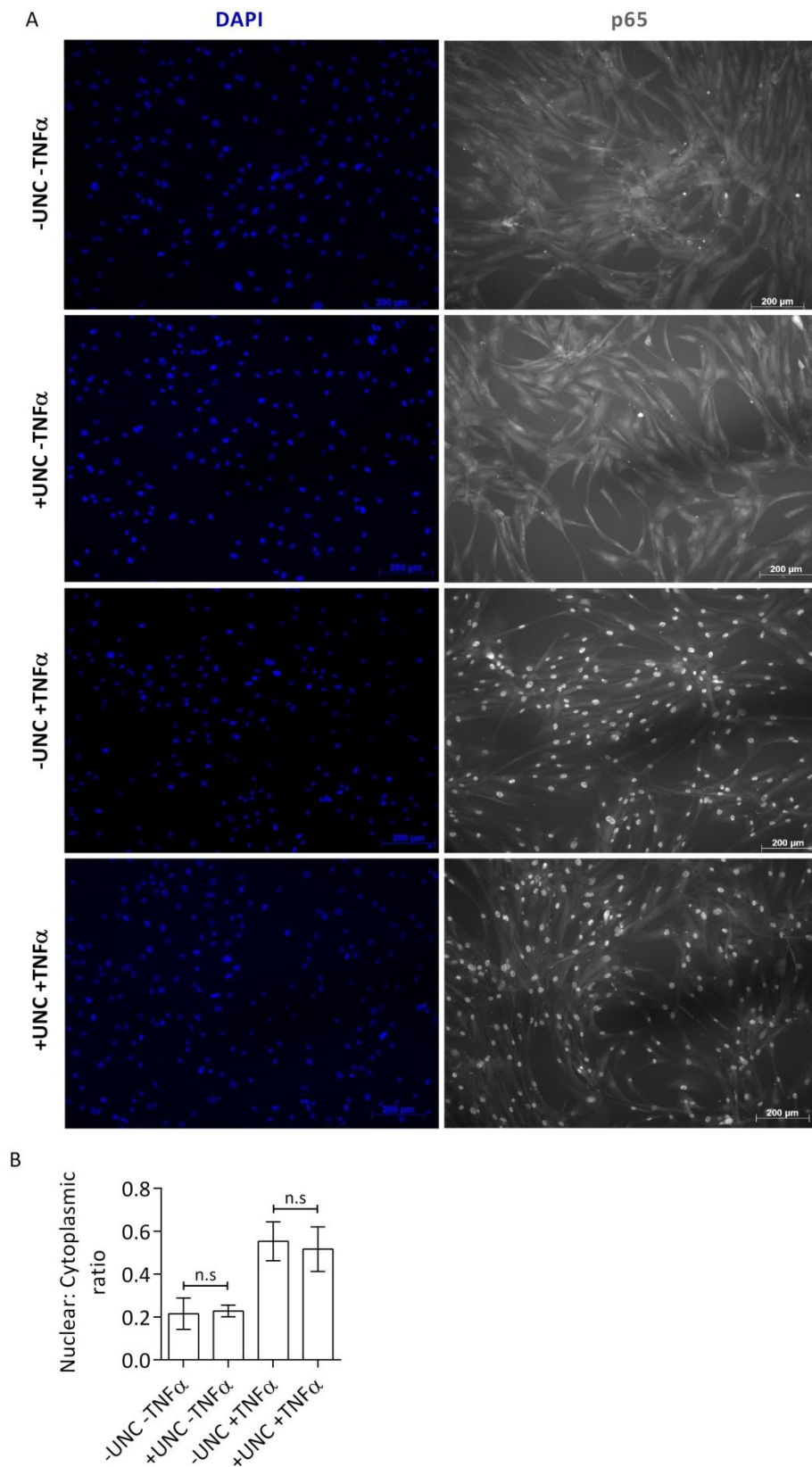


Figure 6.4: Pharmacological inhibition of G9A/GLP does not influence TNF α -mediated nuclear translocation of p65. (A) Immunofluorescence staining for p65 in untreated control (-UNC -TNF α), UNC (+UNC -TNF α), TNF α (-UNC +TNF α) and UNC plus TNF α (+UNC +TNF α) treated cultured hVSMCs. hVSMCs were treated after 7-12 passages of culture. Signals for p65 (Alexa Fluor 488, white) and DAPI counter stained nuclei (blue) are shown.

Scale bars, 200 μm . **(B)** Bar plot showing the nuclear: cytoplasmic ratios of p65 staining in untreated control (-UNC -TNF α), UNC (+UNC -TNF α), TNF α (-UNC +TNF α) and UNC plus TNF α (+UNC +TNF α) treated cultured hVSMCs. hVSMCs were treated after 7-12 passages of culture. Data represent means \pm SEM of 4 experiments using VSMCs derived from independent biopsies. n.s. = no significant difference by one-way ANOVA with *Bonferroni* correction.

6.2.2 Pharmacological inhibition of G9A/GLP potentiates IL-1 α -induced p65 binding to the IL6 promoter, correlating with reduced H3K9me2 levels in cultured hVSMCs.

To investigate whether H3K9me2 acts directly at the *IL6* and *MMP3* promoter to block IL-1 α -induced p65 binding, ChIP for p65 was performed. ChIP revealed p65 bound to the *IL6* promoter in unstimulated and UNC treated cultured hVSMCs, however, p65 binding was greatly enriched by IL-1 α stimulation and this was significantly enhanced by prior UNC treatment (Figure 6.5), correlating with reduced H3K9me2 levels (Figure 5.2 A, B). Enriched levels of p65 were also observed at the NF κ B binding site within the *CCL2* promoter in unstimulated and UNC treated cultured hVSMCs (Figure 6.5). However, neither IL-1 α or IL-1 α in combination with UNC treatment enhanced p65 binding to the *CCL2* promoter (Figure 6.5). In contrast, enrichment of p65 was not observed at reported NF κ B sites or IL1-responsive elements within the *MMP3* promoter (Borghaei et al., 2004; Clark et al., 2008) before or after IL-1 α stimulation with or without prior UNC treatment (Figure 6.5). These findings suggest H3K9me2 acts directly at the *IL6* promoter to block IL-1 α -mediated p65 binding and that *MMP3*, *IL6* and *CCL2* are regulated via different mechanisms.

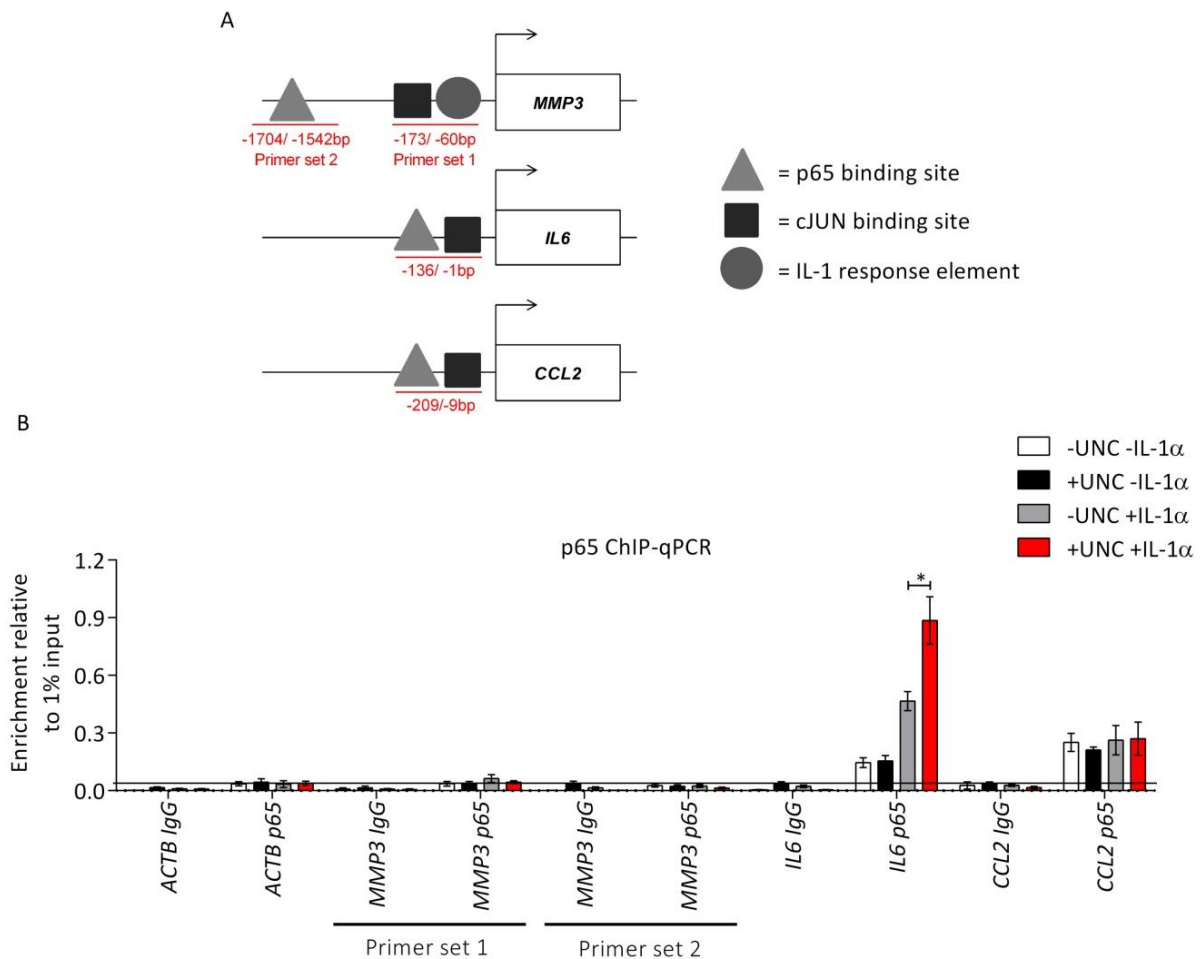


Figure 6.5: Pharmacological inhibition of G9A/GLP potentiates IL-1 α -induced p65 binding to the *IL6* promoter, correlating with reduced H3K9me2 levels in cultured hVSMCs. (A) Schematic indicating the location of the reported p65 binding sites, cJUN binding sites and IL1-responsive elements at the promoters of *MMP3* (Borghaei et al., 2004; Clark et al., 2008; Quinones et al., 1994), *IL6* (Gomard et al., 2010) and *CCL2* (Sutcliffe et al., 2009). Red arrows indicate regions amplified in the ChIP-qPCR analysis. (B) ChIP-qPCR analysis for p65 in untreated control (-UNC -IL-1 α , white bars), UNC (+UNC -IL-1 α , black bars), IL-1 α (-UNC +IL-1 α , grey bars) and UNC plus IL-1 α (+UNC +IL-1 α , red bars) treated cultured hVSMCs (passage 6-15) showing levels of enrichment at the *ACTB* negative control locus and reported p65 binding sites/ IL1-responsive elements within the promoters of *MMP3*, *IL6* and *CCL2* compared with enrichment observed using negative control IgG. Background levels of p65 binding are based on enrichment at the *ACTB* negative control locus and are indicated by a line. Data represent means \pm SEM of 4 experiments using VSMCs derived from independent biopsies. The Asterisk indicates significant difference ($P < 0.05$) by one-way ANOVA with *Bonferroni* correction.

6.2.3 Loss of H3K9me2, by pharmacological inhibition of G9A/GLP, does not influence IL-1 α -induced MAPK phosphorylation.

The MAPK signalling-mediated transcription factor cJUN has also been reported to regulate the expression of MMP and pro-inflammatory genes (Clark et al., 2008; Faggioli et al., 2004; Sutcliffe et al., 2009). I therefore assessed the activity of MAPKs known to phosphorylate cJUN at serine (Ser) 63, which is thought to increase cJUN's transcription factor activity (Klein et al., 2013; Smeal et al., 1992), in response to IL-1 α stimulation with and without prior UNC treatment. Three MAPKs have been identified to phosphorylate cJUN at Ser63, including cJUN N-terminal kinase (JNK), extracellular regulating kinase (ERK1/2) and p38 kinase (p38) (Figure 6.1A) (Kim and Choi, 2015; Sun et al., 2015; Yang et al., 2013). However, JNK has been reported to primarily mediate the phosphorylation of cJUN at Ser63 in different cell types (Morton et al., 2003). IL-1 α /TNF α activate these MAPKs via phosphorylation of JNK at threonine (Thr) 183 and tyrosine (Tyr) 185, ERK1/2 at Thr 202 and Tyr 202 and p38 at (Thr) 180 and (Tyr) 182 (Kim and Choi, 2015; Sun et al., 2015; Yang et al., 2013).

Western blot analysis showed that prior UNC treatment did not influence the level of IL-1 α -induced phosphorylation of p38 (Thr180, Tyr182) (Figure 6.6 A, B), ERK1/2 (Thr202, Tyr204) (Figure 6.6 A, C) or JNK (Thr183, Tyr185) (Figure 6.6 A, D) in cultured hVSMCs. However, UNC treatment potentiated the level of IL-1 α -induced cJUN phosphorylation at Ser63 (Figure 6.6 A, E) without influencing total levels of cJUN (Figure 6.6 A, F) in cultured hVSMCs.

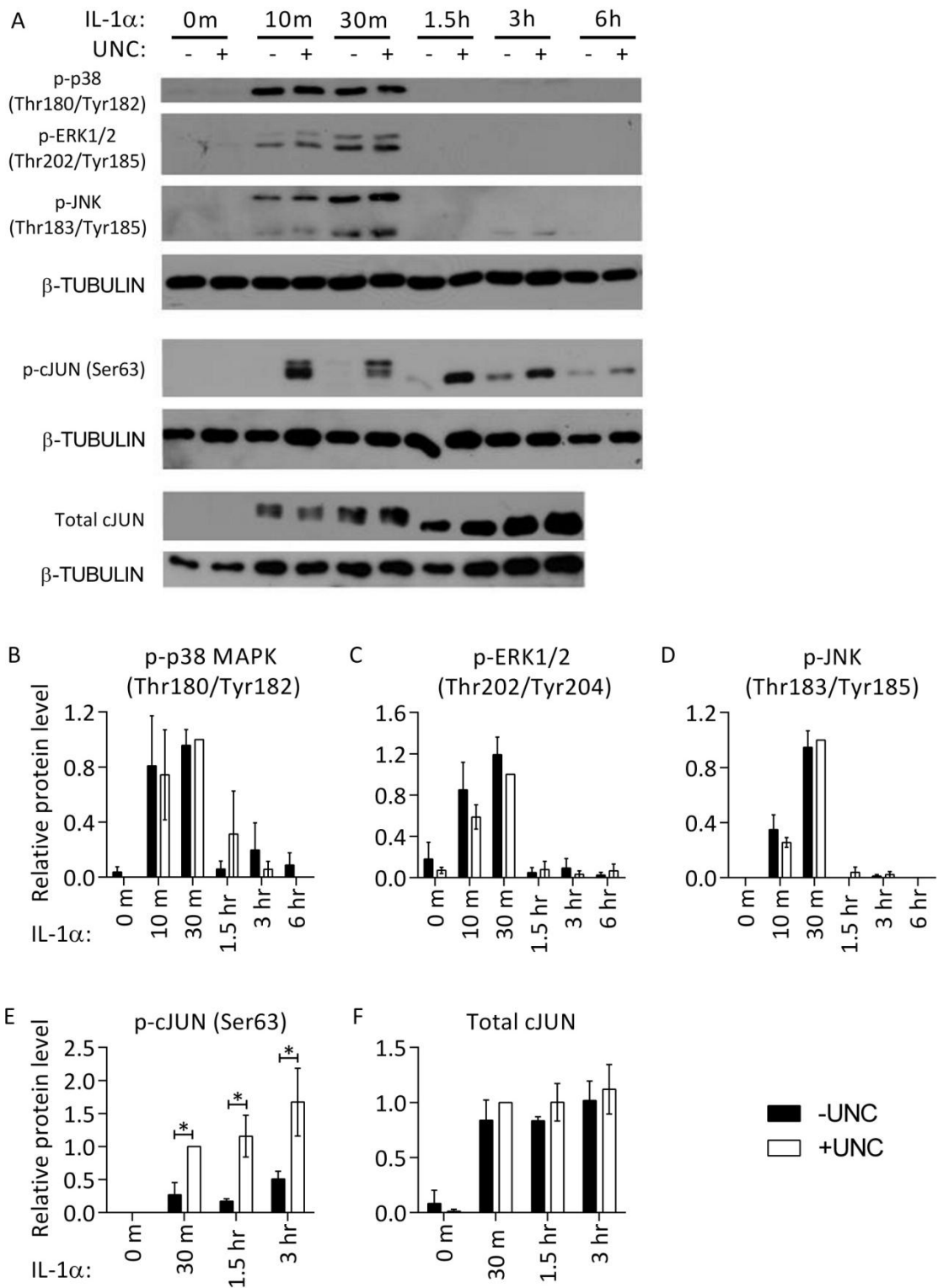


Figure 6.6: Pharmacological inhibition of G9A/GLP does not influence IL-1 α -induced phosphorylation of p38, ERK1/2 or JNK but potentiates IL-1 α -induced cJUN phosphorylation at Ser63. (A) Representative western blot of p38 phosphorylated at Thr183 and Tyr185 (p-p38 Thr180/Tyr182), ERK1/2 phosphorylated at Thr202 and Tyr204 (p-ERK1/2 Thr202, Tyr204), JNK phosphorylated at Thr183 and Tyr185 (p-JNK Thr183/Tyr185), cJUN phosphorylated at Ser63 (p-cJUN Ser63), total cJUN and β -TUBULIN in untreated control and IL-1 α -treated (for 10 mins, 30 mins, 1.5 hr, 3 hr or 6 hr) hVSMCs, without and with prior UNC treatment. hVSMCs were treated after 8-13 passages of culture **(B-E)** Bar plots showing levels of p-p38 (Thr180/Tyr182) **(B)**, p-ERK1/2

(Thr202/Tyr204) **(C)**, p-JNK (Thr83, Tyr185) **(D)**, p-cJUN (Ser63) **(E)** and total cJUN **(F)** in untreated control and IL-1 α -treated (for 10 mins, 30 mins, 1.5 hr, 3 hr or 6 hr) hVSMCs, without and with prior UNC treatment. hVSMCs were treated after 8-13 passages of culture. Data are relative to +UNC +IL-1 α (30 mins) treated hVSMCs and normalised to b-TUBULIN levels. Data represent means \pm SEM of 4 experiments using VSMCs derived from independent biopsies. Asterisks indicate significant differences ($P < 0.05$) by one-way ANOVA with *Bonferroni* correction.

Interestingly, SP600125, a selective small molecule inhibitor of JNK (Han et al., 2001), attenuated IL-1 α -induced *MMP3* expression both with and without prior UNC treatment, correlating with substantially reduced levels of cJUN phosphorylation at Ser63 (Figure 6.7 A-C). However, JNK inhibition did not influence the level of IL-1 α -induced *IL6* or *CCL2* expression (Figure 6.7 D, E). Together, these results suggest cJUN phosphorylation at Ser63 via JNK is necessary for IL-1 α -induced expression of *MMP3* but not for IL-1 α -induced expression of *IL6* or *CCL2*.

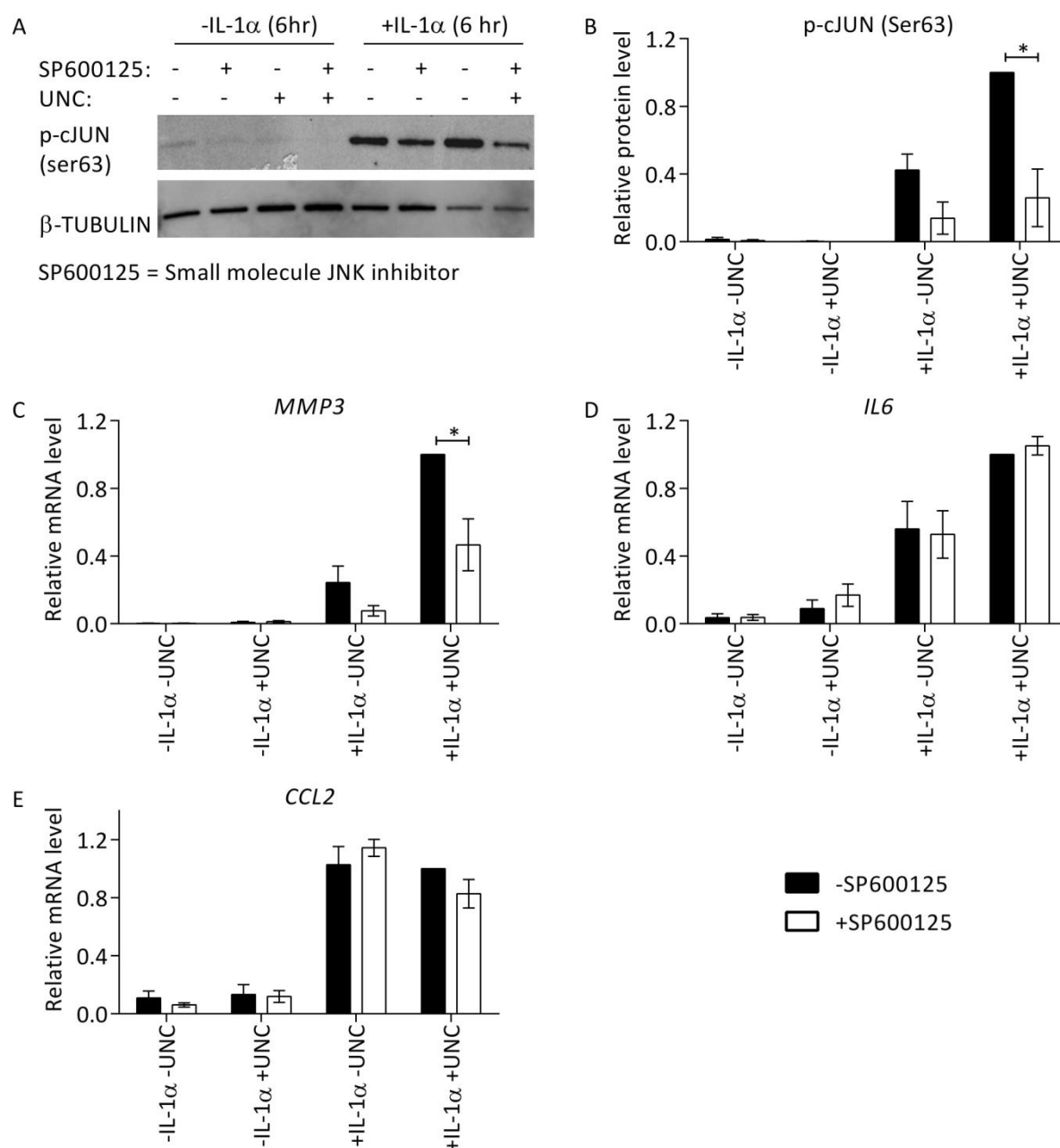


Figure 6.7: IL-1 α -induced *MMP3* expression, but not *IL6* or *CCL2* expression, is dependent on JNK-mediated cJUN phosphorylation at Ser63. (A) Representative western blot of cJUN phosphorylated at serine 63 (p-cJUN Ser63) in untreated control and IL-1 α (6hrs)-treated hVSMCs, cultured to passage 8-13, without and with prior UNC and/ or SP600125 (48 hours)-treatment. (B) Bar plot showing p-cJUN (Ser63) levels in untreated control and IL-1 α -treated hVSMCs, cultured to passage 8-13, without and with prior UNC and/ or SP600125 treatment. Data are relative to +UNC +IL-1 α -SP600125 treated hVSMCs and normalised to b-TUBULIN levels. Data represent means \pm SEM of 4 experiments using VSMCs derived from independent biopsies. Asterisks indicate significant differences by one-way ANOVA with *Bonferroni* correction. (C-F) RT-qPCR analysis of *MMP3* (C), *IL6* (D), and *CCL2* (E) transcript levels in untreated control and IL-1 α (6hrs)-treated hVSMCs, cultured to passage 8-13, without and with prior UNC and/ or SP600125 (48hrs)-treatment. Data are relative to +UNC +IL-1 α -SP600125 treated hVSMCs and normalised to the average of two housekeeping genes (*HPRT1* and *YWHAZ*).

Data represent means \pm SEM of 4 experiments using hVSMCs derived from independent biopsies. Asterisks indicate significant differences ($P < 0.05$) by one-way ANOVA with *Bonferroni* correction.

6.2.4 Pharmacological inhibition of G9A/GLP potentiates IL-1 α -induced cJUN binding to the *MMP3* and *IL6* promoter, correlating with reduced H3K9me2 levels in cultured hVSMCs.

ChIP-qPCR revealed IL-1 α stimulation induced cJUN binding to the *MMP3* and *IL6* promoter and that this was significantly increased by prior UNC treatment in cultured hVSMCs (Figure 6.8). UNC treatment alone did not induce cJUN binding to any of the gene promoters analysed (Figure 6.8). cJUN was not observed to be significantly bound to the *CCL2* promoter under any condition (Figure 6.8).

Taken together, the results described in this chapter suggest H3K9me2 acts directly at the *MMP3* and *IL6* promoter to counteract IL-1 α -induced upregulation by blocking NF κ B (p65) and/or AP-1 (cJUN) transcription factor binding. The findings also suggest that G9A/GLP may regulate JNK's ability to phosphorylate cJUN or cJUN's ability to be phosphorylated by JNK. Alternatively, G9A/GLP may regulate the activity of a phosphatase which targets cJUN.

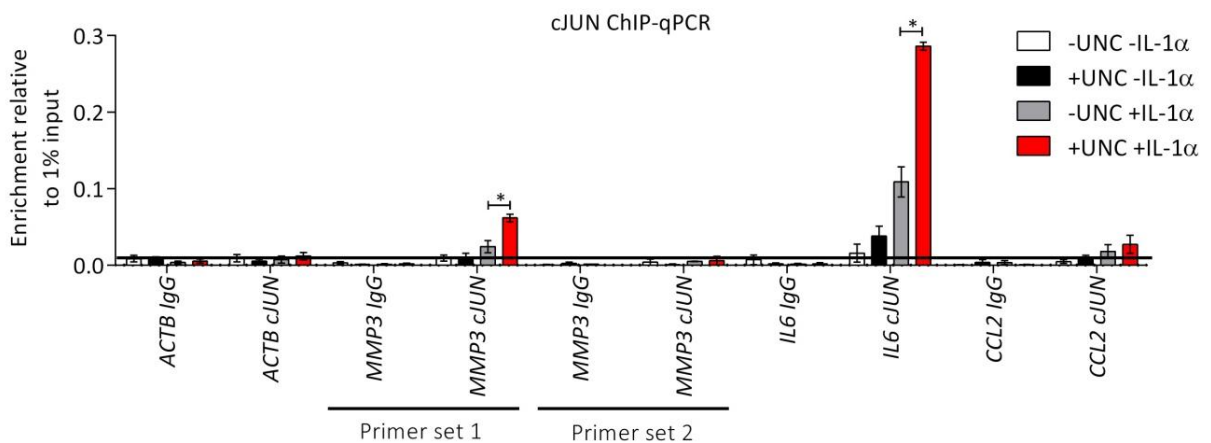


Figure 6.8: Pharmacological inhibition of G9A/GLP potentiates IL-1 α -induced cJUN binding to the *IL6* promoter, correlating with reduced H3K9me2 levels in cultured hVSMCs. ChIP-qPCR analysis for cJUN in untreated control (-UNC -IL-1 α , white bars), UNC (+UNC-IL-1 α , black bars), IL-1 α (-UNC +IL-1 α , grey bars) and UNC plus IL-1 α (+UNC +IL-1 α , red bars) treated cultured hVSMCs (passage 6-15) showing levels of enrichment at the *ACTB* negative control *locus* and regulatory elements within the promoters of *MMP3*, *IL6* and *CCL2* (Figure 6.5 A) compared with the enrichment observed using negative control IgG. Background levels of cJUN are based on enrichment at the *ACTB* negative control *locus* and are indicated by a line. Data represent means \pm SEM of 3 experiments using VSMCs derived from independent biopsies. Asterisks indicate significant differences ($P < 0.05$) by one-way ANOVA with *Bonferroni* correction.

6.3 Summary and Conclusions

The results described in this chapter suggest that G9A/GLP do not influence IL-1 α or TNF α -induced activation of the upstream NF κ B signalling pathway in cultured hVSMCs. However, G9A/GLP inhibition did potentiate IL-1 α -induced p65 binding to the *IL6* promoter (Figure 6.5), concomitant with reduced levels of H3K9me2 (Figure 5.2), suggesting H3K9me2 may act directly at the *IL6* promoter to block p65 binding. No p65 binding was observed at reported p65 consensus sites within the *MMP3* promoter under any condition (Figure 6.5). In contrast p65 was present at the *CCL2* promoter, which is not enriched for H3K9me2 (Figure 5.3 B), at the same level under all conditions (Figure 6.5). The findings also imply that G9A/GLP does not influence IL-1 α -induced MAPK activation in hVSMCs (Figure 6.6). However, G9A/GLP inhibition potentiated IL-1 α -induced cJUN binding to both the *MMP3* and *IL6* promoter (Figure 6.8), concomitant with reduced levels of H3K9me2 (Figure 5.2). No enrichment of cJUN was observed at the *CCL2* promoter under any condition (Figure 6.8). Taken together, these results suggest that H3K9me2 may directly act at the *MMP3* and *IL6* promoter to inhibit inflammatory signal-dependent transcription factor binding. Consistent with this hypothesis, diabetes has been shown to decrease H3K9me2 and increase p65 at the retinal *MMP9* promoter, resulting in increased MMP9 activity (Zhong and Kowluru, 2013b). In addition, the promoters of a subset of NF κ B target genes in mouse macrophages display enriched levels of H3K9me2 that, prior to transcriptional activation, must be diminished through the action of the H3K9me2 demethylase, Aof1 (Saccani and Natoli, 2002; van Essen et al., 2010).

Interestingly, JNK inhibition attenuated the expression of *MMP3* in response to IL-1 α , correlating with reduced cJUN phosphorylation, but did not influence *IL6* or *CCL2* induction (Figure 6.7). These observations imply that *MMP3*, *IL6* and *CCL2* are regulated via different mechanisms in hVSMCs. Furthermore, G9A/GLP inhibition potentiated IL-1 α -induced cJUN phosphorylation at Ser63 (Figure 6.6). Recently, studies have shown that MAPKs can phosphorylate substrates once bound to chromatin (Klein et al., 2013). Therefore, removal of H3K9me2 at target gene promoters could lead to increased IL-1 α -induced recruitment of transcription factor substrates of JNK, including cJUN, which are phosphorylated by JNK once bound to target gene promoters (Klein et al., 2013). This may explain why inhibition of G9A/GLP increases the global level of cJUN phosphorylation at Ser63 in response to IL-1 α stimulation. However, increased phosphorylation of cJUN at Ser63 is known to potentiate its transcriptional activity, although the precise mechanism underlying this remains unclear (Pulverer et al., 1991; Zhu et al., 2014). Therefore, H3K9me2 may not directly act to prevent cJUN binding after IL-1 α -treatment in VSMCs. G9A/GLP could regulate JNK's ability to phosphorylate cJUN or cJUN's ability to be phosphorylated by JNK. Alternatively, G9A/GLP inhibition may reduce the

activity of a phosphatase which targets cJUN. However, a phosphatase which targets phosphorylated cJUN has not yet been identified (Zhu et al., 2014).

CHAPTER 7- DISCUSSION

7.1 Global levels of H3K9me2 and the associated methyltransferase GLP are reduced upon VSMC phenotypic switching.

The results described in this thesis point towards a role for H3K9me2 in the regulation of VSMC phenotype. Global levels of H3K9me2, and the associated methyltransferase GLP, were reduced in phenotypically switched VSMCs *in vitro* and *in vivo*, concomitant with decreased levels of contractile VSMC gene expression. Furthermore, both pharmacological inhibition and siRNA knock down of G9A accelerated the downregulation of contractile VSMC gene expression upon culture. This finding implies reduced levels of H3K9me2 may be causally related to loss of the contractile VSMC state. However, H3K9me2 was absent or present at low levels at contractile VSMC gene promoters independent of their transcriptional state, suggesting H3K9me2 does not act directly at contractile VSMC gene promoters to regulate their expression.

Contractile VSMC genes are reduced rapidly upon vascular injury (Herring et al., 2017; Shi et al., 2013) and are significantly downregulated one day post carotid ligation compared to non-ligated controls (Shi et al., 2013). Contractile VSMC genes are expressed at their lowest levels 7 days post carotid ligation before becoming upregulated around 9 to 28 days post surgery (Allagnat et al., 2016; Shi et al., 2013). Interestingly, H3K9me2 was not significantly reduced in VSMCs within LCCAs until 7 days post carotid ligation and remained downregulated to the same level at day 28 post surgery. These observations further suggest that H3K9me2 does not directly influence the expression of contractile VSMC genes. Moreover, levels of H3K9me2 in VSMC nuclei did not fluctuate between the media, core or cap of atherosclerotic plaque, which are known to express different levels of contractile VSMC genes, providing further evidence to support the hypothesis that H3K9me2 does not directly regulate VSMC contractility. An alternative hypothesis is that H3K9me2 instead regulates the VSMC response to inflammation, which is known to repress the expression of contractile VSMC genes and induce phenotypic switching (Bennett et al., 2016; Yoshida et al., 2013). In support of this theory, H3K9me2 levels were significantly reduced in VSMCs within LCCAs 7 days post carotid ligation concomitant with the infiltration of pro-inflammatory cytokine secreting CD45+ cells into the vessel wall (Alberts-Grill et al., 2012; Tang et al., 2008a), activation of NFkB signalling in VSMCs (Song et al., 2011) and induction of VSMC proliferation (Moura et al., 2007).

Intriguingly, genes activated by identical inflammatory cytokines differ considerably among cell types, despite induction of these genes being dependent on the same activating transcription factors, including NFkB and AP-1 family members (Natoli et al, 2010). It is thought that this context-specificity is due to cell-type specific enhancer activity (Heinz et al., 2015; Zhu et al., 2012). Enhancers are primed via cell-type specific interactions with transcription factors and chromatin modifying

complexes (Heinz et al., 2015; Zhu et al., 2012). Signal dependent transcription factors, such as p65 and cJUN, bind to these primed regions of the genome enabling them to regulate transcription in a cell-type specific manner (Heinz et al., 2015). Therefore it is possible that H3K9me2 plays a role in priming enhancers and therefore regulates cell-type specific gene expression patterns and responses to environmental stimuli.

Enhancers can be located almost anywhere in relation to the gene to be influenced and often relay their regulatory information over vast distances (more than 100Kb and up to 1Mb) (Sanyal et al., 2012). Such enhancer-promoter interactions are enabled by three-dimensional chromatin folding (Sanyal et al., 2012), which is known to be regulated by the transcription factor CTCF (Bulger and Groudine, 2011; de Laat and Duboule, 2013). Interestingly WIZ, a G9A/GLP binding partner, has a binding consensus with a high degree of overlap with that for CTCF (Isbel et al., 2016). Furthermore, CTCF is often detected at the boundaries of H3K9me2- LOCKS (Ciabrelli and Cavalli, 2015; Wen et al., 2009). Based on these findings, H3K9me2 could influence three-dimensional chromatin folding and affect long range inflammation-induced enhancer-promoter interactions. It would therefore be interesting to exploit chromatin conformation capture-derived techniques (Han et al., 2018) to elucidate whether loss of H3K9me2 influences the 3D organisation of VSMC genomic loci containing inflammation-induced genes, in both basal conditions and after inflammatory stimulation.

Genomic profiling has revealed that H3K9me2-decorated megabase scale domains, termed H3K9me2-LOCKS, occupy a great portion of the mammalian genome (Filion and van Steensel, 2010; Lienert et al., 2011; Wen et al., 2009). Whether cellular differentiation coincides with a global increase of H3K9me2-LOCKS has been a matter of debate (Filion and van Steensel, 2010; Lienert et al., 2011; Wen et al., 2009). Wen and colleagues found that H3K9me2 LOCKS cover 10-46% of the genome in differentiated cells compared to only 4% in embryonic stem cells (ESCs), can be lineage-specific and are substantially lost in cancer cell lines (Wen et al., 2009). In agreement with these findings, mass spectrometry-based quantification showed increased global levels of H3K9me2 in mouse fibroblasts compared to pluripotent cells (Sridharan et al., 2013). Additionally, hematopoietic stem and progenitor cells display lower global levels of H3K9me2 compared to mature bone marrow cells (Li et al., 2018). Therefore, H3K9me2-LOCKS might act to repress genomic regions that are no longer required as a cell adopts a certain fate (Jorgensen and Fisher, 2009). In support of this theory, reduction of H3K9me2-LOCKS was observed in epithelial-to-mesenchymal transition (EMT), a process in which cells acquire a multipotent phenotype (McDonald et al., 2011) suggesting these large H3K9me2-decorated domains play a functional role in cell fate specification and reprogramming. However, Filion and van Steensel claim that there are no significant differences in H3K9me2 LOCKS in ESCs compared to differentiated cells and suggest that the algorithm used by Wen et al. may have

may have introduced a detection bias (Filion and van Steensel, 2010). In agreement with Filion and van Steensel, Lienert and colleagues observed no global increase in H3K9me2-LOCKS during neuronal differentiation of embryonic stem cells but instead observed a local gain of H3K9me2 over select genes (Lienert et al., 2011).

Nevertheless, numerous studies report that H3K9me2 patterning is important for silencing lineage-inappropriate genes during differentiation as well as maintaining cell identity, and it must be reset to specify new fates (Chen et al., 2013; Huang et al., 2016; Liu et al., 2018; Rodriguez-Madoz et al., 2017; Wu et al., 2011; Ying et al., 2018). For instance, H3K9me2 has been identified as a barrier for somatic cell nuclear transfer (SCNT)-mediated embryonic genome activation (Liu et al., 2018; Wu et al., 2011) and removal of H3K9me2 by G9A-inhibition has been shown to significantly enhance the developmental competence of SCNT embryos (Huang et al., 2016). Furthermore, mutations in GLP that disrupt its H3K9me1-recognition domain result in reduced H3K9me2 levels, a delay in silencing of pluripotency genes during ESC differentiation and abnormal embryonic development in mice (Liu et al., 2015a). In addition, studies have shown that inhibition of G9A improves the reprogramming efficiency of human primary cells to induced pluripotent stem cells by heterochromatin relaxation and facilitating transcription factor binding (Chen et al., 2013; Rodriguez-Madoz et al., 2017; Ying et al., 2018). With these observations in mind, it is tempting to speculate that loss of H3K9me2 facilitates VSMC phenotypic switching by permitting transcription which is incompatible with the presence of contractile VSMC-specific H3K9me2 marked chromatin territories.

7.2 H3K9me2 inhibits inflammation-induced gene upregulation in VSMCs *in vitro* and *in vivo*.

ChIP identified a subset of IL-1 α /injury-responsive gene promoters enriched for H3K9me2, including *MMP3*, *MMP9*, *MMP12* and *IL6*, in both mouse and human VSMCs. Loss of H3K9me2 significantly increased the expression of MMP and pro-inflammatory mVSMC genes after injury and inflammation, suggesting a functional role of the H3K9me2 mark in regulating the activation of these genes. H3K9me2-mediated regulation of IL-1 α -responsive VSMC gene expression was confirmed in cultured hVSMCs implying the mechanism could be relevant in the context of human CVD. Together, these results suggest H3K9me2 functions to inhibit inflammation-induced gene upregulation in VSMCs via an evolutionary conserved mechanism.

In agreement with my observation that H3K9me2 inhibits inflammation-induced gene upregulation in VSMCs, researchers have shown that VSMCs from diabetic patients display reduced levels of H3K9me2 compared to non-diabetic controls and suggest that dysregulation of H3K9me2 might underlie the vascular complications associated with diabetes (Chen et al., 2017; Villeneuve et al.,

2008a). Chen and colleagues found that loss of H3K9me2, by over expressing the associated demethylase KDM3A, accelerated neointima formation following vascular injury in diabetic rats (Chen et al., 2017).

Several studies report an inverse correlation between H3K9me2 occupancy at MMP and other inflammatory gene promoters and the ability of other cell types to express these genes (Fang et al., 2012; Gesumaria et al., 2015; Liu et al., 2014; Zhong and Kowluru, 2013b). For example, H3K9me2 depletion at the *Mmp9* promoter correlates with elevated *Mmp9* expression in retinal endothelial cells from diabetic rats compared to controls (Zhong and Kowluru, 2013b). Furthermore, solar-stimulated ultraviolet radiation (ssUVR) induces loss of H3K9me2 at the *MMP3* promoter in primary human dermal fibroblasts, correlating with enhanced *MMP3* mRNA levels following ssUVR exposure (Gesumaria et al., 2015). In addition, genetic ablation or pharmacological inhibition of G9A/GLP stimulates the expression of inflammatory genes in mouse embryonic fibroblasts (MEFs) (Fang et al., 2012). Also, similar to what is reported here, reduction of H3K9me2 levels in MEFs further potentiated poly(I:C)-induced upregulation of inflammatory genes (Fang et al., 2012). Moreover, G9A deficient-mutant flies are hypersensitive to RNA virus infection and succumb faster to infection than wild-type controls (Merkling et al., 2015). These observations suggest that G9A/GLP plays a role in an evolutionary conserved mechanism to control genes that are involved in processes that require tight and dynamic regulation and high transcriptional plasticity, including the inflammatory response, in a variety of cell types.

7.3 H3K9me2 hinders inflammation-induced TF binding at target VSMC gene promoters

In hVSMCs, G9A/GLP inhibition did not influence upstream IL-1 α /TNF α -induced NF κ B signalling but significantly increased IL-1 α -induced NF κ B-p65 transcription factor binding to the *IL6* promoter, correlating with reduced H3K9me2 levels. In contrast, enrichment of p65 was not observed at reported NF κ B sites within the *MMP3* promoter after IL-1 α stimulation. Interestingly, inhibition of G9A/GLP potentiated IL-1 α -induced phosphorylation of cJUN at Ser63, a post translational modification which substantially enhances cJUN's transcriptional activity (Morton et al., 2003), without impacting activation of the primary kinases responsible for cJUN phosphorylation, including JNK. In contrast to *IL6*, *MMP3* regulation after IL-1 α stimulation was dependent on JNK activity, suggesting regulation by cJUN. G9A/GLP inhibition potentiated IL-1 α -induced cJUN binding to both the *MMP3* and the *IL6* promoter. Together, these results imply that H3K9me2 prevents binding of both NF κ B and AP1 transcription factors at specific IL-1 α -regulated VSMC genes to possibly block spurious induction of a pro-inflammatory state. Furthermore, *MMP3* and *IL6* appear to be regulated via different mechanisms in VSMCs (Figure 7.1).

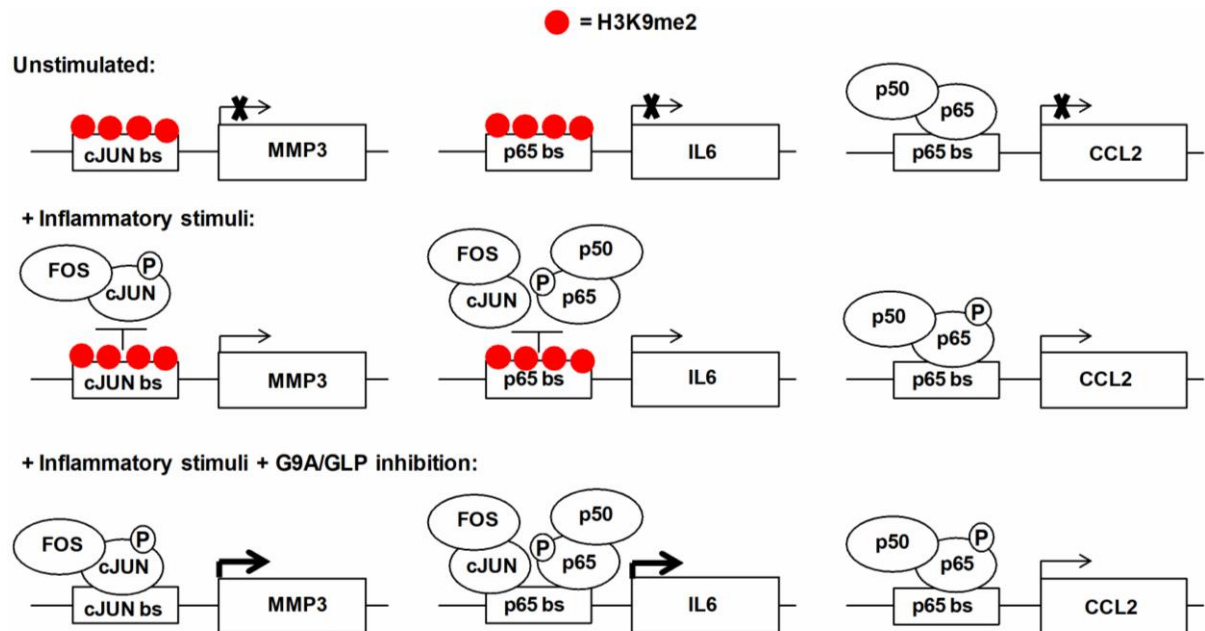


Figure 7.1: Proposed mechanism underlying G9A/GLP-mediated attenuation of inflammation-responsive VSMC gene expression. Binding of AP-1-cJUN and NF κ B-p65 transcription factors at H3K9me2 target genes is increased upon reduction of H3K9me2 levels following G9A/GLP inhibition. Non-H3K9me2 targets such as *CCL2* display transcription factor binding at basal levels resulting in rapid induction upon stimulation. In contrast, H3K9me2 target gene induction is delayed in a context-specific manner, which could be dependent on both specific transcription factor usage and locus-specific chromatin regulation.

In addition to their role as HMTs, several studies report that G9A/GLP can methylate a wide range of non-histone proteins (Figure 1.13) (Biggar and Li, 2015). However, as most of the reported methylation sites have been derived from mass spectrometry analyses, the function of many of these modifications remain unknown. Nevertheless, increasing evidence suggests methylation of non-histone proteins may influence protein stability (Lee et al., 2015), protein-protein interactions (Lee et al., 2010; Ling et al., 2012) and regulate cellular signalling pathways (Biggar and Li, 2015; Pless et al., 2008). Even though binding of p65 and cJUN to many MMP and pro-inflammatory genes is necessary for their expression, they are often not sufficient for their induction (Fanjul-Fernández et al., 2010; Smale and Natoli, 2014). Numerous other transcription factors also play an important role in the upregulation of these inducible genes, including those activated by the JAK-STAT and Smad signalling pathways (Fanjul-Fernández et al., 2010; Smale and Natoli, 2014). Therefore, it is entirely possible that inhibition of G9A/GLP influences the binding of other transcription factors important for the activation of these genes at the transcriptional and/or post transcriptional level. However, if G9A/GLP inhibition influenced the JAK-STAT signalling pathway I would have expected the induction of *CCL2* to be affected upon IL-1 α stimulation which was not observed.

Interestingly, G9A/GLP inhibition potentiated IL-1 α -induced cJUN phosphorylation at Ser63. Recently, studies have shown that MAPKs can phosphorylate substrates once bound to chromatin (Klein et al., 2013). Therefore, removal of H3K9me2 at target gene promoters could lead to increased IL-1 α -induced recruitment of transcription factor substrates of JNK, including cJUN, which are phosphorylated by JNK once bound to target gene promoters (Klein et al., 2013). This may explain why inhibition of G9A/GLP increases the global level of cJUN phosphorylation at Ser63 in response to IL-1 α stimulation. Therefore, it would be interesting to examine whether IL-1 α induces JNK binding at AP1-binding motifs in VSMCs. However, increased phosphorylation of cJUN at Ser63 is known to potentiate its transcriptional activity, although the precise mechanism underlying this remains unclear (Pulverer et al., 1991; Zhu et al., 2014). Phosphorylation of cJUN has been described to alter cJUN's stability, affinity for DNA or protein partners, and nuclear localisation (Bhatt and Ghosh, 2014; Yang et al., 2013). Therefore, H3K9me2 may not directly act to prevent cJUN binding after IL-1 α -treatment in VSMCs. G9A/GLP could regulate JNK's ability to phosphorylate cJUN or cJUN's ability to be phosphorylated by JNK. Alternatively, G9A/GLP inhibition may reduce the activity of a phosphatase which targets cJUN. However, a phosphatase which targets phosphorylated cJUN has not yet been identified (Zhu et al., 2014).

7.4 Limitations of study

For the studies described in this thesis, I used bulk RT-qPCR analysis to examine the effect of G9A/GLP inhibition on VSMC gene expression. This method averages the responses of cell populations and therefore obscures inherent cell-cell heterogeneity restricting the ability to distinguish between the individual responses of different cells within a sample. Therefore, it is not possible to elucidate whether G9A/GLP influences the expression level of particular genes by individual VSMCs or the number of VSMCs expressing the gene. Single cell sequencing would be required to answer this question but would have been a costly preliminary experiment (Ziegenhain et al., 2017). FACS could also help address this problem but the number of genes this method allows you to analyse is limited to the availability of antibodies and the number of colours a flow cytometer can detect.

Many of the experiments described in this thesis were based on analysis using VSMC-specific lineage labelling. As described in section 1.9.1, Myh11-CreER(T2) transgenic mice where the transgene had integrated into the Y chromosome were chosen for breeding onto the C57BL/6 background (Wirth et al., 2008), excluding its application in female mice. Gender has been identified as a risk factor for multiple vascular diseases (Mosca et al., 2011), therefore the use of only male mice in the studies

described in this thesis is a limitation. Furthermore, a potential caveat is that the *Myh11-Cre* is not driven by the endogenous *Myh11* gene. Even though studies report that this Cre-transgene closely recapitulates endogenous gene expression (Nemenoff et al., 2011; Wirth et al., 2008), differences under certain circumstances and the extent to which it may be active in cells which express very low levels of *Myh11* are difficult to determine. However, Dr Joel Chappell did not observe recombination of the reporter in the liver, skeletal muscle or lung apart from within the vasculature within each tissue (Chappell et al., 2016).

For the *in vivo* study, loss of H3K9me2 was not specific to VSMCs (Chen et al., 2017). Therefore, the differences observed in gene expression may have been due to the effects of G9A/GLP inhibition on other cell types, such as bone marrow-derived cells. Introducing the appropriate Cre-deleter transgene onto Flox/Flox mice would address this problem but would involve extensive breeding. I chose to use pharmacologic inhibition, rather than genetic deletion to reduce H3K9me2 levels to comply with the 3R's of animal research.

The experiments performed in this thesis do not definitively show that H3K9me2 acts directly at the promoter of *MMP3*, *MMP9*, *MMP12* and *IL6* to inhibit the inflammation-induced expression of these genes. To investigate whether VSMC gene de-regulation is directly caused by H3K9me2 the CRISPR/dCas9 system (Sander and Joung, 2014) could be used to selectively change H3K9me2 levels locally at specific VSMC promoters. It has been shown that nuclease-mutant Cas9 protein can, when fused to specific protein domains, be used to recruit enzymatic activities to selected *loci* by co-expression with appropriate complementary guide RNAs (gRNA) (Sander and Joung, 2014). It is therefore possible to generate dCas9 fusion proteins with the enzymatic domains of G9A/GLP or JMJD1A, a demethylase which specifically targets H3K9me2 (Loh et al., 2007; Shinkai and Tachibana, 2011), to respectively increase or decrease H3K9me2 levels at target VSMC promoters. This experiment would demonstrate whether levels of H3K9me2 at individual gene promoters are functionally important. I have produced VSV-G pseudotyped lentivirus expressing dCas9 fused with the catalytic SET domain of G9A, which is responsible for H3K9me2 activity, and have used it to transduce cultured hVSMCs. I have also generated gRNA expression plasmids targeting the promoters of *MMP2*, *MMP3* and *CCL2*. I planned to screen for successful gRNAs by transient transfection into cultured hVSMCs but observed extremely low transfection efficiency. Due to time constraints I was not able to optimise the system further.

7.5 Future experiments

Interestingly, stem cell antigen-1 (Sca1), a cell surface protein, is upregulated in cultured compared to *ex vivo* VSMCs, concomitant with reduced levels of H3K9me2 and GLP (Dobnikar et al., 2018). Sca1 is upregulated in VSMCs upon exposure to stimuli known to induce phenotypic switching including culture, injury and inflammation and has been proposed to identify a more plastic VSMC state (Dobnikar et al., 2018). It would be worthwhile exploring if Sca1 plays a functional role in VSMC phenotypic switching before investigating whether the downregulation of H3K9me2 and GLP is linked to the induction of Sca1 expression upon VSMC phenotypic switching. It is tempting to speculate that Sca1+ VSMCs display low global levels of H3K9me2 and represent a more primed state, which readily respond to injury and inflammation.

To determine the functional importance of observed differential H3K9me2-levels in *ex vivo* and cultured VSMCs, I compared H3K9me2 ChIP-seq data to genome-wide expression data (data not shown). However, the H3K9me2 mark was broadly distributed in both *ex vivo* and cultured mVSMCs, consistent with the high abundance of H3K9me2-LOCKS previously identified in differentiated cell types (Filion and van Steensel, 2010; Lienert et al., 2011; Wen et al., 2009). Therefore, using gene-set enrichment analysis I could not identify biological functions previously associated with vascular disease among H3K9me2-marked genes. However, the ChIP-seq data did validate the enriched levels of H3K9me2 observed at IL-1 α -reponsive VSMC gene promoters and absent or low levels of H3K9me2 at contractile VSMC gene promoters observed by ChIP-qPCR (data not shown).

Last year the Henikoff lab published a new method to analyse DNA-protein interactions, which they named CUT&RUN (Cleavage Under Targets and Release Using Nuclease) (Skene and Henikoff, 2017). In CUT&RUN, targeted DNA-protein complexes are isolated directly from the cell nucleus rather than following a precipitation step. To perform CUT&RUN, a specific antibody to the DNA-binding protein of interest and ProtA-MNase is added to permeabilised cells. MNase is tethered to the protein of interest through the ProtA-antibody interaction and MNase cleaves the surrounding, unprotected DNA to release protein-DNA complexes, which can then be isolated and sequenced (Skene and Henikoff, 2017). This technique is reported to give a much higher signal to noise ratio compared to traditional ChIP. CUT&RUN therefore requires one tenth of the sequencing depth of ChIP and permits genomic mapping of histone modifications and transcription factors using extremely low cell numbers (Hainer et al., 2018; Skene and Henikoff, 2017). CUT&RUN has been described to generate robust data from as little as 100 cells for the genome wide mapping of histone modifications (Hainer et al., 2018). Sufficient tissue was not available for genome-wide H3K9me2 mapping after carotid ligation using ChIP. However, CUT&RUN could potentially be used to profile functionally relevant H3K9me2 target genes using low numbers of phenotypically switched VSMCs derived from murine models of vascular disease.

ChIP captures DNA-protein interactions within cell populations at one fixed time point and cannot assess the kinetics of H3K9me2 in single, living cells. Recently, Kimura and colleagues have created sensitive fluorescent genetically encoded histone modification-specific intracellular antibody (mintbody) probes that have been used to monitor changes in histone modifications in living cells (Sato et al., 2013). Such a probe targeting H3K9me2 could be used to examine the dynamics of H3K9me2 in living VSMCs in response to inflammatory stimuli. For example, this tool could be used to explore whether there is a relationship between H3K9me2 levels and the timing of NFkB/AP-1 family transcription factor binding to inflammation-induced gene promoters.

References

- Ackers-Johnson, M., Talasila, A., Sage, A.P., Long, X., Bot, I., Morrell, N.W., Bennett, M.R., Miano, J.M., and Sinha, S. (2015). Myocardin regulates vascular smooth muscle cell inflammatory activation and disease. *Arteriosclerosis, thrombosis, and vascular biology* 35, 817-828.
- Aikawa, M., Sakomura, Y., Ueda, M., Kimura, K., Manabe, I., Ishiwata, S., Komiyama, N., Yamaguchi, H., Yazaki, Y., and Nagai, R. (1997). Redifferentiation of smooth muscle cells after coronary angioplasty determined via myosin heavy chain expression. *Circulation* 96, 82-90.
- Albarrán-Juárez, J., Kaur, H., Grimm, M., Offermanns, S., and Wettschureck, N. Lineage tracing of cells involved in atherosclerosis. *Atherosclerosis* 251, 445-453.
- Alberts-Grill, N., Rezvan, A., Son, D.J., Qiu, H., Kim, C.W., Kemp, M.L., Weyand, C.M., and Jo, H. (2012). Dynamic immune cell accumulation during flow-induced atherogenesis in mouse carotid artery: an expanded flow cytometry method. *Arteriosclerosis, thrombosis, and vascular biology* 32, 623-632.
- Alexander, M.R., and Owens, G.K. (2012). Epigenetic control of smooth muscle cell differentiation and phenotypic switching in vascular development and disease. *Annual review of physiology* 74, 13-40.
- Ali, M.S., Starke, R.M., Jabbour, P.M., Tjounmakaris, S.I., Gonzalez, L.F., Rosenwasser, R.H., Owens, G.K., Koch, W.J., Greig, N.H., and Dumont, A.S. (2013). TNF- α induces phenotypic modulation in cerebral vascular smooth muscle cells: implications for cerebral aneurysm pathology. *Journal of Cerebral Blood Flow & Metabolism* 33, 1564-1573.
- Allagnat, F., Haefliger, J.A., Lambelet, M., Longchamp, A., Berard, X., Mazzolai, L., Corpataux, J.M., and Deglise, S. (2016). Nitric Oxide Deficit Drives Intimal Hyperplasia in Mouse Models of Hypertension. *European journal of vascular and endovascular surgery : the official journal of the European Society for Vascular Surgery* 51, 733-742.
- Anderson, D.R., Poterucha, J.T., Mikuls, T.R., Duryee, M.J., Garvin, R.P., Klassen, L.W., Shurmur, S.W., and Thiele, G.M. (2013). IL-6 and its receptors in coronary artery disease and acute myocardial infarction. *Cytokine* 62, 395-400.
- Azuara, V., Perry, P., Sauer, S., Spivakov, M., Jorgensen, H.F., John, R.M., Gouti, M., Casanova, M., Warnes, G., Merckenschlager, M., *et al.* (2006). Chromatin signatures of pluripotent cell lines. *Nat Cell Biol* 8, 532-538.
- Barski, A., Cuddapah, S., Cui, K., Roh, T.-Y., Schones, D.E., Wang, Z., Wei, G., Chepelev, I., and Zhao, K. (2007). High-Resolution Profiling of Histone Methylations in the Human Genome. *Cell* 129, 823-837.
- Basak, O., van de Born, M., Korving, J., Beumer, J., van der Elst, S., van Es, J.H., and Clevers, H. (2014). Mapping early fate determination in Lgr5+ crypt stem cells using a novel Ki67-RFP allele. *The EMBO journal* 33, 2057-2068.

Baylis, R.A., Gomez, D., and Owens, G.K. (2017). Shifting the Focus of Preclinical, Murine Atherosclerosis Studies From Prevention to Late-Stage Intervention. *Circulation research* *120*, 775-777.

Bennett, M.R., Sinha, S., and Owens, G.K. (2016). Vascular Smooth Muscle Cells in Atherosclerosis. *Circulation research* *118*, 692-702.

Bhatt, D., and Ghosh, S. (2014). Regulation of the NF- κ B-Mediated Transcription of Inflammatory Genes. *Frontiers in Immunology* *5*, 71.

Biasucci, L.M., Liuzzo, G., Fantuzzi, G., Caligiuri, G., Rebuzzi, A.G., Ginnetti, F., Dinarello, C.A., and Maseri, A. (1999). Increasing levels of interleukin (IL)-1Ra and IL-6 during the first 2 days of hospitalization in unstable angina are associated with increased risk of in-hospital coronary events. *Circulation* *99*, 2079-2084.

Biggar, K.K., and Li, S.S.C. (2015). Non-histone protein methylation as a regulator of cellular signalling and function. *Nat Rev Mol Cell Biol* *16*, 5-17.

Bittencourt, D., Wu, D.Y., Jeong, K.W., Gerke, D.S., Herviou, L., Ianculescu, I., Chodankar, R., Siegmund, K.D., and Stallcup, M.R. (2012). G9a functions as a molecular scaffold for assembly of transcriptional coactivators on a subset of glucocorticoid receptor target genes. *Proceedings of the National Academy of Sciences of the United States of America* *109*, 19673-19678.

Borghaei, R.C., Rawlings, P.L., Jr., Javadi, M., and Woloshin, J. (2004). NF-kappaB binds to a polymorphic repressor element in the MMP-3 promoter. *Biochemical and biophysical research communications* *316*, 182-188.

Briot, A., Jaroszewicz, A., Warren, Carmen M., Lu, J., Touma, M., Rudat, C., Hofmann, Jennifer J., Airik, R., Weinmaster, G., Lyons, K., *et al.* (2014). Repression of Sox9 by Jag1 Is Continuously Required to Suppress the Default Chondrogenic Fate of Vascular Smooth Muscle Cells. *Developmental Cell* *31*, 707-721.

Bruna, A., Nicolàs, M., Muñoz, A., Kyriakis, J.M., and Caelles, C. (2003). Glucocorticoid receptor–JNK interaction mediates inhibition of the JNK pathway by glucocorticoids. *The EMBO journal* *22*, 6035-6044.

Bulger, M., and Groudine, M. (2011). Functional and mechanistic diversity of distal transcription enhancers. *Cell* *144*, 327-339.

Cargnello, M., and Roux, P.P. (2011). Activation and function of the MAPKs and their substrates, the MAPK-activated protein kinases. *Microbiology and molecular biology reviews* : *MMBR* *75*, 50-83.

Chang, Y., Ganesh, T., Horton, J.R., Spannhoff, A., Liu, J., Sun, A., Zhang, X., Bedford, M.T., Shinkai, Y., Snyder, J.P., *et al.* (2010). Adding a lysine mimic in the design of potent inhibitors of histone lysine methyltransferases. *Journal of molecular biology* *400*, 1-7.

Chang, Y., Sun, L., Kokura, K., Horton, J.R., Fukuda, M., Espejo, A., Izumi, V., Koomen, J.M., Bedford, M.T., Zhang, X., *et al.* (2011). MPP8 mediates the interactions between DNA

methyltransferase Dnmt3a and H3K9 methyltransferase GLP/G9a. *Nature Communications* 2, 533-533.

Chang, Y., Zhang, X., Horton, J.R., Upadhyay, A.K., Spannhoff, A., Liu, J., Snyder, J.P., Bedford, M.T., and Cheng, X. (2009). Structural basis for G9a-like protein lysine methyltransferase inhibition by BIX-01294. *Nature structural & molecular biology* 16, 312-317.

Chappell, J., Harman, J.L., Narasimhan, V.M., Yu, H., Foote, K., Simons, B.D., Bennett, M.R., and Jorgensen, H.F. (2016). Extensive Proliferation of a Subset of Differentiated, Yet Plastic, Medial Vascular Smooth Muscle Cells Contribute to Neointimal Formation in Mouse Injury and Atherosclerosis Models. *Circulation research*.

Chen, J., Liu, H., Liu, J., Qi, J., Wei, B., Yang, J., Liang, H., Chen, Y., Chen, J., Wu, Y., *et al.* (2013). H3K9 methylation is a barrier during somatic cell reprogramming into iPSCs. *Nature genetics* 45, 34-42.

Chen, J., Zhang, J., Yang, J., Xu, L., Hu, Q., Xu, C., Yang, S., and Jiang, H. (2017). Histone demethylase KDM3a, a novel regulator of vascular smooth muscle cells, controls vascular neointimal hyperplasia in diabetic rats. *Atherosclerosis* 257, 152-163.

Chen, S., Liu, B., Kong, D., Li, S., Li, C., Wang, H., and Sun, Y. (2015a). Atorvastatin Calcium Inhibits Phenotypic Modulation of PDGF-BB-Induced VSMCs via Down-Regulation the Akt Signaling Pathway. *PLoS ONE* 10, e0122577.

Chen, X., El Gazzar, M., Yoza, B.K., and McCall, C.E. (2009). The NF-kappaB factor RelB and histone H3 lysine methyltransferase G9a directly interact to generate epigenetic silencing in endotoxin tolerance. *The Journal of biological chemistry* 284, 27857-27865.

Chen, X., Skutt-Kakaria, K., Davison, J., Ou, Y.L., Choi, E., Malik, P., Loeb, K., Wood, B., Georges, G., Torok-Storb, B., *et al.* (2012). G9a/GLP-dependent histone H3K9me2 patterning during human hematopoietic stem cell lineage commitment. *Genes Dev* 26, 2499-2511.

Chen, Y.C., Wen, Z.H., Lee, Y.H., Chen, C.L., Hung, H.C., Chen, C.H., Chen, W.F., and Tsai, M.C. (2015b). Dihydroaustrasulfone alcohol inhibits PDGF-induced proliferation and migration of human aortic smooth muscle cells through inhibition of the cell cycle. *Marine drugs* 13, 2390-2406.

Chen, Y.J., and Chang, L.S. (2015). NFkappaB- and AP-1-mediated DNA looping regulates matrix metalloproteinase-9 transcription in TNF-alpha-treated human leukemia U937 cells. *Biochimica et biophysica acta* 1849, 1248-1259.

Chettimada, S., Joshi, S.R., Dhagia, V., Aiezza, A., 2nd, Lincoln, T.M., Gupte, R., Miano, J.M., and Gupte, S.A. (2016). Vascular smooth muscle cell contractile protein expression is increased through protein kinase G-dependent and -independent pathways by glucose-6-phosphate dehydrogenase inhibition and deficiency. *American journal of physiology Heart and circulatory physiology* 311, H904-h912.

Chi, P., Allis, C.D., and Wang, G.G. (2010). Covalent histone modifications — miswritten, misinterpreted and mis-erased in human cancers. *Nat Rev Cancer* 10, 457-469.

- Chistiakov, D.A., Melnichenko, A.A., Grechko, A.V., Myasoedova, V.A., and Orekhov, A.N. (2018). Potential of anti-inflammatory agents for treatment of atherosclerosis. *Experimental and molecular pathology* *104*, 114-124.
- Cho, A., and Reidy, M.A. (2002). Matrix metalloproteinase-9 is necessary for the regulation of smooth muscle cell replication and migration after arterial injury. *Circulation research* *91*, 845-851.
- Choi, J., Jang, H., Kim, H., Lee, J.H., Kim, S.T., Cho, E.J., and Youn, H.D. (2014). Modulation of lysine methylation in myocyte enhancer factor 2 during skeletal muscle cell differentiation. *Nucleic Acids Res* *42*, 224-234.
- Choudhary, S., Higgins, C.L., Chen, I.Y., Reardon, M., Lawrie, G., Vick, G.W., 3rd, Karmonik, C., Via, D.P., and Morrisett, J.D. (2006). Quantitation and localization of matrix metalloproteinases and their inhibitors in human carotid endarterectomy tissues. *Arteriosclerosis, thrombosis, and vascular biology* *26*, 2351-2358.
- Christen, T., Verin, V., Bochaton-Piallat, M., Popowski, Y., Ramaekers, F., Debruyne, P., Camenzind, E., van Eys, G., and Gabbiani, G. (2001). Mechanisms of neointima formation and remodeling in the porcine coronary artery. *Circulation* *103*, 882-888.
- Ciabrelli, F., and Cavalli, G. (2015). Chromatin-Driven Behavior of Topologically Associating Domains. *Journal of molecular biology* *427*, 608-625.
- Clark, I.M., Swingler, T.E., Sampieri, C.L., and Edwards, D.R. (2008). The regulation of matrix metalloproteinases and their inhibitors. *The international journal of biochemistry & cell biology* *40*, 1362-1378.
- Clarke, M.C., Talib, S., Figg, N.L., and Bennett, M.R. (2010). Vascular smooth muscle cell apoptosis induces interleukin-1-directed inflammation: effects of hyperlipidemia-mediated inhibition of phagocytosis. *Circulation research* *106*, 363-372.
- Clifford, R.L., John, A.E., Brightling, C.E., and Knox, A.J. (2012). Abnormal Histone Methylation is Responsible for Increased VEGF165a Secretion from Airway Smooth Muscle Cells in Asthma. *Journal of immunology (Baltimore, Md : 1950)* *189*, 819-831.
- Cloos, P.A., Christensen, J., Agger, K., and Helin, K. (2008). Erasing the methyl mark: histone demethylases at the center of cellular differentiation and disease. *Genes Dev* *22*, 1115-1140.
- Davis, P.H., Dawson, J.D., Riley, W.A., and Lauer, R.M. (2001). Carotid intimal-medial thickness is related to cardiovascular risk factors measured from childhood through middle age: The Muscatine Study. *Circulation* *104*, 2815-2819.
- de Laat, W., and Duboule, D. (2013). Topology of mammalian developmental enhancers and their regulatory landscapes. *Nature* *502*, 499-506.
- Delcuve, G.P., Rastegar, M., and Davie, J.R. (2009). Epigenetic control. *Journal of cellular physiology* *219*, 243-250.

Dhagia, V., Alloosh, M., Sturek, M., Gupte, R., and Gupte, S.A. (2014). Abstract 19251: Glucose-6-Phosphate Dehydrogenase Regulates Myocardin and Phenotype of Arterial Smooth Muscle Cells in Metabolic Syndrome Swine and Humans. *Circulation* *130*, A19251.

Diehl, A.G., and Boyle, A.P. (2018). Conserved and species-specific transcription factor co-binding patterns drive divergent gene regulation in human and mouse. *Nucleic Acids Research* *46*, 1878-1894.

Dobnikar, L., Taylor, A., Chappell, J., Oldach, P., Harman, J., Oerton, E., Dzierzak, E., Bennett, M., Spivakov, M., and Jorgensen, H.F. (2018). Disease-relevant transcriptional signatures identified in individual smooth muscle cells from healthy mouse vessels. *Nature communications In Press*.

Doran, A.C., Meller, N., and McNamara, C.A. (2008). The Role of Smooth Muscle Cells in the Initiation and Early Progression of Atherosclerosis. *Arteriosclerosis, thrombosis, and vascular biology* *28*, 812-819.

El Mansouri, F.E., Nebbaki, S.-S., Kapoor, M., Afif, H., Martel-Pelletier, J., Pelletier, J.-P., Benderdour, M., and Fahmi, H. (2014). Lysine-specific demethylase 1-mediated demethylation of histone H3 lysine 9 contributes to interleukin 1 β -induced microsomal prostaglandin E synthase 1 expression in human osteoarthritic chondrocytes. *Arthritis Research & Therapy* *16*, 1-15.

Emini Veseli, B., Perrotta, P., De Meyer, G.R.A., Roth, L., Van der Donckt, C., Martinet, W., and De Meyer, G.R.Y. (2017). Animal models of atherosclerosis. *European Journal of Pharmacology* *816*, 3-13.

English, J.M., and Cobb, M.H. (2002). Pharmacological inhibitors of MAPK pathways. *Trends in Pharmacological Sciences* *23*, 40-45.

ESC (2012). European Cardiovascular Disease Statistics (European Society of Cardiology).

Faggioli, L., Costanzo, C., Donadelli, M., and Palmieri, M. (2004). Activation of the interleukin-6 promoter by a dominant negative mutant of c-Jun. *Biochimica et Biophysica Acta (BBA) - Molecular Cell Research* *1692*, 17-24.

Fang, T.C., Schaefer, U., Mecklenbrauker, I., Stienen, A., Dewell, S., Chen, M.S., Rioja, I., Parravicini, V., Prinjha, R.K., Chandwani, R., *et al.* (2012). Histone H3 lysine 9 di-methylation as an epigenetic signature of the interferon response. *The Journal of Experimental Medicine* *209*, 661-669.

Fanjul-Fernández, M., Folgueras, A.R., Cabrera, S., and López-Otín, C. (2010). Matrix metalloproteinases: Evolution, gene regulation and functional analysis in mouse models. *Biochimica et Biophysica Acta (BBA) - Molecular Cell Research* *1803*, 3-19.

Filion, G.J., and van Steensel, B. (2010). Reassessing the abundance of H3K9me2 chromatin domains in embryonic stem cells. *Nature genetics* *42*, 4; author reply 5-6.

Fleenor, D.L., Pang, I.H., and Clark, A.F. (2003). Involvement of AP-1 in interleukin-1 α -stimulated MMP-3 expression in human trabecular meshwork cells. *Investigative ophthalmology & visual science* *44*, 3494-3501.

Galis, Z.S., and Khatri, J.J. (2002). Matrix metalloproteinases in vascular remodeling and atherogenesis: the good, the bad, and the ugly. *Circulation research* 90, 251-262.

Galis, Z.S., Muszynski, M., Sukhova, G.K., Simon-Morrissey, E., Unemori, E.N., Lark, M.W., Amento, E., and Libby, P. (1994a). Cytokine-stimulated human vascular smooth muscle cells synthesize a complement of enzymes required for extracellular matrix digestion. *Circulation research* 75, 181-189.

Galis, Z.S., Sukhova, G.K., Lark, M.W., and Libby, P. (1994b). Increased expression of matrix metalloproteinases and matrix degrading activity in vulnerable regions of human atherosclerotic plaques. *J Clin Invest* 94, 2493-2503.

Garlanda, C., Dinarello, C.A., and Mantovani, A. (2013). The interleukin-1 family: back to the future. *Immunity* 39, 1003-1018.

Gesumaria, L., Matsui, M.S., Kluz, T., and Costa, M. (2015). Solar-simulated ultraviolet radiation induces histone 3 methylation changes in the gene promoters of matrix metalloproteinases 1 and 3 in primary human dermal fibroblasts. *Experimental dermatology* 24, 384-385.

Ghashghaieina, M., Toulany, M., Saki, M., Bobbala, D., Fehrenbacher, B., Rupec, R., Rodemann, H.P., Ghoreschi, K., Rocken, M., Schaller, M., *et al.* (2011). The NF κ B pathway inhibitors Bay 11-7082 and parthenolide induce programmed cell death in anucleated Erythrocytes. *Cellular physiology and biochemistry : international journal of experimental cellular physiology, biochemistry, and pharmacology* 27, 45-54.

Gomard, T., Michaud, H.A., Tempe, D., Thiolon, K., Pelegrin, M., and Piechaczyk, M. (2010). An NF-kappaB-dependent role for JunB in the induction of proinflammatory cytokines in LPS-activated bone marrow-derived dendritic cells. *PLoS One* 5, e9585.

Gomez, D., and Owens, G.K. (2012). Smooth muscle cell phenotypic switching in atherosclerosis. *Cardiovascular research* 95, 156-164.

Gomez, D., Shankman, L.S., Nguyen, A.T., and Owens, G.K. (2013). Detection of histone modifications at specific gene loci in single cells in histological sections. *Nature methods* 10, 171-177.

Greißel, A., Culmes, M., Napieralski, R., Wagner, E., Gebhard, H., Schmitt, M., Zimmermann, A., Eckstein, H.H., Zerneck, A., and Pelisek, J. (2015). Alternation of histone and DNA methylation in human atherosclerotic carotid plaques. *Thrombosis and haemostasis* 114, 390-402.

Greissel, A., Culmes, M., Napieralski, R., Wagner, E., Gebhard, H., Schmitt, M., Zimmermann, A., Eckstein, H.H., Zerneck, A., and Pelisek, J. (2015). Alternation of histone and DNA methylation in human atherosclerotic carotid plaques. *Thrombosis and haemostasis* 114, 390-402.

Guo, X., and Chen, S.-Y. (2012). Transforming growth factor- β and smooth muscle differentiation. *World Journal of Biological Chemistry* 3, 41-52.

- Gupte, R.S., Ata, H., Rawat, D., Abe, M., Taylor, M.S., Ochi, R., and Gupte, S.A. (2011). Glucose-6-Phosphate Dehydrogenase Is a Regulator of Vascular Smooth Muscle Contraction. *Antioxidants & Redox Signaling* *14*, 543-558.
- Hainer, S.J., Boskovic, A., Rando, O.J., and Fazio, T.G. (2018). Profiling of pluripotency factors in individual stem cells and early embryos. *bioRxiv*.
- Halpert, I., Sires, U.I., Roby, J.D., Potter-Perigo, S., Wight, T.N., Shapiro, S.D., Welgus, H.G., Wickline, S.A., and Parks, W.C. (1996). Matrilysin is expressed by lipid-laden macrophages at sites of potential rupture in atherosclerotic lesions and localizes to areas of versican deposition, a proteoglycan substrate for the enzyme. *Proceedings of the National Academy of Sciences of the United States of America* *93*, 9748-9753.
- Han, J., Zhang, Z., and Wang, K. (2018). 3C and 3C-based techniques: the powerful tools for spatial genome organization deciphering. *Molecular Cytogenetics* *11*, 21.
- Han, Z., Boyle, D.L., Chang, L., Bennett, B., Karin, M., Yang, L., Manning, A.M., and Firestein, G.S. (2001). c-Jun N-terminal kinase is required for metalloproteinase expression and joint destruction in inflammatory arthritis. *J Clin Invest* *108*, 73-81.
- Hao, H., Ropraz, P., Verin, V., Camenzind, E., Geinoz, A., Pepper, M.S., Gabbiani, G., and Bochaton-Piallat, M.L. (2002). Heterogeneity of smooth muscle cell populations cultured from pig coronary artery. *Arteriosclerosis, thrombosis, and vascular biology* *22*, 1093-1099.
- Hautmann, M.B., Madsen, C.S., and Owens, G.K. (1997). A transforming growth factor beta (TGFbeta) control element drives TGFbeta-induced stimulation of smooth muscle alpha-actin gene expression in concert with two CArG elements. *The Journal of biological chemistry* *272*, 10948-10956.
- He, M., Zheng, B., Zhang, Y., Zhang, X.H., Wang, C., Yang, Z., Sun, Y., Wu, X.L., and Wen, J.K. (2015). KLF4 mediates the link between TGF-beta1-induced gene transcription and H3 acetylation in vascular smooth muscle cells. *FASEB journal : official publication of the Federation of American Societies for Experimental Biology* *29*, 4059-4070.
- Heinz, S., Romanoski, C.E., Benner, C., and Glass, C.K. (2015). The selection and function of cell type-specific enhancers. *Nat Rev Mol Cell Biol* *16*, 144-154.
- Herring, B.P., Hoggatt, A.M., Burlak, C., and Offermanns, S. (2014). Previously differentiated medial vascular smooth muscle cells contribute to neointima formation following vascular injury. *Vasc Cell* *6*, 21.
- Herring, B.P., Hoggatt, A.M., Griffith, S.L., McClintick, J.N., and Gallagher, P.J. (2017). Inflammation and vascular smooth muscle cell dedifferentiation following carotid artery ligation. *Physiol Genomics* *49*, 115-126.
- Hess, J., Angel, P., and Schorpp-Kistner, M. (2004). AP-1 subunits: quarrel and harmony among siblings. *Journal of Cell Science* *117*, 5965.
- Huang, J., Dorsey, J., Chuikov, S., Perez-Burgos, L., Zhang, X., Jenuwein, T., Reinberg, D., and Berger, S.L. (2010a). G9a and Glp methylate lysine 373 in the tumor suppressor p53. *The Journal of biological chemistry* *285*, 9636-9641.

- Huang, J., Dorsey, J., Chuikov, S., Zhang, X., Jenuwein, T., Reinberg, D., and Berger, S.L. (2010b). G9a and Glp Methylate Lysine 373 in the Tumor Suppressor p53. *The Journal of biological chemistry* *285*, 9636-9641.
- Huang, J., Zhang, H., Yao, J., Qin, G., Wang, F., Wang, X., Luo, A., Zheng, Q., Cao, C., and Zhao, J. (2016). BIX-01294 increases pig cloning efficiency by improving epigenetic reprogramming of somatic cell nuclei. *Reproduction (Cambridge, England)* *151*, 39-49.
- Huang, W.C., Sala-Newby, G.B., Susana, A., Johnson, J.L., and Newby, A.C. (2012). Classical macrophage activation up-regulates several matrix metalloproteinases through mitogen activated protein kinases and nuclear factor-kappaB. *PLoS One* *7*, e42507.
- Hublitz, P., Albert, M., and Peters, A.H. (2009). Mechanisms of transcriptional repression by histone lysine methylation. *The International journal of developmental biology* *53*, 335-354.
- Hyun, K., Jeon, J., Park, K., and Kim, J. (2017). Writing, erasing and reading histone lysine methylations. *Experimental & Molecular Medicine* *49*, e324.
- Isbel, L., Prokopuk, L., Wu, H., Daxinger, L., Oey, H., and Spurling, A. (2016). Wiz binds active promoters and CTCF-binding sites and is required for normal behaviour in the mouse. *5*.
- Johnson, J.L. (2014). Matrix metalloproteinases and their inhibitors in cardiovascular pathologies: current knowledge and clinical potential. Dove Medical Press Ltd *Volume 2014:1*, Pages 21—36.
- Johnson, J.L. (2017). Metalloproteinases in atherosclerosis. *European Journal of Pharmacology* *816*, 93-106.
- Johnson, J.L., Devel, L., Czarny, B., George, S.J., Jackson, C.L., Rogakos, V., Beau, F., Yiotakis, A., Newby, A.C., and Dive, V. (2011a). A selective matrix metalloproteinase-12 inhibitor retards atherosclerotic plaque development in apolipoprotein E-knockout mice. *Arteriosclerosis, thrombosis, and vascular biology* *31*, 528-535.
- Johnson, J.L., Dwivedi, A., Somerville, M., George, S.J., and Newby, A.C. (2011b). Matrix metalloproteinase (MMP)-3 activates MMP-9 mediated vascular smooth muscle cell migration and neointima formation in mice. *Arteriosclerosis, thrombosis, and vascular biology* *31*, e35-44.
- Johnson, J.L., George, S.J., Newby, A.C., and Jackson, C.L. (2005a). Divergent effects of matrix metalloproteinases 3, 7, 9, and 12 on atherosclerotic plaque stability in mouse brachiocephalic arteries. *Proceedings of the National Academy of Sciences of the United States of America* *102*, 15575-15580.
- Johnson, J.L., George, S.J., Newby, A.C., and Jackson, C.L. (2005b). Divergent effects of matrix metalloproteinases 3, 7, 9, and 12 on atherosclerotic plaque stability in mouse brachiocephalic arteries. *Proceedings of the National Academy of Sciences of the United States of America* *102*, 15575-15580.
- Jorgensen, H.F., and Fisher, A.G. (2009). LOCKing in Cellular Potential. *Cell Stem Cell* *4*, 192-194.

- Kim, E.K., and Choi, E.J. (2015). Compromised MAPK signaling in human diseases: an update. *Archives of toxicology* *89*, 867-882.
- Klein, A.M., Zaganjor, E., and Cobb, M.H. (2013). Chromatin-tethered MAPKs. *Current Opinion in Cell Biology* *25*, 272-277.
- Klose, R.J., and Zhang, Y. (2007). Regulation of histone methylation by demethylination and demethylation. *Nat Rev Mol Cell Biol* *8*, 307-318.
- Kouzarides, T. (2007). Chromatin Modifications and Their Function. *Cell* *128*, 693-705.
- Kowalczyk, M.S., Hughes, J.R., Garrick, D., Lynch, M.D., Sharpe, J.A., Sloane-Stanley, J.A., McGowan, S.J., De Gobbi, M., Hosseini, M., Vernimmen, D., *et al.* (2012). Intragenic enhancers act as alternative promoters. *Mol Cell* *45*, 447-458.
- Kubicek, S., O'Sullivan, R.J., August, E.M., Hickey, E.R., Zhang, Q., Teodoro, M.L., Rea, S., Mechtler, K., Kowalski, J.A., Homon, C.A., *et al.* (2007). Reversal of H3K9me2 by a small-molecule inhibitor for the G9a histone methyltransferase. *Mol Cell* *25*, 473-481.
- Kumar, A., and Lindner, V. (1997a). Remodeling with neointima formation in the mouse carotid artery after cessation of blood flow. *Arteriosclerosis, thrombosis, and vascular biology* *17*, 2238-2244.
- Kumar, A., and Lindner, V. (1997b). Remodeling With Neointima Formation in the Mouse Carotid Artery After Cessation of Blood Flow. *Arteriosclerosis, thrombosis, and vascular biology* *17*, 2238.
- Kurozumi, A., Nakano, K., Yamagata, K., Okada, Y., Nakayamada, S., and Tanaka, Y. (2016). IL-6/STAT3 pathway is critically involved in vascular calcification via histone modification of the RUNX2 promoter in vascular smooth muscle cells.
- Kuzuya, M., Kanda, S., Sasaki, T., Tamaya-Mori, N., Cheng, X.W., Itoh, T., Itohara, S., and Iguchi, A. (2003). Deficiency of gelatinase a suppresses smooth muscle cell invasion and development of experimental intimal hyperplasia. *Circulation* *108*, 1375-1381.
- Kuzuya, M., Nakamura, K., Sasaki, T., Cheng, X.W., Itohara, S., and Iguchi, A. (2006). Effect of MMP-2 deficiency on atherosclerotic lesion formation in apoE-deficient mice. *Arteriosclerosis, thrombosis, and vascular biology* *26*, 1120-1125.
- Lee, G.-L., Wu, J.-Y., Tsai, C.-S., Lin, C.-Y., Tsai, Y.-T., Lin, C.-S., Wang, Y.-F., Yet, S.-F., Hsu, Y.-J., and Kuo, C.-C. (2016). TLR4-Activated MAPK-IL-6 Axis Regulates Vascular Smooth Muscle Cell Function. *International Journal of Molecular Sciences* *17*, 1394.
- Lee, J.-Y., Lee, S.-H., Heo, S.-H., Kim, K.-S., Kim, C., Kim, D.-K., Ko, J.-J., and Park, K.-S. (2015). Novel Function of Lysine Methyltransferase G9a in the Regulation of Sox2 Protein Stability. *PLoS ONE* *10*, e0141118.
- Lee, J., Sayed, N., Hunter, A., Au, K.F., Wong, W.H., Mocarski, E.S., Pera, R.R., Yakubov, E., and Cooke, J.P. (2012). Activation of Innate Immunity is Required for Efficient Nuclear Reprogramming. *Cell* *151*, 547-558.

Lee, J.S., Kim, Y., Kim, I.S., Kim, B., Choi, H.J., Lee, J.M., Shin, H.-J.R., Kim, J.H., Kim, J.-Y., Seo, S.-B., *et al.* (2010). Negative Regulation of Hypoxic Responses via Induced Reptin Methylation. *Molecular cell* 39, 71-85.

Lee, Y.T., Laxton, V., Lin, H.Y., Chan, Y.W.F., Fitzgerald-Smith, S., To, T.L.O., Yan, B.P., Liu, T., and Tse, G. (2017). Animal models of atherosclerosis. *Biomedical Reports* 6, 259-266.

Leung, D.C., Dong, K.B., Maksakova, I.A., Goyal, P., Appanah, R., Lee, S., Tachibana, M., Shinkai, Y., Lehnertz, B., Mager, D.L., *et al.* (2011). Lysine methyltransferase G9a is required for de novo DNA methylation and the establishment, but not the maintenance, of proviral silencing. *Proceedings of the National Academy of Sciences of the United States of America* 108, 5718-5723.

Li, S., Ali, S., Duan, X., Liu, S., Du, J., Liu, C., Dai, H., Zhou, M., Zhou, L., Yang, L., *et al.* (2018). JMJD1B Demethylates H4R3me2s and H3K9me2 to Facilitate Gene Expression for Development of Hematopoietic Stem and Progenitor Cells. *Cell Rep* 23, 389-403.

Liang, J., Liu, E., Yu, Y., Kitajima, S., Koike, T., Jin, Y., Morimoto, M., Hatakeyama, K., Asada, Y., Watanabe, T., *et al.* (2006). Macrophage metalloelastase accelerates the progression of atherosclerosis in transgenic rabbits. *Circulation* 113, 1993-2001.

Libby, P. (2013). Mechanisms of Acute Coronary Syndromes and Their Implications for Therapy. *New England Journal of Medicine* 368, 2004-2013.

Libby, P. (2017). Interleukin-1 Beta as a Target for Atherosclerosis Therapy: Biological Basis of CANTOS and Beyond. *Journal of the American College of Cardiology* 70, 2278-2289.

Libby, P., Ridker, P.M., and Hansson, G.K. (2011). Progress and challenges in translating the biology of atherosclerosis. *Nature* 473, 317-325.

Lienert, F., Mohn, F., Tiwari, V.K., Baubec, T., Roloff, T.C., Gaidatzis, D., Stadler, M.B., and Schubeler, D. (2011). Genomic prevalence of heterochromatic H3K9me2 and transcription do not discriminate pluripotent from terminally differentiated cells. *PLoS genetics* 7, e1002090.

Lim, S., and Park, S. (2014). Role of vascular smooth muscle cell in the inflammation of atherosclerosis. *BMB reports* 47, 1-7.

Ling, B.M.T., Bharathy, N., Chung, T.-K., Kok, W.K., Li, S., Tan, Y.H., Rao, V.K., Gopinadhan, S., Sartorelli, V., Walsh, M.J., *et al.* (2012). Lysine methyltransferase G9a methylates the transcription factor MyoD and regulates skeletal muscle differentiation. *Proceedings of the National Academy of Sciences of the United States of America* 109, 841-846.

Liu, C., Yu, Y., Liu, F., Wei, X., Wrobel, J.A., Gunawardena, H.P., Zhou, L., Jin, J., and Chen, X. (2014). A chromatin activity based chemoproteomic approach reveals a transcriptional repressome for gene-specific silencing. *Nature communications* 5, 5733-5733.

Liu, F., Barsyte-Lovejoy, D., Li, F., Xiong, Y., Korboukh, V., Huang, X.P., Allali-Hassani, A., Janzen, W.P., Roth, B.L., Frye, S.V., *et al.* (2013). Discovery of an in vivo chemical probe of the lysine methyltransferases G9a and GLP. *Journal of medicinal chemistry* 56, 8931-8942.

- Liu, F., Chen, X., Allali-Hassani, A., Quinn, A.M., Wasney, G.A., Dong, A., Barsyte, D., Kozieradzki, I., Senisterra, G., Chau, I., *et al.* (2009). Discovery of a 2,4-diamino-7-aminoalkoxyquinazoline as a potent and selective inhibitor of histone lysine methyltransferase G9a. *Journal of medicinal chemistry* *52*, 7950-7953.
- Liu, N., Zhang, Z., Wu, H., Jiang, Y., Meng, L., Xiong, J., Zhao, Z., Zhou, X., Li, J., Li, H., *et al.* (2015a). Recognition of H3K9 methylation by GLP is required for efficient establishment of H3K9 methylation, rapid target gene repression, and mouse viability. *Genes & Development* *29*, 379-393.
- Liu, R., Leslie, K.L., and Martin, K.A. (2015b). Epigenetic regulation of smooth muscle cell plasticity. *Biochimica et biophysica acta* *1849*, 448-453.
- Liu, T., Zhang, L., Joo, D., and Sun, S.-C. (2017). NF- κ B signaling in inflammation. *Signal Transduction And Targeted Therapy* *2*, 17023.
- Liu, X., Wang, Y., and Gao, Y. (2018). H3K9 demethylase KDM4E is an epigenetic regulator for bovine embryonic development and a defective factor for nuclear reprogramming. *145*.
- Liu, Y., Sinha, S., McDonald, O.G., Shang, Y., Hoofnagle, M.H., and Owens, G.K. (2005). Kruppel-like factor 4 abrogates myocardin-induced activation of smooth muscle gene expression. *The Journal of biological chemistry* *280*, 9719-9727.
- Liu, Y., Sinha, S., and Owens, G. (2003). A transforming growth factor-beta control element required for SM alpha-actin expression in vivo also partially mediates GSKF-dependent transcriptional repression. *The Journal of biological chemistry* *278*, 48004-48011.
- Livet, J., Weissman, T.A., Kang, H., Draft, R.W., Lu, J., Bennis, R.A., Sanes, J.R., and Lichtman, J.W. (2007). Transgenic strategies for combinatorial expression of fluorescent proteins in the nervous system. *Nature* *450*, 56.
- Loh, Y.H., Zhang, W., Chen, X., George, J., and Ng, H.H. (2007). Jmjd1a and Jmjd2c histone H3 Lys 9 demethylases regulate self-renewal in embryonic stem cells. *Genes Dev* *21*, 2545-2557.
- Lu, J., Guo, J.-H., Tu, X.-L., Zhang, C., Zhao, M., Zhang, Q.-W., and Gao, F.-H. (2016). Tiron Inhibits UVB-Induced AP-1 Binding Sites Transcriptional Activation on MMP-1 and MMP-3 Promoters by MAPK Signaling Pathway in Human Dermal Fibroblasts. *PLoS ONE* *11*, e0159998.
- Luttun, A., Lutgens, E., Manderveld, A., Maris, K., Collen, D., Carmeliet, P., and Moons, L. (2004). Loss of matrix metalloproteinase-9 or matrix metalloproteinase-12 protects apolipoprotein E-deficient mice against atherosclerotic media destruction but differentially affects plaque growth. *Circulation* *109*, 1408-1414.
- Majesky, M.W., Horita, H., Ostriker, A., Lu, S., Regan, J.N., Bagchi, A., Dong, X.R., Poczobutt, J., Nemenoff, R.A., and Weiser-Evans, M.C.M. (2017). Differentiated Smooth Muscle Cells Generate a Subpopulation of Resident Vascular Progenitor Cells in the Adventitia Regulated by KLF4. *Circulation research* *120*, 296-311.

- Manderson, J.A., Mosse, P.R., Safstrom, J.A., Young, S.B., and Campbell, G.R. (1989). Balloon catheter injury to rabbit carotid artery. I. Changes in smooth muscle phenotype. *Arteriosclerosis (Dallas, Tex)* 9, 289-298.
- McDonald, O.G., Wamhoff, B.R., Hoofnagle, M.H., and Owens, G.K. (2006). Control of SRF binding to CARG box chromatin regulates smooth muscle gene expression in vivo. *The Journal of Clinical Investigation* 116, 36-48.
- McDonald, O.G., Wu, H., Timp, W., Doi, A., and Feinberg, A.P. (2011). Genome-scale epigenetic reprogramming during epithelial-to-mesenchymal transition. *Nat Struct Mol Biol* 18, 867-874.
- Meijer, C.A., Le Haen, P.A., van Dijk, R.A., Hira, M., Hamming, J.F., van Bockel, J.H., and Lindeman, J.H. (2012). Activator protein-1 (AP-1) signalling in human atherosclerosis: results of a systematic evaluation and intervention study. *Clinical science (London, England : 1979)* 122, 421-428.
- Meir, K.S., and Leitersdorf, E. (2004). Atherosclerosis in the apolipoprotein-E-deficient mouse: a decade of progress. *Arteriosclerosis, thrombosis, and vascular biology* 24, 1006-1014.
- Merkling, S.H., Bronkhorst, A.W., Kramer, J.M., Overheul, G.J., Schenck, A., and Van Rij, R.P. (2015). The Epigenetic Regulator G9a Mediates Tolerance to RNA Virus Infection in *Drosophila*. *PLOS Pathogens* 11, e1004692.
- Metz, R.P., Patterson, J.L., and Wilson, E. (2012). Vascular smooth muscle cells: isolation, culture, and characterization. *Methods in molecular biology (Clifton, NJ)* 843, 169-176.
- Miao, F., Wu, X., Zhang, L., Yuan, Y.C., Riggs, A.D., and Natarajan, R. (2007). Genome-wide analysis of histone lysine methylation variations caused by diabetic conditions in human monocytes. *The Journal of biological chemistry* 282, 13854-13863.
- Mikhaylichenko, O., Bondarenko, V., Harnett, D., Schor, I.E., Males, M., Viales, R.R., and Furlong, E.E.M. (2018). The degree of enhancer or promoter activity is reflected by the levels and directionality of eRNA transcription. 32, 42-57.
- Mishra, M., Flaga, J., and Kowluru, R.A. (2016). Molecular Mechanism of Transcriptional Regulation of Matrix Metalloproteinase-9 in Diabetic Retinopathy. *Journal of cellular physiology* 231, 1709-1718.
- Morton, S., Davis, R.J., McLaren, A., and Cohen, P. (2003). A reinvestigation of the multisite phosphorylation of the transcription factor c-Jun. *The EMBO journal* 22, 3876-3886.
- Mosca, L., Barrett-Connor, E., and Wenger, N.K. (2011). Sex/gender differences in cardiovascular disease prevention: what a difference a decade makes. *Circulation* 124, 2145-2154.
- Moura, R., Tjwa, M., Vandervoort, P., Cludts, K., and Hoylaerts, M.F. (2007). Thrombospondin-1 Activates Medial Smooth Muscle Cells and Triggers Neointima Formation Upon Mouse Carotid Artery Ligation. *Arteriosclerosis, thrombosis, and vascular biology* 27, 2163.

Muller, A., Kramer, S.D., Meletta, R., Beck, K., Selivanova, S.V., Rancic, Z., Kaufmann, P.A., Vos, B., Meding, J., Stellfeld, T., *et al.* (2014). Gene expression levels of matrix metalloproteinases in human atherosclerotic plaques and evaluation of radiolabeled inhibitors as imaging agents for plaque vulnerability. *Nuclear medicine and biology* *41*, 562-569.

Muslin, A.J. (2008). MAPK Signaling in Cardiovascular Health and Disease: Molecular Mechanisms and Therapeutic Targets. *Clinical science (London, England : 1979)* *115*, 203-218.

Nagase, H., Visse, R., and Murphy, G. (2006). Structure and function of matrix metalloproteinases and TIMPs. *Cardiovascular research* *69*, 562-573.

Nair, S.S., Li, D.-Q., and Kumar, R. (2013). A Core Chromatin Remodeling Factor Instructs Global Chromatin Signaling Through Multivalent Reading of Nucleosome Codes. *Molecular cell* *49*, 704-718.

Nakashima, Y., Plump, A.S., Raines, E.W., Breslow, J.L., and Ross, R. (1994). ApoE-deficient mice develop lesions of all phases of atherosclerosis throughout the arterial tree. *Arteriosclerosis and thrombosis : a journal of vascular biology / American Heart Association* *14*, 133-140.

Nakayama, J., Rice, J.C., Strahl, B.D., Allis, C.D., and Grewal, S.I. (2001). Role of histone H3 lysine 9 methylation in epigenetic control of heterochromatin assembly. *Science (New York, NY)* *292*, 110-113.

Ndlovu, M.N., Van Lint, C., Van Wesemael, K., Callebert, P., Chalbos, D., Haegeman, G., and Vanden Berghe, W. (2009). Hyperactivated NF- κ B and AP-1 transcription factors promote highly accessible chromatin and constitutive transcription across the interleukin-6 gene promoter in metastatic breast cancer cells. *Molecular and cellular biology* *29*, 5488-5504.

Nemenoff, R.A., Horita, H., Ostriker, A.C., Furgeson, S.B., Simpson, P.A., VanPutten, V., Crossno, J., Offermanns, S., and Weiser-Evans, M.C. (2011). SDF-1 α induction in mature smooth muscle cells by inactivation of PTEN is a critical mediator of exacerbated injury-induced neointima formation. *Arteriosclerosis, thrombosis, and vascular biology* *31*, 1300-1308.

Newby, A.C. (2005). Dual role of matrix metalloproteinases (matrixins) in intimal thickening and atherosclerotic plaque rupture. *Physiological reviews* *85*, 1-31.

Newby, A.C. (2012). Matrix metalloproteinase inhibition therapy for vascular diseases. *Vascular pharmacology* *56*, 232-244.

Nguyen, A.T., Gomez, D., Bell, R.D., Campbell, J.H., Clowes, A.W., Gabbiani, G., Giachelli, C.M., Parmacek, M.S., Raines, E.W., Rusch, N.J., *et al.* (2013). Smooth muscle cell plasticity: fact or fiction? *Circulation research* *112*, 17-22.

Nurminskaya, M., Beazley, K.E., Smith, E.P., and Belkin, A.M. (2014). Transglutaminase 2 promotes PDGF-mediated activation of PDGFR/Akt1 and beta-catenin signaling in vascular

smooth muscle cells and supports neointima formation. *Journal of vascular research* 51, 418-428.

Ow, J.R., Palanichamy Kala, M., Rao, V.K., Choi, M.H., Bharathy, N., and Taneja, R. (2016). G9a inhibits MEF2C activity to control sarcomere assembly. *Sci Rep* 6, 34163.

Owens, G.K., Kumar, M.S., and Wamhoff, B.R. (2004). Molecular regulation of vascular smooth muscle cell differentiation in development and disease. *Physiological reviews* 84, 767-801.

Pappano, W.N., Guo, J., He, Y., Ferguson, D., Jagadeeswaran, S., Osterling, D.J., Gao, W., Spence, J.K., Pliushchev, M., Sweis, R.F., *et al.* (2015). The Histone Methyltransferase Inhibitor A-366 Uncovers a Role for G9a/GLP in the Epigenetics of Leukemia. *PLoS One* 10, e0131716.

Park, J.W., Shin, I.S., Ha, U.H., Oh, S.R., Kim, J.H., and Ahn, K.S. (2015). Pathophysiological changes induced by *Pseudomonas aeruginosa* infection are involved in MMP-12 and MMP-13 upregulation in human carcinoma epithelial cells and a pneumonia mouse model. *Infection and immunity* 83, 4791-4799.

Perlman, R.L. (2016). Mouse models of human disease: An evolutionary perspective. *Evolution, Medicine, and Public Health* 2016, 170-176.

Peters, A.H., Kubicek, S., Mechtler, K., O'Sullivan, R.J., Derijck, A.A., Perez-Burgos, L., Kohlmaier, A., Opravil, S., Tachibana, M., Shinkai, Y., *et al.* (2003). Partitioning and plasticity of repressive histone methylation states in mammalian chromatin. *Mol Cell* 12, 1577-1589.

Piemonti, L., Calori, G., Lattuada, G., Mercalli, A., Ragogna, F., Garancini, M.P., Ruotolo, G., Luzi, L., and Perseghin, G. (2009). Association between plasma monocyte chemoattractant protein-1 concentration and cardiovascular disease mortality in middle-aged diabetic and nondiabetic individuals. *Diabetes care* 32, 2105-2110.

Pless, O., Kowenz-Leutz, E., Knoblich, M., Lausen, J., Beyermann, M., Walsh, M.J., and Leutz, A. (2008). G9a-mediated lysine methylation alters the function of CCAAT/enhancer-binding protein-beta. *The Journal of biological chemistry* 283, 26357-26363.

Pokholok, D.K., Zeitlinger, J., Hannett, N.M., Reynolds, D.B., and Young, R.A. (2006). Activated Signal Transduction Kinases Frequently Occupy Target Genes. *Science (New York, NY)* 313, 533.

Pradère, J.-P., Hernandez, C., Koppe, C., Friedman, R.A., Luedde, T., and Schwabe, R.F. (2016). Negative regulation of NF- κ B p65 activity by serine 536 phosphorylation. *Science signaling* 9, ra85-ra85.

Pugsley, M.K., and Tabrizchi, R. (2000). The vascular system. An overview of structure and function. *Journal of pharmacological and toxicological methods* 44, 333-340.

Pulverer, B.J., Kyriakis, J.M., Avruch, J., Nikolakaki, E., and Woodgett, J.R. (1991). Phosphorylation of c-jun mediated by MAP kinases. *Nature* 353, 670-674.

- Purcell, D.J., Khalid, O., Ou, C.-Y., Little, G.H., Frenkel, B., Baniwal, S.K., and Stallcup, M.R. (2012). Recruitment of coregulator G9a by Runx2 for selective enhancement or suppression of transcription. *Journal of Cellular Biochemistry* 113, 2406-2414.
- Quinones, S., Buttice, G., and Kurkinen, M. (1994). Promoter elements in the transcriptional activation of the human stromelysin-1 gene by the inflammatory cytokine, interleukin 1. *The Biochemical journal* 302 (Pt 2), 471-477.
- Rader, D.J. (2012). IL-1 and atherosclerosis: a murine twist to an evolving human story. *The Journal of Clinical Investigation* 122, 27-30.
- Rensen, S.S.M., Doevendans, P., and van Eys, G. (2007). Regulation and characteristics of vascular smooth muscle cell phenotypic diversity. *Netherlands Heart Journal* 15, 100-108.
- Ridker, P.M., Everett, B.M., Thuren, T., MacFadyen, J.G., Chang, W.H., Ballantyne, C., Fonseca, F., Nicolau, J., Koenig, W., Anker, S.D., *et al.* (2017). Antiinflammatory Therapy with Canakinumab for Atherosclerotic Disease. *The New England journal of medicine* 377, 1119-1131.
- Rodriguez-Madoz, J.R., San Jose-Eneriz, E., Rabal, O., Zapata-Linares, N., Miranda, E., Rodriguez, S., Porciuncula, A., Vilas-Zornoza, A., Garate, L., Segura, V., *et al.* (2017). Reversible dual inhibitor against G9a and DNMT1 improves human iPSC derivation enhancing MET and facilitating transcription factor engagement to the genome. *PLOS ONE* 12, e0190275.
- Rong, S., Zhao, X., Jin, X., Zhang, Z., Chen, L., Zhu, Y., and Yuan, W. (2014). Vascular calcification in chronic kidney disease is induced by bone morphogenetic protein-2 via a mechanism involving the Wnt/beta-catenin pathway. *Cellular physiology and biochemistry : international journal of experimental cellular physiology, biochemistry, and pharmacology* 34, 2049-2060.
- Ross, M., and Pawlina, W. (2011). *Histology: a text and atlas: with collerated cell and molecular biology* (Lippincott Williams & Wilkins).
- Saccani, S., and Natoli, G. (2002). Dynamic changes in histone H3 Lys 9 methylation occurring at tightly regulated inducible inflammatory genes. *Genes Dev* 16.
- Sander, J.D., and Joung, J.K. (2014). CRISPR-Cas systems for editing, regulating and targeting genomes. *Nature biotechnology* 32, 347-355.
- Sanyal, A., Lajoie, B.R., Jain, G., and Dekker, J. (2012). The long-range interaction landscape of gene promoters. *Nature* 489, 109-113.
- Sato, Y., Mukai, M., Ueda, J., Muraki, M., Stasevich, T.J., Horikoshi, N., Kujirai, T., Kita, H., Kimura, T., Hira, S., *et al.* (2013). Genetically encoded system to track histone modification in vivo. *Sci Rep* 3, 2436.
- Sayers, R.L., Sundberg-Smith, L.J., Rojas, M., Hayasaka, H., Parsons, J.T., Mack, C.P., and Taylor, J.M. (2008). FRNK Expression Promotes Smooth Muscle Cell Maturation During Vascular Development and After Vascular Injury. *Arteriosclerosis, thrombosis, and vascular biology* 28, 2115.

- Scheller, J., Chalaris, A., Schmidt-Arras, D., and Rose-John, S. (2011). The pro- and anti-inflammatory properties of the cytokine interleukin-6. *Biochimica et Biophysica Acta (BBA) - Molecular Cell Research* 1813, 878-888.
- Schober, A. (2008). Chemokines in vascular dysfunction and remodeling. *Arteriosclerosis, thrombosis, and vascular biology* 28, 1950-1959.
- Sedger, L.M., and McDermott, M.F. (2014). TNF and TNF-receptors: From mediators of cell death and inflammation to therapeutic giants – past, present and future. *Cytokine & Growth Factor Reviews* 25, 453-472.
- Selzman, C.H., Miller, S.A., Zimmerman, M.A., Gamboni-Robertson, F., Harken, A.H., and Banerjee, A. (2002). Monocyte chemotactic protein-1 directly induces human vascular smooth muscle proliferation. *American Journal of Physiology-Heart and Circulatory Physiology* 283, H1455-H1461.
- Shah, A., Oldenburg, A., and Collas, P. (2014). A hyper-dynamic nature of bivalent promoter states underlies coordinated developmental gene expression modules. *BMC genomics* 15, 1186.
- Shankar, S.R., Bahirvani, A.G., Rao, V.K., Bharathy, N., Ow, J.R., and Taneja, R. (2013). G9a, a multipotent regulator of gene expression. *Epigenetics* 8, 16-22.
- Shankman, L.S., Gomez, D., Cherepanova, O.A., Salmon, M., Alencar, G.F., Haskins, R.M., Swiatlowska, P., Newman, A.A., Greene, E.S., Straub, A.C., *et al.* (2015). KLF4-dependent phenotypic modulation of smooth muscle cells has a key role in atherosclerotic plaque pathogenesis. *Nat Med* 21, 628-637.
- Shi, G., Field, D.J., Long, X., Mickelsen, D., Ko, K.-a., Ture, S., Korshunov, V.A., Miano, J.M., and Morrell, C.N. (2013). Platelet factor 4 mediates vascular smooth muscle cell injury responses. *Blood* 121, 4417-4427.
- Shi, Y., Desponts, C., Do, J.T., Hahm, H.S., Schöler, H.R., and Ding, S. (2008). Induction of Pluripotent Stem Cells from Mouse Embryonic Fibroblasts by Oct4 and Klf4 with Small-Molecule Compounds. *Cell Stem Cell* 3, 568-574.
- Shi, Y., Lan, F., Matson, C., Mulligan, P., Whetstine, J.R., Cole, P.A., and Casero, R.A. (2004). Histone demethylation mediated by the nuclear amine oxidase homolog LSD1. *Cell* 119.
- Shinkai, Y., and Tachibana, M. (2011). H3K9 methyltransferase G9a and the related molecule GLP. *Genes Dev* 25, 781-788.
- Singh, P., and Zheng, X.L. (2014). Dual regulation of myocardin expression by tumor necrosis factor-alpha in vascular smooth muscle cells. *PLoS One* 9, e112120.
- Sinha, S., Iyer, D., and Granata, A. (2014). Embryonic origins of human vascular smooth muscle cells: implications for in vitro modeling and clinical application. *Cellular and Molecular Life Sciences* 71, 2271-2288.
- Skene, P.J., and Henikoff, S. (2017). An efficient targeted nuclease strategy for high-resolution mapping of DNA binding sites. *eLife* 6, e21856.

- Smale, S.T., and Natoli, G. (2014). Transcriptional Control of Inflammatory Responses. *Cold Spring Harbor Perspectives in Biology* 6, a016261.
- Smeal, T., Binetruy, B., Mercola, D., Grover-Bardwick, A., Heidecker, G., Rapp, U.R., and Karin, M. (1992). Oncoprotein-mediated signalling cascade stimulates c-Jun activity by phosphorylation of serines 63 and 73. *Molecular and cellular biology* 12, 3507-3513.
- Snippert, H.J., van der Flier, L.G., Sato, T., van Es, J.H., van den Born, M., Kroon-Veenboer, C., Barker, N., Klein, A.M., van Rheenen, J., Simons, B.D., *et al.* (2010). Intestinal crypt homeostasis results from neutral competition between symmetrically dividing Lgr5 stem cells. *Cell* 143, 134-144.
- Song, Y., Wu, F., and Wu, J. (2016). Targeting histone methylation for cancer therapy: enzymes, inhibitors, biological activity and perspectives. *Journal of hematology & oncology* 9, 49.
- Song, Z., Jin, R., Yu, S., Rivet, J.J., Smyth, S.S., Nanda, A., Granger, D.N., and Li, G. (2011). CD40 is essential in the upregulation of TRAF proteins and NF-kappaB-dependent proinflammatory gene expression after arterial injury. *PLoS One* 6, e23239.
- Sottiurai, V.S., Yao, J.S., Batson, R.C., Sue, S.L., Jones, R., and Nakamura, Y.A. (1989). Distal anastomotic intimal hyperplasia: histopathologic character and biogenesis. *Annals of vascular surgery* 3, 26-33.
- Speer, M.Y., Yang, H.Y., Brabb, T., Leaf, E., Look, A., Lin, W.L., Frutkin, A., Dichek, D., and Giachelli, C.M. (2009). Smooth muscle cells give rise to osteochondrogenic precursors and chondrocytes in calcifying arteries. *Circulation research* 104, 733-741.
- Sprague, A.H., and Khalil, R.A. (2009). Inflammatory Cytokines in Vascular Dysfunction and Vascular Disease. *Biochemical pharmacology* 78, 539-552.
- Sridharan, R., Gonzales-Cope, M., Chronis, C., Bonora, G., McKee, R., Huang, C., Patel, S., Lopez, D., Mishra, N., Pellegrini, M., *et al.* (2013). Proteomic and genomic approaches reveal critical functions of H3K9 methylation and heterochromatin protein-1gamma in reprogramming to pluripotency. *Nat Cell Biol* 15, 872-882.
- Steitz, S.A., Speer, M.Y., Curinga, G., Yang, H.Y., Haynes, P., Aebbersold, R., Schinke, T., Karsenty, G., and Giachelli, C.M. (2001). Smooth muscle cell phenotypic transition associated with calcification: upregulation of Cbfa1 and downregulation of smooth muscle lineage markers. *Circulation research* 89, 1147-1154.
- Stenmark, K.R., Yeager, M.E., El Kasmi, K.C., Nozik-Grayck, E., Gerasimovskaya, E.V., Li, M., Riddle, S.R., and Frid, M.G. (2013). The adventitia: essential regulator of vascular wall structure and function. *Annual review of physiology* 75, 23-47.
- Stoner, L., Lucero, A.A., Palmer, B.R., Jones, L.M., Young, J.M., and Faulkner, J. (2013). Inflammatory biomarkers for predicting cardiovascular disease. *Clinical biochemistry* 46, 1353-1371.
- Strahl, B.D., and Allis, C.D. (2000). The language of covalent histone modifications. *Nature* 403, 41-45.

Suganuma, T., Mushegian, A., Swanson, S.K., Abmayr, S.M., Florens, L., Washburn, M.P., and Workman, J.L. (2010). The ATAC Acetyltransferase Complex Coordinates MAP Kinases to Regulate JNK Target Genes. *Cell* 142, 726-736.

Sun, Y., Liu, W.Z., Liu, T., Feng, X., Yang, N., and Zhou, H.F. (2015). Signaling pathway of MAPK/ERK in cell proliferation, differentiation, migration, senescence and apoptosis. *Journal of receptor and signal transduction research* 35, 600-604.

Sutcliffe, A.M., Clarke, D.L., Bradbury, D.A., Corbett, L.M., Patel, J.A., and Knox, A.J. (2009). Transcriptional regulation of monocyte chemotactic protein-1 release by endothelin-1 in human airway smooth muscle cells involves NF- κ B and AP-1. *British Journal of Pharmacology* 157, 436-450.

Sweis, R.F., Pliushchev, M., Brown, P.J., Guo, J., Li, F., Maag, D., Petros, A.M., Soni, N.B., Tse, C., Vedadi, M., *et al.* (2014). Discovery and development of potent and selective inhibitors of histone methyltransferase G9a. *ACS medicinal chemistry letters* 5, 205-209.

Tachibana, M., Matsumura, Y., Fukuda, M., Kimura, H., and Shinkai, Y. (2008). G9a/GLP complexes independently mediate H3K9 and DNA methylation to silence transcription. *The EMBO journal* 27, 2681-2690.

Tachibana, M., Sugimoto, K., Nozaki, M., Ueda, J., Ohta, T., Ohki, M., Fukuda, M., Takeda, N., Niida, H., Kato, H., *et al.* (2002). G9a histone methyltransferase plays a dominant role in euchromatic histone H3 lysine 9 methylation and is essential for early embryogenesis. *Genes Dev* 16, 1779-1791.

Tachibana, M., Ueda, J., Fukuda, M., Takeda, N., Ohta, T., Iwanari, H., Sakihama, T., Kodama, T., Hamakubo, T., and Shinkai, Y. (2005). Histone methyltransferases G9a and GLP form heteromeric complexes and are both crucial for methylation of euchromatin at H3-K9. *Genes & development* 19, 815-826.

Tak, P.P., and Firestein, G.S. (2001). NF- κ B: a key role in inflammatory diseases. *Journal of Clinical Investigation* 107, 7-11.

Tang, P.C., Qin, L., Zielonka, J., Zhou, J., Matte-Martone, C., Bergaya, S., van Rooijen, N., Shlomchik, W.D., Min, W., Sessa, W.C., *et al.* (2008a). MyD88-dependent, superoxide-initiated inflammation is necessary for flow-mediated inward remodeling of conduit arteries. *J Exp Med* 205, 3159-3171.

Tang, R.H., Zheng, X.L., Callis, T.E., Stansfield, W.E., He, J., Baldwin, A.S., Wang, D.Z., and Selzman, C.H. (2008b). Myocardin inhibits cellular proliferation by inhibiting NF- κ B(p65)-dependent cell cycle progression. *Proceedings of the National Academy of Sciences of the United States of America* 105, 3362-3367.

Thienpont, B., Aronsen, J.M., Robinson, E.L., Okkenhaug, H., Loche, E., Ferrini, A., Brien, P., Alkass, K., Tomasso, A., Agrawal, A., *et al.* (2017). The H3K9 dimethyltransferases EHMT1/2 protect against pathological cardiac hypertrophy. *The Journal of Clinical Investigation* 127, 335-348.

Thomas, A.C., Sala-Newby, G.B., Ismail, Y., Johnson, J.L., Pasterkamp, G., and Newby, A.C. (2007). Genomics of foam cells and nonfoamy macrophages from rabbits identifies arginase-

I as a differential regulator of nitric oxide production. *Arteriosclerosis, thrombosis, and vascular biology* 27, 571-577.

Thyberg, J., Blomgren, K., Hedin, U., and Dryjski, M. (1995). Phenotypic modulation of smooth muscle cells during the formation of neointimal thickenings in the rat carotid artery after balloon injury: an electron-microscopic and stereological study. *Cell and tissue research* 281, 421-433.

Thyberg, J., Blomgren, K., Roy, J., Tran, P.K., and Hedin, U. (1997). Phenotypic modulation of smooth muscle cells after arterial injury is associated with changes in the distribution of laminin and fibronectin. *The journal of histochemistry and cytochemistry : official journal of the Histochemistry Society* 45, 837-846.

Tiwari, V.K., Stadler, M.B., Wirbelauer, C., Paro, R., Schubeler, D., and Beisel, C. (2012). A chromatin-modifying function of JNK during stem cell differentiation. *Nature genetics* 44, 94-100.

Tousoulis, D., Oikonomou, E., Economou, E.K., Crea, F., and Kaski, J.C. (2016). Inflammatory cytokines in atherosclerosis: current therapeutic approaches. *European heart journal* 37, 1723-1732.

Turner, E.C., Huang, C.L., Govindarajan, K., and Caplice, N.M. (2013). Identification of a Klf4-dependent upstream repressor region mediating transcriptional regulation of the myocardin gene in human smooth muscle cells. *Biochimica et biophysica acta* 1829, 1191-1201.

Turunen, M.P., Aavik, E., and Yla-Herttuala, S. (2009). Epigenetics and atherosclerosis. *Biochimica et biophysica acta* 1790, 886-891.

Uehling, D.E., and Harris, P.A. (2015). Recent progress on MAP kinase pathway inhibitors. *Bioorganic & Medicinal Chemistry Letters* 25, 4047-4056.

van Essen, D., Zhu, Y., and Sacconi, S. (2010). A feed-forward circuit controlling inducible NF-kappaB target gene activation by promoter histone demethylation. *Mol Cell* 39, 750-760.

van der Heiden, K., Cuhlmann, S., Luong, Le A., Zakkar, M., and Evans, Paul C. (2010). Role of nuclear factor kappaB in cardiovascular health and disease. *Clinical Science* 118, 593.

Vedadi, M., Barsyte-Lovejoy, D., Liu, F., Rival-Gervier, S., Allali-Hassani, A., Labrie, V., Wigle, T.J., Dimaggio, P.A., Wasney, G.A., Siarheyeva, A., *et al.* (2011). A chemical probe selectively inhibits G9a and GLP methyltransferase activity in cells. *Nature Chemical Biology* 7, 566-574.

Villeneuve, L.M., Reddy, M.A., Lanting, L.L., Wang, M., Meng, L., and Natarajan, R. (2008a). Epigenetic histone H3 lysine 9 methylation in metabolic memory and inflammatory phenotype of vascular smooth muscle cells in diabetes. *Proceedings of the National Academy of Sciences of the United States of America* 105.

Villeneuve, L.M., Reddy, M.A., Lanting, L.L., Wang, M., Meng, L., and Natarajan, R. (2008b). Epigenetic histone H3 lysine 9 methylation in metabolic memory and inflammatory phenotype of vascular smooth muscle cells in diabetes. *Proceedings of the National Academy of Sciences of the United States of America* 105, 9047-9052.

- von Scheidt, M., Zhao, Y., Kurt, Z., Pan, C., Zeng, L., Yang, X., Schunkert, H., and Lusic, A.J. (2017). Applications and Limitations of Mouse Models for Understanding Human Atherosclerosis. *Cell metabolism* 25, 248-261.
- Wang, Z., Zang, C., Rosenfeld, J.A., Schones, D.E., Barski, A., Cuddapah, S., Cui, K., Roh, T.Y., Peng, W., Zhang, M.Q., *et al.* (2008). Combinatorial patterns of histone acetylations and methylations in the human genome. *Nature genetics* 40, 897-903.
- Watanabe, S., Mu, W., Kahn, A., Jing, N., Li, J.H., Lan, H.Y., Nakagawa, T., Ohashi, R., and Johnson, R.J. (2004). Role of JAK/STAT pathway in IL-6-induced activation of vascular smooth muscle cells. *American journal of nephrology* 24, 387-392.
- Webb, K.E., Henney, A.M., Anglin, S., Humphries, S.E., and McEwan, J.R. (1997). Expression of Matrix Metalloproteinases and Their Inhibitor TIMP-1 in the Rat Carotid Artery After Balloon Injury. *Arteriosclerosis, thrombosis, and vascular biology* 17, 1837.
- Weber, C., and von Hundelshausen, P. (2017). CANTOS Trial Validates the Inflammatory Pathogenesis of Atherosclerosis: Setting the Stage for a New Chapter in Therapeutic Targeting. *Circulation research* 121, 1119-1121.
- Wen, B., Wu, H., Shinkai, Y., Irizarry, R.A., and Feinberg, A.P. (2009). Large histone H3 lysine 9 dimethylated chromatin blocks distinguish differentiated from embryonic stem cells. *Nature genetics* 41, 246-250.
- WHO (2015). Cardiovascular diseases (CVDs). In Fact sheet N°317, M. centre, ed. (World Health Organisation).
- Wirth, A., Benyo, Z., Lukasova, M., Leutgeb, B., Wettschureck, N., Gorbey, S., Orsy, P., Horvath, B., Maser-Gluth, C., Greiner, E., *et al.* (2008). G12-G13-LARG-mediated signaling in vascular smooth muscle is required for salt-induced hypertension. *Nat Med* 14, 64-68.
- Wirth, A., Benyó, Z., Lukasova, M., Leutgeb, B., Wettschureck, N., Gorbey, S., Örsy, P., Horváth, B., Maser-Gluth, C., Greiner, E., *et al.* (2007). G12-G13–LARG–mediated signaling in vascular smooth muscle is required for salt-induced hypertension. *Nature Medicine* 14, 64.
- Wu, X., Li, Y., Xue, L., Wang, L., Yue, Y., Li, K., Bou, S., Li, G.P., and Yu, H. (2011). Multiple histone site epigenetic modifications in nuclear transfer and in vitro fertilized bovine embryos. *Zygote (Cambridge, England)* 19, 31-45.
- Xie, S., Issa, R., Sukkar, M.B., Oltmanns, U., Bhavsar, P.K., Papi, A., Caramori, G., Adcock, I., and Fan Chung, K. (2005). Induction and regulation of matrix metalloproteinase-12 in human airway smooth muscle cells. *Respiratory Research* 6, 148-148.
- Xiong, Y., Li, F., Babault, N., Dong, A., Zeng, H., Wu, H., Chen, X., Arrowsmith, C.H., Brown, P.J., Liu, J., *et al.* (2017). Discovery of Potent and Selective Inhibitors for G9a-Like Protein (GLP) Lysine Methyltransferase. *60*, 1876-1891.
- Xu, J., and Shi, G.-P. (2014). Vascular wall extracellular matrix proteins and vascular diseases. *Biochimica et biophysica acta* 1842, 2106-2119.

Yamada, S., Wang, K.-Y., Tanimoto, A., Fan, J., Shimajiri, S., Kitajima, S., Morimoto, M., Tsutsui, M., Watanabe, T., Yasumoto, K., *et al.* (2008). Matrix Metalloproteinase 12 Accelerates the Initiation of Atherosclerosis and Stimulates the Progression of Fatty Streaks to Fibrous Plaques in Transgenic Rabbits. *The American journal of pathology* *172*, 1419-1429.

Yang, Q., Lu, Z., Singh, D., and Raj, J.U. (2012). BIX-01294 treatment blocks cell proliferation, migration, and contractility in ovine fetal pulmonary arterial smooth muscle cells. *Cell proliferation* *45*, 335-344.

Yang, S.H., Sharrocks, A.D., and Whitmarsh, A.J. (2013). MAP kinase signalling cascades and transcriptional regulation. *Gene* *513*, 1-13.

Ye, N., Ding, Y., Wild, C., Shen, Q., and Zhou, J. (2014). Small molecule inhibitors targeting activator protein 1 (AP-1). *Journal of medicinal chemistry* *57*, 6930-6948.

Ying, Z., Xiang, G., Zheng, L., Tang, H., Duan, L., Lin, X., Zhao, Q., Chen, K., Wu, Y., Xing, G., *et al.* (2018). Short-Term Mitochondrial Permeability Transition Pore Opening Modulates Histone Lysine Methylation at the Early Phase of Somatic Cell Reprogramming. *Cell Metab.*

Yoshida, K., Maekawa, T., Zhu, Y., Renard-Guillet, C., Chatton, B., Inoue, K., Uchiyama, T., Ishibashi, K.-i., Yamada, T., Ohno, N., *et al.* (2015). The transcription factor ATF7 mediates lipopolysaccharide-induced epigenetic changes in macrophages involved in innate immunological memory. *Nature Immunology* *16*, 1034.

Yoshida, T., Yamashita, M., Horimai, C., and Hayashi, M. (2013). Smooth muscle-selective inhibition of nuclear factor-kappaB attenuates smooth muscle phenotypic switching and neointima formation following vascular injury. *Journal of the American Heart Association* *2*, e000230.

Zhang, B.F., Jiang, H., Chen, J., Guo, X., Hu, Q., and Yang, S. (2018). KDM3A inhibition attenuates high concentration insulin-induced vascular smooth muscle cell injury by suppressing MAPK/NFkappaB pathways. *International journal of molecular medicine* *41*, 1265-1274.

Zhang, J., Gao, Q., Li, P., Liu, X., Jia, Y., Wu, W., Li, J., Dong, S., Koseki, H., and Wong, J. (2011). S phase-dependent interaction with DNMT1 dictates the role of UHRF1 but not UHRF2 in DNA methylation maintenance. *Cell Research* *21*, 1723-1739.

Zhang, Q., Lenardo, M.J., and Baltimore, D. (2017). 30 Years of NF-kappaB: A Blossoming of Relevance to Human Pathobiology. *Cell* *168*, 37-57.

Zhang, T., Termanis, A., Özkan, B., Bao, Xun X., Culley, J., de Lima Alves, F., Rappsilber, J., Ramsahoye, B., and Stancheva, I. (2016). G9a/GLP Complex Maintains Imprinted DNA Methylation in Embryonic Stem Cells. *Cell Reports* *15*, 77-85.

Zhong, Q., and Kowluru, R.A. (2013a). Regulation of matrix metalloproteinase-9 by epigenetic modifications and the development of diabetic retinopathy. *Diabetes* *62*.

Zhong, Q., and Kowluru, R.A. (2013b). Regulation of matrix metalloproteinase-9 by epigenetic modifications and the development of diabetic retinopathy. *Diabetes* *62*, 2559-2568.

Zhou, V.W., Goren, A., and Bernstein, B.E. (2011). Charting histone modifications and the functional organization of mammalian genomes. *Nature reviews Genetics* 12, 7-18.

Zhu, J., Zhang, J., Huang, H., Li, J., Yu, Y., Jin, H., Li, Y., Deng, X., Gao, J., Zhao, Q., *et al.* (2014). Crucial Role of C-Jun Phosphorylation at Ser63/73 Mediated by PHLPP Protein Degradation in the Cheliosisin A (Chel A) Inhibition of Cell Transformation. *Cancer prevention research (Philadelphia, Pa)* 7, 1270-1281.

Zhu, Y., van Essen, D., and Sacconi, S. (2012). Cell-type-specific control of enhancer activity by H3K9 trimethylation. *Mol Cell* 46, 408-423.

Ziegenhain, C., Vieth, B., Parekh, S., Reinius, B., Guillaumet-Adkins, A., Smets, M., Leonhardt, H., Heyn, H., Hellmann, I., and Enard, W. (2017). Comparative Analysis of Single-Cell RNA Sequencing Methods. *Mol Cell* 65, 631-643.e634.